

Optimisation in Plant Operations for a 100 MW Central Receiver CSP Plant with Focus on the Plant Operating Strategies

by
Oelof Abraham Jakobus de Meyer

*Dissertation presented for the degree of Doctor of Philosophy in the
Faculty of Engineering at Stellenbosch University*



Supervisor: Prof Frank Dinter
Co-supervisor: Prof Saneshan Govender

March 2017

Declaration

By submitting this dissertation electronically, I declare that the entirety of the work contained therein is my own, original work, that I am the sole author thereof (save to the extent explicitly otherwise stated), that reproduction and publication thereof by Stellenbosch University will not infringe any third party rights and that I have not previously in its entirety or in part submitted it for obtaining any qualification.

This dissertation includes three original papers published in peer-reviewed journals, peer-reviewed conference proceedings or books and one unpublished publications. The development and writing of the papers (published and unpublished) were the principal responsibility of myself and, for each of the cases where this is not the case, a declaration is included in the dissertation indicating the nature and extent of the contributions of co-authors

Date: 21 August 2017

Abstract

As South Africa progresses towards a more diverse energy mix, it is essential to comprehend both the contribution and implications that renewable energy generating technologies have on the electric grid. Therefore, this dissertation emanated from Eskom's directive aims to acquire a comprehensive understanding of the technical, financial, and operational aspects of running a plant that is built on concentrating solar central receiver technology. Independent Power Producers (IPPs) and Concentrated Solar Power (CSP) plant operators across the globe predominantly adopt the Maximise Power Generation operating strategy. It is necessary to determine the means to optimise the plant operations as a varying operating strategy is envisioned for the plant. Therefore, this research investigated the effects of an array of varying operating strategies imposed upon the plant, which is an essential exercise to determine the possible role of CSP within the South African electric grid. Three boundary conditions determine the operations of a CSP plant: weather conditions; plant status; and operating strategy. After an extensive literature review, it is established that no publically available model is available to optimise the plant operations under the aforementioned conditions. Therefore, a simulation model was developed in the current research to optimise the plant under these boundary conditions.

The basic design of Eskom's 100 MW CSP project was used as the reference plant in developing the simulation model. Subsequently, the simulation results and performance curves of each subsystem within the plant, i.e. the heliostat field, receiver and power block, are validated against other commercially available simulation models. The operational logic is implemented in the validated model to objectively simulate the plant operations considering the specified boundary conditions.

The developed simulation model successfully demonstrated through simulation the effects that (i) weather conditions, (ii) plant status and (iii) operating strategies have on both, the plant performance and operational capabilities of the central receiver technology. The advantages that this model offers over the other similar simulation models available in literature are as follows: provides a detailed, up to seven-day forecast, of the plant operations; implements time resolution of 15 minutes increasing the transients and results accuracy; provides user flexibility to specify the precise boundary conditions imposed on plant operations; offers capability of comparing various simulations or operating strategies by providing key performance and financial indicators.

The dissertation and developed model offers Eskom and the system operator with the required tools to address the specific business needs, also identified by the Eskom Power Plant Engineering Institute (EPPEI) program. The resulting cost of generation, performance indicators and operational capabilities demonstrated are to assist in future Power Purchase Agreements (PPA) and national policy formulations.

Uittreksel

Met Suid-Afrika wat tans besig is om sy energiesamevatting te diversifiseer, is dit noodsaaklik om 'n allesomvattende geheelbeeld oor die bydrae en implikasies wat hernubare energie krag-opwek tegnologieë op die elektriese netwerk bied. Hierdie tesis het daarom voortgespruit uit Eskom se leiding om 'n volle begrip te kry oor die tegniese, finansiële, en operasionele aspekte van 'n kragstasie wat gebruik maak van die gekonsentreerde sonsentrale-opvangertegnologie. Onafhanklike Krag Producente (OKP) en Gekonsentreerde Sonkrag (GSK) stasieoperateurs reg oor die wêreld implementeer gewoonlik die 'Maksimum Krag Opwekking' bedryfstrategie. Hierdie tesis ondersoek die effekte op die kragstasie wanneer 'n verskeidenheid van bedryfstrategieë geïmplementeer word, 'n noodsaaklike oefening om die potensiale rol van GSK te bepaal in Suid-Afrika se elektriese netwerk. Met 'n verskeidenheid van bedryfstrategieë beoog vir die kragstasie, is dit dus noodsaaklik om die optimalisering van die kragstasie se bedrywigheede te bepaal. Drie randvoorwaardes bepaal die optimalisering van die kragstasie se bedrywigheede: die weerstoestand; status van die kragstasie; en bedryfstrategie. Die literatuuroorsig het aangewys dat daar geen publieke simulasiemodelle beskikbaar is om te voldoen aan die optimalisering van die kragstasie se bedrywigheede met hierdie randvoorwaardes nie. Daarom was 'n simulasiemodel geskep om die optimalisering aan te spreek.

Die basiese ontwerp van Eskom se 100 MW GSK projek was gebruik as die verwysingskragstasie in die ontwikkeling van die simulasiemodel. Gevolglik was die simulasiereultate en prestasiekrommes van elke substelsel in die kragstasie, nl. die heliostaatveld, ontvanger en krag blok, bekragtig teenoor ander kommersiële beskikbare simulasiemodelle. Die operasionele logika is geïmplementeer in die bekragtigte simulasiemodel om objektief die kragstasie se bedrywigheede te simuleer met verskeie bedryfstrategieë.

Die simulasiemodel kon dus suksesvol demonstreer, deur simulatie, die effekte wat (i) die weerstoestand, (ii) status van die kragstasie en, (iii) bedryfstrategie plaas op die kragstasie se prestasie en operasionele vermoëns. Die voordeel wat die simulasiemodel bied oor ander soortgelyke simulasiemodelle beskikbaar in literatuur, is soos volg: bied 'n gedetailleerde, tot sewe-dae voorspelling, van die kragstasie se bedrywigheede; implementeer 'n tydresolusie van 15 minute om die kragstasie oorgang te verbeter asook beter akkuraatheid; bied die gebruiker vryheid om die presiese randvoorwaardes te spesifiseer wat op kragstasie se bedrywigheede geplaas word; en die simulasiemodel is in staat om verskillende simulaties of bedryfstrategieë te vergelyk deur middel van prestasie en finansiële aanwysers.

Die tesis en ontwikkelde simulasiemodel bied Eskom en die elektriese netwerkoperateur die noodsaaklike gereedskap om die spesifieke besigheids-behoefte aan te spreek, ook deur die Eskom Kragstasie Ingenieursinstituut (EKII) geïdentifiseer. Die simulasiemodel se resultate, nl. koste van kragopwekking, prestasie-aanwysers en operasionele vermoëns, kan bydrae met toekomstige kragaankoop-ooreenkomste en nasionale beleidsformulerings.

I dedicate this to my mother, Debbie Steyn
For your unconditional love, support and sacrifices

Acknowledgements

I hereby acknowledge the Eskom Power Plant Engineering Institute for funding this research. The Eskom Control and Instrumentation departmental managers, Prudence Madiba, Dieter Huppe, Khaya Sobuwa, Xolelwa Sibozza and Mapula Majola for your continued support.

The following Eskom colleagues have played an instrumental role in the success of this dissertation, my professional and academic career. First and foremost, Devan Naidoo, you kept pushing my boundaries to reach the potential you saw in me, without you, none of this would have been possible. Secondly, the Solar-1 CSP engineering team, Vikesh Rajpaul, Viren Heera, Dhelia Raman, Irshaad Vawda, Johan Stegman, Mbali Mtshali and Zama Luswani. The Owner's Engineering team, for bestowing us with your knowledge and expertise with regards to the solar industry. Special thanks to Xavier Garcia-Casals and Felix Tellez for your mentorship and the work you contributed towards this dissertation.

My industrial mentor, Prof. Saneshan Govender. You inspired me to achieve the impossible and broaden my horizons. Thank you for keeping me on the right path, calming my storms and encourage me to greatness. Your tact, humbleness, and dedication are key qualities I would always remember.

Prof. Frank Dinter, my academic supervisor. The wealth of knowledge and experience you contributed to my life and this research is invaluable. It was a pleasure working with you, thank you for always having my best interests at heart.

Completing this research as part-time studies required a lot of sacrifices and I would like to thank my family and friends for their support during this time. Michael Dafel, you played an instrumental role from start to finish, I will be forever grateful for your contribution. Chiriez Dafel, Steven Howard and Luke Ware, thanks for always listening and helping me to maintain a balanced lifestyle.

My Steyn and Dafel family, Adel de Meyer, Pieter Jansen van Rensburg and Gavin Anderson, you always believed in me even when I doubted myself.

TABLE OF CONTENTS

	Page
1. RESEARCH PROJECT	13
1.1. THE GENESIS OF THE PROJECT	13
1.2. OBJECTIVES	14
1.3. MOTIVATION.....	14
1.4. METHODOLOGY	15
2. LITERATURE REVIEW	16
2.1. INTRODUCTION	16
2.1.1. Renewables in South Africa	16
2.1.2. Contribution of Renewables to the Electric Grid	16
2.1.3. REIPPPP: Policy Framework of Power Sector in South Africa	18
2.2. TARIFF SYSTEM IN SOUTH AFRICA	19
2.2.1. Levelized Cost of Energy (LCOE)	19
2.2.2. System Generation Cost	19
2.3. SOLAR THERMAL POWER GENERATION	20
2.4. MOLTEN SALT CENTRAL RECEIVER TECHNOLOGY DEVELOPMENT	22
2.4.1. Solar One, 1982-1988 (Barstow, California, USA)	22
2.4.2. Solar Two, 1996-1999 (Barstow, California, USA).....	23
2.4.3. Gemasolar, 2011 (Fuentes de Andalucía, Seville, Spain)	23
2.4.4. Crescent Dunes, 2014 (Tonopah, Nevada, USA).....	24
2.5. WATER/STEAM CENTRAL RECEIVER TECHNOLOGY DEVELOPMENT....	25
2.5.1. PS10, 2007 (Andalusia, Seville, Spain).....	25
2.5.2. PS20, 2009 (Andalusia, Seville, Spain).....	25
2.5.3. Ivanpah, 2013 (Mojave Desert, California, USA).....	25
2.5.4. Khi Solar One, 2016 (Upington, Northern Cape, South Africa)	26
2.6. CONTROL SYSTEM DEVELOPMENT AND LESSONS LEARNED.....	26
2.6.1. Solar One.....	27
2.6.2. Solar Two	29

2.6.3. Gemasolar.....	31
2.7. PLANT OPERATIONS.....	31
2.7.1. Plant Operating Philosophy.....	32
2.7.2. Collector Field Aiming Strategy and Control Systems.....	35
2.8. OPERATING STRATEGIES.....	36
2.8.1. Maximise Power Generation.....	38
2.8.2. Maximise Plant Revenue under various Boundary Conditions.....	39
2.8.3. Minimise Energy Dumping.....	40
2.8.4. Optimise Electric Grid Operation.....	41
2.9. COMMERCIAL SOFTWARE AND TOOLS.....	43
3. MODEL DEVELOPMENT.....	46
3.1. INTRODUCTION.....	46
3.2. MODEL OVERVIEW.....	47
3.3. SITE LOCATION AND WEATHER DATA.....	48
3.4. HELIOSTAT FIELD.....	49
3.4.1. Heliostat Field Aiming Strategy.....	49
3.4.2. Heliostat Field Characteristics.....	49
3.4.3. Corresponding Performance and Flux Map.....	50
3.4.4. Heliostat Field Model Configuration.....	52
3.5. RECEIVER.....	54
3.5.1. Mathematical Model.....	55
3.5.2. Step 1: Determine Heat Transfer Fluid Mass Flow Rate.....	58
3.5.3. Step 2: Determine Surface and Tube Temperature.....	58
3.5.4. Receiver Efficiency.....	58
3.5.5. Receiver Pressure Drop.....	59
3.5.6. Receiver Tube Strain.....	59
3.5.7. Receiver Operating Regimes and Weather Prediction.....	60
3.5.8. Receiver Model Configuration.....	62
3.6. POWER BLOCK.....	63

3.7.	THERMAL ENERGY STORAGE.....	65
3.8.	AUXILIARIES	65
3.8.1.	Heliostat Field	66
3.8.2.	Receiver Pump.....	67
3.8.3.	Hot TES Pump.....	69
3.8.4.	Feedwater Heater Pumps	70
3.8.5.	Balance of Plant.....	70
3.8.6.	Air Cooled Condenser	70
3.8.7.	Fixed Parasitics.....	70
4.	MODEL RESULTS.....	71
4.1.	HELIOSTAT FIELD	71
4.2.	RECEIVER THERMOGRAPHIC AND COLORMAP REPRESENTATION	72
4.2.1.	Receiver Flux Map	74
4.2.2.	Surface Tube Temperature	76
4.2.3.	Radiation Losses.....	76
4.2.4.	Convection Losses.....	77
4.2.5.	Receiver Efficiency	78
4.2.6.	Heat Transfer Fluid Temperatures.....	78
4.2.7.	Inner Tube Temperature	79
4.2.8.	Tube Thermal Strain.....	80
4.3.	RECEIVER PERFORMANCE CURVE.....	80
4.3.1.	Constant Wind Speed, Variant Ambient Temperatures	80
4.3.2.	Wind Speed Effects	81
4.4.	POWER BLOCK PERFORMANCE	84
5.	MODEL VALIDATION.....	87
5.1.	HELIOSTAT FIELD MODEL.....	87
5.2.	RECEIVER MODEL.....	88
5.3.	POWER BLOCK MODEL	90
6.	SIMULATION RESULTS.....	95

6.1.	MAXIMISE POWER GENERATION.....	95
6.1.1.	Short Term Simulation Results	95
6.1.2.	Annual Simulation Results	98
6.2.	MAXIMISE PLANT REVENUE	101
6.3.	MINIMISE ENERGY DUMPING.....	102
6.3.1.	Short Term Simulation Results	103
6.3.2.	Annual Simulation Results	105
6.4.	OPTIMISE ELECTRIC GRID.....	106
6.4.1.	Complimentary Services to Wind Generation.....	106
6.4.2.	Complimentary Services to PV Generation	108
6.4.3.	Complimentary Services to Wind and PV Generation.....	109
6.4.4.	Complimentary Services Summary	110
6.4.5.	Base Load Operations.....	111
6.4.6.	Peaking Operations.....	114
7.	CONCLUSION.....	115
7.1.	SUMMARY OF FINDINGS	115
7.2.	CONCLUSION.....	118
7.3.	FURTHER RESEARCH DEVELOPMENTS	120
	REFERENCES.....	122
	APPENDIX A: SOLAR-1 DESIGN PARAMETERS	
	APPENDIX B: DELSOL3 FLUX MAP AND ERRORS	
	APPENDIX C: SIMULATION MODEL: STEP-BY-STEP GUIDE.....	

LIST OF FIGURES

Figure 1: System seasonal demands with Wind and PV contribution (Eskom, 2015b) .17	17
Figure 2: Average system seasonal demand and residual load (Eskom, 2015b).....	17
Figure 3: Average tariffs per Bid Window in REIPPPP (DoE, 2016b).....	20
Figure 4: Molten salt two-tank central receiver system, (Solar Reserve, 2014).....	21
Figure 5: Schematic of Solar One pilot plant (Falcone, 1986)	22
Figure 6: Gemasolar CSP plant located in Seville, Spain (Torresol Energy, 2010).....	24
Figure 7: Crescent Dune located in Tonopah, Nevada (Solar Reserve, 2016)	24
Figure 8: CSP plants, PS20 (left) and PS10 (right), in Seville, Spain. (Guasti, 2015)...	25
Figure 9: Three units of Ivanpah in the Mojave Desert. (BrightSource Energy, 2014) .	26
Figure 10: Cavity receivers (left) (JG Afrika, 2017). Aerial view (right) (CMI, 2017) .	26
Figure 11: Visual representation of operating modes of Solar One, Table 1	28
Figure 12: Receiver and power block decoupled (Lovegrove and Stein, 2012).....	29
Figure 13: Energy collection system steady-state operation (Zavoico, 2001).....	32
Figure 14: Power generation system steady-state operation (Zavoico, 2001)	32
Figure 15: MIP plant valuation framework, adapted (Kost et al., 2013)	37
Figure 16: DYESOPT modelling approach used, adapted (Guedez et al., 2013).....	38
Figure 17: Review on commercial software and tools (De Meyer et al., 2014).....	43
Figure 18: Review on commercial software and tools (De Meyer et al., 2014).....	45
Figure 19: Basic overview of model developed	48
Figure 20: Graphical representation of DELSOL3 flux map	51
Figure 21: 96 Flux maps equally spaced by declination angle (Wagner, 2008).....	52
Figure 22: Heliostat field model configuration, interfacing and outputs.....	53
Figure 23: Receiver serpentine flow regimes with cross over flow halfway.....	54
Figure 24: Receiver thermal resistance network at the receiver tube cross section	55
Figure 25: (a) Determine Q_{in} and $THTF(o)$ (b) Determine T_s and T_t	58
Figure 27: Receiver operations with weather predicting element incorporated [15min]	61
Figure 28: Receiver model configuration, interfacing and outputs	62
Figure 29: TS-Diagram representing the power block design point values	63
Figure 30: Power block configuration and design point conditions	64
Figure 31: Head loss associated with the receiver pump.....	68
Figure 32: Heliostat field optical efficiency in relation to the zenith angle	72

Figure 33: Receiver thermographic and colormap representation a) DELSOL3 incident flux map (b) receiver efficiency (c) panel inner tube temperatures (d) receiver surface temperatures (e) radiation losses (f) convective losses.	73
Figure 34: Receiver incident flux map on 1 st January at 08h00 (left) and 16h00 (right)	75
Figure 35: Receiver incident flux map on 1 st July at 08h00 (left) and 16h00 (right)	75
Figure 36: Surface tube temperatures at 08h00 on 1 st January (left) and 1 st July (right)	76
Figure 37: Radiation losses at 08h00 on 1 st January (left) and 1 st July (right)	77
Figure 38: Convection losses on 1 st January at 08h00 (left) and 16h00 (right)	77
Figure 39: Receiver efficiency on 1 st July at 08h00 (left) and 16h00 (right)	78
Figure 40: HTF temperatures at 08h00 on 1 st January (left) and 1 st July (right)	79
Figure 41: Inner tube temperatures at 08h00 on 1 st January (left) and 1 st July (right)	79
Figure 42: Tube strain analysis at 08h00 on 1 st January (left) and 1 st July (right)	80
Figure 43: (a) Ambient temperature effects on the receiver efficiency, no wind speeds (b) Correlation between the highest and lowest ambient temperature effect. (c) Average receiver performance with regards to ambient temperature	81
Figure 44: (a) Wind speed effects on the receiver efficiency, at reference temperature (b) Correlation between the highest and the lowest wind speed effects (c) Average receiver performance with regards to wind speed	82
Figure 45: (a) Ambient temperature effects on the receiver efficiency, no wind speeds (b) Correlation between highest and lowest ambient temperature effects.	83
Figure 46: Annual wind speed occurrences	83
Figure 47: (left) Turbine output, thermal energy supplied to steam generator system (right) Power block performance curve	84
Figure 48: (a) Steam generator system's heat transfer fluid output temperature effects (b) Power block performance curve w.r.t. thermal energy supplied	85
Figure 49: (left) Steam generator system's HTF output temperature effects (right) Power block performance curve w.r.t. thermal energy supplied	85
Figure 50: Heliostat field optical efficiency	88
Figure 51: SAM: Effect of receiver curtailment on heliostat field optical efficiency	88
Figure 52: Receiver performance curve validation	89
Figure 53: Results comparison in the HTF mass flow rate through the receiver	90
Figure 54: Power block performance validation	94
Figure 55: Weather conditions as input to simulation model	96
Figure 56: Graphical representation of receiver operations	96
Figure 57: Hot TES dispatch profile and state of charge	97

Figure 58: Power block operations under optimised maximise power generation.....	97
Figure 59: Power block, optimised part load (left) and non-optimised (right).....	98
Figure 60: Annual receiver performance curve correlation between the two models ..	100
Figure 61: Annual generation breakdown comparison with generation occurrences...	100
Figure 62: Weather conditions for period with limited solar resource availability	102
Figure 63: Hot TES dispatch profile, optimising dispatch during higher paying tier ..	102
Figure 64: Maximise power generation (left), and minimise energy dumping (right) .	103
Figure 65: Maximise power generation (left), and minimise energy dumping (right) .	103
Figure 66: Hot TES dispatch profile, optimised to minimise energy dumping	104
Figure 67: Minimum turbine output required to avoid energy dumping	104
Figure 68: Generation profile, wind and CSP offering continuous output.....	106
Figure 69: Annual generation profile, CSP providing complimentary service to wind	107
Figure 70: Annual generation profile and availability, wind and CSP generation	107
Figure 71: Generation profile, PV and CSP with continuous output.....	108
Figure 72: Annual generation profile, CSP with complimentary services to PV	108
Figure 73: Annual generation profile and availability, PV and CSP generation	108
Figure 74: Generation profile, Wind-PV and CSP for continuous output.....	109
Figure 75: Annual generation profile, CSP with complimentary services to Wind-PV	109
Figure 76: Annual generation profile and availability, Wind-PV and CSP generation	109
Figure 77: Hot TES dispatch control, maintaining sufficient capacity in hot TES	111
Figure 78: Power block dispatch profile to the grid, base load capability.....	111
Figure 79: Base load operations while maintaining a higher turbine output	112
Figure 80: Weather conditions applicable for the low DNI period	112
Figure 81: Hot TES dispatch during low DNI periods	113
Figure 82: Lower turbine output during low DNI periods.....	113
Figure 83: CSP offering base load capabilities to the system demonstrated	113
Figure 84: ‘Peaking’ capabilities demonstrated during low DNI period.....	114
Figure B.1: Heliostat compensation for induced errors to field performance	B.1
Figure B.2: Constant heliostat field, effect on performance due to induced errors	B.2
Figure C.1: Model-3 Opening window	C.2
Figure C.2: ‘Start Simulation’ graphical user interface	C.3
Figure C.3: Maximise Power Generation operating strategy sub-window.....	C.5

Figure C.4: Maximise Power Generation, user specified turbine start-up at 05h00.....	C.6
Figure C.5: Report sheet. Simulation model results with graphical representations....	C.7
Figure C.6: Weather and heliostat field report - summary	C.8
Figure C.7: Ambient conditions under which the plant operations were optimised.....	C.8
Figure C.8: Heliostat field optical efficiency and energy deflected from receiver.....	C.9
Figure C.9: Receiver operational report – summary.....	C.9
Figure C.10: Graphical representation of receiver operations	C.10
Figure C.11: Graphical representation of cold TES charge and discharge profiles ...	C.11
Figure C.12: Extraction from 'Results' sheet, rows 128-139	C.11
Figure C.13: Power block operational report – summary.....	C.12
Figure C.14: Power block dispatch profile and efficiency	C.12
Figure C.15: Graphical representation of hot TES charge and discharge profiles	C.12
Figure C.16: Plant auxiliary consumption and financial report.....	C.13
Figure C.17: Plant auxiliary consumption	C.13
Figure C.18: System demand; represent residual load, wind, PV and CSP.	C.14
Figure C.19: Results sheet. Detailed plant performance, weather conditions and financial indicators	C.15
Figure C.20: Maximise Power Generation, user specified turbine start-up.....	C.16
Figure C.21: Receiver operational report – summary.....	C.17
Figure C.22: Graphical representation of receiver operations	C.17
Figure C.23: Graphical representation of cold TES charge and discharge profiles ...	C.18
Figure C.24: Graphical representation of hot TES charge and discharge profiles	C.18
Figure C.25: Optimised Maximise Power Generation.....	C.19
Figure C.26: Receiver operational report – summary.....	C.20
Figure C.27: Graphical representation of receiver operations	C.20
Figure C.28: Power block operational report – summary.....	C.21
Figure C.29: Power block dispatch profile and efficiency	C.21
Figure C.30: Graphical representation of hot TES charge and discharge profiles	C.22
Figure C.31: Maximise Plant Revenue, Time-of-day Tariff – Optimise Net Power..	C.23
Figure C.32: Power block dispatch profile and efficiency	C.23
Figure C.33: Hot TES dispatch profile	C.24
Figure C.34: Change TES size, adapted from Figure C.31	C.25
Figure C.35: Receiver curtailment due to TES size reduction	C.25

Figure C.36: Increase in turbine start/stops due to reduction in TES (left), Reduce turbine start/stops by delaying turbine start-up (right).....	C.26
Figure C.37: Minimise energy dumping operating strategy	C.28
Figure C.38: Heliostat field optical efficiency, no solar energy deflected	C.28
Figure C.39: Receiver operations, no solar energy deflected	C.28
Figure C.40: Reduce turbine start/stops by delaying turbine start-up	C.29
Figure C.41: Hot TES dispatch control highlighting areas of constraint.....	C.29
Figure C.42: Complimentary services to Wind generation	C.31
Figure C.43: CSP complimentary services to wind generation, stacked line	C.31
Figure C.44: Increase in deflected solar energy for complimenting wind generation	C.32
Figure C.45: Power block dispatch profile, complimenting wind generation	C.32
Figure C.46: CSP complimentary services to wind generation, stacked line	C.33
Figure C.47: CSP storage acting as a ‘battery’ for PV generation	C.33
Figure C.48: CSP complimentary services, wind/PV generation, stacked line	C.34
Figure C.49: Power block dispatch profile to the grid, base load capability	C.35
Figure C.50: Hot TES dispatch control, maintaining sufficient capacity in hot TES.	C.35
Figure C.51: Peaking operations simulation set up	C.35
Figure C.52: Power block dispatch profile to the grid, peaking capability	C.36
Figure C.53: Comparison of simulation results executed in Section 3 presented in the ‘Compare SimResults’ sheet	C.38
Figure C.54: Comparison of the simulation results for the receiver performance	C.39
Figure C.55: TES size reduction (left) 12 hours (right) 8 hours	C.40
Figure C.56: Receiver shutting down due to TES state of charge	C.40
Figure C.57: Comparison of the simulation results, power bock performance	C.41
Figure C.58: Comparison of the simulation results, overall plant performance.....	C.42
Figure C.59: Comparison of the simulation results, plant revenue generated.....	C.43
Figure C.60: Ambient conditions and heliostat performance for high DNI period	C.44
Figure C.61: Weather conditions applicable for the high DNI period.....	C.44
Figure C.62: Receiver output curtailed due to hot TES state of charge	C.45
Figure C.63: Receiver operation shut down due to full hot TES.....	C.46
Figure C.64: Hot TES dispatch, reducing turbine start/stop for energy conservation	C.46
Figure C.65: Receiver output curtailed due to hot TES state of charge	C.47
Figure C.66: Time-of-day tariff boundary conditions on turbine output.....	C.47

Figure C.67: Field operations before optimised in Minimise Energy Dumping	C.48
Figure C.68: Hot TES discharge and charge profile.....	C.49
Figure C.69: Turbine output increased to 110 % nominal output	C.49
Figure C.70: Hot TES discharge and charge profile.....	C.50
Figure C.71: Receiver output curtailed due to hot TES state of charge	C.50
Figure C.72: CSP complimentary services to wind generation, stacked line	C.50
Figure C.73: Hot TES discharge and charge profile.....	C.51
Figure C.74: CSP complimentary services to PV generation, stacked line	C.51
Figure C.75: CSP complimentary services to wind and PV generation, stacked line	C.52
Figure C.76: Base load operations while maintaining a higher turbine output	C.52
Figure C.77: Comparison of the simulation results, receiver performance	C.53
Figure C.78: Comparison of the simulation results, power block performance	C.54
Figure C.79: Comparison of the simulation results, plant performance	C.55
Figure C.80: Comparison of the simulation results, plant revenue generated.....	C.55
Figure C.81: Ambient conditions and heliostat performance for low DNI period	C.56
Figure C.82: Weather conditions applicable for the low DNI period.....	C.56
Figure C.83: Receiver output not curtailed in low DNI period	C.57
Figure C.84: Receiver output not curtailed, sufficient capacity in hot TES.....	C.58
Figure C.85: Receiver operation shut down due to full hot TES.....	C.58
Figure C.86: Receiver operation shut down due to full hot TES.....	C.58
Figure C.87: ‘Maximise Power Generation’, low DNI and ambient temperatures	C.59
Figure C.88: Power block operations for ‘Maximise Plant Revenue’	C.59
Figure C.89: Heliostat field optical efficiency and deflected solar energy	C.60
Figure C.90: CSP complimentary services to wind generation, stacked line	C.61
Figure C.91: Hot TES dispatch profile to provide complimentary services to wind..	C.61
Figure C.92: CSP complimentary services to PV generation, stacked line	C.61
Figure C.93: CSP complimentary services to wind and PV generation, stacked line	C.62
Figure C.82: Weather conditions applicable for the low DNI period.....	C.62
Figure C.94: Hot TES dispatch during low DNI periods	C.63
Figure C.95: Turbine output during low DNI periods	C.63
Figure C.96: Optimise for low turbine output	C.64
Figure C.97: Re-optimised hot TES dispatch during low DNI periods.....	C.64

Figure C.98: Re-optimised lower turbine output during low DNI periods.....	C.64
Figure C.99: ‘Peaking’ capabilities demonstrated during low DNI period	C.65
Figure C.100: Comparison of the simulation results, receiver performance	C.66
Figure C.101: Comparison of the simulation results, power bock performance	C.66
Figure C.102: Comparison of the simulation results, plant performance	C.67
Figure C.103: Comparison of the simulation results, plant revenue generated.....	C.67

LIST OF TABLES

Table 1: Steady state operation modes for Solar One (Alpert and Kolb, 1988).....	27
Table 2: Energy collection system steady state operation modes (Zavoico, 2001).....	33
Table 3: Energy collection system transients (Zavoico, 2001).....	33
Table 4: Energy collection system steady state operation modes (Zavoico, 2001).....	34
Table 5: Power Generation system transients (Zavoico, 2001).....	34
Table 6: Aiming strategies and their functions (Grobler and Gauche, 2014).....	35
Table 7: Solar-1 Project Basic Design documentation (Eskom, 2012a).....	46
Table 8: Heliostat field design and characteristics correlation.....	50
Table 9: Performance output of DELSOL3 at design point, insolation at 950 W/m ²	51
Table 10: Nu correlation for forced convection over cylinder with surface roughness .	57
Table 11: Receiver operating philosophy boundary conditions.....	60
Table 12: Power block design point conditions (Eskom, 2012c).....	63
Table 13: Parasitics consumption for Solar-1 basic design (Eskom, 2012a).....	66
Table 14: Parasitics consumption comparison, SAM and Solar-1 basic design.....	66
Table 15: Receiver parasitics at design point.....	69
Table 16: Heliostat field efficiency as a function of the solar angles.....	71
Table 17: Correlation between Basic Design and receiver model performance.....	89
Table 18: Turbine heat and mass balance correlation.....	91
Table 19: Condenser and feedwater heaters heat and mass balance correlation.....	92
Table 20: Steam generator heat and mass balance correlation.....	93
Table 21: Annual simulation results, comparative overview.....	99
Table 22: Comparison in simulation results for SAM's hot TES dispatch profile.....	101
Table 23: Key plant performance indicators optimised, 'Minimise Energy Dumping' 105	
Table 24: Plant performance indicators, complimentary services to Wind and/or PV. 110	
Table A.1: Plant design parameters.....	A.1
Table A.2: Plant operational parameters.....	A.2
Table C.1: Plant revenue comparison between two variances in simulation model... C.30	
Table C.2: List of operating strategies with specified user inputs in Section 3..... C.36	
Table C.3: List of operating strategies simulated with specified user inputs..... C.45	

SYMBOL	DESCRIPTION	UNIT
A	Surface area or cross-sectional area	m ²
AUX	Auxiliary consumption	Wh
C_p	Heat capacitance	J/kgK
D	Receiver diameter	m
d	Tube diameter	m
E	Unit of electrical energy or Electricity generation per year	kWh or MWh
F	Adjustment Factor	-
f	Friction factor	-
F	Fuel expenditures in the year t	\$ or R
Full	State of charge in thermal storage tank	%
g	Gravitational acceleration	m/s ²
h	Heat transfer coefficient	W/m ² K
H, h	Height or hydraulic head	m
I	Investment expenditures in the year t	\$ or R
k	Surface roughness or resistance coefficient factor	-
k	Thermal conductivity	W/mK
L	Length	m
l	Length	m
\dot{m}	Mass flow rate	kg/s
M	Operations and maintenance expenditures in the year t	\$ or R
n	Economic life of the system	y
N	Number of	-
<i>nday</i>	Number of days included in the selection	day
Nu	Nusselt number	-
P	Pressure	Pa
P	Power	W
\dot{Q}	Thermal energy	W
r	Discount rate	%
r	Radius or radial	m
R	Thermal resistance	K/W
Re	Reynolds number	-
T	Temperature	K
t	Time	a or h or s
tt	Tube thickness	m
V	Heat transfer fluid velocity	m/s
α	Coefficient of thermal expansion	1/K
ε	Emissivity	-
ε	Tube strain	-
σ	Stefan Boltzmann's constant	W/m ² K ⁴

η	Efficiency	%
ρ	Density	kg/m ³
ρ	Receiver reflectivity	-
ν	Poisson's ratio	-

SUBSCRIPT

<i>45</i>	Tube bend of 45°
<i>90</i>	Tube bend of 90°
<i>amb</i>	Ambient
<i>avg</i>	Average
<i>cold</i>	HTF from cold storage tank
<i>cond</i>	Conduction
<i>conv</i>	Convection
<i>DP</i>	Design point
<i>e</i>	Electrical energy
<i>ext</i>	External
<i>f</i>	Friction
<i>field</i>	Heliostat field
<i>film</i>	Film, area between surface and surroundings or fluid
<i>FRES</i>	Fluctuating infeed
<i>gross</i>	Gross energy or gross power
<i>H</i>	Heliostat field
<i>hot</i>	HTF from hot storage tank
<i>HTF</i>	Heat transfer fluid
<i>i</i>	Time or tube inside or internal or inlet
<i>in</i>	Energy transferred to HTF or inside tube
<i>inlet-vessel</i>	Receiver inlet vessel protection system
<i>limit</i>	Flux limit
<i>load</i>	Load demand curve
<i>m</i>	Average between two temperatures (mean) or hydraulic minor losses
<i>min</i>	Minimum
<i>nat</i>	Natural, influenced by natural convection
<i>nodes</i>	Nodes in flux map
<i>normal</i>	Normal operating mode
<i>o</i>	Tube outside or output or outlet
<i>panel</i>	Receiver panel
<i>PB</i>	Power block
<i>pump</i>	Associated pump

<i>PV</i>	PV generation
<i>rad</i>	Radiation
<i>rec</i>	Receiver
<i>ref</i>	Energy reflected
<i>res</i>	Residual load
<i>s</i>	Receiver surface
<i>STB</i>	Standby operating mode
<i>surr</i>	Surroundings
<i>t</i>	Thermal energy or time or tube
<i>TES</i>	Thermal Energy Storage
<i>tot</i>	Total
<i>total</i>	Total value of expression
<i>tower</i>	Receiver tower
<i>tube</i>	Receiver tube inside
<i>warmup</i>	Warmup operating mode
<i>wind</i>	Wind generation or wind energy
θ	Tangential
<i>l</i>	Longitudinal
<i>r</i>	Radial

ABBREVIATIONS

ACC	Air Cooled Condenser
BCS	Beam Characterization System
BoP	Balance of Plant
CO ₂	Carbon Dioxide
COP17	17 th session of the Conference of the Parties
CSP	Concentrated Solar Power
DAPS	Dynamic Aim Processing System
DCS	Distributed Control System
DEA	Department of Environmental Affairs
DNI	Direct Normal Irradiation
DoE	Department of Energy
DP	Design Point
EPPEI	Eskom Power Plant Engineering Institute
FW	Feed Water
FWH	Feed Water Heater
HAC	Heliostat Array Controller
HC	Heliostat Controller
HP	High Pressure
HTF	Heat Transfer Fluid
IP	Intermediate Pressure

IPP	Independent Power Producer
IPPPP	Independent Power Producer Procurement Program
IRP	Integrated Resource Plan
IRR	Internal Rate of Return
ITD	Initial Temperature Differential
LCOE	Levelized Cost of Energy
LP	Low Pressure
NCC	National Control Centre
NDP	National Development Plan
NERSA	National Energy Regulator of South Africa
NREL	National Renewable Energy Laboratory
O&M	Operating & Maintenance
PH	Preheater
PPA	Power Purchase Agreement
PS	Planta Solar
PV	Photovoltaic
REIPPPP	Renewable Energy Independent Power Producer Procurement Program
SAM	System Advisory Model
SAPS	Static Air Processing System
SGS	Steam Generating System
SH	Superheater
SM	Solar Multiple
TES	Thermal Energy Storage
TMY	Typical Meteorological Year
VSD	Variable Speed Drive

OTHER

R	South Africa Rand (ZAR)
\$	United States Dollar (USD)

1. RESEARCH PROJECT

1.1. The Genesis of the Project

Eskom is in the advance stage of procuring a 100 MW_e Concentrating Solar Power (CSP) plant, colloquially referred to as Solar-1. With the aim to diversify Eskom's generation mix, Solar-1 will be Eskom's first operated and maintained CSP plant. This research project emanates from Eskom's directive to acquire a better understanding of the technical, financial, and operational aspects of running a plant that is built on concentrating solar central receiver technology. More specifically, Eskom identified the need to understand the operating capabilities of this plant within the South African electric grid. During the design phase of Solar-1, an array of operating strategies was identified in order to demonstrate the role and value that CSP with storage offers to the electric grid. These operating strategies range from maximising power generation to the base load and peaking operations. Once Solar-1 is commissioned, the bidder would be tasked to demonstrate these operating strategies. With varying operating strategies envisioned for the plant, it is, therefore, necessary to determine how to optimise the plant operations.

In contrast, when an Independent Power Producer (IPP) operated plant is considered, the operating strategy followed is predetermined by the Power Purchase Agreement (PPA). The plant design is optimised to adhere to the PPA. Therefore, plant operations are already considered and developed in the plant's 'Operating Philosophy'. IPPs and other CSP plant operators around the globe follow predominantly a maximise power generation operating strategy. This helps them to yield maximum revenue when a flat rate tariff structure is considered. The Department of Energy (DoE) introduced a time-of-day tariff structure from Bid Window 3 (BW) to the Renewable Energy Independent Power Producers Procurement Program (REIPPPP). Since, the higher paying tariff period commences during the peak time, this boundary condition especially affects the plant design and operations.

The publically available models and tools relating to the central receiver technology assist in the calculation of the annual plant performance predictions and estimation of cost of energy. This valuable information enables upfront design decisions and conclusions relating to the plant's design parameters, installation and operating costs, performance, and financial viability. However, these models are not catering for user's flexibility regarding operating strategies and various tariff structures. This is the reason why this research project focuses on the development of a model to cater for the following requirements: user input flexibility, appropriate operating strategies available pertinent to the user's objectives, flexible periods in which the plant's operation are simulated, and various tariff structures reflecting the appropriate PPA. The novel contribution of this research project separates the developed model from the other models that focus on the annual plant performance predictions, or those whose limitations are imposed on the implemented operating strategies.

With the developed model, the user is empowered to optimise the plant operations under any boundary conditions imposed on the plant. With an objective to maximise the plant

revenue, the user can be represented by the plant operator. He can also be represented by the system operator, requiring peak time operations capabilities from the plant. Lastly, the model compares the simulation results in a holistic manner. This is to inform the user about the best operating strategy to consider while analysing the key performance and financial indicators.

1.2. Objectives

In order to acquire the operational capabilities of the central receiver technology, the following research objectives are identified:

- Investigating in operation simulation, the effect of (i) weather conditions, (ii) plant status and (iii) operating strategy on the operational capabilities of the plant;
- Identifying the performance and financial indicators for the purpose of comparing various operating strategies within the same time period;
- Delivering a plant generation forecast for a maximum period of seven days, based on the implemented operating strategy; and
- Establishing the relationship between the plant and electric grid, specifically, the value that CSP with storage capabilities offers the grid.

1.3. Motivation

More than 90 % of the country's energy requirements are fulfilled and generated by Eskom. To generate such an amount of energy, the energy utility employs various energy generation sources such as coal-fired, nuclear, gas and hydro power stations. Eskom has therefore accumulated a vast amount of experience in understanding the relationship between the plant's operations of these energy generating technologies and the electric grid. Due to the influx of renewable energies to the electric grid, Eskom (the system operator) needs to redevelop its operational capabilities. The Eskom Power Plant Engineering Institute (EPPEI) was established to address the Eskom's business needs. This research project, funded by EPPEI, aims to develop competencies within Eskom relating to the CSP industry.

Simulation models are utilised by the system operators to forecast the energy requirements of the country. It also predicts the amount of power that each of the generating plants can deliver, at any given time period. During a meeting held with a subject matter expert at Eskom's National Control Centre (NCC), it was identified that one of the major problems for the system operator is its inability to generate forecasts for renewable energy sources such as wind, photo-voltaic (PV) and CSP. As the contribution of these renewable sources of energy to the electric grid is growing by each year, forecasting requirements are a necessity. The system operator currently relies on the forecast supplied by the plant operators, but this information is not always reliable. In fact, in some instances, this information is not even provided. The system operator ideally prefers a generation forecast of the plant for a seven-day period (Candy, 2014) to meet the energy requirements of the country and plan maintenance periods and plant outages. For this forecast generation weather prediction is required.

Looking beyond Eskom's owned generation technologies; power generated by IPPs is purchased by the system operator. The introduction of REIPPPP in South Africa opened new challenges and opportunities for growth and development within Eskom. As Eskom had no prior experience in renewables, especially CSP, the need to acquire competencies in these plant's operational capabilities are of great value to the utility. Non-dispatchable renewable power generating technologies such as wind and PV systems offer the electric grid with low generating costs. Furthermore, the fast deployment of these technologies aided during times when the electric grid was constrained. One of the advantages of CSP with storage capabilities in comparison to the wind and PV systems is that it can be dispatched to the system. With this flexibility introduced in a plant's operation and various PPAs in place, the need for optimisation of plant operations emerged. In order to fully unlock the potential that CSP with storage can offer Eskom, there is a need to investigate and understand its operational capabilities and operating strategies.

With the anticipated different PPAs in place, as mentioned in the REIPPPP Bid Window 3.5, the effects of a time-of-day tariff structure on plant operations are investigated. This study aims to inform the policymakers and plant designers about the capabilities and limitations of CSP plant operations associated to the PPA. Currently, IPPs and other CSP plant operators around the world follow predominantly a maximise power generation operating strategy. This research further investigates the effects of varying operating strategies imposed upon the plant, which is an essential exercise to determine the role of CSP within the electric grid. As South Africa progresses towards a more diversified energy mix, it is crucial to have a deep understanding about the contribution and implications that renewable energy generating technologies have on the electric grid.

As stated above, Eskom is currently procuring a CSP plant. The Solar-1 project requires the winning bidder to produce a 100 MW_e CSP plant, with a minimum 60 % capacity factor. Eskom's objective for the plant is, therefore, to acquire a full understanding of the operational aspects associated with this generating technology. The developed model assists in achieving this understanding. Particularly, it demonstrates to the electric grid's stakeholders, the values and capabilities of CSP with storage can offer to the grid. The various operating strategies developed and provided by this study will be tested and implemented once the plant is commissioned.

1.4. Methodology

The literature review shows that there is no publically available model that could calculate the data required to address the current research objectives. A simulation model is, therefore, developed using Solar-1 basic design as the reference plant. With the simulation results of each subsystem of the plant, i.e. the heliostat field as well as the receiver and power block, their performance is validated against other commercially available simulation models. With the subsystems validated, the operational logic is introduced to simulate the plant operations under various boundary conditions. These results demonstrate both the plant performance and operational capabilities. The research objectives are thus achieved.

2. LITERATURE REVIEW

2.1. Introduction

2.1.1. Renewables in South Africa

In response to the 2008 blackouts as well as to meet the country's energy demands, the South African government introduced the REIPPPP. Renewable energy based technologies offer short lead times. Since 2011, through the competitive bidding process, 92 IPPs contributed 6,237 MW to the electric grid (DoE, 2015). South Africa's Integrated Resource Plan (IRP) 2010-2030 policy document sets out the long-term energy requirements for the country. In the revised IRP 2010, for the year 2030, allocations for the following technologies have been set out: a total generation capacity of 9,200 MW wind, 8,400 MW through PV and 1,200 MW through CSP (DoE, 2013). Eskom generates power for the majority of South Africa's energy demand from coal, nuclear, hydro energy, gas and pumped storage stations. Since, Eskom represents a vertically integrated model in the power sector, it has the supply chain of electricity under its control. That is, in addition to serve as the system operator, the energy utility generates, transmits, and distributes power. IPPs participate in the electricity market through a signed PPA with Eskom. In the financial year 2014-15, Eskom sold 216,274 GWh from which 6,022 GWh was from IPP purchases (Eskom, 2015a). However, in the financial year 2015-16, IPP purchases increased to 9,033 GWh whereas the total Eskom sales decreased to 214,487 GWh (Eskom, 2016). In order to secure a solid base load for the future generation, the addition of 9,600 MW of nuclear power source has been allocated to the IRP 2010. The IRP 2010 prioritises nuclear energy, even though, its usage requires strict regulations, higher costs and negative public sentiments. However, the South African government remains committed to the nuclear energy expansion (DoE, 2016a).

2.1.2. Contribution of Renewables to the Electric Grid

During the peak times, when the power usage is the highest, Eskom urged the consumers to lower their power consumption in order to meet the country's energy demands. Although in 2015-16, the REIPPPP contributed 9,033 GWh of renewable energy (wind and PV) to the electric grid, it could not essentially support the system (see Figure 1). During winters, the energy demand is even higher, especially in the evenings. As less power is generated from the renewables due to the meteorological conditions, the high energy demands is not met. Since, the days are longer and warmer in summers, more power is generated from the wind in the afternoons. The data presented in Figure 1 represents the early deployment of wind and PV generating plants in the year 2015. The contribution profile from wind and/or PV will change as more plants are dispersed around the country. However, this research utilises the 2015 system data obtained from the system operator. This data includes demand profile, aggregate wind generation, and aggregate PV generation.

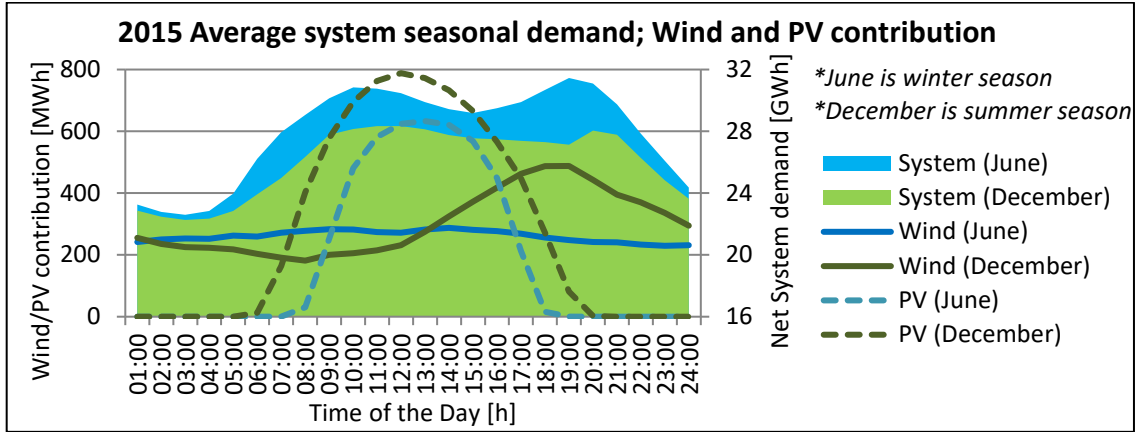


Figure 1: System seasonal demands with Wind and PV contribution (Eskom, 2015b)

The term residual load was introduced to express the status of the system with an influx of non-dispatchable renewables or intermitted energy sources, in a better way (Lunz *et al.*, 2015). The residual load $E_{res}(t)$ is the difference between the load demand curve, $E_{load}(t)$, and the fluctuating infeed, $E_{FRES}(t)$:

$$E_{res}(t) = E_{FRES}(t) - E_{load}(t) \quad (1)$$

In the South African electric grid, the fluctuating infeed consists of wind and PV, hence,

$$E_{FRES}(t) = E_{wind}(t) + E_{PV}(t) \quad (2)$$

Applying the residual load theorem as per Equations 1 and 2, the resulting residual load is illustrated in Figure 2. Additionally, this figure provides a collective overview of the average seasonal distribution amongst the system demand and residual load. At the end of 2015, the installed capacity per generating technology was: Wind 969/9,200 MW; PV 965/8,400 MW; and CSP 150/1,200 MW (Eskom, 2015b). Although, without proper storage capabilities in wind and PV generation, it is unlikely to fully meet the morning and afternoon peak energy demands within the electric grid. CSP with storage offers an alternative solution with its inherent dispatchability potential (Dinter and Busse, 2016).

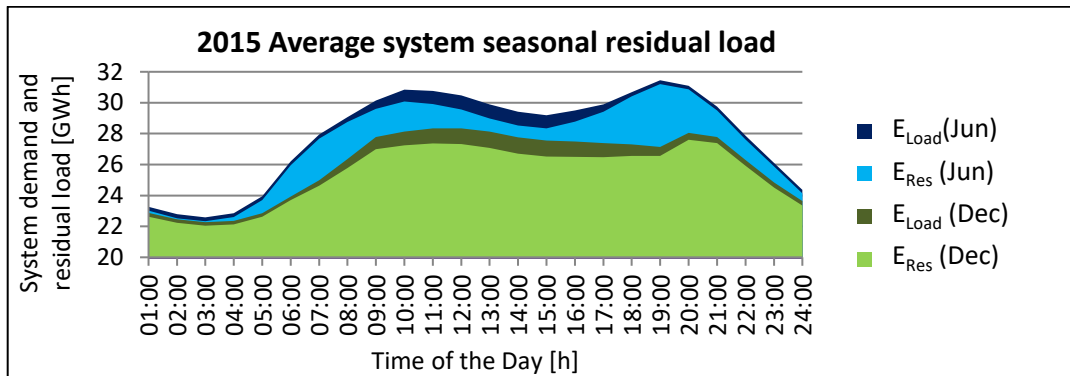


Figure 2: Average system seasonal demand and residual load (Eskom, 2015b)

2.1.3. REIPPPP: Policy Framework of Power Sector in South Africa

In order to support the country's short- and long-term economic and social objectives, the country needs a strong network of economic and energy infrastructure. These objectives were set out in the National Development Plan (NDP) for South Africa (The Presidency, 2014). According to NDP, development of an additional 29,000 MW of electricity by 2030 is required. Also, 10,900 MW of the existing capacity has to be decommissioned. For fulfilling these requirements, new plants generating about 40,000 MW are required. In order to balance the decarbonisation of the power sector and to add different energy generation sources in South Africa's electric grid, it is anticipated that more of the renewable energy technologies are used. The NDP strives for a balance between responding to climate change concerns as well as employing the least-cost power generation technologies to sustain economic growth. The implementation of the NDP is set forth in legislation, policies and regulations.

The Minister of Energy, in consultation with National Energy Regulator of South Africa (NERSA), determines the required new capacity to be implemented. This new energy requirement is determined in accordance with section 34(1) of the Electricity Regulation Act, 2006 (Act No. 4 of 2006) and the Electricity Regulations on New Generation Capacity (published as GNR. 399 in Government Gazette No. 34262 dated 04 May 2011). The indicative capacity to be allocated to various generating technologies is set out in the Integrated Resource Plan for Electricity 2010-2030 (published as GN 400 in Government Gazette No. 34263 dated 06 May 2011). The new generation capacity derived from the nuclear power technology is excluded by the Minister.

The procurement of new generation follows the procurement process under the DoE's Independent Power Producer Procurement Program (IPPPP). The IPPPP Unit was established by the DoE, National Treasury and the Development Bank of South Africa. Its sole purpose was to secure electrical energy from the private sector for renewable and non-renewable energy sources. In accordance with the Electricity Regulations on New Generation Capacity, Section 6(3), the Minister of Energy may determine the identity of the buyer of new generation. Section 10 stipulates that the buyer is able to recover, the full amount of the costs incurred by the buyer for purchasing of the new generation capacity. This transpires when the Regulator determines license conditions relating to prices, charges and tariffs. The South African government favoured a competitive tender approach, as opposed to the feed-in tariffs more commonly used by international governments, for procuring renewable energy capacity. Tenders are structured as a 'rolling bid-window' programme to ensure competitive pressure among bidders, resulting in reduced pricing. (DoE, 2016b)

In the recent years, a conflict amongst certain quarters of South Africa has emerged. This is due to poor understanding on how the policy framework implicated various stakeholders within the power sector. The main instigator is the outdated IRP. The IRP is a policy document that allows all power sector stakeholders to amalgamate to the NDP of the country. It establishes the objectives and requirements needed to achieve the energy demands based on the economic growth, environmental factors, generating technologies costs, fuel costs and other applicable factors. It is revised every two years by the DoE.

The first IRP was published by the South African DoE in 2009. In March 2011, the IRP 2010-2030 was promulgated by the DoE. Based on the new data for the aforementioned factors, a new, updated draft IRP was published in 2013. But, in this draft, the introduction of newly built nuclear power generators was delayed. Therefore, this IRP version was rejected by the government and Cabinet. The anticipated IRP 2016 draft was published by the DoE in November 2016. Various power sector stakeholders were not satisfied with its content and projections. The sentiments amongst various stakeholders were that the strategical activities of South Africa are politically influenced, and the best electricity generation mix for South Africa was not considered. (DoE, 2017)

2.2. Tariff System in South Africa

2.2.1. Levelized Cost of Energy (LCOE)

The LCOE value expresses the conventional cost of any power generation technology. The formula for LCOE in Equation 3 (IRENA, 2015) can be used for comparing different power generation technologies. It is an economic assessment of the power generating technology over the plant's lifetime. It takes into account the average total cost to build and operate the plant in relation to the total amount of energy output over that lifetime. The LCOE represents the minimum cost at which the generated power should be sold, in order to achieve a 'break-even' at the end of the plant's life. Hence, LCOE is the driving factor for investing in a particular plant, and reflects the plant's ability to compete with other technologies. It is important to understand which parameters are to be included in the LCOE calculation. In order to have realistic comparisons between the systems, it is important to know what all parameters need to be considered while calculating LCOE. All the assumptions made and the additional costs are to be stated. Another factor which all investments incur is its financing costs.

$$LCOE = \frac{\sum_{t=1}^n \frac{I_t + M_t + F_t}{(1+r)^t}}{\sum_{t=1}^n \frac{E_t}{(1+r)^t}} \quad (3)$$

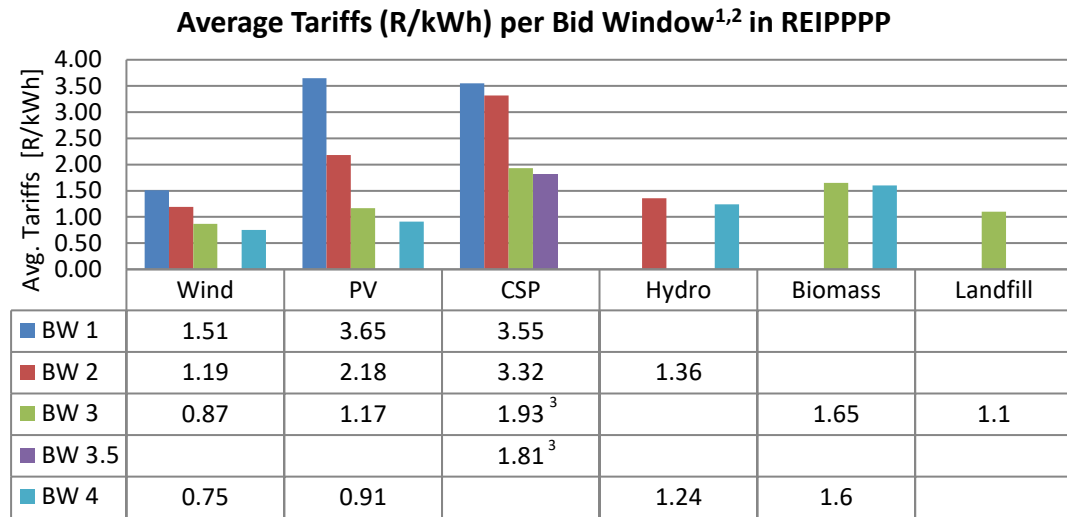
Where, I_t , M_t , F_t and E_t represent the investment cost, operating and maintenance cost, fuel cost and electricity generated in year (t), respectively. r and n represent the discount rate and plant's lifetime, respectively.

2.2.2. System Generation Cost

The system generation cost pertains to the cost incurred by the system operator when purchasing power from the generation plant. The cost per unit power sold to the electric grid is determined by the PPA. In the financial year 2014-15, Eskom reported in its annual results that it paid R2.17/kWh on average to the renewable IPPs. In the 2014-15 financial year, 1,795 MW of the 3,887 MW capacity contracted was connected to the grid. The average load factor of 30.9 % was reported for renewable IPPs (Eskom, 2015a). The annual report for the financial year 2015-16 states that 2,145 MW of the 3,901 MW

contracted was connected to the grid (Eskom, 2016). The total amount of energy purchases from IPPs for this period was 9,033 GWh. The average load factor of 30.7 % was reported for renewable IPPs. For this financial year, a calculated value of R2.15/kWh¹ was determined as the weighted average cost for renewables. (DoE, 2016b)

It is represented in Figure 3 that the average tariffs for the various renewable energy generations have declined considerably since the first Bid Window of the REIPPPP. The price for wind power reduced by 50 % from Bid Window 1 to Bid Window 4, whereas PV decreased by 75 %.



Note 1: Fully indexed price, inflation adjusted to April 2016. Note 2: Price weighted to technology and its relative, projected annual energy contribution (P50). Note 3: Average base rate only, peaking rate is 270 % of the base rate.

Figure 3: Average tariffs per Bid Window in REIPPPP (DoE, 2016b)

2.3. Solar Thermal Power Generation

Solar central receiver technologies utilise direct solar irradiation for power generation. The sunrays are reflected onto a central receiver to raise the temperature of a heat transfer fluid. Large tracking mirrors, also known as heliostats are used for this purpose. The heat transfer fluid in the heating loop of the solar energy collection system drives a traditional Rankine cycle operating on steam. The heat transfer fluid can be a molten salt, steam, oil or air. It depends on the technology used and the desired operating temperatures. In this research project, a molten salt, two-tank central receiver with a traditional Rankine cycle operating on steam is studied. It is illustrated in the Figure 4.

¹ Eskom Integrated Report 2015/16 reported 1.71 R/kWh as the average cost for renewable IPPs. This is in contrast with the 2.17 R/kWh reported in Eskom's Integrated Reported 2014/15. The calculated value of 2.15 R/kWh is based on the weighted production figures from wind and PV under Bid Window 1 and Bid Window 2 tariffs ~ April 2015.

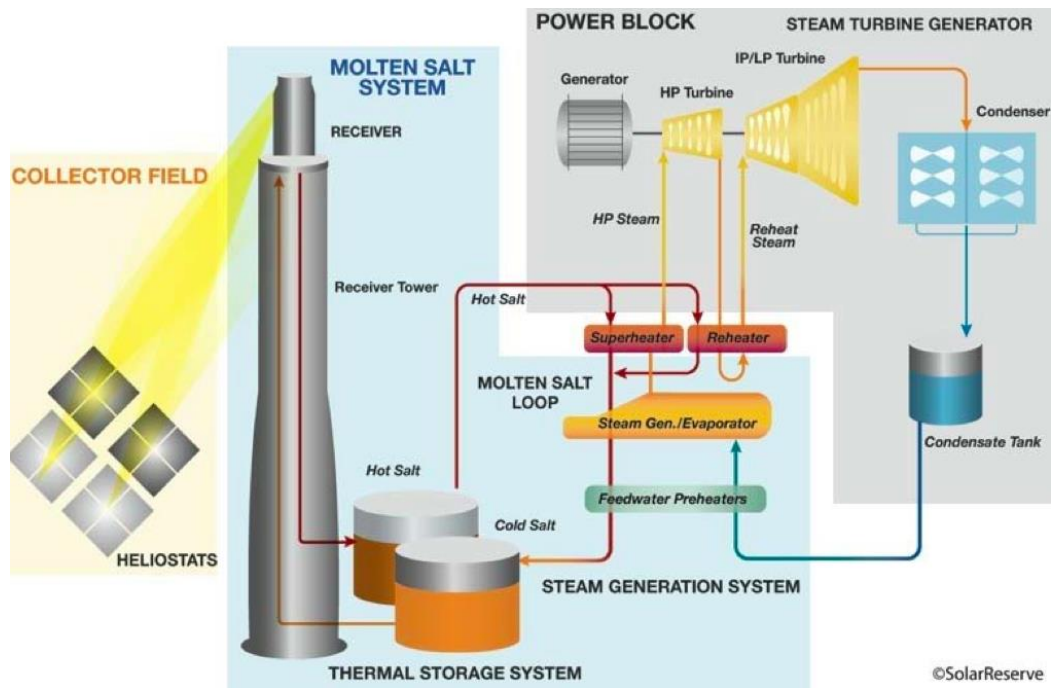


Figure 4: Molten salt two-tank central receiver system, (Solar Reserve, 2014)

In 1986, Falcone published a handbook on solar central receiver design (Falcone, 1986). According to Falcone, a well-designed automated control system can increase the plant's reliability, performance and energy output. It was documented in this book that the control system of these plants was more complex than a conventional power plant. This increased complexity is, in part, due to the unique factors that are relevant to the operation of a central receiver plant. These factors include daily plant start-up and shutdown, cloud transients, load changes, plant operating mode changes, heliostat field control and tracking. In 2001, Zavoico published a 'Design Basis' document for a generic molten salt central receiver power plant (Zavoico, 2001). This document summarised the experience, lessons learned and proposed design innovations from designing, constructing, operating and maintaining Solar Two. In 2011, Kolb published a report evaluating possible next-generation high-temperature molten salt central receivers (Kolb, 2011). Although this research project did not explore next-generation high-temperature molten salt central receivers, it discussed the trend followed in the development of molten salt central receiver technologies. For a global overview of pilot, commercial, and planned CSP plants a comprehensive review of the current status of these plants literatures by Behar *et al.* (2013) and Reddy *et al.* (2013) should be considered.

In this literature review, the progress and technological developments in the central receiver power plants was investigated. The review specifically focuses on the control systems, operating philosophy and operational experiences of receiver power plants. This investigation will help form an understanding of the dynamic behaviour of the process control in these plants. The literature on the commercial power plants developed after Solar Two is limited due to the competitive nature in the solar industry between the developers. However, the maturity of the technology found in literature is sufficient to

approximate the design, operating philosophy and control systems. The simulation tools that are available in the industry for design, optimisation, feasibility studies and performance analysis of the power plants are also considered.

2.4. Molten Salt Central Receiver Technology Development

2.4.1. Solar One, 1982-1988 (Barstow, California, USA)

The largest solar central receiver power plant was constructed in California's Mojave Desert in the year 1981. This pilot plant operated from 1982 to 1988, and had the capacity to generate 10 MW_e or 7 MW_e from 4 hours of thermal storage. The plant configuration is illustrated in the schematic diagram (Figure 5). The heat transfer fluid used in this plant was water. It was boiled and converted into superheated steam to propel the Rankine cycle. The solar energy collection system consisted of 1,818 heliostats, each with a reflective area of 39.9 m² and annual clean reflectivity of 0.903. The heliostat field reflected 70 % of the annual incident solar energy to the receiver. The energy losses were from cosine, shading, blocking and spillage. A 90.8 m tower housed a 24-panel receiver with an annual average efficiency of 70 %. The receiver produced 40 MW_t of 426 °C superheated steam at full load, and 4 MW_t superheated steam at partial load conditions. The receiver which was 13.7 m high and had a diameter of 7 m, had an absorptance of 0.97. (Alpert and Kolb, 1988)

The storage system of this power plant consisted of a tank, a thermal charging and a discharging loop. The heat transfer oil flowed through the bed of packed rock and sand, which enabled the store of energy as sensible heat. The turbine-generator gross efficiency was 33 % when operating off the receiver-generated superheated steam, delivering 12.5 MW_{e-gross}. The turbine-generator gross efficiency dropped to 24 % when operating on the steam from the storage system. (Alpert and Kolb, 1988)

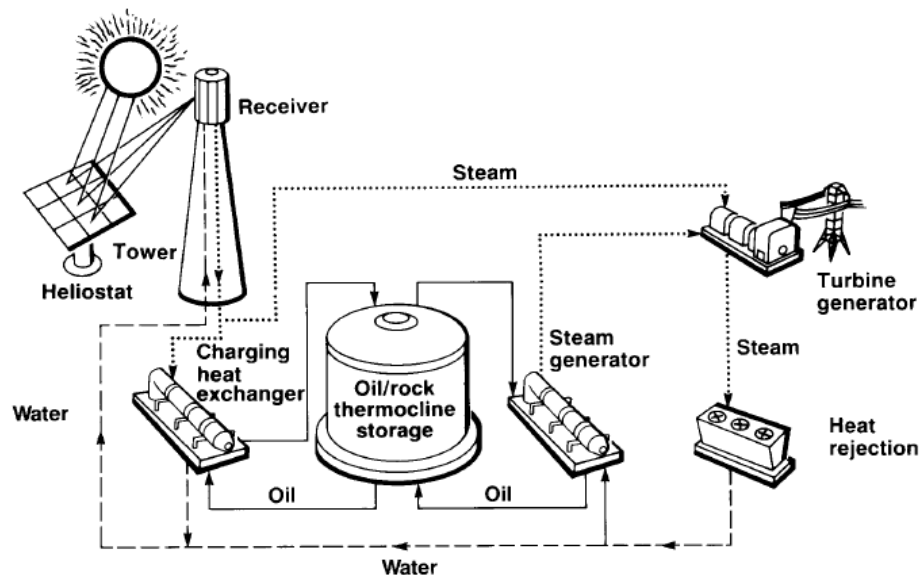


Figure 5: Schematic of Solar One pilot plant (Falcone, 1986)

Based on the report published by Radosevich in 1988, the Solar One's six-year test and power generation program proved that the operating technology was reliable. Further, the plant operated with low environmental impact and high social acceptance (Radosevich, 1988). It was observed in the demonstration phase of the Solar One that direct coupling of the receiver to the turbine configuration causes the turbine to drop offline during cloud transients. Higher thermodynamic losses from the thermal storage system were also observed. Further developments on the central receiver technologies were investigated in the testing phase. This escalated the development of Solar Two Project. The project considered all the drawbacks and shortcomings of Solar One. (Tyner *et al.*, 1995)

2.4.2. Solar Two, 1996-1999 (Barstow, California, USA)

Solar Two was a modified and updated version of Solar One with improvements and new demonstration objectives. The heliostat field, tower structure and 10 MW_e turbine, including the balance of plant infrastructure were reused for this project. New components were added to the plant. These were a 42 MW_t external receiver, 110 MW_t two-tank molten salt thermal storage, 35 MW_t steam generator system (535 °C temperature and 100 bar pressure), and a master control system (Kelly and Singh, 1995). The objectives of this project were twofold. It was to validate the technical features of the nitrate salt technology, receiver, thermal storage and steam generator and to reduce the technical and economic risks associated with the technology by increasing the capital, operation and maintenance costs database (Goswami and Kreith, 2007). The core difference between Solar One and Solar Two was the heat transfer fluid. The heat transfer fluid used in Solar Two was a nitrate salt mixture, commonly called the molten salt, with 60 wt % of sodium nitrate (NaNO₃) and 40 wt % of potassium nitrate (KNO₃).

The plant successfully demonstrated the potential of nitrate salt technology. Some key results were as follows: a receiver efficiency of 88 %, thermal storage system efficiency over 97 %, gross Rankine turbine cycle efficiency of 34 %, and an overall plant peak conversion efficiency of 13.5 %. The collector field availability was between 85-95 %. It was less than the projected 98 % value. The Solar Two power plant was comparatively smaller than the conventional power plants and hence was not competitive with them. More efficient designs could be prepared for larger plants that could benefit economically. The maintenance costs are also distributed while designing larger plants. These economic benefits are achieved along with more power generation. The first commercial molten salt central receiver plant, Gemasolar, was developed and was commercially operational since 2011. (Goswami and Kreith, 2007)

2.4.3. Gemasolar, 2011 (Fuentes de Andalucía, Seville, Spain)

Gemasolar (Figure 6), also known as Solar Tres in earlier literatures, started operating in 2011. It generated 19.9 MW_e power using molten salt as heat transfer fluid and storage medium. Its 120 MW_t external cylindrical receiver, which is installed on a 140 m tower, is powered by a heliostat field consisting of 2,650 heliostats. Each heliostat has a reflecting area of 115 m² (Kolb, 2011). The molten salt operating temperatures range between 290 °C and 565 °C. It is kept in a two-tank storage system which can operate for

15 hours at full load. Burgaleta (2012) released a report elaborating the key points for the operation of the Gemasolar plant. This report focused on the results obtained from the plant's one-year of operation. It highlighted that the technology's robustness is demonstrated in its successful operation. Apart from reporting on a high plant availability factor, a milestone of 12 consecutive days of operation was achieved (Burgaleta *et al.*, 2012). Another report published by Garcia in 2012, discoursed on one year of operational experience from Gemasolar (Garcia and Calvo, 2012).



Figure 6: Gemasolar CSP plant located in Seville, Spain (Torresol Energy, 2010)

2.4.4. Crescent Dunes, 2014 (Tonopah, Nevada, USA)

Crescent Dunes (illustrated in Figure 7), was commissioned in February 2014. It generates 110 MW_e on 10 hours of full load storage. In present, it is one of the largest two-tank molten salt central receiver power plants in the world with a capacity factor of 52 %. The heliostat field of this power plant consists of 10,347 heliostats, each with a reflecting area of 62 m^2 (Wang, 2014). An external receiver with a power rating of 565 MW_t , located on the 185 m high tower, raises the molten salt temperature up to $560 \text{ }^\circ\text{C}$ (Gould, 2011). It is expected that the future of the solar towers would mainly rely on the plant design of Crescent Dune and its operating capabilities.



Figure 7: Crescent Dune located in Tonopah, Nevada (Solar Reserve, 2016)

2.5. Water/Steam Central Receiver Technology Development

2.5.1. PS10, 2007 (Andalusia, Seville, Spain)

Planta Solar 10 (PS10) (see Figure 8), is the world's first commercialised central receiver CSP plant. It was commissioned in 2007 and it generates 11 MW_e of power at 45 bar pressure. The heliostat field consists of 624 heliostats, each with a reflecting area of 120 m². The heliostats concentrate the solar energy onto a steam operated cavity receiver to create a steam at 300 °C. This cavity receiver is installed on a 115 m high tower. The receiver has a steam storage capability of 30 minutes, which results in a capacity factor of 24 %. (Lovegrove and Stein, 2012)

2.5.2. PS20, 2009 (Andalusia, Seville, Spain)

In 2009, Planta Solar 20 (PS20) was commissioned featuring several technological improvements from its predecessor, PS10 (see Figure 8). PS20 has a more efficient receiver and thermal storage system. The improvements in the control and operational systems resulted in an overall improvement and enhancement in the plant's performance. The heliostat field consists of 1,255 heliostats, each with a reflecting area of 120 m². The 165 m high tower houses a steam operated cavity receiver which is capable of producing steam at 300 °C for a turbine-generator. It generates 20 MW_e power at 45 bar pressure. The plant has a one-hour steam storage capability and a capacity factor of 27 %. (Lovegrove and Stein, 2012)



Figure 8: CSP plants, PS20 (left) and PS10 (right), in Seville, Spain. (Guasti, 2015)

2.5.3. Ivanpah, 2013 (Mojave Desert, California, USA)

In 2013, Ivanpah was commissioned in Mojave Desert of California. It has three units. All the three units generate a combined power of 377 MW_e. Each unit has a 140 m high tower, housing an external steam-operated receiver. The three heliostat fields combined have a total number of 173,500 heliostats in it. Each heliostat has a reflecting area of 15.2 m². Its power block, which operates at 160 bar pressure and 565 °C temperature has no thermal storage. (Brightsource, 2014)



Figure 9: Three units of Ivanpah in the Mojave Desert. (BrightSource Energy, 2014)

2.5.4. Khi Solar One, 2016 (Upington, Northern Cape, South Africa)

Khi Solar One, which generates 50 MW_e of power, is the first commercially operated solar thermal power plant with a tower in South Africa (see Figure 10). The plant consists of 4,120 heliostats, each with a reflecting area of 140 m². These heliostats reflect the incoming rays of the sun to three cavity receivers that are located on a 200 m high tower. The superheated steam at 530 °C is generated in the receiver for the Rankine cycle operating at 130 bar pressure. In the tower, a natural draft is induced over the fin blades of the air-cooled condenser. A cooling effect is thus achieved as a result of heat dissipation from the condenser.



Figure 10: Cavity receivers (left) (JG Afrika, 2017). Aerial view (right) (CMI, 2017)

2.6. Control System Development and Lessons Learned

The following sections highlight the main developments and operational experiences of the control system and operating philosophy of Solar One and Solar Two. As Solar One and Solar Two were pilot or demonstration plants, extensive data is available on them. However, very limited literature is available on the commercially operated plants. Any information published on these plants could be beneficial to the industry. This information could be on those projects that failed or the ones that were successful and met the desired outcomes. However, disclosure of such information to the public and the developers of solar energy power plants may lead to loss of competitive advantage of their developers over the other developers in the industry.

2.6.1. Solar One

Various independent controllers within the heliostat field, the receiver, the thermal storage, the power block and the balance of the plant, were integrated in the Solar One power plant. The control was either achieved manually from the plant operators or autonomously from the plant operating software. The plant used a data acquisition system which recorded the control and monitored the data. It was also used in the validation process of the SOLERGY computer code. The plant was designed to operate in eight steady-state modes. These operating modes varied in the process flow regimes between the heliostat field, receiver, thermal storage and power generation subsystems. A brief description of the various modes is discussed in Table 1 and is schematically illustrated in Figure 11.

Table 1: Steady state operation modes for Solar One (Alpert and Kolb, 1988)

<p><u>Mode 1: Turbine Direct</u></p> <p>Steam from receiver directed at turbine-generator only, thermal storage system is bypassed.</p>	<p><u>Mode 5: Storage Charging</u></p> <p>Steam from receiver charges thermal storage system. Turbine-generator is inactive</p>
<p><u>Mode 2: Turbine Direct and Charging</u></p> <p>Steam from receiver directed to turbine-generator and thermal storage system.</p>	<p><u>Mode 6: Storage Discharging</u></p> <p>Thermal storage system generates steam for turbine-generator. Receiver and heliostat field is inactive.</p>
<p><u>Mode 3: Storage Boosted</u></p> <p>Steam generated from thermal storage system is used to supplement steam generated in the receiver.</p>	<p><u>Mode 7: Dual Flow</u></p> <p>Steam from receiver directed to turbine-generator and thermal storage system. Thermal storage system generates steam for turbine-generator.</p>
<p><u>Mode 4: In-Line Flow</u></p> <p>Steam from receiver charges thermal storage system. Thermal storage system generates steam for turbine-generator.</p>	<p><u>Mode 8: Inactive</u></p> <p>Heliostat field, receiver, thermal storage and turbine-generator are inactive. Supporting systems are only active.</p>

The Solar One's operating philosophy was as follows. The plant operates in Mode 1 on days with clear sky. The thermal storage is not required on such days. Mode 2 is adopted when the receiver's thermal power exceeds the maximum capability of the turbine. This typically happens mid-day time with clear sky. In the mornings and evenings when the insolation is lower, the plant operates in Mode 3. In this mode, the thermal storage supplements the steam from the receiver. The operating philosophy made provision for cloud transients by reducing its effect on the turbine by operating in Mode 4. However, the plant efficiency in Mode 4 is lower than in Mode 1 as the maximum power output reduces. This is due to the temperature limitations on the heat transfer oil and temperature differences across the heat exchangers. In Mode 5, the thermal energy of the receiver is stored when power generation is not required. On overcast days or during the night, the plant operates in Mode 6. In Mode 7, the turbine-generator operates by receiving steam

from both the receiver and thermal storage system. This operating condition dampens the effect of cloud transients. When the operation of all major plant systems, heliostat field, receiver, thermal storage system and turbine-generator is not required, the plant is operated in Mode 8. In this mode the balance of plant systems remains active. (Alpert and Kolb, 1988)

Lessons learned from Solar One are as follows: From the eight modes of operation, only three modes were routinely used, namely Modes 1, 5 and 8. The heliostat field could not supply the required thermal energy to the receiver to operate in Mode 2. This indicates that the Solar Multiple (SM) was not greater than one. This assumption was confirmed by the fact that the size of the solar field was reduced before construction in order to reduce the costs. Due to some control related difficulties, other modes of operation were not favoured. However, Mode 1 was the most efficient operating mode. The thermal energy storage system was charged every ten days to provide auxiliary steam during start-ups. This approach was used due to the fact that the service steam was not provided by an electric boiler. (Alpert and Kolb, 1988)

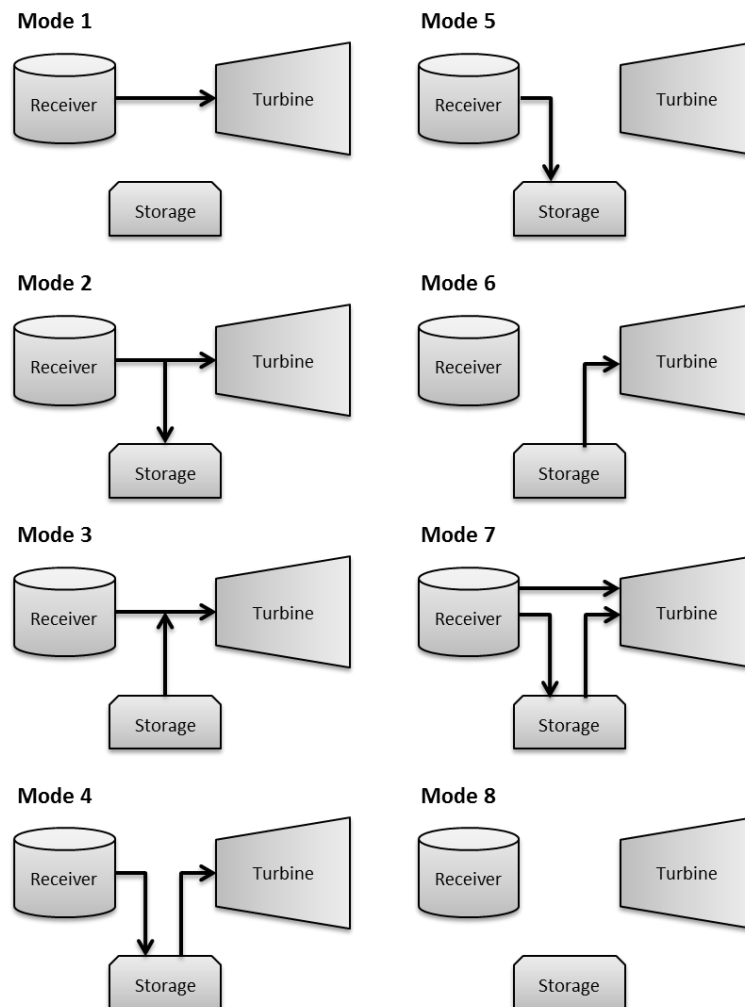


Figure 11: Visual representation of operating modes of Solar One, Table 1

2.6.2. Solar Two

In 2002, Litwin published a report on the lessons learned from Solar Two, reviewing the most significant components such as the mechanical design, control and instrumentation, panel fabrication, site construction and receiver system operation. In this section, various aspects on control system, and control and instrumentation are elaborated. In 2002, Pacheco also published a comprehensive report on Solar Two, 'Final Test and Evaluation Results of the Solar Two Project'.

The operating principals of a molten salt two-tank central receiver plant are discussed in this section. In this plant, the molten salt is pumped from the cold storage tank which is maintained at the temperature of 288 °C, through the receiver. The solar radiation reflected from the heliostat field is directed towards the tank, where the salt is heated up to the desired temperature of 565 °C. When power generation is required, the molten salt from the hot storage tank, maintained at 565 °C, is pumped through a steam generator to produce a high-pressure superheated steam for powering a conventional Rankine turbine-generator. The molten salt is thereafter pumped back to the cold storage tank, so that it could be reused later for retrieving thermal energy from the receiver. The steam generation system, decoupled from the energy collection system (see Figure 12), operates independently during the day time, night time and in overcast weather conditions. (Pacheco, 2002)

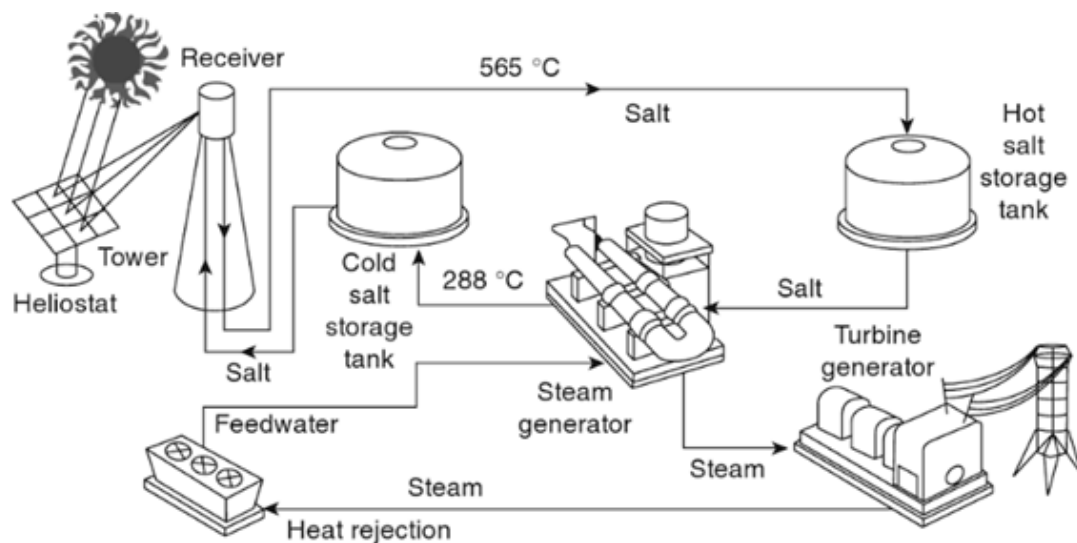


Figure 12: Receiver and power block decoupled (Lovegrove and Stein, 2012)

The implemented heliostat field control system accounts for any errors and misalignment in its aiming strategy in order to direct and reflect the incoming solar radiation with minimal losses onto the central receiver. The accuracy of the heliostat tracking is measured with the Beam Characterisation System (BCS), which assesses the reflected beam quality in terms of a flux map. In Solar Two, the recorded heliostat tracking errors

were more than that in Solar One. This is because the sun position algorithm was incorrectly converted from the FORTRAN to the C programming language. There were problems in coordinate conversation made by the BCS software algorithm. The improper operating procedures and degrading heliostat controller hardware were also the reason for this. These identified problem areas were addressed and compared to Solar One's 1.5 mrad accuracy requirement. Solar Two resulted in a 4.14 mrad value. The higher tracking errors and lower beam quality resulted in a lower heliostat field efficiency, which ultimately affected the overall performance of the plant. The lessons learned from Solar Two indicated that a control system capable of correcting many heliostat tracking errors are required utilising numerous BCS measurements. A highly automated BCS system would assist in resolving error sources. (Pacheco, 2002)

The control and operating modifications made in the heliostat field included three software-based systems for managing the flux distribution incident on the receiver. The Static Aim Processing System (SAPS) adjusts the heliostat by aiming points at the intervals of ± 10 minutes to minimise the spillage. The heliostat's image changes the size and shape with respect to the sun's position. The Dynamic Aim Processing System (DAPS) is a receiver protection system which ensures that the allowable receiver design flux limit of 850 kW/m^2 is not exceeded. This is achieved by checking the predicted flux patterns every few seconds and re-adjusting the heliostat's aiming points. The software-based system called the 'Preheat Processor' preheats during start-up of the empty receiver by distributing the flux over the entire receiver area. (Pacheco, 2002)

The receiver control algorithm allowed for automatic operation and is capable of re-adjusting the incident flux on the receiver. The main purpose of the algorithm is to ensure that the molten salt set point temperature of $565 \text{ }^\circ\text{C}$ is maintained and to limit the thermal fatigue of the receiver tubes. This was achieved initially by using three independent control signals. The design team, however, simplified the control algorithm by introducing a 'Cloud Standby' operating setting. The final receiver control algorithm successfully controlled the outlet temperature of the molten salt throughout the plant operational life, even during the cloud transients. This final receiver control algorithm consisted of a feed-forward signal from eight photometers, measuring incident power on the receiver, four per flow regime, and the outlet temperature feedback signal of the molten salt. (Pacheco, 2002)

As is the case for any other power station, it is a common practice to use various control systems for different power plant systems. In Solar Two, each system namely, turbine generator, heat tracer, heliostat control, molten salt system and steam system had its own independent control system. To operate the plant, signals are exchanged between these systems. However, in Solar Two the information exchange was not reliable, and operator intervention was required. Therefore, use of a fully integrated control system for the entire plant was proposed. (Litwin, 2002)

Litwin and Pacheco documented several shortcomings learned in their reports. It is advised to review those reports for additional information that is not captured in this section. This section highlighted the main aspects with regards to the control systems and operational experience which will be the focus area of this research project.

2.6.3. Gemasolar

Gemasolar incorporated innovative ideas within the heliostat field aiming strategy and control systems. An important parameter incorporated was the estimation of Direct Normal Irradiation (DNI). The DNI is required for forecasting the plant performance based on its current status. The estimation of DNI forecast was done between 24 to 48 hours. It assisted the operator in plant optimisation. It prevents the plant from reaching its thermal storage capacity during operation. It benefits the plant from colder ambient conditions by generating power and it reduces the number of times the turbine starts and stops. The satellite images and a hemispheric camera are used for cloud predictions. They assist the operator during plant operation, in preventing the solidification of molten salts in the receiver due to insufficient solar flux reflected onto the receiver. A highly advanced control system with thermography cameras assisted in the heliostat aiming strategy. It ensured that a desired thermal flow and temperature is achieved for the receiver. The thermography cameras also assisted in daily receiver start-ups and shutdowns. (Burgaleta *et al.*, 2012)

2.7. Plant Operations

This section is dedicated to commercial plants introduced after Solar Two. In this section the strengths and shortcomings of the earlier developed plants, such as Solar One and Solar Two, are used for the development of new commercial plants. This section assumes that plants such as PS10, PS20, Gemasolar, Ivanpah, Crescent Dunes and Khi would have considered these developments. However, Ivanpah, Crescent Dunes and Khi are more technological advanced than PS10, PS20 and Gemasolar.

The industrialists prefer to invest in tested and proven technologies. Although, while designing the commercial power plants the engineering design team considers the research carried out by the academicians. This research project focus on the two-tank molten salt central receiver technology, thus the following sections will only elaborate on the control systems, operating philosophy and operating strategies envisioned for these plants. The two-tank molten salt central receiver power plant can be divided into three main systems: the collector field, the molten salt system and the power block. The receiver acts as a coupling component between the heliostat field and the molten salt system, whereas the steam generator links the molten salt system with the power block. These three main systems and common components are represented in Figure 4.

The Distributed Control System (DCS) or Master Control System is responsible for integrated control and monitoring of all the systems. A control system hierarchy coordinates the information transfer between various systems and sub-systems. The plant has an automated control system. However, operators can intervene and issue commands to any system or subsystem in the control room through the operating desk's Human Machine Interface.

2.7.1. Plant Operating Philosophy

A decoupling system, which is present between the energy collection system and the power generation system, gives the two-tank molten salt central receiver plant edge over others. These two systems can operate independently from one another. However, the degree of freedom is limited by the thermal energy storage tank level. The energy collection system consists of the collector field system, receiver system, heat tracing system and thermal energy storage system. The power generation system consists of the thermal energy storage system, steam generator system and turbine-generator system. The steady-state operations of these two systems are represented in Figure 13 and Figure 14.

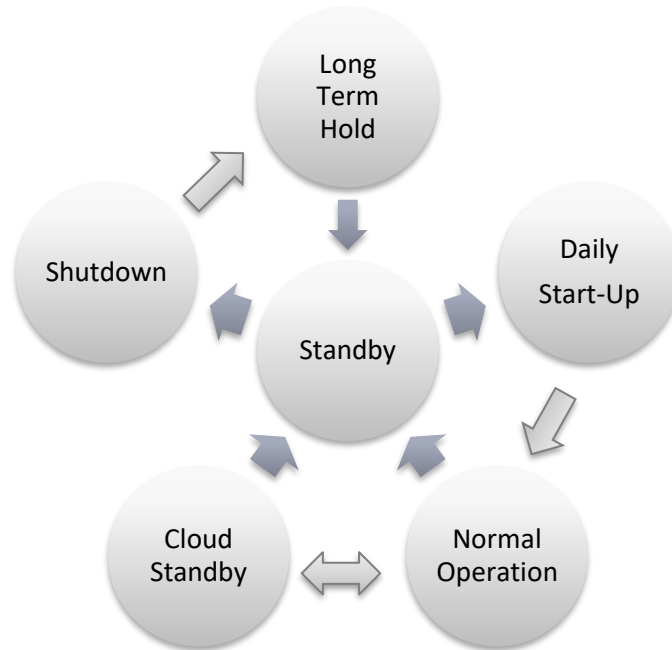


Figure 13: Energy collection system steady-state operation (Zavoico, 2001)

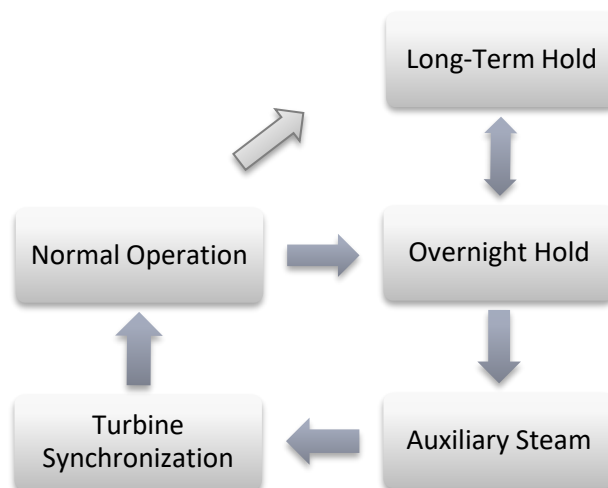


Figure 14: Power generation system steady-state operation (Zavoico, 2001)

The six steady-state operational modes for the energy collection system and the corresponding transients are presented in Table 2 and Table 3, respectively.

Table 2: Energy collection system steady-state operation modes (Zavoico, 2001)

<p>1) <u>Long-Term Hold</u></p> <ul style="list-style-type: none"> - Heliostats in stow position - Receiver Drained - Electric heat tracing system inactive 	<p>4) <u>Normal Operation</u></p> <ul style="list-style-type: none"> - Electric heat tracing circuits are deactivated - Heliostat follow aiming strategy - Receiver flow rate controlled to maintain desired outlet temperature
<p>2) <u>Standby</u></p> <ul style="list-style-type: none"> - Heliostats focused at standby aiming points - Receiver pump in operation - Molten salt flowing in riser, receiver bypass line and down comer - Electric heat tracing circuits active for preheat of molten salt flow path 	<p>5) <u>Cloud Standby</u></p> <ul style="list-style-type: none"> - All heliostats are focused on receiver - Receiver flow rate controlled to achieve outlet temperature of 510 °C - Molten salt recirculated to cold storage tank until cloud dissipates
<p>3) <u>Daily Start-Up</u></p> <ul style="list-style-type: none"> - Electric heat tracing circuits are active - Heliostats selected by DAPS focused on receiver at selected aiming points - Receiver pump in operation - Reaching the desired inlet level of receiver, the pump is switched to pressure control to maintain a minimum flow to the receiver - Salt is circulated to cold storage tank until desired outlet temperature is reached for hot storage tank 	<p>6) <u>Daily Shutdown</u></p> <ul style="list-style-type: none"> - Operation mode is changed to Standby mode - Heliostat normal aiming points moved to standby aiming points - Inlet vessel vented to atmosphere - Receiver drained by gravity

Table 3: Energy collection system transients (Zavoico, 2001)

<p><u>Long-Term Hold to Standby</u></p> <ul style="list-style-type: none"> - Heliostats moved from stow position to standby aiming points - Heat tracing circuits heat riser, receiver bypass line and down comer to 260 °C - Receiver pump started - Flow initiated from cold storage 	<p><u>Daily Start-Up to Normal</u></p> <ul style="list-style-type: none"> - Receiver filled by flooding - Establish serpentine flow - Flow rate corresponding to clear sky conditions - Heliostat aiming strategy to normal operation initiated - Flow rate controlled to achieve 565 °C outlet temperature 	<p><u>Standby to Long-Term Hold</u></p> <ul style="list-style-type: none"> - Heliostats standby aiming points deactivated - Heliostat stow position - Receiver pump stopped - Electric heat trace circuits deactivated
<p><u>Standby to Daily Start-Up</u></p> <ul style="list-style-type: none"> - Receiver inter-panel piping temperature raised, 315 °C - Heliostats selected for preheating by DAPS moved to preheat aiming points 	<p><u>Normal to Standby</u></p> <ul style="list-style-type: none"> - Heliostats aiming strategy to standby aiming points - Inlet vessel vented to atmosphere - Receiver drained 	<p><u>Cloud Standby to Standby</u></p> <ul style="list-style-type: none"> - Heliostats aiming strategy to standby aiming points - Inlet vessel vented to atmosphere - Receiver drained
<p><u>Daily Start-Up to Standby</u></p> <ul style="list-style-type: none"> - Heliostats selected for preheating by DAPS moved from preheat aiming points to standby aiming points 	<p><u>Normal to Cloud Standby</u></p> <ul style="list-style-type: none"> - Flow rate controlled to achieve 510 °C outlet temperature 	<p><u>Cloud Standby to Normal</u></p> <ul style="list-style-type: none"> - Flow rate controlled to achieve 565 °C outlet temperature

The five steady-state operational modes for the power generation system and the corresponding transients are presented in Table 4 and Table 5, respectively.

Table 4: Energy collection system steady-state operation modes (Zavoico, 2001)

<p>1) <u>Long-Term Hold</u></p> <ul style="list-style-type: none"> - Steam generator is drained - Electric heat trace circuits inactivated - Steam drum immersion heater inactivated 	<p>3) <u>Auxiliary Steam</u></p> <ul style="list-style-type: none"> - Nominal saturated steam flow rate established by auxiliary steam generator - Sealing steam delivered to shaft seals - Vacuum established in condenser - Preheat piping system and other equipment achieved from auxiliary steam
<p>2) <u>Overnight Hold</u></p> <ul style="list-style-type: none"> - Regulating pump cold salt to steam generator to keep steam drum hot - Steam production rate at 0 kg/s - Steam turbine rotated by turning gear - Steam drum immersion heaters de-energized at overnight hold temperature set points 	<p>4) <u>Turbine Synchronization</u></p> <ul style="list-style-type: none"> - Live steam flow (400 °C, 80 bar) established - Turbine-generator synchronized with grid - Minimum turbine-generator output (MW_e) is established - Steam drum immersion heaters de-energized at normal operating temperature set points
<p>5) <u>Normal Operation</u></p> <ul style="list-style-type: none"> - Extraction feedwater heaters active - Live steam flow (550 °C, 125 bar) established - Turbine-generator at full load established - Steam drum immersion heaters de-energized at normal operating temperature set points 	

Table 5: Power Generation system transients (Zavoico, 2001)

<p><u>Long-Term Hold to Overnight Hold</u></p> <ul style="list-style-type: none"> - Electric heat trace system heat steam generator heat exchangers and inter-vessel piping to 260 °C - Steam generator regulating pump started 	<p><u>Overnight Hold to Long-Term Hold</u></p> <ul style="list-style-type: none"> - Regulating pump stopped - Electric heat trace system turned off
<p><u>Overnight Hold to Auxiliary Steam</u></p> <ul style="list-style-type: none"> - Auxiliary steam generator started - Saturated steam flow established, shaft seals - Vacuum is drawn in condenser - Makeup water for auxiliary steam generator provided by variable speed, positive displacement auxiliary feedwater pump 	<p><u>Normal Operation to Overnight Hold</u></p> <ul style="list-style-type: none"> - Regulating cold salt started - Mixed salt at inlet of superheater reduced relating to allowable rate of temperature change of 500 °C/h - Output of turbine reduced - Live steam throttle valve to condenser open - Heat exchanger temperatures reduced 285 °C - Auxiliary steam for turbine shaft seals
<p><u>Auxiliary Steam to Turbine Synchronization</u></p> <ul style="list-style-type: none"> - Steam generator system circulation pump started with speed increased to achieve a 500 °C/h increase rate at inlet of superheater - When live steam achieves superheated conditions of 60 °C, turbine is accelerated to synchronize with the grid - Live steam throttle valve to condenser, closed - Minimum turbine output (MW_e) established 	<p><u>Turbine Synchronization to Normal Operation</u></p> <ul style="list-style-type: none"> - Turbine control transferred from evaporator pressure control to speed control - Extraction feedwater heaters activated - Reheater activated - Regulating flow of cold salt reduced relating to allowable rate of temperature change in heat exchangers of 500 °C/h - Hot salt flow rate increased to design value

Table 5 (Continued): Power Generation system transients (Zavoico, 2001)

<u>Turbine Synchronization to Overnight Hold</u>	
-	Turbine output reduced
-	Live steam throttle valve to condenser, activated
-	Turbine tripped, live steam throttled to condenser
-	Heat exchanger temperatures reduced to 285 °C
-	Auxiliary steam for turbine shaft seals activated

2.7.2. Collector Field Aiming Strategy and Control Systems

The heliostat field is responsible for tracking the sun and reflecting the direct solar radiation onto the receiver. The implemented aiming strategy determines the aiming point for each heliostat. The aiming strategy plays a vital role in the heat transfer from the receiver to the molten salt, receiver's protection, receiver material thermal fatigue, and daily start-up and shut-down operations. The aiming strategies presented in Table 6, are used at commercial power plants or experimental facilities. These are identified in the literature review by Grobler and Gauche (2014).

Table 6: Aiming strategies and their functions (Grobler and Gauche, 2014)

Aiming Strategy	Function
Abengoa Solar	Distribute flux evenly over centre (75 %) of plate
Gemasolar	Lower peak flux and temperature gradients
Solar Two	Remove heliostats causing flux density to surpass limit
Plataforma Solar de Almería	Keep temperature between the allowable limits
THEMIS	Real-time flux distribution optimisation through flux estimation and TABU meta-heuristic algorithm
Jülich	Real-time flux distribution through ray tracing and ant colony optimisation
Combined strategy	Flux distribution and mass flow rate optimisation
Ivanpah	Flux and temperature optimisation through weather measurements and visual and infra-red photography

There are three levels of control within the collector field system: the DCS, the Heliostat Array Controller (HAC) and the Heliostat Controller (HC). The DCS is responsible for controlling, monitoring and supervising the running of steady-state operation mode. The instructions obtained from the DCS are sent to the HAC depending on the operating mode to control the heliostat field accordingly. The field status and alarms are reported back to the DCS by HAC. Each HAC consists out a BCS, SAPS and DAPS. It provides with the command instructions and time from the master clock station to the HC of each heliostat under its control. (Zavoico, 2001)

The BCS is an automated system which calibrates each heliostat individually by setting an aiming point on the BCS target. The heliostat reflected images are shifted up or down

from the centre of the receiver, using SAPS, to achieve an evenly distributed flux over the receiver area. Depending on the implemented heliostat aiming strategy, the SAPS can be replaced with an equivalent functional system, as presented by Grobler and Gauche (2014). The DAPS is used for daily pre- and post-heat of the receiver. (Zavoico, 2001)

The HC solar tracking mechanism can operate either on an open-loop or closed-loop system. In a closed-loop system, the solar position is determined by using sensors to track the trajectory of the sun's position. This system is more accurate, even though the cloud transients negatively affect its ability to track the sun. In an open-loop system, the solar position is calculated by an astronomical formula that relates the sun's position to the system geometry. During the cloud transients, open-loop systems are recommended for larger solar fields due to their lower cost and higher reliability. (Behar *et al.*, 2013)

2.8. Operating Strategies

The terms 'Operating Strategy' and 'Operating Philosophy' are often used interchangeably to describe the manner in which a plant is operated in order to achieve the set-out plant performance indicators. The Operating Strategy refers to the specific design and operating nature of the plant, i.e. to adhere to the PPA. Whereas the control of the process plant is achieved through the Operating Philosophy. Thus, the plant's operating philosophy strives to satisfy the plant operating strategy. In the case of CSP plants, the thermal energy storage plays a vital role in the operating philosophy and the operating strategy. The renewable energy technologies such as wind turbines and PV installations are considered as non-dispatchable systems due to their type of operation. Investment decisions for these types of plants rely primarily on scale, energy yield and total capacity. The type of operation for these plants is straightforward. As the plant generates power, it delivers the electric energy to the grid. CSP plants with storage on the other hand have other factors that require consideration. The operating strategy chosen for the plant directly influences the interdependencies between the turbine capacity, solar field size and thermal energy storage. (Kost *et al.*, 2013)

As the ultimate goal of the plant operations is to satisfy the operating strategy, each strategy influences the plant's design. The plant design also has a LCOE associated to it. Thus, the operating strategy indirectly influences the LCOE. If more than one operating strategy is envisioned for the plant, the plant requires more flexibility to adhere to the different operating regimes. The aim of the Eskom's Solar-1 project is to acquire full understanding of the technical, financial and operational aspects that are associated with the concentrating solar central receiver technology. As this is a demonstration plant, the plant designed has to be flexible enough to 'demonstrate' various operating strategies. The four main operating strategies identified by Garcia Casals *et al.* (2012) for the Eskom Solar-1 project are to Maximise Power Generation, Maximise Plant Revenue, Minimise Energy Dumping and Optimise Electric Grid Operation. (Garcia-Casals *et al.*, 2012)

These operating strategies are typically followed by the industry or IPPs and they form a part of the system operator's tools to meet the energy demand of the country. Although, these operating strategies do not benefit the interests of an IPP, in certain cases the plant

forms part of the utility’s fleet of power generation capabilities. This relationship is commonly referred to as a vertically integrated model within the power sector, where the utility, e.g. Eskom, owns the supply chain of electricity. This includes generation, transmission, distribution and management of the electric grid.

By investigating the various operating strategies, it can be concluded that the operating strategy greatly influences the design and operation of these plants (Garcia-Casals *et al.*, 2012, Kost *et al.*, 2013 and Guedez *et al.*, 2013). The model used by Kost *et al.* (2013) investigated an optimal layout decision for the operation of CSP plants within Spain’s electric grid. This model optimised the size of the solar field and the thermal storage in relation to a fixed turbine size of 100 MW_e for a parabolic trough plant. Although the study is applied to a parabolic trough plant, the same principles still apply. This is illustrated in Figure 15. An optimal operating strategy for the proposed plant was obtained from this model. This model also yields the insight for plant investors, grid operators and regulators.

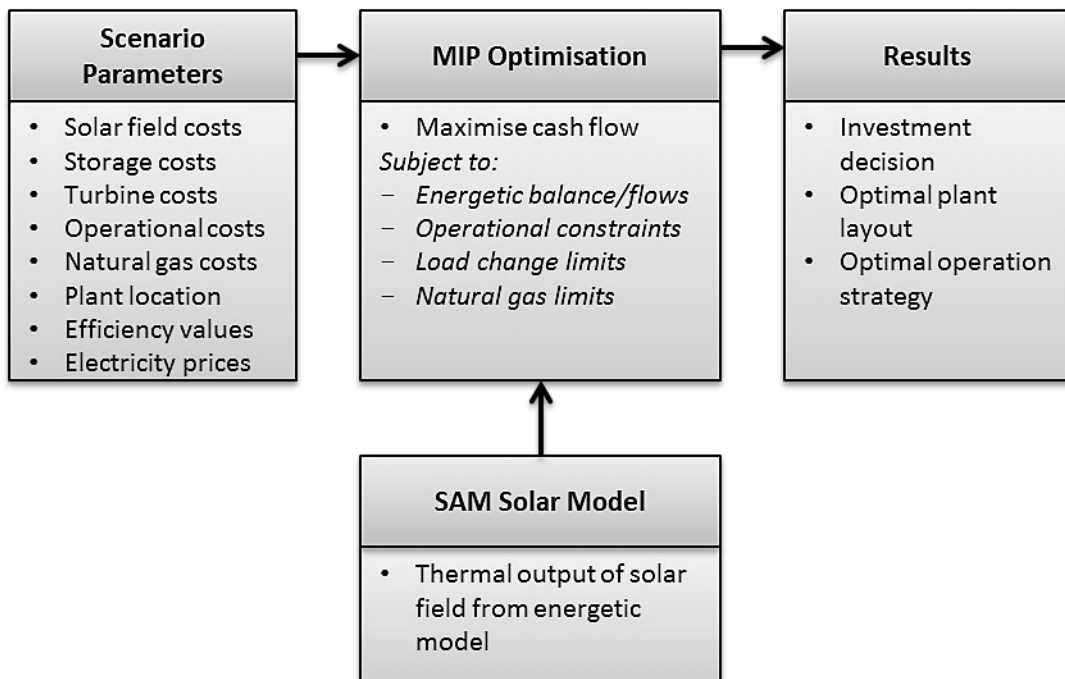


Figure 15: MIP plant valuation framework, adapted (Kost *et al.*, 2013)

Guedez *et al.* (2013) in their study investigated the optimum configuration required for a plant for a specific site location by considering various price-based grid integration strategies. The study was carried out on on-site locations within Spain, and it was concluded that the plant operating strategy relates to an optimum solar field size and storage size. A quasi-steady state model of the entire system, assisted by KTH Royal Institute of Technology’s in-house tool DYESOFT, was used for the thermodynamic design of the plant, illustrated in Figure 16. The main function of this model was to derive an economically viable power plant for each operating strategy, measured in terms of LCOE and Internal Rate of Return (IRR). It was indicated from the results of this study

that despite the operating strategy adopted, a large plant configuration would yield minimum electricity costs and maximum IRR. However, for smaller plant designs a peak operating strategy is more beneficial.

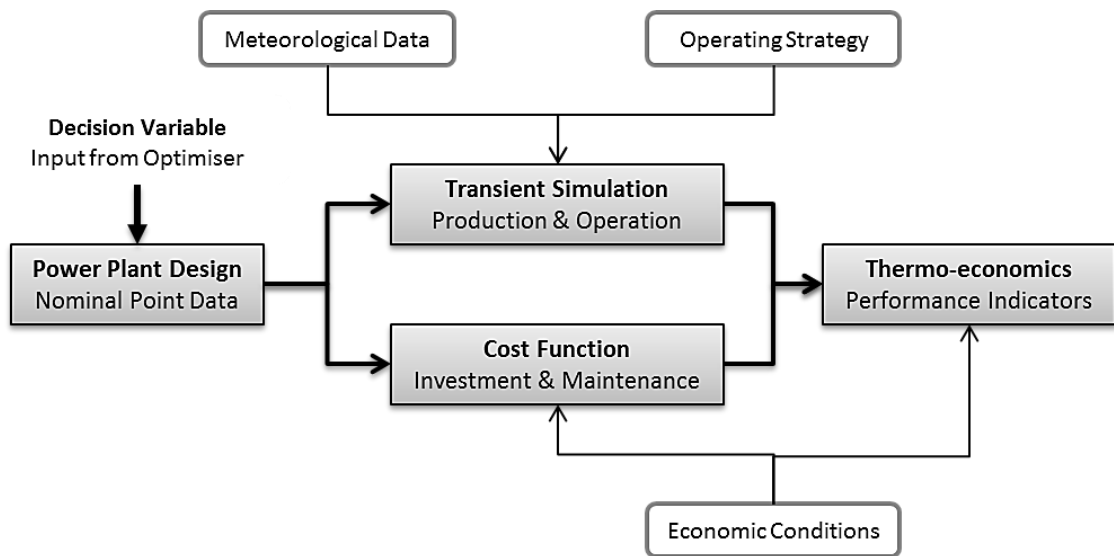


Figure 16: DYESOPT modelling approach used, adapted (Guedez et al., 2013)

The study conducted by Guedez in 2016, analysed the effect of market conditions on the profitability of a South Africa based CSP plant (Guédez *et al.*, 2016). The results of this modelling illustrated the trade-offs between minimising investment and maximising profits under three scenarios. These scenarios were based on the incentive programs and wholesale electricity prices. The optimal plant configuration for each scenario highlighted the profitability that the storage offered under the time-of-day tariff structure. An economic evaluation of the plant configurations resulted in the LCOE being used as the performance indicator. Thus, the study performed by Guedez focused on the ‘Maximising Revenue’ operating strategy when a time-of-day tariff structure is considered. Also, an optimal plant configuration is associated with LCOE. This research approach is typically applicable when the plant operator is an IPP with a PPA in place.

As highlighted in the objectives and motivation of this research project, this research focuses on an array of operating strategies imposed on the plant. The maximising plant revenue is one of the many aspects that are considered in this project. The value of a CSP storage in this research is not related to the financial value, but rather on the benefits and capabilities that CSP offers to the electric grid, and not the plant operator. To further assist the discussion, operating strategies applicable to this research project, identified by Garcia-Casals during the design phase of Solar-1, are as summarised below.

2.8.1. Maximise Power Generation

The ‘Maximise Power Generation’ operating strategy is the most commonly used operational strategy in nearly all renewable energy generating technologies. This operating strategy is followed by the IPPs from Bid Window 1 to Bid Window 3 of the

REIPPPP. The PPA in these Bid Windows awarded a fixed price for all generations where conditions such as, contribution to the regulation and ancillary services are not required. Accordingly, no system boundaries are imposed on the plant. The ‘Maximise Power Generation’ and ‘Maximise Plant Revenue’ operating strategies coincide when a flat rate tariff structure is considered. The objectives of these strategies include maximising the electric generation that will result in a lower LCOE and higher capacity factor.

This operation strategy is closely linked to the first commercial development phase from all renewable energy technologies. This is clearly evident in the first three Bid Windows of the REIPPPP as South Africa entered the renewable energy market at this time. In efforts to reduce the technology generation costs and to establish a commercial market, this operating strategy is ideal for emerging markets, offering lower LCOE values. However, the plants operating under the ‘Maximise Power Generation’ strategy may become a burden for the electric grid once renewable contributions grow to a certain amount. In such cases, the generating technologies providing flexibility to the electrical grid can provide assistance by integrating with the ‘Maximise Power Generation’ operating strategies. Furthermore, by fixating on the ‘Maximise Power Generation’ operating strategy, the generating technologies offering other operational capabilities may elude the system operator or stakeholders of the electric grid.

Since, in this operating strategy the boundaries of the system analysis are set at the plant boundaries, a lower LCOE and higher capacity factor are achievable. Beyond these boundary conditions, the broader implications of the entire electric grid are not considered. Therefore, the plant operator is able to optimise the plant operations in order to maximise the electricity generation while minimising the operational costs. The following plant operations are considered for the optimisation. Maximising the retrieval of energy from the solar collection system, minimising energy dumping associated with a full state of charge in the hot thermal storage tank, minimising the impact of the plant start-ups and shut-downs; and power block efficiency associated with part load.

2.8.2. Maximise Plant Revenue under various Boundary Conditions

The primary objective of any plant operator or IPP is to operate under the ‘Maximise Plant Revenue’ operating strategy. In this operating strategy, the key factors are the techno-economic and regulatory conditions that are imposed upon the plant operations. These conditions are observed in REIPPPP’s Bid Window 3 and Bid Window 3.5 for CSP where a base tariff and a peaking factor component are awarded in the PPA. This is commonly known as two-tier tariff structure or time-of-day tariff structure. As the plant design is determined by the implemented operating strategy, the plants operating under Bid Window 3.5 would be designed differently from the plants from Bid Window 1 and Bid Window 2, where a flat rate tariff structure is in place. This constraint was confirmed by the study undertaken by Guedez *et al.* (2016). The plants from Bid Windows with the peaking factor component prioritise generation during this period. Thus, these plants would be operated in a different manner. When the operations are not optimal, the plant may sacrifice its operating efficiency, but more revenue is recovered from the peaking factor time period.

As in the case for IPPs participating in the electricity market operating under this operating strategy, system boundaries imposed on the plant are set out in the PPA. For Bid Window 3.5, the ideal operating times for the plant are determined from the peaking factor tariff, base tariff and no payment time periods. Thus, the plant operator optimises the plant operations to generate electricity during these time periods to maximise the plant revenue. The factors that are considered in optimising the plant revenue are to lower operational costs and maximise electric generation, by prioritising generation in higher-paying periods.

The pricing of complementary, regulatory and ancillary services beyond electricity generation offers an additional source of income. Plants such as CSP with storage capabilities could benefit from these services with appropriate pricing structures in place. In South Africa, the PPA designates Eskom as the ‘buyer’ of electricity. With Eskom representing a vertically integrated model in the power sector, the PPA could be drawn up, in such a way that the pricing for complementary, regulatory and ancillary services are catered for, compensating the plant and benefitting the electric grid.

2.8.3. Minimise Energy Dumping

The ‘Minimise Energy Dumping’ operating strategy is considered within almost all of the operating strategies. Energy dumping refers to the act of defocusing the heliostats from the receiver’s ‘dumping’ potential energy. This act affects the plant efficiency. The two leading causes for energy dumping that are worth mentioning are discussed briefly. Firstly, the hot Thermal Energy Storage (TES) when fully charged causes the receiver to shut down or curtails its operation. Secondly, particular heliostats are defocused from the receiver in order to prevent the receiver material to exceed its maximum incident solar flux limit. The deflected solar energy should not be mistaken for spillage. The spillage is induced by the reflecting image induced by the heliostat. A distorted image due to canting or heliostat’s aiming errors increases the spillage on the receiver. The spillage is involuntary energy loss from the heliostat field where the energy reflected onto the receiver falls outside the receiver’s domain (Garcia, *et al.*, 2015). The deflected energy is intentionally deflected from the receiver by the heliostat field. The receiver control system, DAPS, implements this safety precaution through the heliostat field aiming strategy.

In order to prevent energy dumping, the plant optimises its hot TES dispatch. This is done to ensure that the TES does not reach its thermal capacity limit. Additionally, optimisation in the aiming strategy of the heliostat field can be done, so that the reflected sun rays stay within the flux limit of the receiver. In the ‘Minimise Energy Dumping’ operating strategy, all the plant operations are prioritised to ensure that no or minimal energy dumping occurs. The implementation of a weather predicting system can further enhance the optimisation capabilities of the plant regarding dispatch forecasting and peak flux limits on the receiver.

2.8.4. Optimise Electric Grid Operation

The ‘Optimise Electric Grid Operation’ operating strategy is subjectively biased to the system operator’s point of view. In this case, boundary conditions are imposed on the plant by the system operator. This results in the optimisation of plant operations by the plant operator. Although this operating strategy is predominantly applicable to generating plants within the vertically integrated model, plants participating in the electricity market could be subjected to this operating strategy through the PPA. The conditions in the PPA could include providing ancillary services to the electric grid, as per Eskom’s Ancillary Services Technical Requirements document (Eskom, 2013). The objectives of the operating strategy ‘Optimise Electric Grid Operation’ include factors such as regulatory requirements, complementary services, lower electricity system generation costs and the environmental impacts relating to the generation of electricity.

The electricity generating plants may become a burden on the electric grid, once the electric grid reaches its threshold number of plants operating under the ‘Maximise Power Generation’ operating strategy. For this reason, the capabilities of other generating technologies, such a CSP, are demonstrated for optimising the electric grid operations. Appropriate regulatory requirements that support the introduction of various technologies to the electric grid and achieving an ideal electric grid are currently not developed in the South African context. Subsequently, demonstrating various capabilities of the generating technology, the potential and value within the electric grid are unlocked. Each operating strategy present in the ‘Optimise Electric Grid Operation’ has a different objective.

South Africa is known for its system constraints with an increase in demand during morning and evening peak times. The ‘Covering Peak Periods’ operating strategy can be utilised during these peak periods. Due to CSP’s storage capabilities, the value of this operating strategy has been appreciated in the REIPPPP Bid Window 3 and Bid Window 3.5. The power generating from these plants during peak periods compensated 270 % of the base tariff. In this instance, both the generating plant and electric grid benefitted from the operating strategy implemented. Hence, the ‘Maximise Plant Revenue’ operating strategy is being applied along with the ‘Covering Peak Periods’.

One of the objectives of the system operator, especially in a vertically integrated model, is to minimise the electricity generation costs. The purchasing costs of electricity from the IPPs are determined in the PPA. The PPA for the current Bid Windows in the REIPPPP stipulates that Eskom is obligated to purchase the electricity from the IPP whenever the IPP is able to generate power for the electric grid. Thus, the cost parameter to optimise for the system is on the Eskom generating fleet, as all power generated from the IPPs are accounted for as per the PPA. The cost of generation from IPPs should not implicate the system operator objectives in the ‘Minimise Electricity Generation Costs’ operating strategy. The Electricity Regulations on New Generation Capacity, Section 10, stipulates “*the buyer is able to recover, the full amount of the costs incurred by the buyer for purchasing of the new generation capacity*” (DoE, 2011).

As Eskom’s fleet was designed to operate at full load, i.e. base load operations, additional technical challenges are induced when operating certain power plants under part load

conditions. A high penetration from variable renewable power generation on a constrained electric power system induces curtailment on the nonflexible fleet. This leads to higher cost. For the load shifting, thermal or electric storage is thus required to reduce the curtailment on the fleet (Denholm and Hand, 2011). The non-dispatchable renewables such as wind and PV can be integrated with the electric grid. This integration can be further accompanied by some complementary services which aim to provide flexibility to the grid by introducing dispatchability potential of CSP. The dispatchability potential of Andasol 3, a parabolic trough CSP plant with 7.5 hours of thermal storage, was published by Dinter and Gonzalez (2013). Therefore, the flexibility in the dispatch potential of a generating plant with storage, such as CSP, provides stability to the less dispatchable generating plants of other renewable energy technologies. In case, when cloud cover causes reduction in the output generation of a PV plant, the generation from the CSP storage supplements this offset. The Eskom's generation fleet was not intended to provide flexibility to the system. During times when the system is constraint, the aid of wind and PV generation is welcomed. However, during surplus capacity the Eskom fleet is curtailed to offtake the generation from these plants. Along with the low-quality coal used, the oil is required to stabilise the flames in the boiler.

The last operational strategy to consider is the impact associated with electricity generation on the environment. The Department of Environmental Affairs (DEA) published the National Climate Change Response Policy White Paper of 2011 shortly before the 17th session of the Conference of the Parties (COP17) to the United Nations Framework. The White Paper established the overarching policy framework for South Africa's climate change response. South Africa committed at COP17 to lower the country's carbon emissions. The carbon emissions trajectory is to peak in the period 2020 to 2025 with ranges specified at a lower limit of 398 Mt carbon dioxide (CO₂) per annum, and an upper limit of 583 and 614 MtCO₂ for 2020 and 2025 respectively. The emissions will plateau for up to 10 years following a decline in absolute terms where the lower limit of 212 MtCO₂ and upper limit of 428 MtCO₂ are envisioned by 2050. Considering this mentioned scenario, the objectives of the system operator are clearly defined. As the power sector in South Africa contributes up to 45.08 % of the National Green House Gas emissions, it is essential that the system operator optimises the electric generation from its generating energy mix. The IRP 2010-2030 policy document diversified the future energy mix of South Africa by implementing these conditions. (DEA, 2014)

This research project focuses on demonstrating the operating strategies of complimentary services to wind and/or PV generation, base load operations and peaking operations. These operating strategies are pertinent to the power generation plant, with boundary conditions imposed by the system operator. The operating strategies such as Minimise system electric generation cost and Environmental impact associated with electricity generation are applicable to the complete South African electric grid. Thus, model encompassing all generation within the electric grid is required at a system operator level.

2.9. Commercial Software and Tools

A physical model or complex system can be converted into a digital prototype by developing a simulation model of the system's underlying physics on a computer (Winsberg, 2002). Simulation models are predominantly developed for two reasons in the CSP industry. Firstly, in order to secure funding for the project, investors prefer to invest in a technology when the estimates and data provided are both realistic and indicate a reasonable rate of return on the investment (Alpert and Kolb, 1988). Therefore, simulation models are used to calculate the energy performance of the proposed plant. This is done to estimate the potential annual energy production by using a verified and bankable Typical Meteorological Year (TMY) data as an input. Secondly, the simulation models are used by the design engineers for optimisation and in feasibility studies to evaluate alternative designs. These models are also used in operating strategies to enhance the component or the system's performance. In addition, the simulation models assist plant or system operators to estimate and predict the plant performance for a given period under various boundary conditions. The literature review conducted investigates the various computer codes, simulation models, software and tools used in the industry, with the focus and relevance to the central receiver technology. The results are seen in Figure 17.

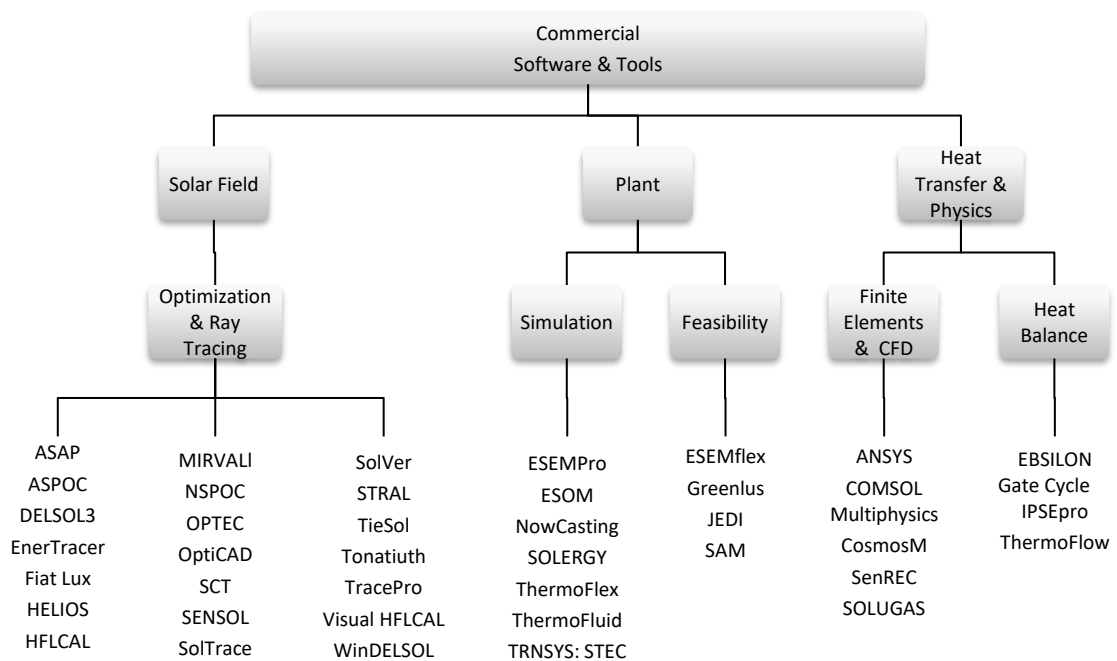


Figure 17: Review on commercial software and tools (De Meyer et al., 2014)

The review concluded that the development of ray tracing software and heliostat field optimisation tools are well developed for the central receiver CSP technology. In a review by Bode *et al.* (2012), the concluding remarks highlighted that the codes can be divided into two categories, detailed plant performance simulation and optimal field layout

design. Bode further highlighted that the codes present under these categories are very similar. In this current literature review, a similar conclusion was made. It was found that the ray tracing tools used Monte Carlo ray tracing techniques. These tools subsequently calculated the heliostat field performance. The capabilities of these software packages differed somewhat. However, where certain tools focused on the optical analysis of the heliostats, or to calculate heliostat field performances, other tools are able to perform receiver flux mapping and optimisation of the heliostat field layout.

In order to simulate the plant's performance, the heliostat field performance is required. Thus, software packages with the capability of simulating plant performances rely on other software packages, tools or modules. For example, the System Advisor Model (SAM) software package serves as an interface between the user and the other underlying tools. DELSOL3 or the PTGen code developed by Wagner (2008), interface with SAM for optimising the heliostat field layout and tower height, subsequently calculating the heliostat field performance required for the plant simulation by SAM. For the power block, TRNSYS is used to determine the power block performance based on input from SAM. Thus, the plant performance is achieved with three various sub-models. (De Meyer *et al.*, 2014)

Various literatures have elaborated in more detail about the simulation models and tools that are discussed above (Ho, 2008, Bode and Gauche, 2012 and Morin, 2010). A detailed report was given by De Meyer *et al.*, (2014) investigating various simulation models and tools, a summary is presented in Figure 18. (De Meyer *et al.*, 2014)

The objective of investigating the various simulation programmes that are publically available was to establish a baseline for this research. From this review, it is concluded that none of the models available fulfil the functional requirements set out in the research objectives. These objectives were to optimise the plant operations under the following boundary conditions, weather conditions, plant status and operating strategy implemented; and to deliver a plant generation forecast for a period of seven days. The software package SAM is able to simulate the plant performance under various conditions. SAM is widely accepted by the solar industry and consists of various models developed at the National Renewable Energy Laboratory (NREL), Sandia National Laboratories, the University of Wisconsin, and other organisations. However, limitations in the operational flexibility exist. SAM is not developed to optimise plant operations, but to produce an hourly output of a renewable energy system over a single year. Thus, SAM provides the performance predictions for a plant and estimates the cost of energy. Due to SAM's credibility, it will be used in the validation of the newly developed model in this research.

Software Platform	Purpose							Capabilities										Lisence			Source	References
	Computational Fluid Dynamics	Feasibility	Finite Elements	Heat Balance	Ray- Tracing	Simulation	HelioStat Field Optimisation	Feasibility Economic Impacts	Feasibility Technology	Finite Modelling Mechanical	Finite Modelling Thermal	Heat Transfer Fluid Analysis	HelioStat Field Design Optimisation	Optical Analysis Ray- Tracing	Power Block	System Plant Simulation Performance	Commercial Lisence	Free Lisence	Private Use			
ANSYS	X	X	X						X	X	X	X					X			ANSYS	ANSYS, 2014	
ASAP					X												-			Breault	Breault, 2014	
ASPOC		X			X		X					X	X				X			Nevada Software	ASPOC, 2014	
COMSOL Multiphysics	X	X	X						X	X	X						X			COMSOL	COMSOL, 2014	
DELSOL3		X					X		X			X				X	X			SANDIA	Kistler, 1986	
EnerTracer					X									X			-			CIEMAT PSA	Blanco et al., 2000	
EPSILON		X		X		X		X	X						X	X	X			STEAG, DLR	EPSILON, 2014	
ESEMflex		X						X	X			X							X	Sun to Market	Sun to Market, 2014	
ESEMpro						X						X		X	X	X			X	Sun to Market	Sun to Market, 2014	
ESOM						X		X				X		X	X	X			X	Sun to Market	Sun to Market, 2014	
Fiat Lux					X									X					X	CIEMAT PSA	Tellez, 2013	
GateCycle				X		X						X			X		X			GE	GateCycle, 2014	
Greenius		X				X		X	X							X	X			DLR	Buck, 2013	
Helios					X									X					X	SANDIA	Ho, 2008	
HFLCAL							X					X					X			DLR	Bode et al., 2012	
IPSEpro		X		X				X	X			X			X	X	X			SimTech	IPSEpro, 2014	
NowCasting						X		X								X	X			Sun to Market	Sun to Market, 2014	
NSPOC		X					X					X	X			X	X			Nevada Software	NSPOC, 2014	
OPTEC					X									X						-	Schoffel et al., 1991	
OptiCAD					X									X					X	OptiCAD	OptiCAD, 2014	
SAM		X				X	X	X	X			X				X			X	NREL	SAM, 2014	
SCT					X									X					X	CIEMAT PSA	Tellez, 2013	
SenRec	X	X	X						X	X	X	X							X	SENER	Martin, 2007	
SENSOL		X			X	X	X	X	X			X	X			X			X	SENER	Martin, 2007	
SOLERGY		X				X			X							X			X	SANDIA	Alpert et al., 1988	
SolTrace					X									X					X	NREL	SolTrace, 2014	
SOLUGAS	X	X	X						X	X	X	X							X	DLR	Buck, 2013	
SolVer		X			X	X		X	X			X	X			X			X	Solucar / Abengoa	Garcia, 2007	
ThermoFlow		X		X				X	X			X			X	X	X			ThermoFlow	ThermoFlow, 2014	
TieSol					X		X					X	X						X	Tietronix	Izygon et al., 2011	
Tonatiuh					X									X					X	Google-Code	Tonatiuh, 2014	
TracePro					X									X					X	Lambda	Lambda, 2014	
TRNSYS (STEC)		X		X		X			X						X	X	X		X	DLR	Schwarzbozl, 2006	
Visual HFLCAL					X		X					X	X						X	DLR	Schwarzbolz et al, 2009	
WINDELSOL					X		X					X	X						X	SANDIA	Tellez, 2013	

Figure 18: Review on commercial software and tools (De Meyer et al., 2014)

3. MODEL DEVELOPMENT

3.1. Introduction

This research project investigates the operational capabilities of the first Eskom owned CSP plant. It represents a generation plant within the vertically integrated model of the power sector. An array of operating strategies is envisioned to be implemented and demonstrated for this plant. The commercial models and tools that were publicly available did not offer the flexibility required in simulating the plant performance under various dynamic boundary conditions such as weather conditions, plant status and operating strategy.

A model was developed based on the plant basic design of the Solar-1 project, to analyse the plant performance under the above mentioned boundary conditions. This plant design is referred as the ‘case study plant’ in this study. The sub-system performance of the heliostat field, receiver and power block has been validated against similar models or tools that are commercially available. Focus on the research objectives was made while developing the model. Therefore, the simulation results should conclude these objectives. To consider the role of weather conditions and in order to optimize the plant operations, a weather prediction system was also introduced.

The Eskom 100 MWe CSP Project, Solar-1 or the Eskom Kiwano CSP plant, is the first CSP project within Eskom Holdings SOC. Eskom contracted the services of a consultant to act as Owner’s Engineer in the development, construction and commission of this demonstration plant in Upington, Northern Cape, South Africa. The Owner’s Engineer utilised Eskom’s User Requirements Specification and developed a Basic Engineering Design. This section elaborates on the main design parameters that were utilised in the development of the simulation model. It is important to note that all the optimisations in the design itself has been executed and reviewed by Eskom Engineering and the Owner’s Engineer. The aim of this research project is not to optimise any design of the plant, but to utilise the plant parameters as it is and develop a simulation model to represent the plant operations for optimisation. The following literature is recommended for optimisation in CSP plant design: Wagner (2008), Morin (2010) and Augsburger (2013). The following Owner’s Engineer design documents were considered as the basis for this simulation model. These are represented in Table 7. All the plant design parameters used in the model are presented in APPENDIX A: Solar-1 Design Parameters.

Table 7: Solar-1 Project Basic Design documentation (Eskom, 2012a)

DOCUMENT	DOC. NUMBER
General Documents	
Basic Design Report	S1GM000MEM0002
Site Location	S1GM000DRW0002
Site Meteorological Data	S1GM000MEM0008
Operation Strategies	S1GM000MEM0015

DOCUMENT	DOC. NUMBER
Mechanical	
Mechanical general design criteria	S1MC000SPC0001
Steam generator specification and data sheet	S1MC009SPC0001
Receiver Specification and data sheet	S1MC019SPC0001
TES Specification and data sheet	S1MC033SPC0003
Inlet and outlet vessels specification and data sheet	S1MC033SPC0004
Steam turbine and generator specification and data sheet	S1MC011SPC0001
Heliostats specification and data sheet	S1MC018SPC0001
Molten salts pumps specification and data sheet	S1MC033SPC0001
Molten salts specification and data sheet	S1MC033SPC0002
Process	
General Process Design Criteria	S1PR000SPC0001
Parametric analysis and plant performance	S1PR000MEM0001
ADD I - Parametric analysis and plant performance	S1PR000MEM0001
ADD II - Parametric analysis and plant performance	S1PR000MEM0001
ADD III - Parametric analysis and plant performance	S1PR000MEM0001
Solar modelling report	S1PR000MEM0002
Conventional modelling report and conventional heat balances	S1PR000MEM0003
Performance report ADD I - Performance report	S1PR000MEM0004
Molten salts description. Thermal properties and melting	S1PR033MEM0001
Molten Salts Heat and Mass Balance	S1PR000DRW0001
Process flow diagram	S1PR000DRW0002
Electrical	
Electrical general design criteria	S1EL000MEM0001
Key single line diagram	S1EL000DRW0002
Layout electrical equipment	S1EL000DRW0003
Load list	S1EL000LIS0001
Control and Instrumentation	
General I&C design criteria	S1CI000MEM0001
Plant control Philosophy	S1CI000MEM0002
Molten salt system control philosophy	S1CI033MEM0001
Steam system control philosophy	S1CI006MEM0001
Heliostats calibration and local control specification	S1CI018SPC0001
Control architecture	S1CI000DRW0002

3.2. Model Overview

After reviewing the available platforms for developing the model, Microsoft Excel software package has been selected due to its Macro functionality and Visual Basic interfacing. The entire model is built on the Microsoft Visual Basic for Application 7.0 platform. In order to achieve the overall functionality prescribed in the research objectives and various sub-components such as heliostat field, receiver, power block etc., have been developed and integrated in a holistic manner to represent the CSP plant. Various macros within the Microsoft Excel software were utilised to implement the overlaying control, i.e. operating philosophy and operating strategy. A basic user form serves as an interface between the model and the user to ease the simulation process. A complete ‘Step-by-Step’ guide has been supplemented in APPENDIX C. The user is urged to follow the guide in

order to extract the full benefit and flexibility offered by this model. A visual interpretation of the overall model developed is presented in Figure 19. The following sections elaborate on the development of each sub-system of the model.

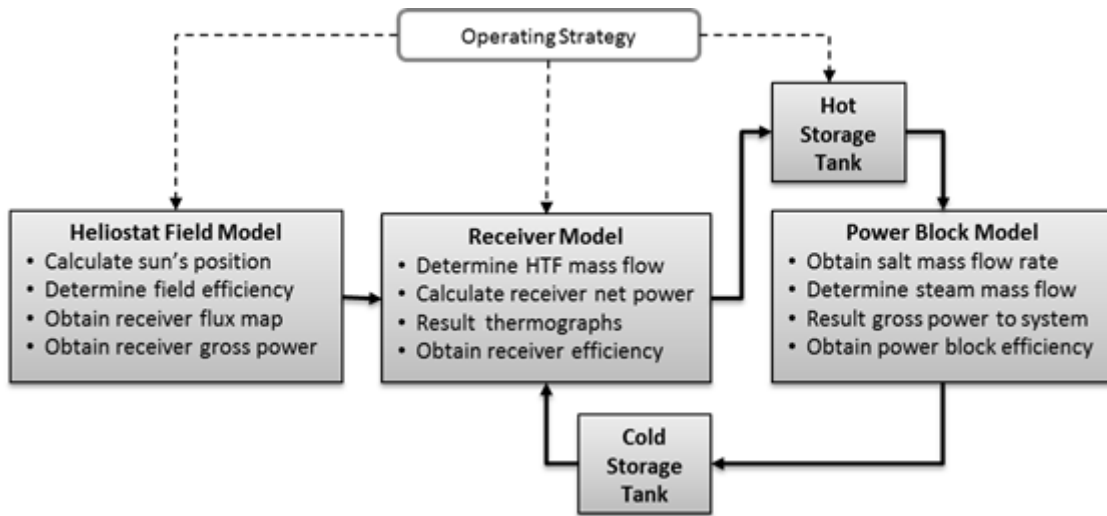


Figure 19: Basic overview of model developed

The user inputs are given to the model by using the Graphical User Interface. These inputs are the date on which simulation was started, duration and time resolution, the plant status at the start of simulation, financial parameters, and the implemented operating strategy. The model utilises these inputs to obtain the appropriate TMY data set which contains the ambient temperature, wind speed, humidity and DNI. Based on the operating strategy selected and the specified boundary conditions, the model optimises the plant operations pertaining to the user inputs. The simulation results are presented in a report format along with the detailed values in the Excel workbook. A series of various simulations can be executed from which the model is able to compare, e.g. comparisons based on plant performances and financial indicators.

3.3. Site Location and Weather Data

The case study plant is located in Upington, Northern Cape, South Africa with the coordinates: latitude -28.482431, longitude 21.096990 and elevation 858 m. The time resolution of the model is set up to either one hour or 15 minutes interval by using the corresponding TMY data. The 15 minutes resolution provides a more realistic representation of the plant operations, as the transients are represented in a better manner. The resulting TMY data is based on a statistical analysis of SolarGIS multiyear time series of solar resource and meteorological data. The SolarGIS data are obtained and calculated by these models using the meteorological, atmospheric and satellite input data as well as on-site measurements from three different sites. A detailed report on this study with an appropriate weather data is also available. (GeoModel, 2011; Eskom, 2012b)

3.4. Heliostat Field

The heliostat field model was a replicate of the case study plant's designed heliostat field. The heliostat field is an important component of the solar energy collection system of the plant. Its primary function is to direct the incoming sun rays to the receiver in the most efficient manner. Based on the sun's position relative to the field, the reflected solar beams onto the receiver portray a flux map on the receiver surface. The DNI received by the field, the cosine and air attenuation losses, shadowing and blocking experienced within the field as well as spillage on the receiver, are some of the parameters that influence the characteristics of the flux map. The most important element regarding the flux map is the aiming strategy implemented by the heliostat field.

3.4.1. Heliostat Field Aiming Strategy

The first and foremost operational aspect of the CSP plant is the heliostat field aiming strategy. For the heliostat field model, a single heliostat field aiming strategy is used. Minor modifications to the aiming strategy are implemented during optimisation of the plant operations. The 'One-Dimensional Smart Aiming Strategy' (Kistler, 1986) implemented allows the heliostat images to spread out along the height of the receiver until spillage starts to increase. The smaller images of the inner heliostats that have the best efficiency or reflectivity are spread out over several aiming points. The images from the outer heliostats, that have bigger images and are less focused, are aimed towards the centre of the receiver. This minimises the effects of peak flux and flux gradients on the receiver. During times when the peak flux exceeds the receiver material's designed flux limit of 1000 kW/m^2 , the DAPS deflect heliostats contributing to the peak flux. This diverted energy is recorded as 'deflected energy' in the model. The heliostat field control system, DAPS, is responsible for this safety aspect.

The heliostat field layout and aiming strategy influence the flux map resulting on the receiver surface. Heliostat errors and mirror cleanliness are further contributing factors. Heliostat field characteristics can be expressed as the result of the effects that these factors have on the field optical efficiency. In order to obtain a flux map to be used for the receiver model, the heliostat field characteristics of the heliostat field model should correlate with the case study plant.

3.4.2. Heliostat Field Characteristics

The heliostat field of the case study plant is designed at a Solar Multiple or SM of 2.4. The Solar Multiple represents the ratio of the receiver net thermal output at design point to the energy required by the Steam Generating System (SGS) to generate power at nominal conditions. The SM is also defined as the solar field aperture area expressed as a function of the power cycle capacity (SAM, 2014). The Design Point (DP) refers to a point in time in a year that represents the conditions for which the plant is designed for. Design point, thus, results in the nominal output conditions of the plant. The field consists of 11,298 individual heliostats, each with a height and width of 11.60 m and 10.64 m respectively. These heliostats contribute to the total mirror area of $1,338,384 \text{ m}^2$. The

simulation tool, DELSOL3 (Kistler, 1986), has been selected to replicate the case study plant's heliostat field. As DELSOL3 is used to interface in the popular simulation software tool SAM (SAM, 2014), it was deemed suitable for this research project. The designing of the heliostat field relating to the case study plant, obtaining the heliostat field performance and the corresponding flux map is done by using DELSOL3.

The first step in designing the heliostat field was to create a 'Fortran Input File' required by DELSOL3. This input file corresponds with the design parameters of the case study plant. The design point selected, Day 80 or equinox at noon, correlates to the design point of Solar-1. After DELSOL3 executes the input file, the output files are created. During the second step of this process, a new input file is created for the performance run on the designed heliostat field. DELSOL3 uses the output files from the previous step in addition to the new input file during this execution. The heliostat field characteristics, expressed as efficiencies, from the second step is compared to case study plant represented in Table 8. At the design point, the heliostat field optical efficiency is 53.57 %. This percentage corresponds to the DELSOL3 efficiency of 53.80 %. The slight deviation between the heliostat fields is as the result of the heliostat field layout and aiming strategy implemented in each design. In the case study plant, the owner engineers specified the location of each heliostat and the aiming strategy to be implemented. In this research, DELSOL3 was used to optimise the heliostat field layout. The DELSOL3's predetermined options were used to determine the aiming strategy.

Table 8: Heliostat field design and characteristics correlation

Design Parameter		Solar-1 Basic Design					DELSOL3 Output file		
Number of heliostats		11 298					11 198		
Total mirror area [m ²]		1 338 384					1 340 000		
Heliostat height [m]		11.60					11.60		
Heliostat width [m]		10.64					10.64		
Ratio reflective area to profile		0.97					0.96		
Solar-1	Day	Hour	Cosine	Shadow	Block	Air Att.	Spillage	Total	
Basic Design	80	0	79.0 %	100 %	98.2 %	91.0 %	92.7 %	53.57 %	
DELSOL3	Day	Hour	Cosine	Shadow	Block	Air Att.	Spillage	Total	
Output File	80	0	80.0 %	100 %	98.0 %	92.0 %	91.8 %	53.80 %	

3.4.3. Corresponding Performance and Flux Map

DELSOL3 provides the performance and corresponding flux map for both the given parameters and the design at a specific point in time. The results obtained from the output file after the performance run is executed and the second step is also shown in Table 9. This performance data is compared with the Solar-1 plant performance at the design point. It shows that they fit quite well together.

Table 9: Performance output of DELSOL3 at design point, insolation at 950 W/m^2

Parameters	Solar-1, Basic Design	DELSOL3 OUTPUT
Gross Power onto Receiver	651.80 MW _t	654.00 MW _t
Reflectivity Loss	45.60 MW _t	45.78 MW _t
Radiation/Convection Loss	29.90 MW _t	29.94 MW _t
Piping Loss	0.50 MW _t	0.56 MW _t
Thermal Power Tower Base	575.80 MW _t	577.73 MW _t
Power to Storage	336.10 MW _t	337.01 MW _t
Power to Turbine	239.70 MW _t	240.72 MW _t
Thermal/Electric Efficiency	0.417	0.417
Gross Electric Power	100.00 MW _e	100.43 MW _e
Electrical Parasitics	12.51 MW _e	12.56 MW _e
Net Electric Power	87.49 MW _e	87.87 MW _e

During the flux map retrieval process from DELSOL3, it has been determined that the corresponding flux map related to the design is affected by the heliostat errors and aiming strategy. DELSOL3 optimises the heliostat field according to the values specified in the ‘Input File’, i.e. the aiming strategy to be used, and the error source values. Based on these inputs, DELSOL3 provides a heliostat field to the specified ‘Net Electric Power Output’. Through an iteration process, DELSOL3 continuously adds heliostats to the field to achieve the desired ‘Net Electric Power Output’. The total heliostat field efficiency is affected by the error values the user provides. The higher error values lead to more spillage in the field. This leads to change in the total heliostat field efficiency. To compensate these losses, DELSOL3 adds more heliostats. However, this action effectively increases the field losses as a bigger field is now considered. The graphical representations of these flux maps, relating to heliostat errors, are provided in APPENDIX B. Thus, the final heliostat errors selected for the heliostat field were based on the Solar-1 basic design error values and corresponding number of heliostats in the heliostat field. The flux map obtained at design point is represented in Figure 20. By changing the user inputs in the DELSOL3 input file, various flux maps are accessible throughout the year for the same heliostat field design.

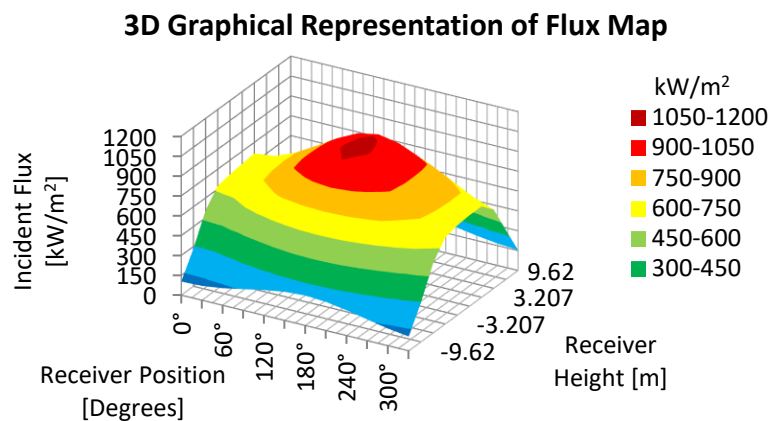


Figure 20: Graphical representation of DELSOL3 flux map

3.4.4. Heliostat Field Model Configuration

The aim of the flux maps is to determine the energy flux on the receiver for any given time-of-day throughout the year. Therefore, the energy flux on the receiver can be represented as a function of the solar position and reference DNI value. This methodology was developed by Wagner (2008). It can generate a number of flux maps for various solar positions followed by interpolating it. Six months between the winter solstice and summer solstice were considered to obtain an equally spaced distribution. These maps are equally spaced by declination angle, from eight specifically selected days. The days are selected based on the following equation (Wagner, 2008):

$$Day_i = 355 - \text{floor} \left(\frac{\arccos(-1 + 2(i - 1))}{(nday - 1)} \cdot \frac{(355 - 172)}{\pi} \right) \quad (4)$$

Where $nday$ is the number of days included in the selection, and i can have any value from 1 to $nday$. The numbers 355 and 172 represent the day of the year on which the summer and winter solstice occur, respectively.

The 96 equally spaced flux maps are represented in Figure 21. By interpolating the azimuth and zenith angles accordingly, the flux map for the receiver on any day and time can, thus, be obtained. Wagner conducted a sensitivity analysis and verified that the error associated with 96 flux maps are accurate within 0.53 %. (Wagner, 2008)

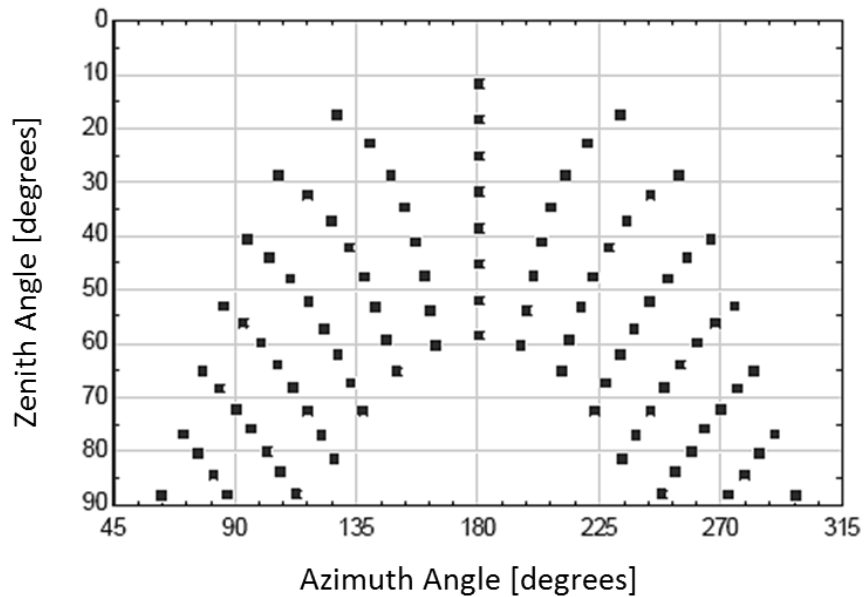


Figure 21: 96 Flux maps equally spaced by declination angle (Wagner, 2008)

The developed heliostat field model uses these 96 distinct flux maps. The interpolated flux maps are then normalized with the DNI from the TMY data file. The excessive flux is catered for by ‘defocusing’ some heliostats at the required node. The defocused flux is

recorded. The defocused flux affects the overall plant performance. Once the interpolated flux map is adjusted to the receiver design limitations and ambient conditions of the DNI, the receiver model utilises this flux map to calculate the total gross power onto the receiver. Subsequently, the receiver's thermal losses, net thermal power and efficiency can be determined.

In conclusion, a graphical representation of the configuration and interfaces present in the developed heliostat field model are illustrated in Figure 22. DELSOL3 was used to design the heliostat field to represent a similar field used in the case study plant. The designed field was used to obtain 96 flux maps. These flux maps and their corresponding heliostat field optical efficiencies are recorded in the heliostat field model database. The heliostat field model utilises the user inputs, simulation start date and time to calculate the corresponding solar angles. These solar angles are used in a lookup table to provide the model with an interpolated flux map and the corresponding heliostat field optical efficiencies. The flux map is further adjusted by the weather conditions and receiver flux limit boundary conditions. Two sets of information are provided to the receiver model, that is, the adjusted flux map and gross thermal power on the receiver. The methodology followed in the heliostat field model is further supported by a similar approach for the developed model in the plant design optimisation (Augsburger, 2013).

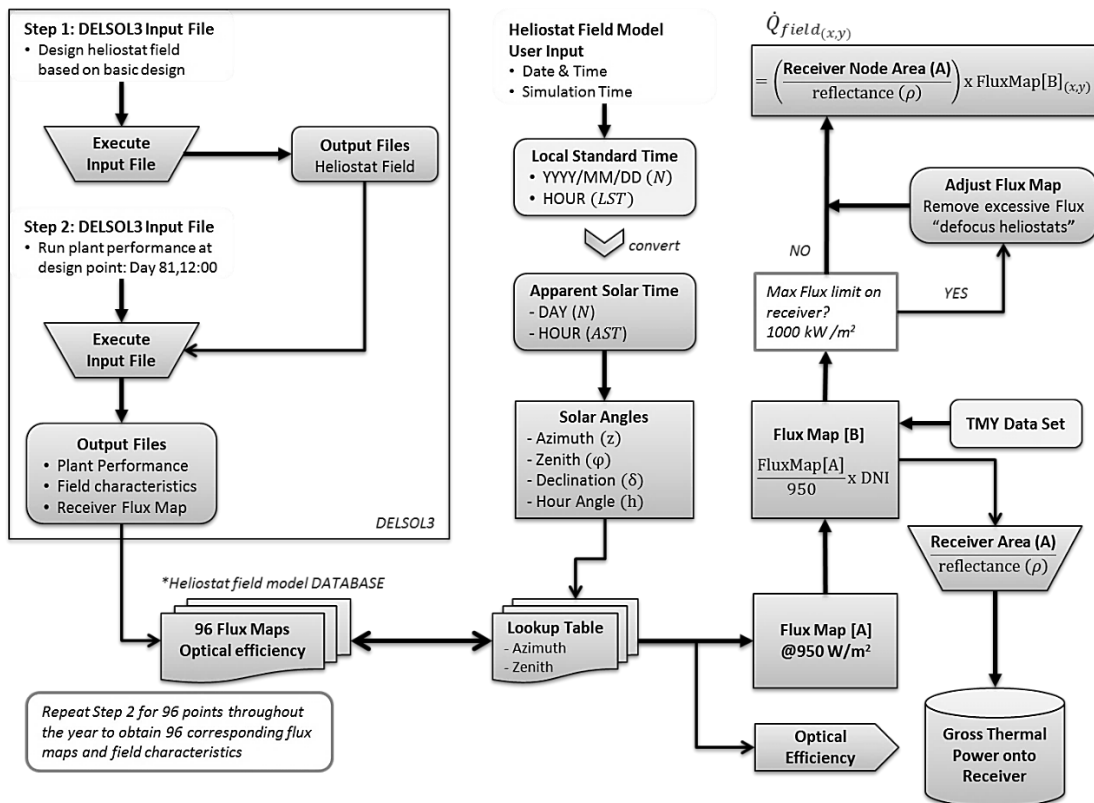


Figure 22: Heliostat field model configuration, interfacing and outputs

3.5. Receiver

This Section on the receiver’s model has been published by De Meyer *et al.* in 2015. The receiver design and heliostat field aiming strategy play a vital role in the heat transfer efficiency of the receiver. In molten salt external receivers, the common operating temperature of the Heat Transfer Fluid (HTF) or molten salt ranges between 285 °C to 565 °C. The optimum output temperature of 565 °C is achieved by adjusting the mass flow rate of the molten salt through the receiver. The receiver of the case study plant has two serpentine flow regimes through the panels with a cross over flow commencing halfway, as illustrated in Figure 23. The solar radiation which is reflected onto the receiver causes a rise in the temperature of the molten salt by the means of heat transfer. By investigating the published work on molten salt external receiver operating temperatures, the corresponding receiver tube surface temperatures and heat losses, the developed model results in a detailed thermographic representation of the receiver. The receiver flux map is used as input for the steady state model to determine: i) the HTF mass flow rate through the receiver to obtain the desired molten salt output temperature of 565 °C, ii) the receiver’s surface temperatures, iii) the receiver’s tube temperatures, iv) the receiver’s efficiency, v) the pressure drop across the receiver, and vi) the tube strain per panel.

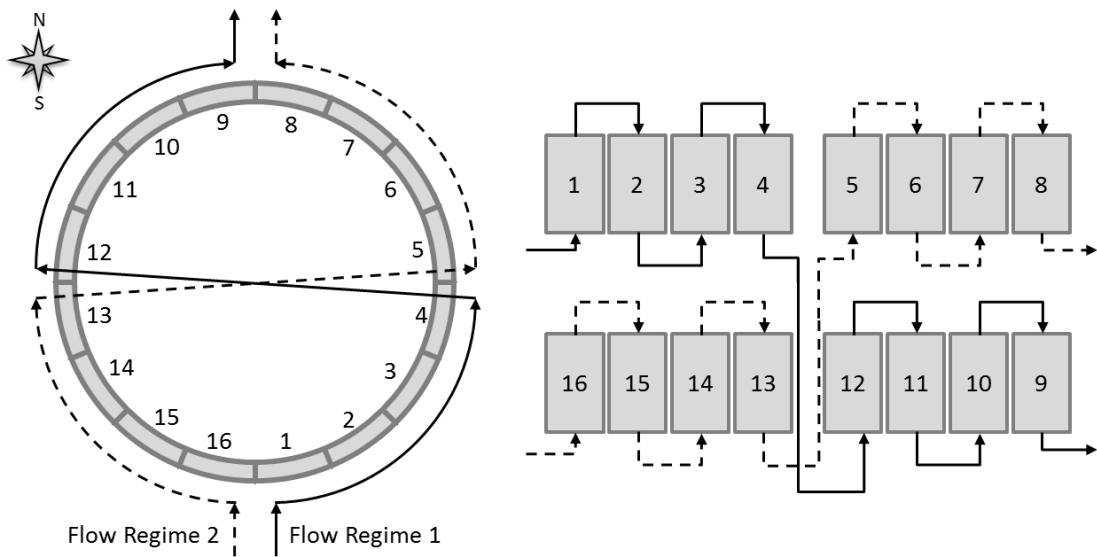


Figure 23: Receiver serpentine flow regimes with cross over flow halfway.

The external receiver consists of 16 panels with tube diameters and thickness of 50 mm and 1.5 mm, respectively. The molten salt enters the receiver from the south through Panel 1 and Panel 16, and exits from the north through Panels 8 and 9, as illustrated in Figure 23. The heliostat design, field layout, aiming strategy and incident thermal power onto the receiver at design point correlates with a 652 MW_t receiver at an optical height of 208 m. The receiver dimensions are as follows, diameter of 16.32 m and height of 19.24 m. The flux maps generated using DELSOL3, are obtained from the heliostat field model as described in Section 3.4.4.

The thermal resistance concept (Cengel, 2009) was utilised to derive the thermal resistance network (De Meyer *et al.*, 2015). Representing the receiver, the thermal resistance network is illustrated in Figure 24 at the tube cross-section. This steady state heat transfer model is used to determine the receiver temperatures from the known variables such as ambient conditions, incident flux onto the receiver and heat transfer fluid mass flow rate with an inlet temperature.

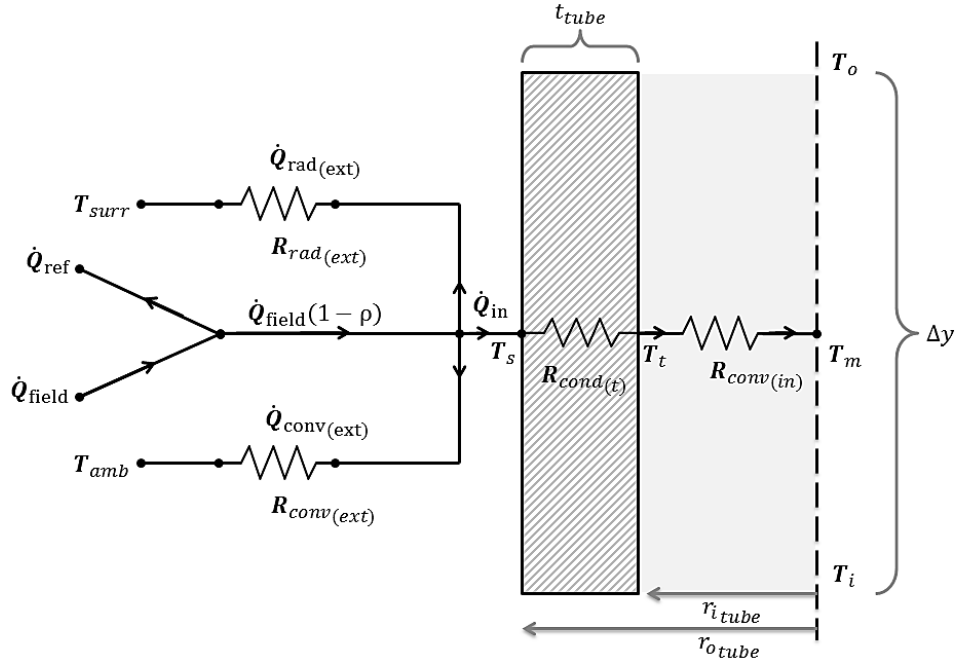


Figure 24: Receiver thermal resistance network at the receiver tube cross section

3.5.1. Mathematical Model

A list of all the design parameters used in the receiver model is supplemented in APPENDIX A. Recalling the receiver thermal resistance network, illustrated in Figure 24, the following energy balance is applicable.

$$\dot{Q}_{field} - \dot{Q}_{ref} = \dot{Q}_{field}(1 - \rho) = \dot{Q}_{in} + \dot{Q}_{conv(ext)} + \dot{Q}_{rad(ext)} \quad (5)$$

The incident flux onto the receiver (\dot{Q}_{field}) results from the flux map obtained from the heliostat field model and the reflected radiation (\dot{Q}_{ref}) from the receiver is influenced by the receiver reflectivity (ρ). The energy transferred to the heat transfer fluid (\dot{Q}_{in}) is subjected to the incident flux onto the receiver, the reflected radiation, the external thermal radiation loss ($\dot{Q}_{rad(ext)}$) and the external convective heat loss ($\dot{Q}_{conv(ext)}$). The convection losses, radiation losses and the resulting thermal energy transfer to heat transfer fluid are expressed as:

$$\dot{Q}_{conv(ext)} = \frac{(T_s - T_{amb})}{R_{conv(ext)}} \quad (6)$$

$$\dot{Q}_{rad(ext)} = \frac{(T_s - T_{surr})}{R_{rad(ext)}} \quad (7)$$

$$\dot{Q}_{in} = \frac{(T_s - T_t)}{R_{cond(t)}} = \frac{(T_t - T_m)}{R_{conv(in)}} = \frac{(T_s - T_m)}{R_{cond(t)} + R_{conv(in)}} = \dot{m}C_p(T_o - T_i) \quad (8)$$

The receiver temperatures are represented by surface temperature (T_s), ambient temperature (T_{amb}), surrounding or sky temperature (T_{surr}), inner tube temperature (T_t), heat transfer fluid mean temperature (T_m) and heat transfer fluid inlet (T_i) and outlet (T_o) temperatures. The heat transfer fluid heat capacitance and mass flow rate are expressed as C_p and \dot{m} respectively. The thermal resistance (R) for each of the abovementioned expressions are:

$$R_{rad(ext)} = \frac{1}{h_{rad(ext)}A_s} \quad (9)$$

$$R_{conv(ext)} = \frac{1}{h_{conv(ext)}A_s} \quad (10)$$

$$R_{cond(t)} = \frac{L_t}{k_t A_t} \quad (11)$$

$$R_{conv(in)} = \frac{1}{h_{conv(in)}A(in)} \quad (12)$$

The corresponding exposed surface area ($A_s = d_o \cdot N_t \cdot H_{rec}/N_{nodes}$) is used for radiation and convection losses. The cross-sectional area (A_t) is used for the conduction of heat from the outer tube area to the inner tube area. The tube cross sectional length (L_t) is equivalent to the tube thickness (tt). The thermal conductivity of the tube (k_t) is applicable to the tube's conductive resistance (R_{cond}). The heat transfer coefficients (h) for the external radiative resistance ($R_{rad(ext)}$), the external convection resistance ($R_{conv(ext)}$) and the internal convection resistance ($R_{conv(in)}$) are respectively expressed as follows:

$$h_{rad(ext)} = \varepsilon\sigma(T_s^4 - T_{surr}^4)/(T_s - T_{surr}) \quad (13)$$

$$h_{conv(ext)} = (h_{nat}^{3.2} + h_{wind}^{3.2})^{1/3.2} \quad (14)$$

$$h_{conv(in)} = \frac{k_{HTF}Nu_{HTF}}{r_i} \quad (15)$$

with,

$$h_{nat} = \frac{k_{film}Nu_{nat}}{H_{rec}} \quad (16)$$

$$h_{wind} = \frac{k_{film}Nu_{wind}}{D_{rec}} \quad (17)$$

where, ε and σ are the receiver emissivity and Stefan Boltzmann's constant, respectively. The mixed external convection heat transfer coefficient ($h_{conv(ext)}$) was determined by Wagner (2008) and Siebers and Kraabel (1984) in their studies. The heat transfer coefficients for natural convection (h_{nat}) and forced convection or wind (h_{nat}) are obtained by determining the Nusselt numbers for each. Nusselt numbers for natural convection (Nu_{nat}), forced convection (Nu_{wind}) and internal forced convection (Nu_{HTF}) are determined as per Cengel (2009) or Siebers and Kraabel (1984). The receiver dimensions are height (H_{rec}), external diameter (D_{rec}) and receiver inner tube radius (r_i). The thermal conductivity for air (k_{film}) is determined at film temperature, whereas for the heat transfer fluid (k_{HTF}), it is determined at the bulk fluid temperature.

The Nu correlation is applicable for forced convection over a cylinder with various surface roughness (k_s) and corresponding Reynolds numbers, with the effective surface roughness represented as $k_s = r_o/D_{rec}$. (Wagner, 2008). These are presented in Table 10

Table 10: Nu correlation for forced convection over cylinder with surface roughness

	Reynolds Number (Re) ranges	Nusselt Number (Nu) correlation
$k_s/D = 0$ (smooth cylinder)		
(1)	All Re	$Nu = 0.3 + 0.488 \cdot Re^{\frac{1}{2}} \left(1 + \left(\frac{Re}{282000} \right)^{\frac{5}{8}} \right)^{\frac{4}{5}}$
$k_s/D = 75$ (10^{-5})		
(2)	$Re \leq 7.0$ (10^5)	Use correlation (1)
(3)	7.0 (10^5) $< Re < 2.2$ (10^7)	$Nu = 2.57$ (10^{-3}). $Re^{0.98}$
(4)	$Re \geq 2.2$ (10^7)	$Nu = 0.0455 \cdot Re^{0.81}$
$k_s/D = 300$ (10^{-5})		
(5)	$Re \leq 1.8$ (10^5)	Use correlation (1)
(6)	1.8 (10^5) $< Re < 4.0$ (10^6)	$Nu = 0.0135 \cdot Re^{0.98}$
(7)	$Re \geq 4.0$ (10^6)	Use correlation (4)
$k_s/D = 900$ (10^{-5})		
(8)	$Re \leq 1.0$ (10^5)	Use correlation (1)
(9)	$Re > 1.0$ (10^5)	Use correlation (4)
Note: Fluid properties evaluated at film temperature		

3.5.2. Step 1: Determine Heat Transfer Fluid Mass Flow Rate

An initial average surface temperature is assigned to each panel, from 450 °C to 650 °C. From the incident flux map and Equations 6-7, the thermal losses for each panel are calculated to obtain the total thermal loss of the receiver. The resulting energy transferred to the heat transfer fluid (\dot{Q}_{in}) is obtained from Equation 5. The heat transfer fluid mass flow rate is calculated for each flow regime in the receiver using Equation 8.

3.5.3. Step 2: Determine Surface and Tube Temperature

In the second step, each panel is divided into the number of nodes corresponding to the incident flux map. Starting with the first node in the first panel of each flow regime, see Figure 25(a), the thermal losses for the node are calculated and the resulting energy transferred to the heat transfer fluid is obtained. With the heat transfer input temperature known, the output temperature is obtained using Equation 8 from the calculated heat transfer fluid mass flow rate. The bulk fluid temperature can thus, be obtained to determine the corresponding tube (T_t) and the surface (T_s) temperature, respectively, from Equation 8.

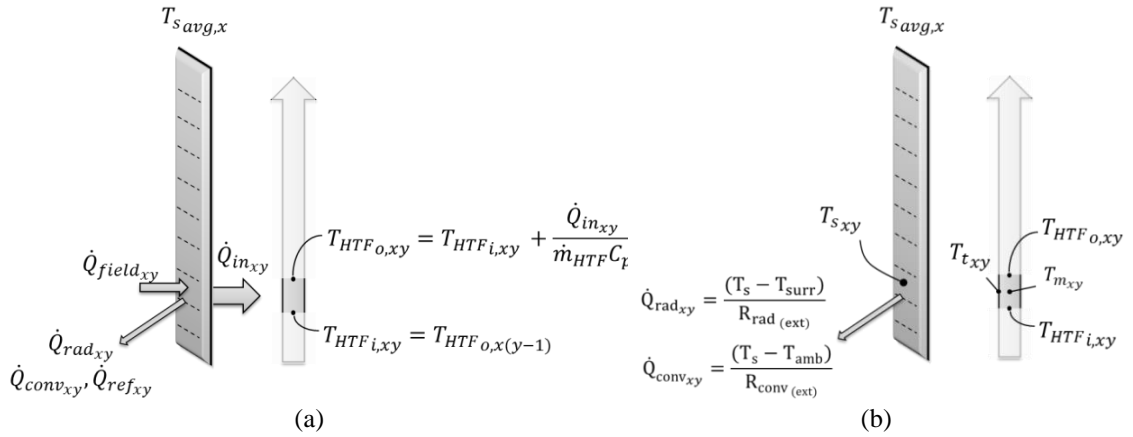


Figure 25: (a) Determine \dot{Q}_{in} and $T_{HTF(o)}$ (b) Determine T_s and T_t

3.5.4. Receiver Efficiency

As illustrated in Figure 25(b), from the newly calculated surface temperature the resulting heat losses are recalculated for the node. The aggregated heat transferred from all the nodes in each flow regime to the heat transfer fluid is re-evaluated and corresponding mass flow rate is recalculated accordingly. From the Equation 8, it is evident that any deviation in the amount of heat transferred to the heat transfer fluid will induce a corresponding mass flow rate. The process is iterated until the final surface temperatures are obtained. The receiver efficiency can thus be calculated utilizing the following equation:

$$\eta_{rec} = \frac{\dot{Q}_{in}}{\dot{Q}_{tot}} = \frac{\dot{Q}_{in}}{\dot{Q}_{in} + \dot{Q}_{rad(ext)} + \dot{Q}_{conv(ext)} + \dot{Q}_{ref}} \quad (18)$$

3.5.5. Receiver Pressure Drop

The receiver's pump is sized according to the pressure drop in the tower and across the receiver. It is, therefore, important to analyse the pressure drop in the receiver. The pressure drop is influenced by various factors such as the heat transfer fluid mass flow rate, the receiver's height, the number of panels used, the tube diameter and tube thickness. This is evident in the total system loss equation for losses in pipe systems (White, 2008), with the pressure drop correlation being, $\Delta P = \rho gh$.

$$\Delta h_{tot} = h_f + \sum h_m = \frac{V^2}{2g} \left(\frac{fl}{d} + \sum k \right) \quad (19)$$

Head loss due to friction (h_f) and minor losses (h_m) in the receiver tube are accounted for in 2 x 45° and 2 x 90° elbows, each with a resistance coefficient factor of 16 and 30, respectively (Crane, 1986). The pipe entrance and exit resistance coefficients are 0.78 and 1, respectively. The friction factor for turbulent flow in rough pipes (Govender, 2013) is given as follows:

$$f = 0.18Re^{-0.2} \quad (20)$$

3.5.6. Receiver Tube Strain

The receiver is subjected to operation conditions where the temperature is changed daily. This imposes thermal stresses within the material. Furthermore, the incident flux onto the receiver results in creation of a temperature gradient across the material. This temperature gradient makes the receiver's material sensitive to the thermal shocks that are caused during the cloud transients. It is therefore also important to have a heliostat field aiming strategy that allows even distribution of flux on the receivers. To calculate the mechanical strain resulting due to a temperature gradient, these equations are applicable: (Pacheco, 2002), (Kolb, 2011)

$$\varepsilon = \alpha \left(\frac{T_s - T_t}{2(1 - \nu)} + \frac{T_s + T_t}{2} - T_{avg} \right) \quad (21)$$

where,

$$T_{avg} = T_m + \frac{1}{\pi} \left(\frac{T_s + T_t}{2} - T_m \right) \quad (22)$$

The tube strain and average temperature of the cross section are represented as ε and T_{avg} , respectively. The coefficient of thermal expansion and Poisson's ratio is represented by α and ν , respectively. From the calculations of the receiver pressure drop, the internal pressure per tube can be obtained. For calculating the stresses across the tube wall resulting from the internal pressure (P_i) and thermal gradient (ΔT), further analysis is undertaken. The stresses such as radial (P_r), tangential (P_θ) and longitudinal (P_l) stresses are calculated using thick wall pressure vessel calculations ($t/d > 1/20$). The stresses resulting from internal pressure and thermal gradient across the tube walls are noted by Budynas and Nisbett (2008), Neises *et al.* (2014) and Rodreiguez-Sanchez *et al.* (2014).

3.5.7. Receiver Operating Regimes and Weather Prediction

Before a normal receiver operation can occur, the receiver has to be heated up for approximately 1 hour and 15 minutes. During the warm-up sequence of the receiver, the heliostats are used to heat up the receiver with the available DNI. For this, the heliostat field control system is used. The receiver requires 70 % of the minimum gross operating thermal power onto its surface to initiate the warm-up sequence. The minimum mass flow rate of the heat transfer fluid through the receiver is achieved in 30 minutes before the normal operation. During the warm-up, the heat transfer fluid is pumped from the cold storage tank and circulated back to the cold storage tank. The heat tracing is activated during the warm-up sequence in order to prevent freezing in the pipes and the equipment. (Alpert and Kolb, 1988)

The receiver operating philosophy has been set up in the model with these boundary conditions, see Table 11. In order for the receiver to operate in ‘Normal’ operation mode, a minimum gross thermal power (P_{min}) is required on the receiver. The model utilises the TMY data set to obtain ambient conditions determining the heliostat field and receiver operations. In addition, a weather prediction system has been implemented to avoid unnecessary receiver start-ups when insufficient DNI is available, to maintain the operation during the receiver normal operating regime. It is standard practice to use one-hour time resolutions in annual performance models. However, when daily operations of the plant are considered, 15 min time resolutions are recommended to represent more accurate transients of the receiver operations.

Table 11: Receiver operating philosophy boundary conditions

	Gross Thermal Power on Receiver Surface	Receiver Pump Operating Conditions	Receiver Status	Operating Mode
Legend	P_{gross}	Pump	Hot	Mode
Warm-Up	$> 70 \% (P_{min})$	OFF ON = 30 min before Normal	+0.25 for each 15 min interval	1
Normal	$> P_{min}$	ON	= 1.25	3
Cloud	$< P_{min}$	ON, if Mode (t+2) =Normal	-0.25 for each cloud transient	0

The receiver model results, weather predictions and the effect of the receiver operating regimes are illustrated in Figure 26 and Figure 27. Using Table 11 as reference, the legend P_{gross} represents the total incident power received from the heliostat field onto the receiver. The legend HOT indicates the receiver status, i.e. how warm the receiver is. 0 is used for cold conditions, and 1.25 when receiver is ready for normal operations. The receiver’s pump operation is indicated by the legend PUMP. It indicates flow through the receiver. The value ‘1’ corresponds to the flow through the receiver, and a value of ‘0’ for no flow. The legend MODE represents the receiver operational mode where 0 represents ‘OFF’, 1 is for ‘Warm-Up’, 3 is for ‘Normal Operation’ and 0 represents the ‘Cloud Transients’.

Analysing the results from Figure 26 and Figure 27, the one-hour time resolution did not accurately represent the receiver operations of warm-up sequence and cloud transients. In the one-hour time resolution, the receiver is heated up when sufficient that is more than 70 % of the minimum gross power is put onto the receiver. In the next time step, a fraction (25 %) was used to heat up the receiver to normal operating conditions. The remaining energy was utilised under normal receiver operations. At time 14h00 to 15h00 (Figure 26), when the cloud was observed, it did not activate the cloud transient mode. However, in Figure 27 the cloud transients and its resulting effects on the receiver's operations are clearly observed. Although, the one-hour time resolution did not best represent the daily operations of the receiver, in terms of warm-up sequence and cloud transients, it was necessary to set up the model to accommodate both the time intervals. This was done for validation against other simulation models that utilise hourly intervals and to accommodate data sets available only in hourly format such as system demand, wind and PV generation profiles that are obtained from the National Control. The hourly simulation was modelled to best represent the receiver operations and deemed adequate for demonstration purposes.

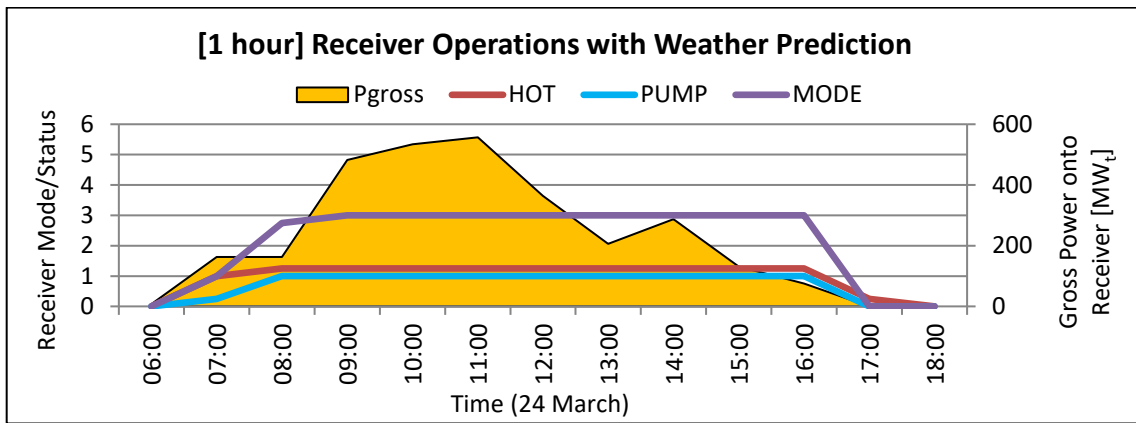


Figure 26: Receiver operations with weather predicting element incorporated [1 hour]

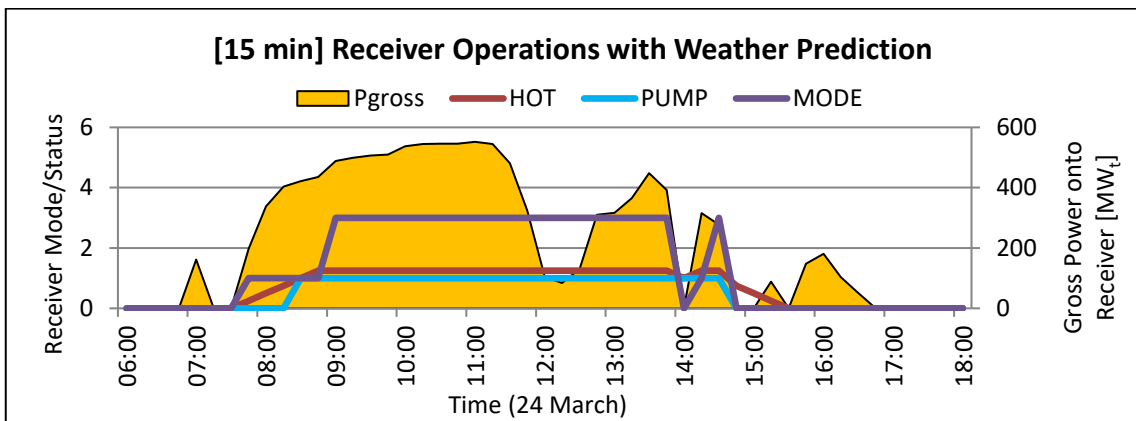


Figure 27: Receiver operations with weather predicting element incorporated [15 min]

3.5.8. Receiver Model Configuration

The receiver model interfaces with the heliostat field model and thermal storage system. The meteorological conditions such as temperature and wind speed are obtained from the TMY data file and these affect the performance of the receiver. The receiver operating regimes are implemented as per the Section 3.5.7. In addition, the weather predicting system is also included. The operating parameters such as receiver's net thermal energy absorbed, receiver's thermal losses, HTF mass flow rate, HTF outlet temperature, and receiver's efficiency, are calculated from the receiver model. The receiver net thermal energy absorbed is used to update the status of the hot TES. Subsequently, the cold TES tank is updated with the amount of HTF dispatched to the receiver. The receiver model is capable of generating thermographic and colormap representations of the heliostat field flux distribution over receiver surface, tube strain per panel and receiver's efficiency. It can also be used for generating temperature profiles of the surface, inner tube and HTF. This functionality has been made available to the user in the stand-alone 'Receiver Model: Thermographs and Colormaps'.

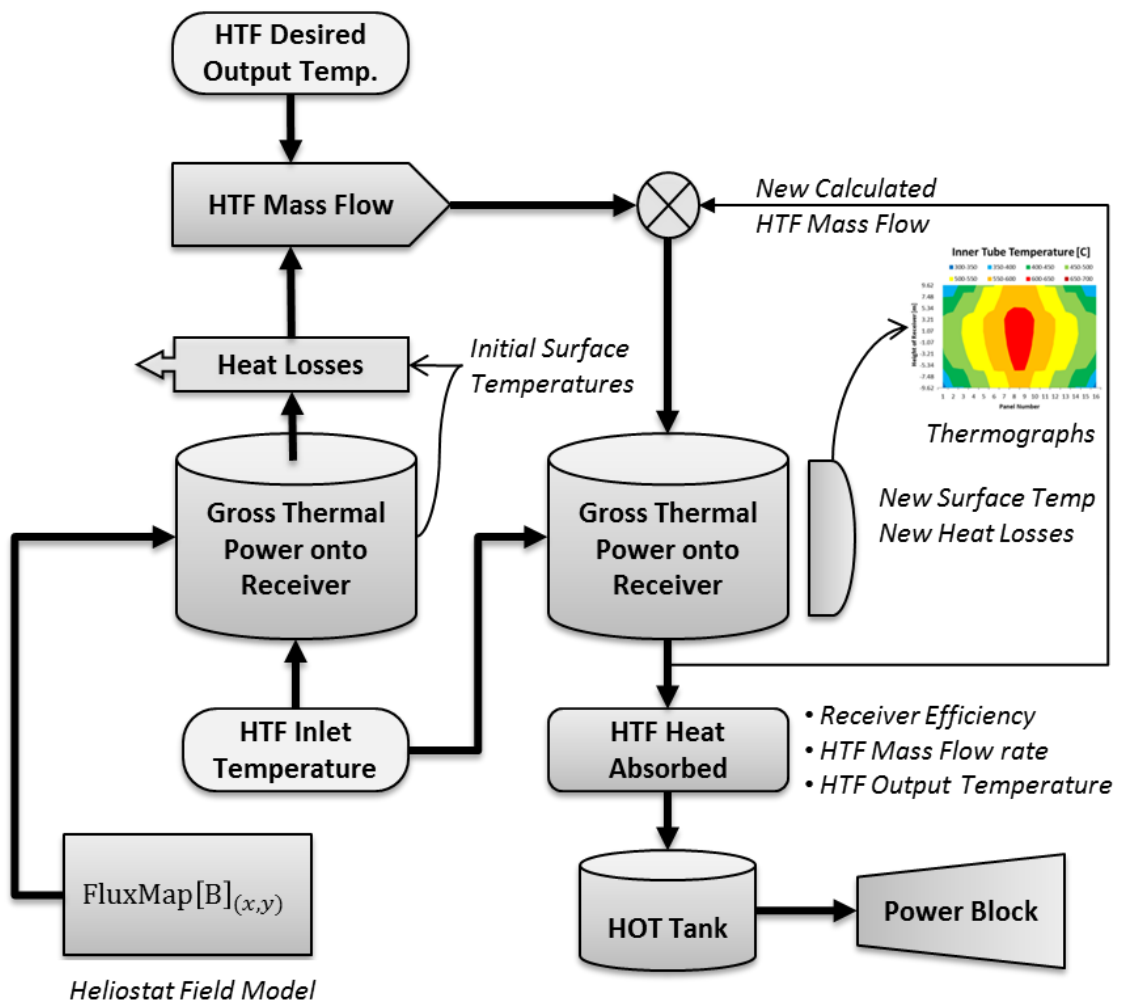


Figure 28: Receiver model configuration, interfacing and outputs

3.6. Power Block

The power block of the case study plant is designed to generate 100 MW at design point. The optimisation of the power block configuration has been catered for in the basic design (Eskom, 2012c). The resulting configuration consists of a turbine with five steam extraction points. The high-pressure (HP) turbine's steam extraction is reheated for the intermediate-pressure (IP) turbine. An air-cooled condenser condenses the low-pressure (LP) turbine's steam to saturated water. This feedwater (FW) is heated through a series of five feedwater heaters (FWH). An open- and four closed-feedwater heaters are used. The steam generator system consists of a preheater (PH), boiler, superheater (SH) and reheater (RH). A simplified TS-diagram of the power block is represented in Figure 29 with its configuration and design point conditions (in Figure 30). The power block is created using the design point conditions. The efficiency of the power block is affected as these conditions changes. The design point conditions are represented in Table 12.

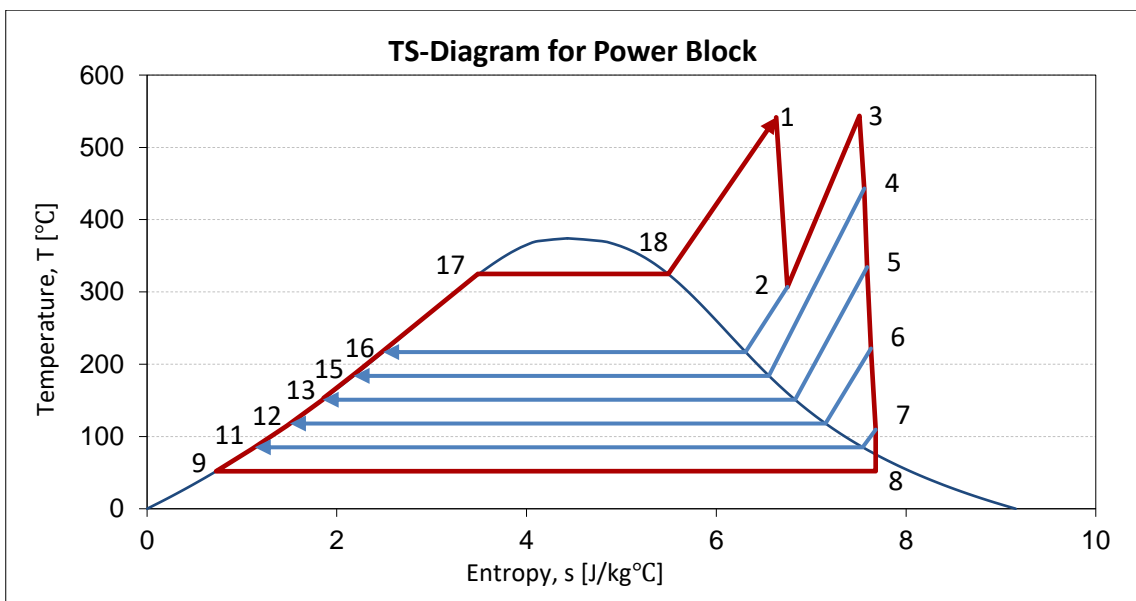


Figure 29: Simplified TS-Diagram representing the power block design point values

Table 12: Power block design point conditions (Eskom, 2012c)

Design Parameter	Value	Unit
Turbine-Generator Output(gross)	100	[MW _e]
Turbine HP inlet pressure	120	[bar]
Turbine HP inlet temperature	541	[°C]
Ambient Temperature	32	[°C]
ACC ITD	20	[°C]
HTF mass flow	570	[kg/s]
HTF input temperature	565	[°C]
HTF desired output temperature	289	[°C]

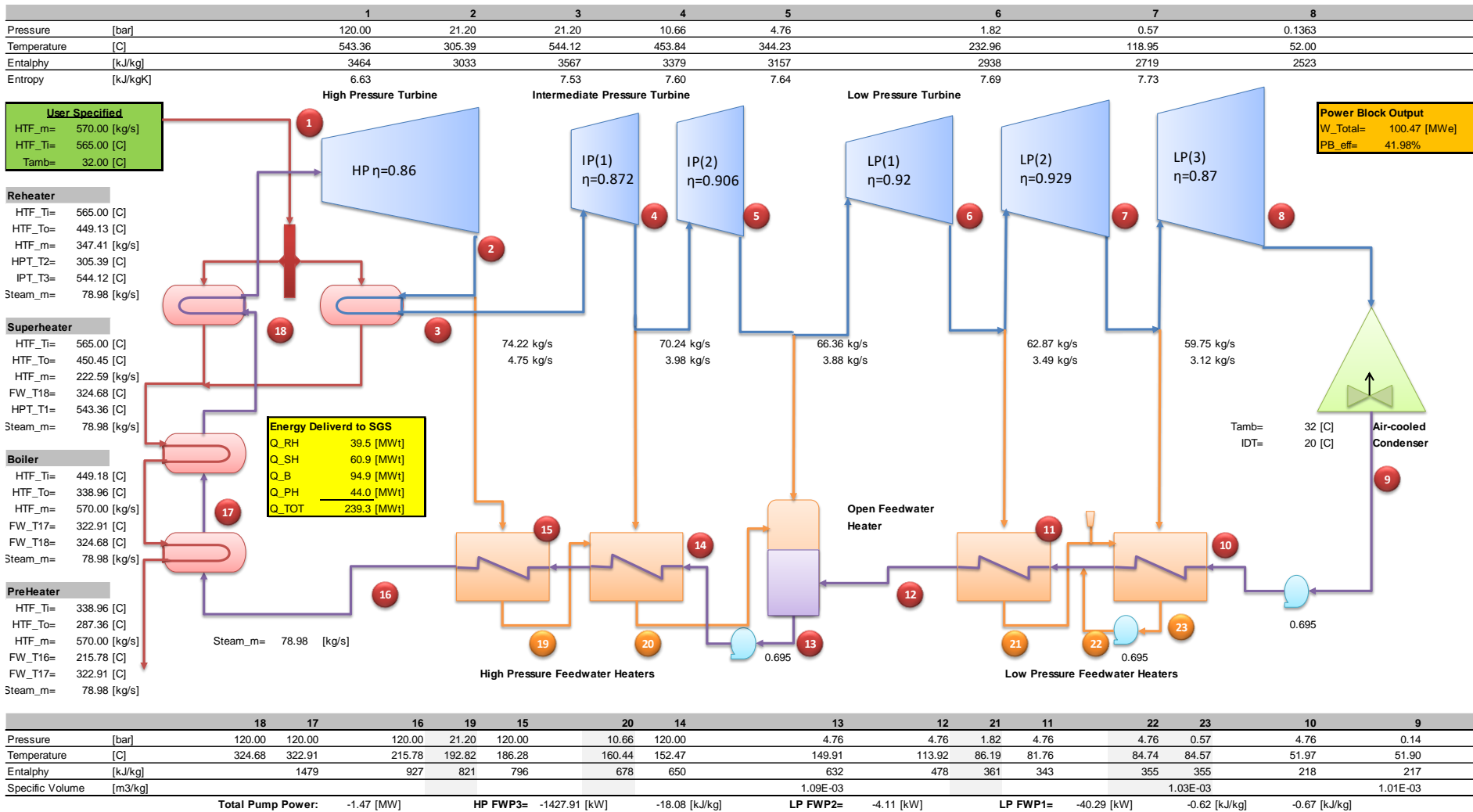


Figure 30: Power block configuration and design point conditions

Once the design parameters are set, the power block operates under these design parameters as reference operating parameters. The power block outputs are affected by changing these operating conditions. The steam generator's boiler pressure for the HP turbine is fixed at 120 bar, and for the IP turbine at 21.79 bar. The pressure drop across the feedwater heaters are not taken into consideration. The turbine-generator output is controlled by the molten salt inlet temperature and mass flow rate to the SGS. The turbine-generator output is decreased by reducing the energy input to the SGS, i.e. molten salt mass flow rate and temperature. The feedwater mass flow rate through the boiler is controlled to achieve the 120 bar inlet pressure to the HP turbine. The performance curve for the power block is obtained by simulating the power block under various conditions, including part-load operations. The power block model has been made available to the user in the stand-alone 'Power Block Model: Operating Conditions'.

3.7. Thermal Energy Storage

The thermal energy storage system stores the energy required for the steam generator system to produce steam. The HTF in the solar collecting system, molten salt, is stored in the cold tank at 288 °C and pumped to the receiver during receiver operations. Sufficient DNI is required to heat up the molten salt to the desired temperature. The heated molten salt, at 565 °C, is pumped to the hot storage tank before it is utilised in the SGS to generate steam for the turbine. This configuration separates the solar collecting system from the power generation system. This is the big advantage of CSP plants with molten salt as HTF and storage medium. The design parameters of the storage system are supplemented in APPENDIX A. The developed model utilises the storage system to optimise the dispatchability potential of the plant. It plays an important role in optimising the plant according to the implemented operating strategy.

3.8. Auxiliaries

The plant auxiliaries are informed by the equipment list and single line diagram of the basic design from the case study plant (Eskom, 2012a). One of the largest contributors to the auxiliaries of the plant is the receiver molten salt pump. It is responsible for pumping the cold molten salt from the cold storage tank to the receiver placed at the top of the tower. The detailed auxiliary consumptions for the plant at design point and the annual performance are shown in Table 13. The Balance of Plant (BoP) consumed the most auxiliary power whereas heat tracing in the pipes consumed the least. It should be noted that the auxiliary consumption indicated in Table 13 for the basic design of Solar-1 is pertinent to the operating strategy implemented and operating philosophy followed.

The case study plant is replicated in SAM using the design parameters of Solar-1. The annual auxiliary consumptions from SAM's simulation results are reported in Table 14. The comparison in Table 14 shows a deviation between the annual total plant parasitics. The deviation is primarily due to the parasitic load of the receiver pump. The inclusion of an inlet vessel in the Solar-1 plant receiver's design is the reason for the difference observed in the receiver pump values. The inlet vessel is the part of the receiver protection system, and it accounted for an additional 4.5 GWh_e power used in the receiver pump due

to an increased pressure drop. Thus, when the receiver inlet vessel is excluded, Solar-1 receiver auxiliary consumption is 10.0 GWh_e. The adjusted value correlates with the 10.3 GWh_e reported by SAM. The adjusted total plant parasitics for Solar-1 is 47.8 GWh_e. The deviation in the total plant parasitics is less than 1.5 %.

Table 13: Parasitics consumption for Solar-1 basic design (Eskom, 2012a)

Parasitics	Annual Performance		Design Point	
Heliostat Field Tracking Power	3.1	GWh _e	0.600	MW _e
Receiver pump	14.5	GWh _e	5.578	MW _e
Hot TES pump	3.3	GWh _e	0.729	MW _e
Balance of Plant	21.6	GWh _e	3.391	MW _e
ACC	4.3	GWh _e	1.527	MW _e
Pipe Tracing	0.6	GWh _e	0.101	MW _e
Fixed Parasitics	4.8	GWh _e	0.555	MW _e
Total Plant Parasitics	52.3	GWh_e	12.51	MW_e

Table 14: Parasitics consumption comparison, SAM and Solar-1 basic design

Parasitics – Annual Performance	SAM		Solar-1	
Heliostat field tracking power	3.1	GWh _e	3.1	GWh _e
Receiver pump	10.3	GWh _e	14.5	GWh _e
Hot TES pump	3.4	GWh _e	3.3	GWh _e
Balance of plant	21.7	GWh _e	21.6	GWh _e
ACC	4.8	GWh _e	4.3	GWh _e
Pipe tracing	0.0	GWh _e	0.6	GWh _e
Fixed parasitics	4.8	GWh _e	4.8	GWh _e
Total Plant Parasitics	48.5	GWh_e	52.3	GWh_e

The simulation results from SAM showed similarity in the auxiliary consumption when compared to the performance of Solar-1’s basic design, mainly for following the same operating strategy. Therefore, SAM’s auxiliary consumption approximations were used in the development of the research project’s model. The following section represents the auxiliary consumption unless otherwise stated, these approximations were obtained from SAM’s simulation results. It also discusses the approximations and calculations that are found similar to the level of detail from an engineering basic design. Therefore, only major system components are considered in these calculations. The purpose of this section is to have representation of the plant parasitics in the model.

3.8.1. Heliostat Field

The heliostat field with the tracking power of 0.6 MW_e is used during receiver ‘Normal’ operation when all the available heliostats are focused onto the receiver. During the warm-up sequence, the ‘preheat processor’ is utilised to aim the required heliostats to the receiver. The remaining heliostats that are not used in the process are kept at stand-by mode. Once the receiver is warmed up and ready for normal operations, the stand-by heliostats come into operation, thus reflecting solar energy onto the receiver. For this

reason, during warmup sequence, an adjustment factor ($F_{H,STB}$) is added to the normal operating auxiliary consumption. See Equation 24, where, $F_{H,STB} = 1.3$.

$$AUX_{H(normal)} = 0.6 MW_e \quad (23)$$

$$AUX_{H(warmup)} = AUX_{H(normal)} \cdot F_{H,STB} \quad (24)$$

During cloud transients, Zavoico (2001) reported that all the available heliostats are focused on the receiver. To achieve an outlet temperature of 510 °C, the HTF mass flow is maintained. However, the receiver model obtains only gross thermal power incident on the receiver. In the case of a cloud transient, the TMY data set, report a lower DNI value to the heliostat field model, subsequently calculating a lower gross thermal power input for the receiver model. Nonetheless, the auxiliary consumption for the heliostat field remains at 0.6 MW_e as all the available heliostats are in use. A cloud transient in the receiver model is recorded when the gross thermal power onto the receiver is less than the minimum gross thermal power required for normal operating conditions. It is determined by the weather prediction system whether to shut down the receiver or keep it warm till the cloud passes. The heliostats are stowed when the receiver is shut down. If sufficient solar energy is available, atleast 70 % of the minimum gross thermal power, the receiver is kept warm. In this scenario, selected heliostats are focused onto the receiver while others are in standby mode. The auxiliary consumption is conservatively assumed to be the same as normal operating conditions.

During receiver curtailment, selected heliostats focus on the receiver while others are set to standby mode. An adjustment factor ($F_{H,rec}$) is implemented to represent the auxiliary power consumption of the heliostats in operation. Similarly, when heliostats are defocused due to the maximum receiver flux limitations, the extra auxiliary consumption is accounted with an adjustment factor ($F_{H,limit}$). Therefore, auxiliary consumption for the heliostat field under these conditions is:

$$AUX_{H(warmup)} = AUX_{H(normal)} \cdot F_{H,Rec} \cdot F_{H,Limit} \quad (25)$$

3.8.2. Receiver Pump

The receiver pump auxiliary consumption is determined by the pressure drop in the tower riser and across the receiver. Pressure drop across the receiver is calculated as per Section 3.5.5 and Equation 19. The receiver flow configuration is a series of straight and bend tubes. This configuration with associated friction factors are adapted from Wagner, 2008. The turbulent flow present in the receiver is established from the HTF minimum design flow rate of 168 kg/s. With the HTF input and output temperatures at 288 °C, the resulting Reynolds number is 10,008, thus indicating a turbulent flow. The schematic diagram presented in Figure 31, illustrates the head loss associated with the receiver pump.

With turbulent flow established, Equation 20 from Section 3.5.6 is used to determine the friction factor in the receiver tubes. The following equations express the pressure drop in the receiver section (Crane, 1986):

$$\Delta P_{45} = \rho 16f \frac{V_{tube}^2}{2} \quad (26)$$

$$\Delta P_{90} = \rho 30f \frac{V_{tube}^2}{2} \quad (27)$$

$$\Delta P_{tube} = \rho f \frac{H_{rec}}{d_{i,tube}} \frac{V_{tube}^2}{2} \quad (28)$$

$$\Delta P_{panel} = 2\Delta P_{45} + 4\Delta P_{90} + \Delta P_{tube} \quad (29)$$

$$\Delta P_{rec} = \sum_{i=1}^n \Delta P_{panel,i} + g\rho_{HTF,hot}(2 + H_{rec}) \quad (30)$$

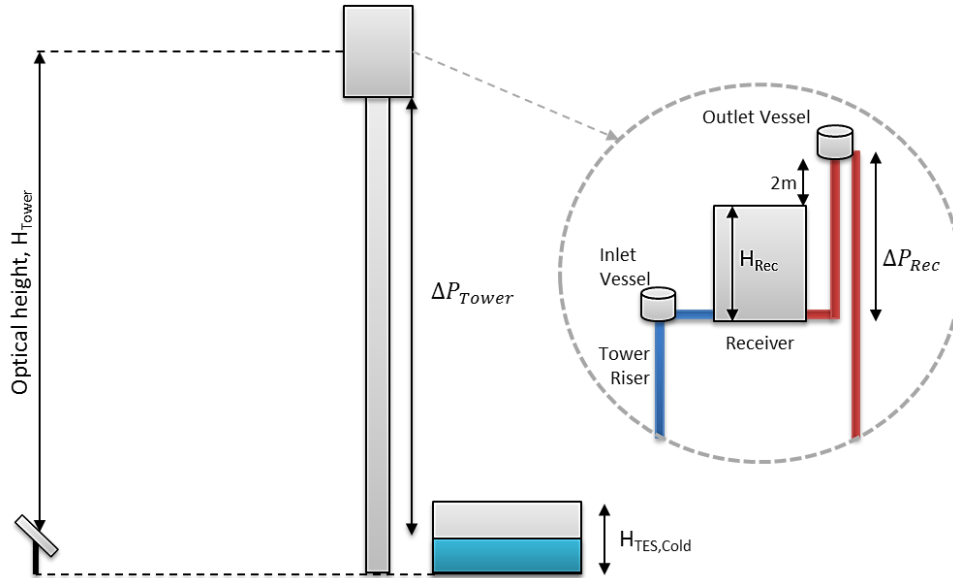


Figure 31: Head loss associated with the receiver pump

The receiver pump is a vertical turbine pump with Variable Speed Drive (VSD). It is located on the top of the cold molten salt tank. The shaft length of 20 m allows for suction directly from the salt tank. Therefore, the following equation is applicable before the molten salt is pumped up the tower riser:

$$\Delta P_{COLD, TES} = g\rho_{HTF,cold}H_{cold, TES} \cdot (1 - Full_{cold, TES}) \quad (31)$$

where, $Full_{cold, TES}$ represents the tank level in percentage. The optical height of the receiver is 208 m and the pressure drop in the tower riser can be expressed as follows:

$$\Delta P_{tower} = g\rho_{HTF,cold}(H_{tower} - H_{cold,TES} - 0.5H_{Rec}) \quad (32)$$

The inlet vessel, represented in Figure 31, is part of the receiver protection system. Although the simulation model SAM does not account for this protection mechanism, the pressure drop associated with the inlet vessel was taken into account to more accurately represent the case study plant. As reported in Table 15, the basic design of the case study plant accounted for the pressure drop in the inlet vessel with a factor of 1.456. The following table presents the parasitics associated with the receiver pump at design point, with and without the presence of the inlet vessel. The receiver inlet vessel pressure drop factor selected for the model was 1.33. Due to the difference in pressure drop calculations between the model and the case study plant basic design, the inlet vessel factor was reduced. Although a correlation between SAM and the model is observed, the inlet vessel factor also acknowledges the design and protection system of Solar-1.

Table 15: Receiver parasitics at design point

Parameter at DP	SAM	Solar-1	Model
HTF mass flow rate [kg/s]	1361	1361	1363
Receiver Pump [MW]	4.17	3.83	4.11
Receiver Pump with inlet vessel [MW]	NA	5.57	5.46
Factor	NA	1.456	1.330

Therefore, the total pressure drop associated to the receiver pump and corresponding auxiliary consumption expressed as:

$$\Delta P_{total} = (\Delta P_{COLD,TES} + \Delta P_{tower} + \Delta P_{Rec}) \cdot F_{inlet-vessel} \quad (33)$$

$$AUX_{rec,pump} = \frac{\dot{m}_{HTF} \cdot \Delta P_{total}}{\rho_{HTF,cold} \cdot \eta_{pump}} \quad (34)$$

Where, η_{pump} represents the efficiency of the receiver pump.

3.8.3. Hot TES Pump

Molten salt is pumped from the hot thermal energy storage tank to the steam generator. The pressure drop associated with the steam generator components and interconnecting piping is accounted for in the following correlation representing the auxiliary consumption of the hot TES pump:

$$AUX_{SGS} = (\dot{m}_{SGS} - 0.6)/1000 \quad (35)$$

3.8.4. Feedwater Heater Pumps

The parasitics associated with the power block is determined from the power block model. The following correlation represents the auxiliary consumption for all the feedwater pumps in the power block:

$$AUX_{PB} = 0.0144(P_{PB,gross} + 1.81) \quad (36)$$

3.8.5. Balance of Plant

The parasitics associated with the BoP as a function of the nameplate capacity of the power block. This is represented by the following correlation:

$$AUX_{BoP} = (46.945 \cdot P_{PB,gross} - 84.561)/1000 \quad (37)$$

3.8.6. Air Cooled Condenser

The Air Cooled Condenser (ACC) parasitics have been established during the development of the power block model. In order to achieve the required heat dissipation from the ACC, the airflow through it is controlled. The fans required to attain the desired airflow determine the auxiliary power for the ACC, and is expressed in the following equations:

$$\dot{Q}_{ACC} = \dot{m}_{air} C_{p,air} \Delta T \quad (38)$$

3.8.7. Fixed Parasitics

The fixed parasitics are represented by the following correlation. The correlation represents the auxiliary consumption of the entire plant regardless of the mode of operation.

$$AUX_{fixed} = 0.55 [MW_e] \quad (39)$$

4. MODEL RESULTS

A simulation model of the case study plant representing a digital prototype of the physical system has been developed. In order to appreciate the plant operations within the developed model, each system's performance is demonstrated under various boundary conditions. Within the heliostat field model, the sun's relative position to the heliostat and the receiver's efficiency results in the overall optical efficiency of the heliostat field. In case of the models for the receiver and the power block, the ambient conditions and heat transfer fluid inlet temperature contribute to the performance of the system. The following sections elaborate on each system's performance simulated under various boundary conditions.

4.1. Heliostat Field

The heliostat field model utilises 96 distinct points to represent the heliostat field performance and to infer the corresponding receiver flux map. The model determines the solar angles from the sun's current position and interpolates between the representing solar angles associated with the 96 points. Therefore, the performance curve of the heliostat field is conveyed as the optical efficiency of the heliostat field in relation to the solar angles throughout the year. The heliostat field optical efficiency as a function of solar angles, zenith and azimuth, is represented in Table 16. The azimuth angle at zero degrees represents true North.

These optical efficiencies are only applicable to geographical location and field design off the case study plant. The zenith angle has a greater effect on the heliostat field optical efficiency than the azimuth angle, as noted from the Table 16. The heliostat field has a circular layout and mirrored around 180°, i.e. from East to West. Therefore, as the sun moves across the sky from East to West, the optical efficiency associated with the azimuth angle stays relatively the same. That is if the sun would have moved horizontally across the sky, the zenith angle remains the same. This is due optics in ray tracing and the corresponding incoming angles. As the optics involved with the zenith angle has a greater effect on the optical efficiency of the field, it is considered to represent the heliostat field's performance curve (see Figure 32).

Table 16: Heliostat field efficiency as a function of the solar angles

		Azimuth Angle											
		0°	30°	60°	90°	120°	150°	180°	210°	240°	270°	300°	330°
Zenith Angle	0.5°	49.5	49.5	49.5	49.5	49.5	49.5	49.5	49.5	49.5	49.5	49.5	49.5
	7°	49.3	49.3	49.3	49.3	49.2	49.2	49.2	49.2	49.2	49.3	49.3	49.3
	15°	48.6	48.6	48.5	48.5	48.5	48.4	48.4	48.4	48.5	48.5	48.5	48.6
	30°	47.4	47.4	47.3	47.2	47.2	47.1	47.1	47.1	47.2	47.2	47.3	47.4
	45°	46.1	46.0	45.9	45.8	45.7	45.6	45.6	45.6	45.7	45.8	46.0	46.0
	60°	42.8	42.8	42.6	42.5	42.3	42.2	42.2	42.3	42.4	42.6	42.7	42.9
	75°	32.9	32.9	32.7	32.5	32.3	32.2	32.3	32.4	32.5	32.7	32.9	33.1
	85°	19.9	20.0	19.8	19.6	19.5	19.4	19.4	19.6	19.8	19.9	20.1	20.2

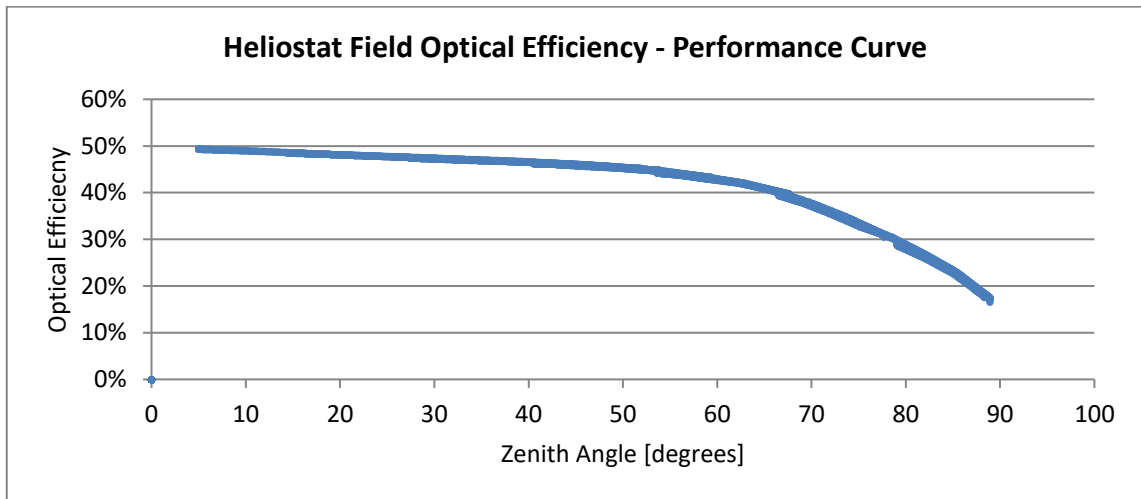


Figure 32: Heliostat field optical efficiency in relation to the zenith angle

4.2. Receiver Thermographic and Colormap Representation

The detailed thermographic and colormap representations of the receiver, highlights the importance of the heliostat field’s aiming strategy. The aim of the thermographic and colormap representations is to assist the plant operator in making informed decisions regarding the receiver operations and heliostat field aiming strategy. The thermographs emphasise the relationship between the receiver’s design, its configuration and incident flux distribution onto the receiver. Various operational and design interpretations can be made about the receiver’s design and configuration using these results.

The thermographs and colormaps are obtained by the methodology followed for the receiver model development which is discussed in Section 3.5 (De Meyer *et al.*, 2015). Through an iterative process, the heat transfer fluid mass flow rate, inner tube and surface temperatures are calculated from the incident flux map, ambient conditions and heat transfer fluid inlet temperature. The corresponding thermal losses are obtained and the receiver efficiency is determined. The receiver’s thermographic and colormap representation further provides a useful tool in tube strain analysis and receiver design considerations. For illustrative purposes, the following results have been obtained for the case study plant’s receiver operating at design point on the noon of 21 March. The following figures are the resulting thermographs and colormaps of the receiver: Figure 33(a) incident flux map, Figure 33(b) the receiver efficiency, Figure 33(c) the resulting surface temperatures and Figure 33(d) the corresponding inner tube temperatures. Thermal losses, radiation and convective heat loss are represented in Figure 33(e) and Figure 33(f) respectively.

The thermographs and colormaps rendered attainable through the accompanying Receiver Model, are serving a supplementary purpose to the plant operator. These graphs are not used and analysed in the model. They provide a graphical overview of the operation of the receiver. These graphs offer similar functionality as the heat and mass balance diagrams demonstrating the operation of a Rankine cycle in the power block.

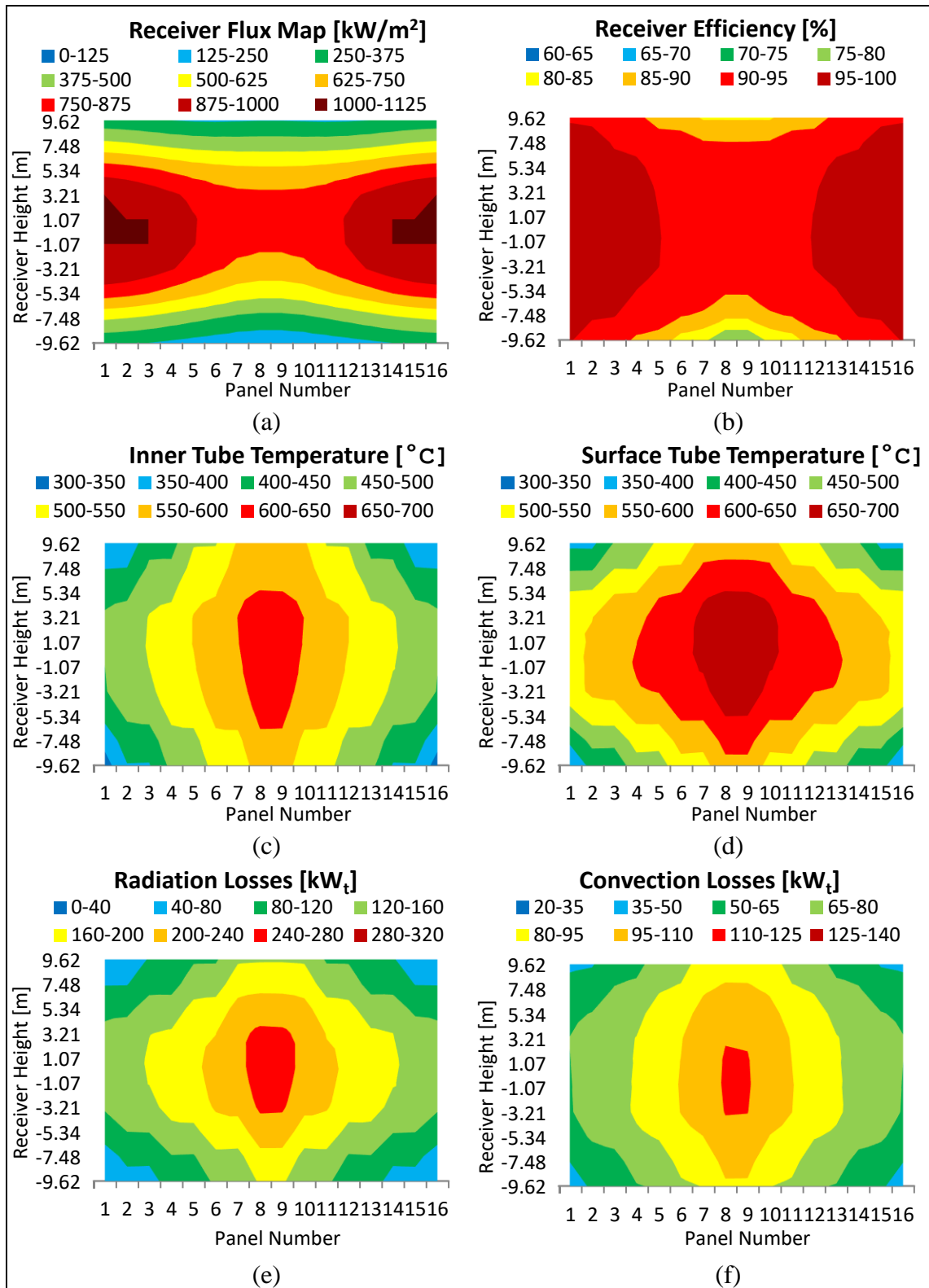


Figure 33: Receiver thermographic and colormap representation a) DELSOL3 incident flux map (b) receiver efficiency (c) panel inner tube temperatures (d) receiver surface temperatures (e) radiation losses (f) convective losses

In order to fully understand the representations of the thermographs and colormaps, the receiver flow regime and panel configuration should be considered. Recalling Figure 23, the receiver serpentine flow regime and cross over flow halfway is applicable. The thermographs and colormaps present the 16 panels of the receiver on the x-axis with the receiver's height on the y-axis. The HTF enters the receiver from the south side, through Panels 1 and 16, and exit the receiver from the north side, through Panels 8 and 9.

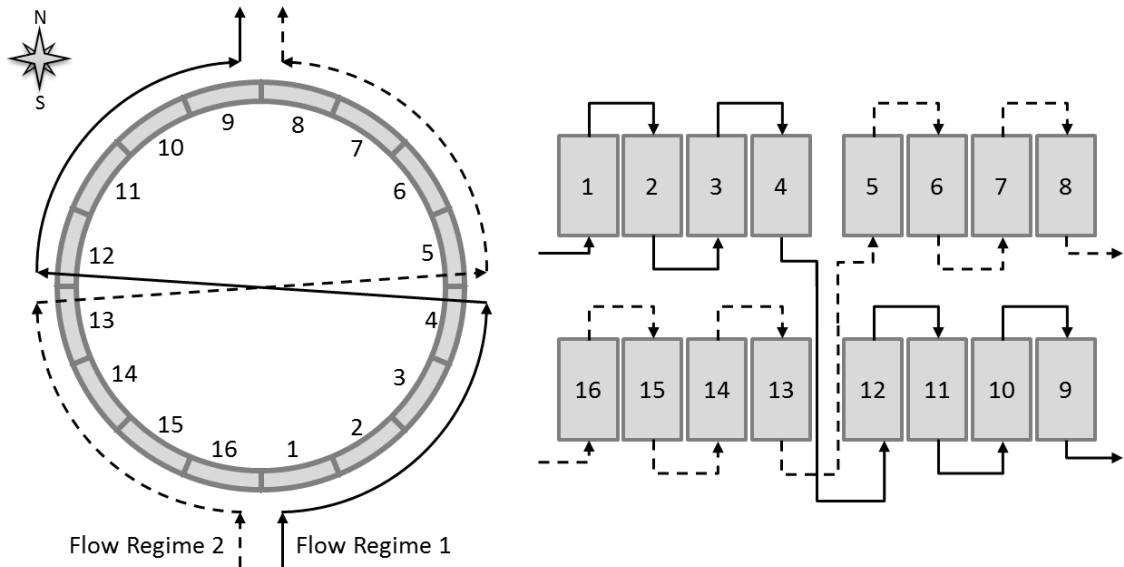


Figure 23: Receiver serpentine flow regimes with cross over flow halfway.

Two days are considered to compare and further express the operation of the receiver. The first day was 1st of January. It was a summer day where high DNI is observed with relatively high ambient temperatures and low wind speeds. The second day considered was the 1st July which represents a winter day where lower DNI is observed with low ambient temperatures and higher wind speeds. The solar angles analysed are selected at 08h00, 12h00 and 16h00. At noon, the incident flux distribution on the receiver is almost symmetrical around the receiver, as illustrated in Figure 33(a). Thus, flow regime 1 and flow regime 2 receive equal amounts of thermal energy. This results in similar temperature profiles, Figure 33(d), and thermal loss representations, Figure 33(e) and Figure 33(f). Therefore, emphasis is placed on the solar angles at 08h00 and 16h00 to demonstrate the effect of more incident flux on one of the two flow regimes. Furthermore, the effect of the ambient temperatures, wind speeds and DNI on the receiver are explored.

4.2.1. Receiver Flux Map

As the sun rises in the east, the heliostats on the west side of the receiver, intercepts the incoming sunrays the best. This means that minimal optical loss takes place from the heliostat to the point of focus on the receiver. When Figure 34(left) is considered, a higher concentration of incident flux is observed on the west side of the receiver, Panels 9-16. Similarly, the same phenomenon is observed in the afternoons when the sun sets in the west, with higher incident flux on the east side of the receiver, Figure 34 (right). The

resulting incident flux distribution on the receiver is influenced by the amount of DNI bestowed onto the heliostat field and the solar angle. On the 1st of January, the average DNI at 08h00 and 16h00 is 1,022 W/m² and 1,042 W/m², respectively. The flux limit of 1,000 kW/m² on the receiver's surface is accounted for 0.92 % and 1.28 %. Subsequently, the energy dumping occurred at 08h00 and 16h00. Since the DNI is similar for both the above mentioned times, the flux maps obtained are almost similar in size and shape. However, when the DNI changes, the incident flux map changes in shape and size. This is illustrated in Figure 35. On 1st of July, the average DNI at 08h00 and 16h00 is 308 W/m² and 439 W/m², respectively. The flux limit was not reached in this case. Therefore, the energy dumping was not induced. The differences between the two flux maps are noted in the size and concentration of incident flux. Since, the same heliostat field aiming strategy was implemented, the solar angles determine the shape of the incident flux distribution, whereas the amount of DNI determines its size.

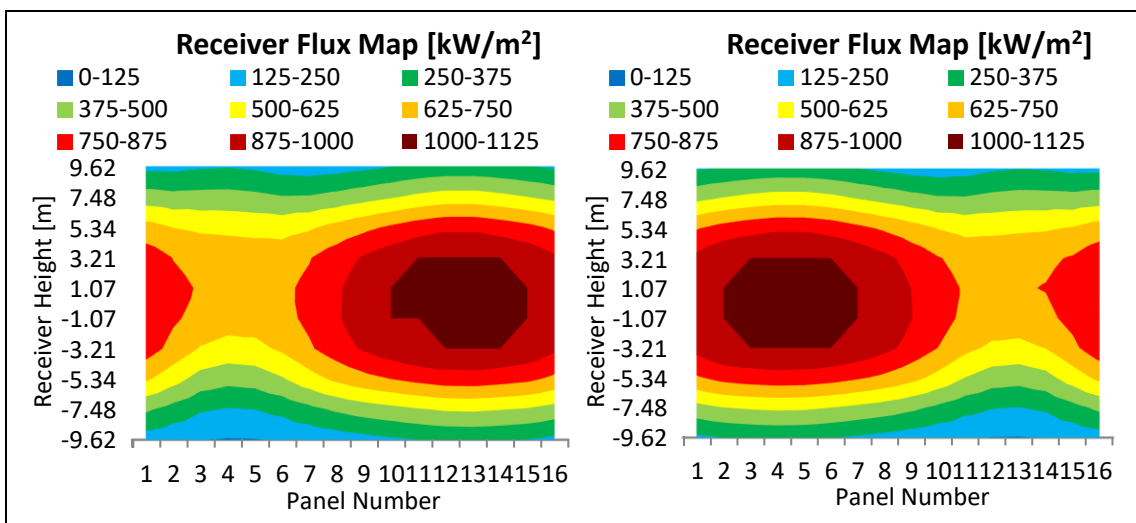


Figure 34: Receiver incident flux map on 1st January at 08h00 (left) and 16h00 (right)

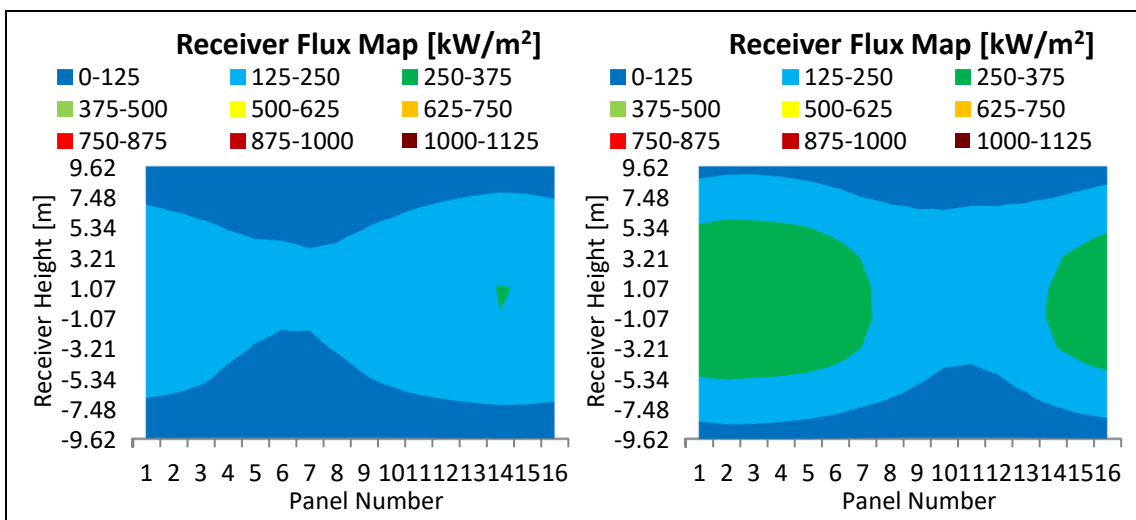


Figure 35: Receiver incident flux map on 1st July at 08h00 (left) and 16h00 (right)

4.2.2. Surface Tube Temperature

The surface temperature of the receiver is probably the most important variable measured in the receiver operations. To avoid the operation outside the designed flux temperatures and since no direct method for measuring the incident flux on the receiver is available, surface temperatures of the receiver are measured. This is achieved by using thermocouples in the receiver tube wall as well as in the thermographic cameras. In order to determine the incident flux applied, an indirect method involving the mathematical calculations using the receiver surface temperatures as input is done. This approach is similar to the developed receiver model in this research. However, in the receiver model, the incident flux on the receiver is known and the surface temperatures are determined. The receiver's tube surface temperatures are represented in Figure 36. It is noted that there is a relationship between the incident flux on the receiver and its surface temperature. The highest surface temperatures are observed where the HTF exits, that is Panels 8 and 9 where the HTF temperatures are around 565 °C. The mid-section of the receiver had the highest temperature. This is because of the presence of higher incident flux in this location than the outer sides. The effect of the HTF temperature on the surface temperature is observed in Panel 12, where 'colder' molten salt from the east side of the receiver with less incident flux, is crossed over to the west side of the receiver with higher incident flux side.

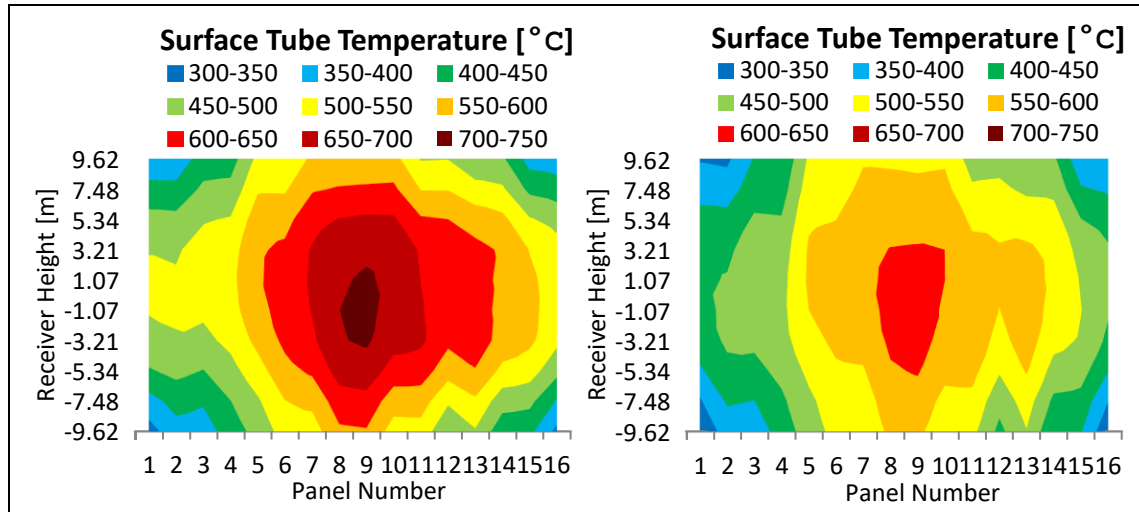


Figure 36: Surface tube temperatures at 08h00 on 1st January (left) and 1st July (right)

4.2.3. Radiation Losses

The radiation losses are dependent on the surface temperature and sky temperature. This is expressed in Equation 40. Therefore, higher thermal energy losses due to radiation are expected where surface temperatures are high. The radiation losses in Figure 37 correlate with the surface temperatures in Figure 36.

$$\dot{Q}_{rad(ext)} = \varepsilon\sigma(T_s^4 - T_{surr}^4)A_s \quad (40)$$

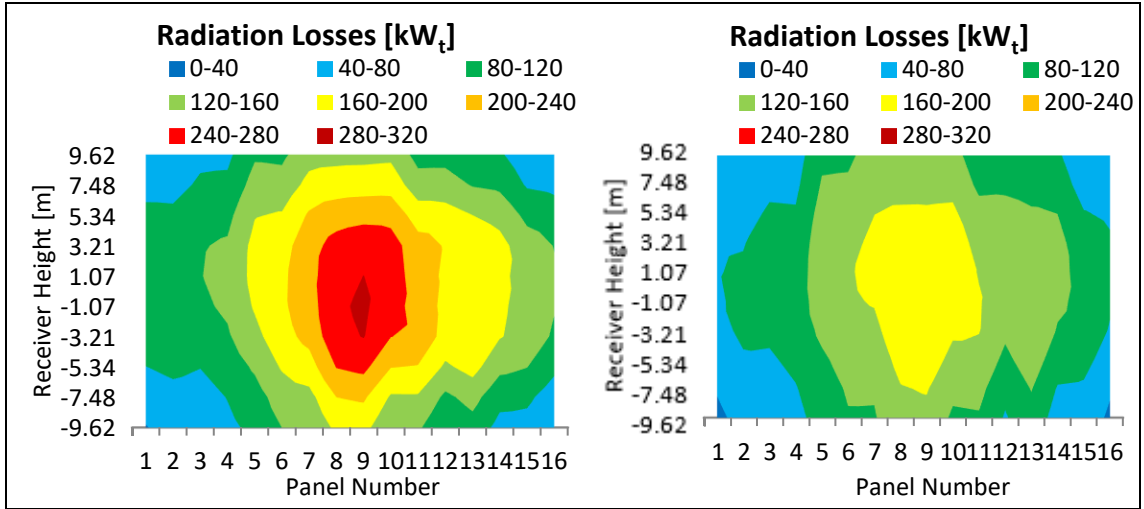


Figure 37: Radiation losses at 08h00 on 1st January (left) and 1st July (right)

4.2.4. Convection Losses

The convective heat transfer, represented by Equation 41, is influenced by two factors, the ambient temperature and the wind speed. The effects of the wind speed are captured in the heat transfer coefficient ($h_{conv(ext)}$). In order to illustrate the effects of wind on the receiver, colormaps with similar surface temperatures are used for comparison. The average surface temperature of the receiver at 08h00 and 16h00 on 1st of January is 545 °C. However, ambient temperatures are 20.9 °C and 32.7 °C, with wind speeds of 3.1 m/s and 5.9 m/s, respectively. The resulting heat transfer coefficients under these conditions are 23.2 W/m² and 25.8 W/m². The convective heat loss at 08h00 is 12 MW_t and at 16h00 is 13.1 MW_t. Therefore, the effect of wind speed on the convective heat loss is more visible than its effect on the temperature difference. It is illustrated in Figure 38.

$$\dot{Q}_{conv(ext)} = h_{conv(ext)}(T_s - T_{amb})A_s \quad (41)$$

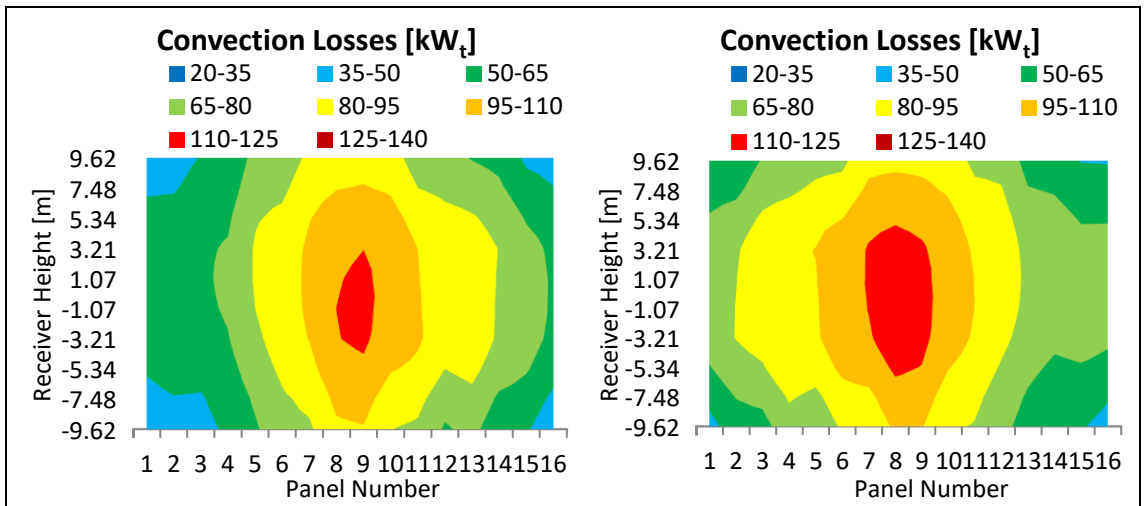


Figure 38: Convection losses on 1st January at 08h00 (left) and 16h00 (right)

4.2.5. Receiver Efficiency

The receiver efficiency is a representation of the relationship between the incident flux on the receiver and the thermal energy transferred to the HTF. Under any given circumstance, the range of the HTF temperature remains relatively the same. Therefore, higher surface temperatures are always expected at the last panels where the HTF exits the receiver. It has been noted in Figure 36 that surface temperatures increase amongst higher incident flux. Therefore, high surface temperatures results in higher thermal losses. However, the thermal losses fluctuate around the same magnitude due to the surface temperatures increasing or decreasing only marginally as a result of change in the incident flux. It is for this reason that higher receiver efficiencies are observed where high incident flux concentrations are present. Hence, the effect of thermal losses is minor. The receiver's efficiency reduces when lower DNI is received by the heliostat field or when the incident flux is low on the receiver.

Considering Figure 39, it is clear that lower receiver efficiencies are reported where the incident flux concentrations are low and thermal losses are high, i.e. higher surface temperatures. Figure 33(b) showed higher DNI resulting in a higher overall receiver efficiency, whereas in Figure 39 lower DNI values resulted in a low overall receiver efficiency.

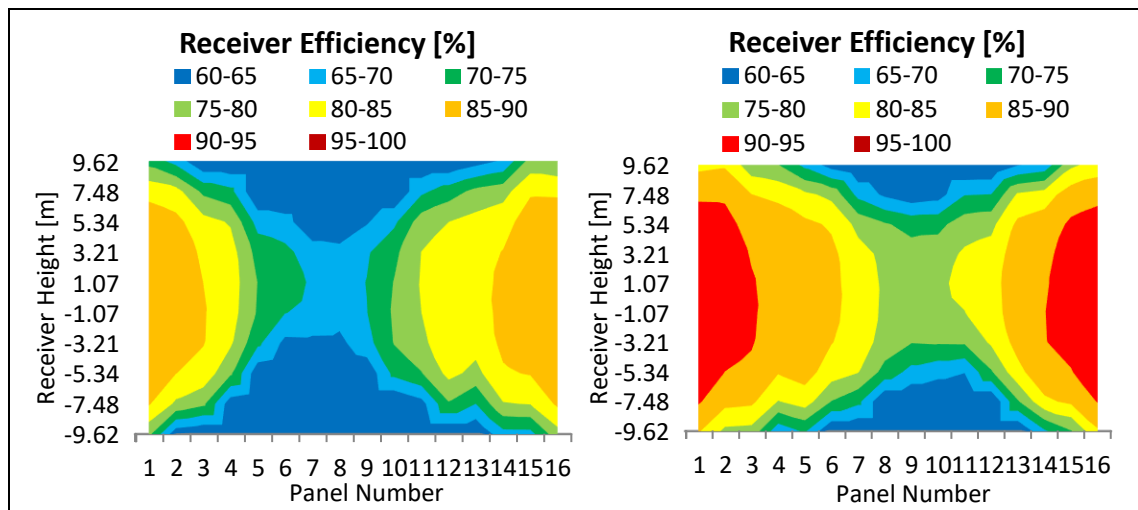


Figure 39: Receiver efficiency on 1st July at 08h00 (left) and 16h00 (right)

4.2.6. Heat Transfer Fluid Temperatures

The HTF is effectively a cooling mechanism of the receiver. By the means of forced convection, that is the receiver pumps ‘cold’ molten salt through the receiver, heat transfer from the receiver to the HTF occurs. The mass flow rate of the HTF is controlled to achieve the desired temperature of 565 °C at the receiver's exit. Therefore, the HTF mass flow rate has a direct relationship with the level of incident flux concentrated on the receiver. On 1st of January at 08h00, the thermal energy transferred to the HTF was 563 MW_t, resulting in total mass flow rate of 1345 kg/s. The thermal energy transferred

to the HTF on 1st of July at 08h00 was 97.5 MW_t, resulting in a total mass flow rate of 233 kg/s. The temperature rise in the HTF is illustrated in Figure 40 for both the days. It is interesting to note the effect of the cross over flow from Figure 40(right). The cross over flow, for flow regime 1, occurs between Panels 4 and 12. The ‘colder’ HTF fluid enters Panel 12 where ‘hotter’ HTF exits Panel 13. Higher concentration of incident flux is present on Panels 13-16 in comparison to the Panels 1-4, as illustrated in Figure 35(left). Therefore, the temperature rises in flow regime 2, i.e. HTF entering from Panel 16 and crossing over at Panel 13, is faster as in flow regime 1.

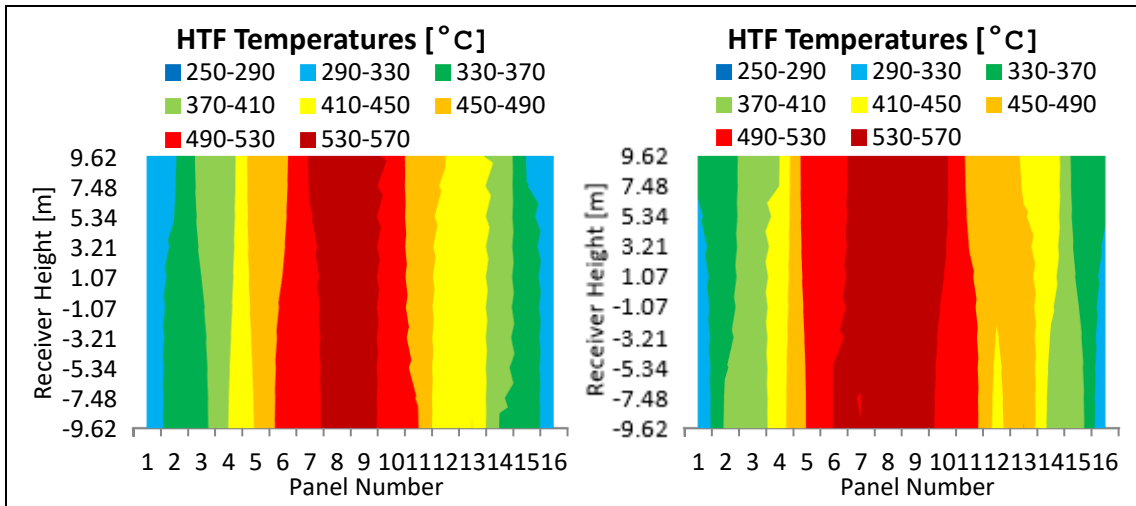


Figure 40: HTF temperatures at 08h00 on 1st January (left) and 1st July (right)

4.2.7. Inner Tube Temperature

The inner tube temperatures represented in Figure 41, present similarities between the surface temperatures in Figure 36 and HTF temperatures in Figure 40. The inner tube temperatures play a significant role in tube strain analysis.

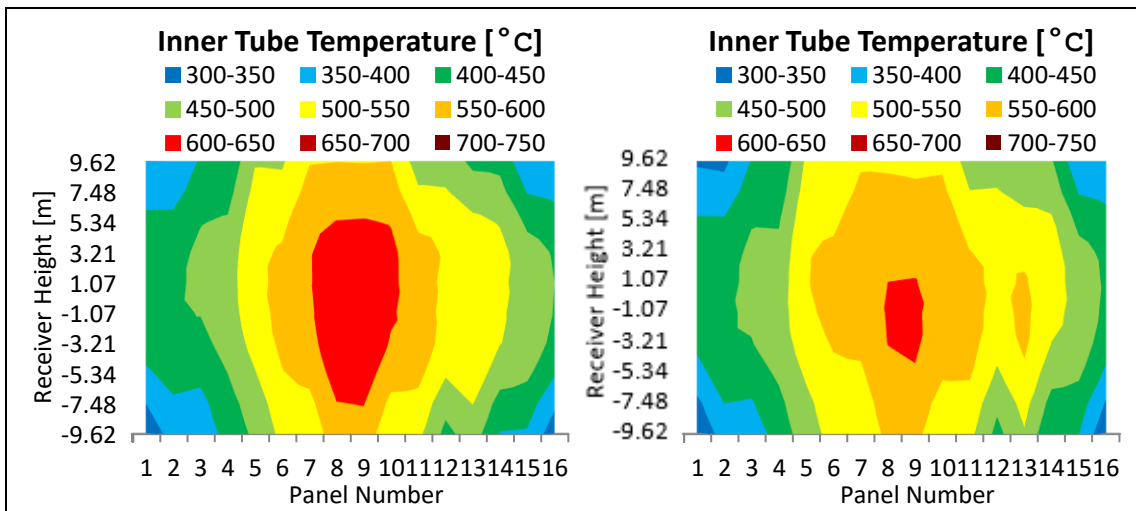


Figure 41: Inner tube temperatures at 08h00 on 1st January (left) and 1st July (right)

4.2.8. Tube Thermal Strain

In the receiver operation and maintenance, tube strain analysis is of particular interest. The receiver panels have been designed to undergo a number of thermal stress cycles in their lifetime. By inducing excessive or additional thermal strain on the receiver panel, thermal fatigue is increased, and ultimately the lifetime of the panel is reduced. Utilising thermal strain analysis, the aiming strategy of the heliostats can be adopted to redistribute the flux in the event when the recorded thermal strain exceeds design recommendations. It is suspected that areas with high surface temperatures would result in high thermal strain. However, as illustrated in Figure 36 and Figure 41, areas with high surface temperatures have an underlying high inner tube temperature, resulting in lower thermal strain as shown in Figure 42. Therefore, high surface temperatures do not necessarily lead to higher tube's thermal strain. From the tube thermal strain analysis, the panels where HTF enters the receiver are subjected to a higher thermal strain, resulting in a lower inner tube temperature with higher surface temperatures. The thermal strain further increases in magnitude with an increase in incident flux. This is due to the rise in the temperature of the receiver's surface while the inner tube temperature stays relatively in the same magnitude, i.e. marginal increase.

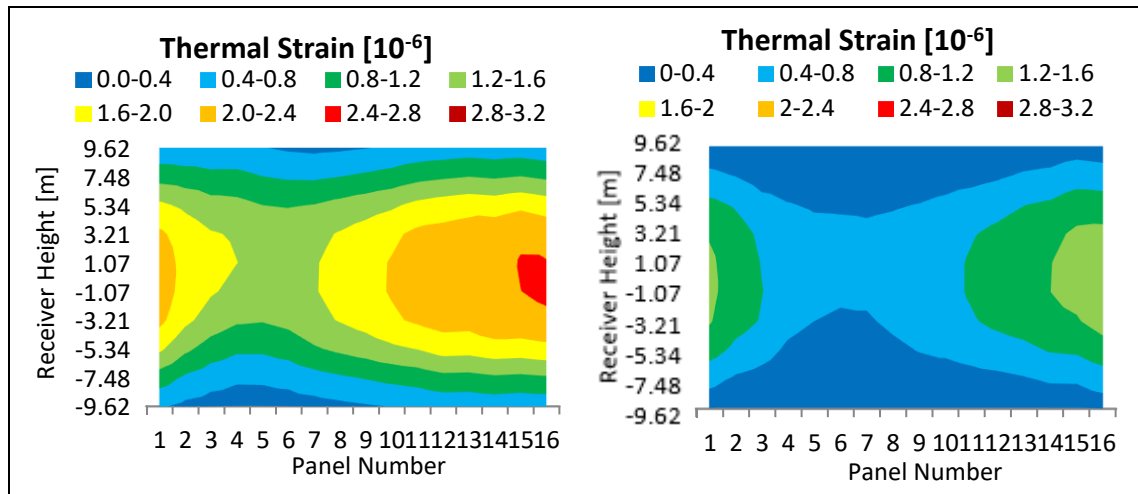


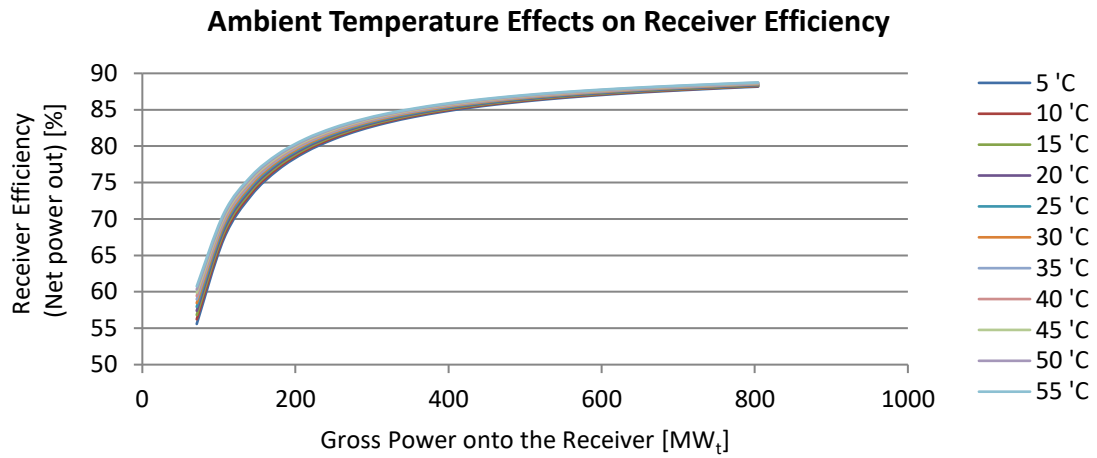
Figure 42: Tube strain analysis at 08h00 on 1st January (left) and 1st July (right)

4.3. Receiver Performance Curve

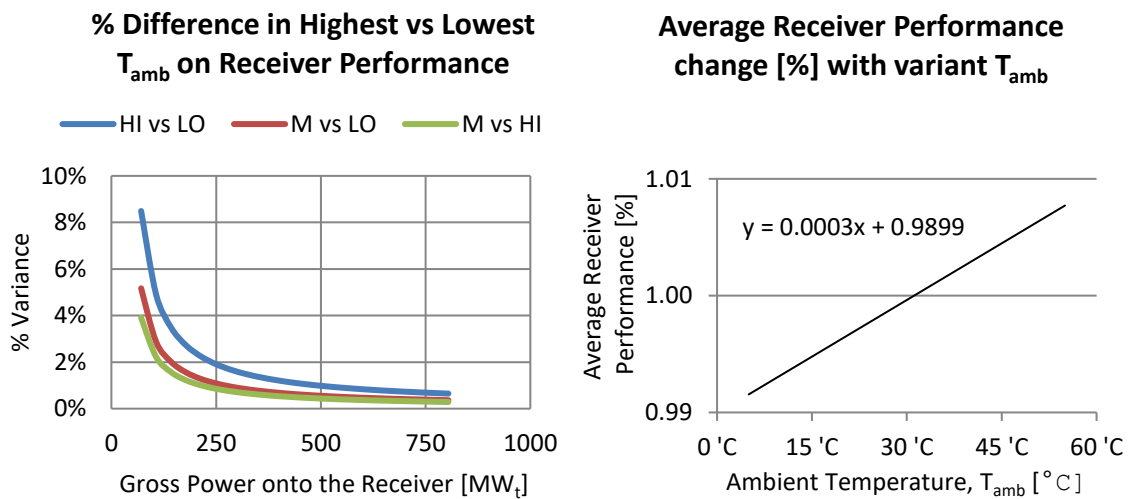
4.3.1. Constant Wind Speed, Variant Ambient Temperatures

The effects of the ambient temperature on the receiver's efficiency with no wind speed were simulated. The results are presented below in Figure 43(a). The variances between the highest (HI) and the lowest (LO) temperatures are presented in Figure 43(b). The variance in the receiver's performance is observed to be less than 3-5 % for low incident flux onto the receiver. The performance at 30 °C is taken as reference. The variance between the high-and-low temperatures to the reference is less than 2 % for low incident

flux on the receiver, and less than 0.5 % for the higher-end spectrum. Thus, the reference ambient temperature for the receiver performance is taken at 30 °C (Figure 43(c)).



(a)



(b)

(c)

Figure 43: (a) Ambient temperature effects on the receiver efficiency, no wind speeds
 (b) Correlation between the highest and lowest ambient temperature effect.
 (c) Average receiver performance with regards to ambient temperature

4.3.2. Wind Speed Effects

The various wind speeds, at reference ambient temperature of 30 °C, and their effects on the receiver efficiency were simulated. The results are presented in Figure 44(a). The variances between the highest (HI) and lowest (LO) wind speed are presented in Figure 44(b). A high variance in receiver's performance is observed at high wind speeds and low incident flux onto the receiver. When the reference wind speed is taken as 3 m/s, the variance between the high wind speeds and reference wind speeds were reduced slightly, that is less than 5 % for low incident flux onto the receiver. Whereas the low

wind speeds are less than 2 % for low incident flux on the receiver, and less than 0.2 % for the higher-end spectrum. Thus, the reference wind speed for the receiver performance is taken at 3 m/s (see Figure 44(c)).

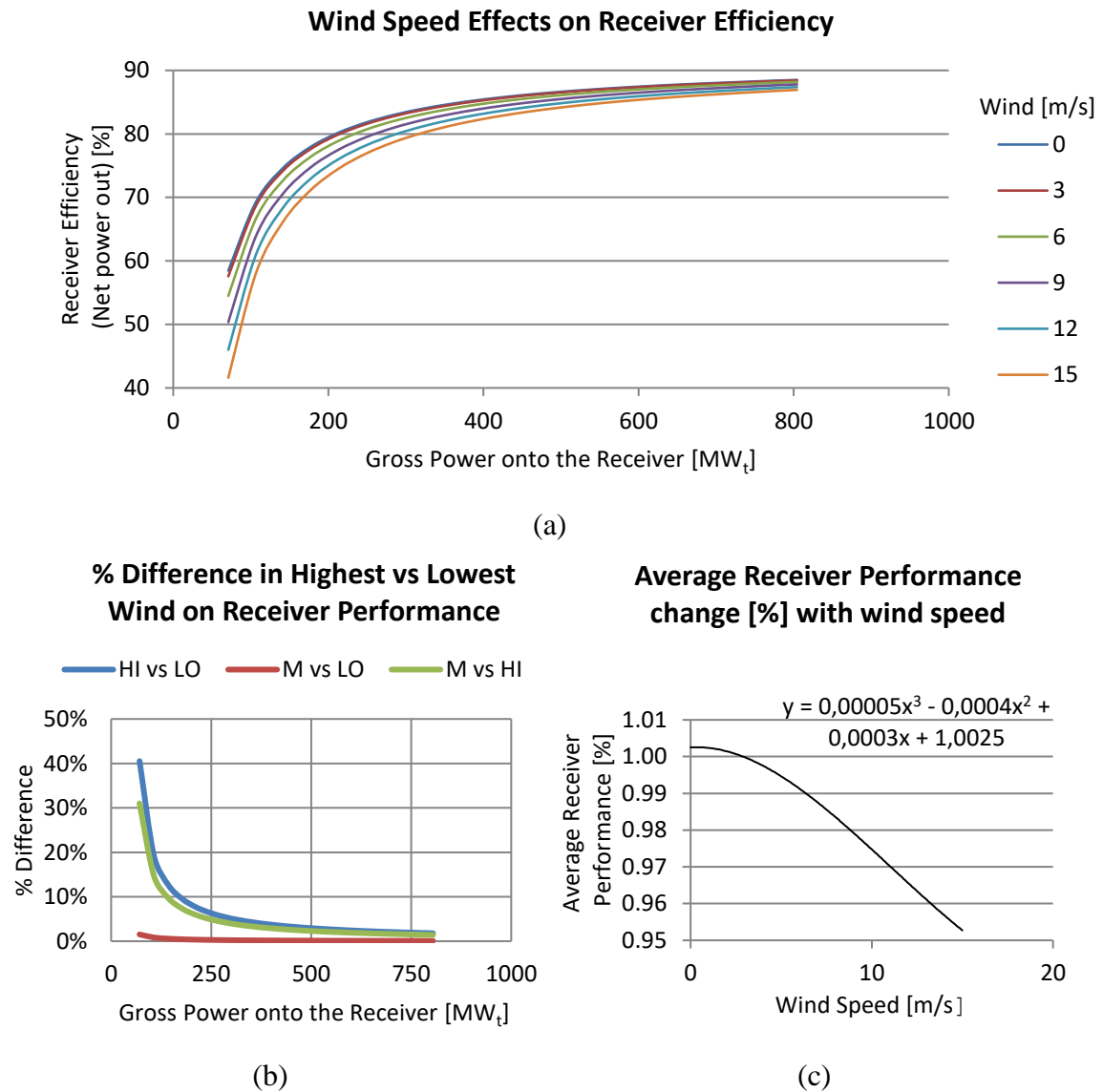


Figure 44: (a) Wind speed effects on the receiver efficiency, at reference temperature
 (b) Correlation between the highest and the lowest wind speed effects
 (c) Average receiver performance with regards to wind speed

A sensitivity analysis was performed under the reference wind speed conditions. Simulating the receiver performance subjected to various wind speeds as illustrated in Figure 45(a), a very high variance in receiver performance is observed with very high wind speeds of 9-15 m/s. However, this only occurred at very low incident flux onto the receiver. When the receiver's performance is analysed at the higher-end spectrum, the effects of wind speeds on the receiver efficiency are reduced to less than 2.5 %. This is reproduced in Figure 45(b). The hourly occurrences of various wind speeds throughout

the year were investigated, and is illustrated in Figure 46. The reference wind speed occurred more frequently, when these wind speeds were coupled with the available DNI. In the high variance of receiver performance, observed at higher wind speeds, the occurrence account less than 0.02-1 % of the time.

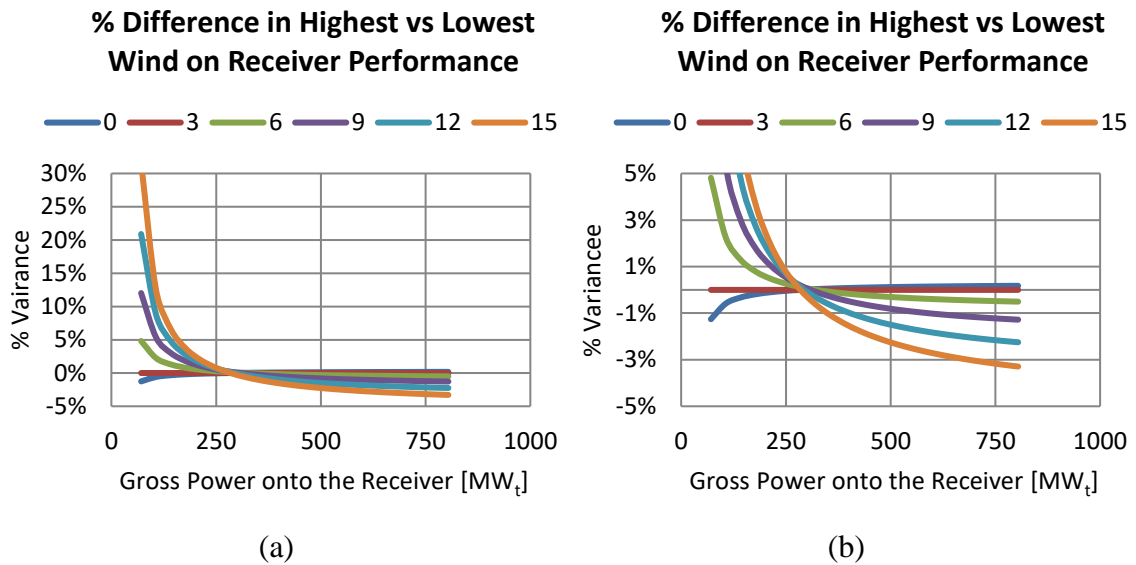


Figure 45: (a) Ambient temperature effects on the receiver efficiency, no wind speeds (b) Correlation between the highest and lowest ambient temperature effects.

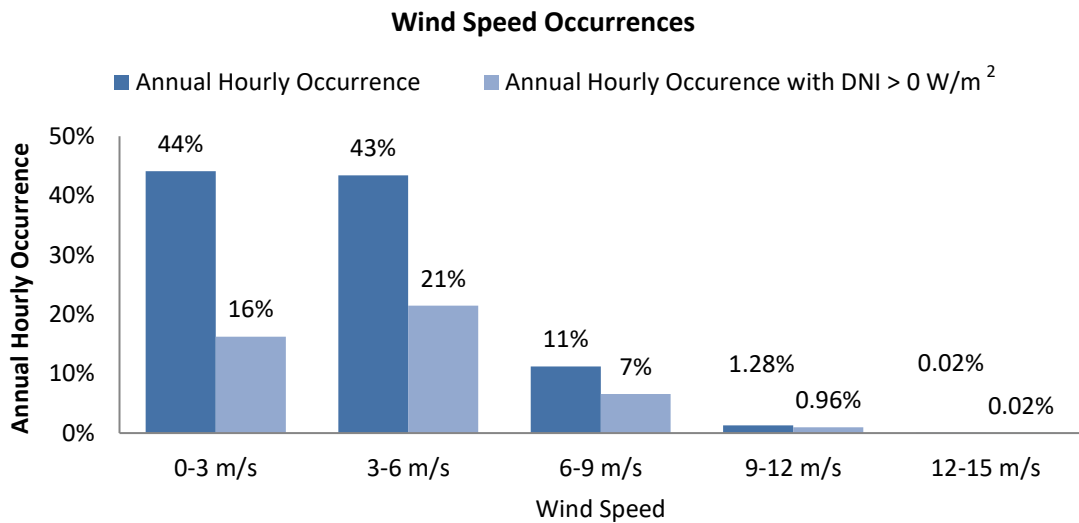


Figure 46: Annual wind speed occurrences

The following equations represent the receiver's performance. The effects of ambient temperatures are represented in Equation 42, whereas the effects of various wind speeds are represented in Equation 43. The receiver's efficiency is represented by Equation 44 and Equation 45 with the corresponding heat transfer fluid mass flow rate obtained through Equation 46.

$$\eta_{T_{amb}} = 0.0003 \cdot T_{amb} + 0.9899 \quad (42)$$

$$\eta_{wind} = 0.00005 \cdot wind^3 - 0.0004 \cdot wind^2 + 0.0003 \cdot wind + 1.0025 \quad (43)$$

$$\dot{Q}_{in,HTF} = P_{gross} \cdot \eta_{T_{amb}} \cdot \eta_{wind} \quad (44)$$

$$\eta_{rec} = \frac{\dot{Q}_{in,HTF}}{P_{gross}} \quad (45)$$

$$\dot{Q}_{in,HTF} = \dot{m}C_{p,HTF}(T_{o,HTF} - T_{i,HTF}) \quad (46)$$

4.4. Power Block Performance

The design parameters of the power block are fixed at the design point. By changing the operating parameters of the power block, the performance changes accordingly. The thermal energy supplied to the SGS from the hot storage tank affects the turbine power output, and it resulted in Figure 47 (left). When the thermal energy is reduced on the steam generator, the output of the turbine is reduced, making part-load operations achievable. The power block performance curve is a power block efficiency vs turbine output curve is shown in Figure 47 (right). Furthermore, the steam generator system's heat transfer fluid output temperature is presented in Figure 48 (left). The thermal energy supplied to the steam generator system in relation to the power block efficiency is presented in Figure 48 (right).

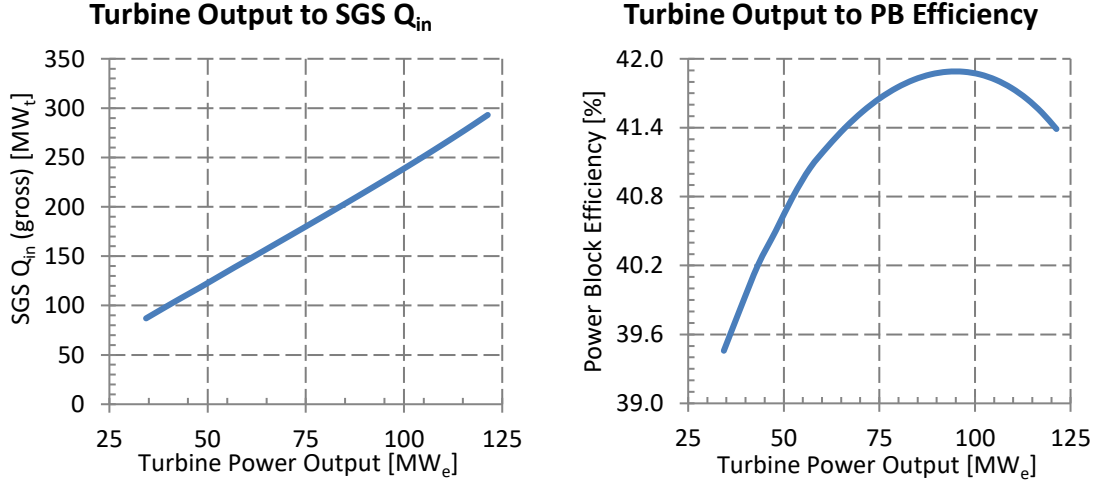


Figure 47: (left) Turbine output, thermal energy supplied to steam generator system (right) Power block performance curve

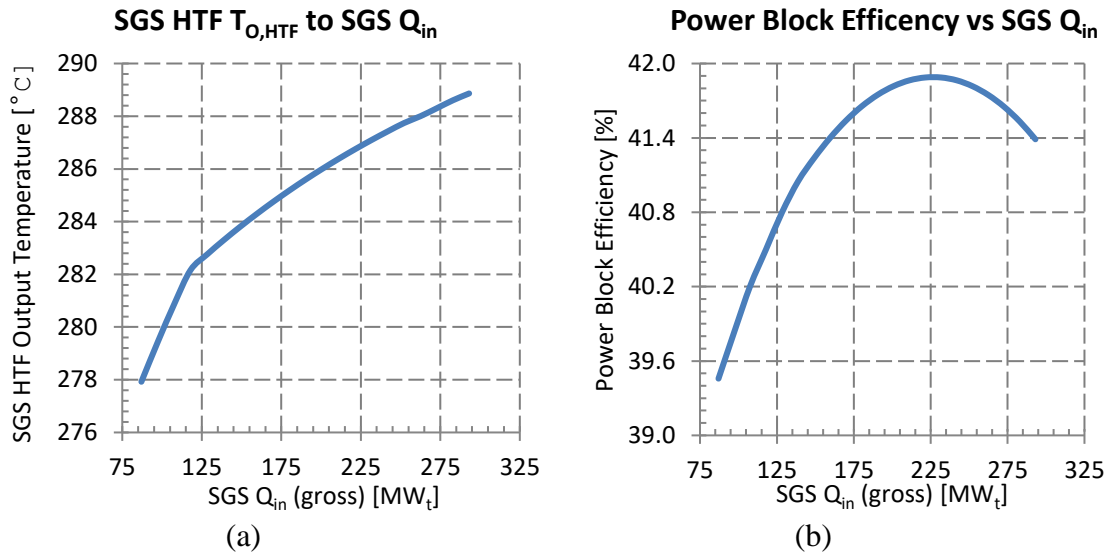


Figure 48: (a) Steam generator system's heat transfer fluid output temperature effects
(b) Power block performance curve w.r.t. thermal energy supplied

The effects of the ambient temperature on the performance of the power block are considered and presented in Figure 49. The Initial Temperature Differential (ITD) of the ACC influences the performance of the turbine. The ITD of the case study plant's ACC is set at 20 °C. The effects of the ITD on the turbine's performance are illustrated in Figure 49 (left) and Figure 49 (right). The linear relationship between the ambient temperature and turbine power output is due to the optimisation within the power block under various ambient conditions (Wagner, 2008).

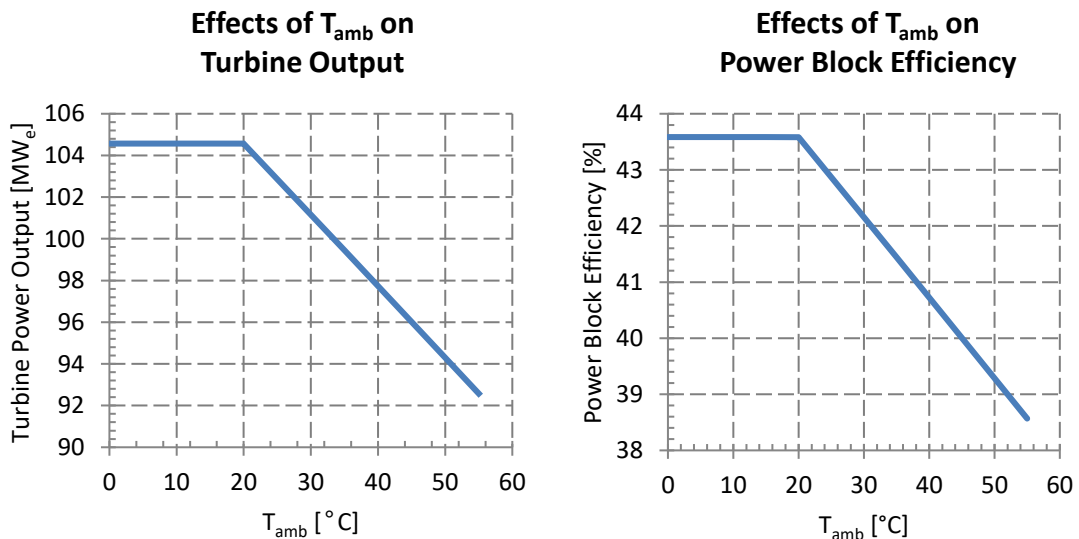


Figure 49: (left) Steam generator system's HTF output temperature effects
(right) Power block performance curve w.r.t. thermal energy supplied

The following equations represent the power block performance. The power block performance at design point with ambient temperature at 32 °C, is represented by Equation 47. The effect of the ambient temperature on the power block performance is represented by Equation 48.

$$P_{PB@DP} = 0.4256 \cdot \dot{Q}_{in,SGS} - 2.0873 \quad (47)$$

$$\eta_{T_{amb}} = 1.109 - 0.0034 \cdot T_{amb} \quad (48)$$

where $T_{amb} \geq 20$ °C and $\eta_{T_{amb}} = 1.041$ for $T_{amb} < 20$ °C. Thus, the power block performance can be represented by Equation 49 and Equation 50.

$$P_{PB} = P_{PB@DP} \cdot \eta_{T_{amb}} \quad (49)$$

$$\eta_{PB} = \frac{P_{PB}}{\dot{Q}_{in,SGS}} \quad (50)$$

5. MODEL VALIDATION

It is important to have the developed model validated against other commercially available software and tools. Although these models and tools could not satisfy the objective requirements of this research, their functionality and results have been tested, interrogated and generally accepted within the industry. The first and foremost commercially available software package used for validation is SAM (SAM, 2014). SAM is a performance and financial model for renewable energy power systems and projects (De Meyer *et al.*, 2014). It is used to derive an estimate of cost of energy to the grid-connected power plants or projects. The predictions are made on the basis of the installation and operating costs that are associated with user-specified system design parameters. SAM also interfaces with the models developed by NREL, Sandia National Laboratories, the University of Wisconsin and other organisations to represent the cost and performance of the project. DELSOL3 or the PTGen code developed by Wagner (2008), interface with SAM for optimising the heliostat field layout and tower height, subsequently calculating the heliostat field performance required for the plant simulation. The receiver performance is based on the methodology developed and implemented by Wagner (2008). Furthermore, the power block performance is determined using the power block interfaces with TRNSYS.

SAM is recognised by the solar industry. Its heliostat field, receiver and power block performances are used for validating the currently developed model. The plant design parameters used in developing the model are applied in SAM to replicate the case study plant. In both the cases, the validation was carried out using the same TMY data. The heliostat field, receiver and power block performance are further correlated with the basic design documentation of the Eskom 100 MW_e CSP project (Eskom, 2012a).

5.1. Heliostat Field Model

The SAM replica model was used to obtain the optical efficiency of the heliostat field throughout the year. The optical efficiency of the heliostat field is determined by the sun's position, i.e. the solar angles relative to the heliostat and tower. Therefore, the optical efficiency of the heliostat field was plotted against the sun's position, the zenith angle. The correlation between SAM and the heliostat field model is presented in Figure 50. The annual results of both the models display a good comparison in terms of optical efficiency. The results from the SAM model showed various isolated points under the trend line. When the hot TES reaches its full capacity, curtailment of the receiver occurs. This explains the isolated points observed in the results. This phenomenon is illustrated in Figure 51. However, the optical efficiencies of the developed heliostat field model represented in Figure 50 are taken in isolation. The simulation results do not account for the effect of receiver curtailment or receiver flux limitations.

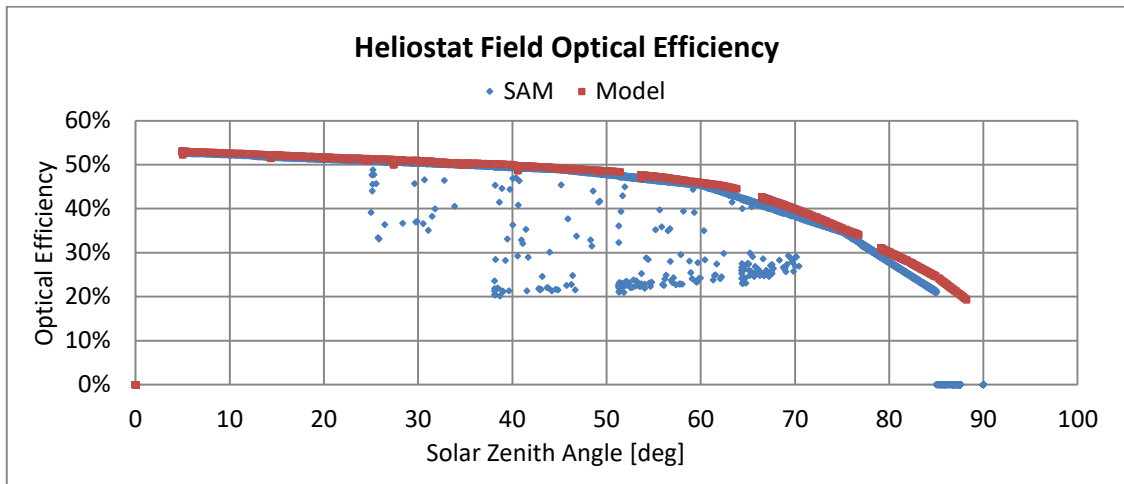


Figure 50: Heliostat field optical efficiency

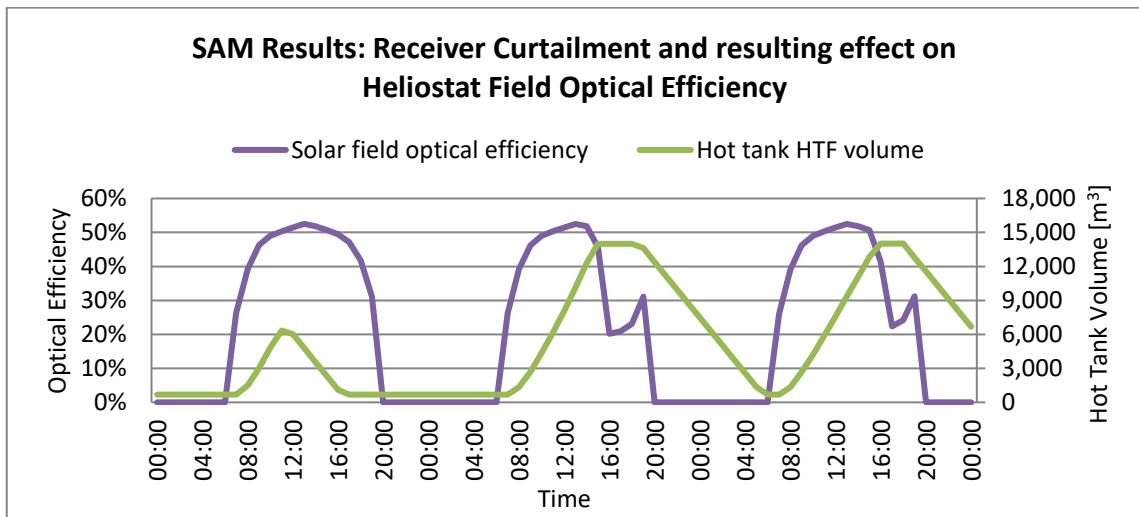


Figure 51: SAM: Effect of receiver curtailment on heliostat field optical efficiency

5.2. Receiver Model

The developed receiver thermal model is validated at design point, e.g. autumn equinox at noon, against the basic design of the case study plant. The parameters affecting the receiver performance are aiming strategy from heliostat field or in other words the incident flux map applied, DNI on the heliostat field, ambient temperature, relative humidity and wind speed. The performances of both receivers at design point are compared in Table 17, when the conditions were alike. Slight deviations are observed between the receivers due to the implementation of different heliostat aiming strategies in each model. The aiming strategy also influences the temperature profile that results in change in the amount of heat loss from the surface. The minor increase in the incident power onto the receiver observed in the model is due to the total mirror area of the heliostat field being slightly larger as indicated previously in Table 8. The receiver efficiencies on both receivers are in agreement with less than 1 % difference.

Table 17: Correlation between Basic Design and receiver model performance

Parameter	Solar-1 Basic Design	Model
Molten salt mass flow through receiver	1360.9 kg/s	1430.0 kg/s
Incident power onto receiver	651.8 MW _t	662.8 MW _t
Reflectivity losses	45.60 MW _t	46.40 MW _t
Radiation losses	18.30 MW _t	24.21 MW _t
Convection losses	11.60 MW _t	10.24 MW _t
Net Power	576.2 MW _t	581.9 MW _t
Receiver efficiency	88.41 %	87.80 %

Furthermore, the receiver's performance curve is used to validate the receiver performance against the SAM simulation results. A comparative overview of this is shown in Figure 52. The parameters affecting the receiver performance are kept similar in both the simulations by utilising the same TMY data. For both receivers the design parameters and the working weather conditions are the same. Therefore, the only variance that can occur is the due to the aiming strategy implemented and the calculations in the receiver's thermal losses. Considering the results obtained from SAM, the data points represent the operation of the receiver throughout the year. Data points have been categorised under three ambient temperatures ranges, ± 2 °C; 20 °C, 30 °C and 40 °C. Although the data points differ in magnitude only, i.e. slightly higher receiver efficiency, the results concur with those obtained from the receiver model.

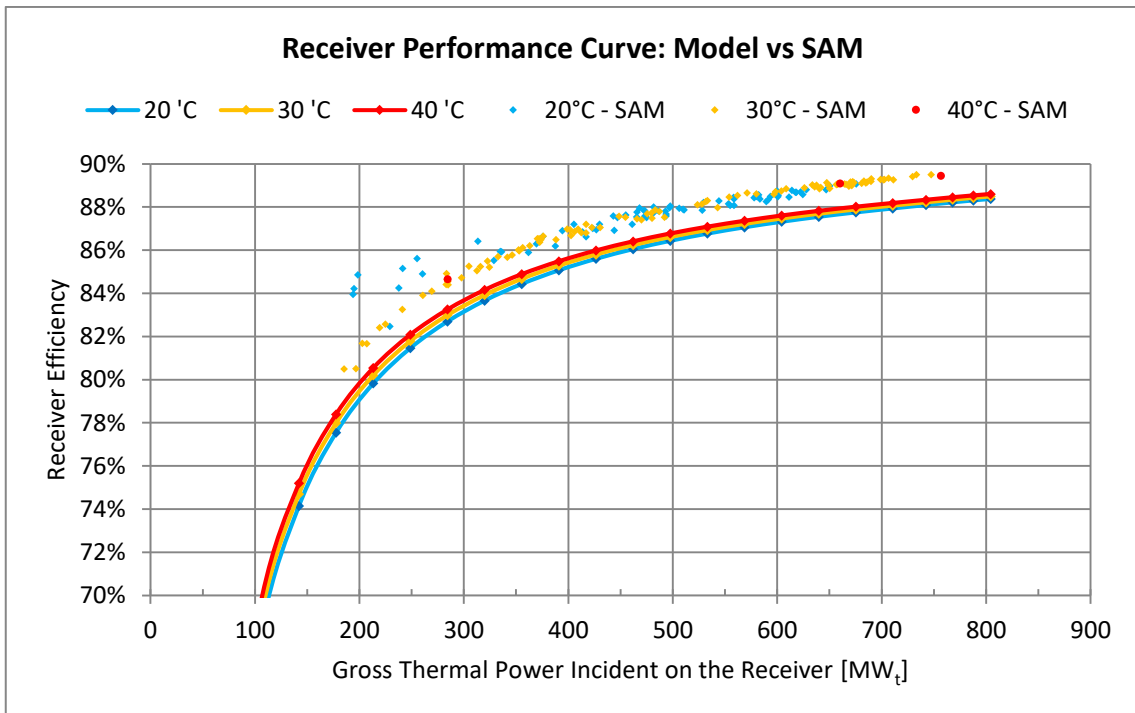


Figure 52: Receiver performance curve validation

Although the comparison indicates a marginal higher receiver performance in the results from SAM, the underlying trend line is in agreement with the performance curve of the receiver model. The method and calculations used in the receiver model are very detailed, whereas a simplified approach is used in SAM for computing purposes. Nevertheless, the variances between the two models are 1-2 % and deemed fit for purpose. Considering the HTF mass flow rate through the receiver under various thermal energy incident on the receiver, the results from the two models are in agreement as represented in Figure 53. Only three temperature ranges were considered in Figure 52, whereas the results from Figure 53 encompassed the entire receiver operation range.

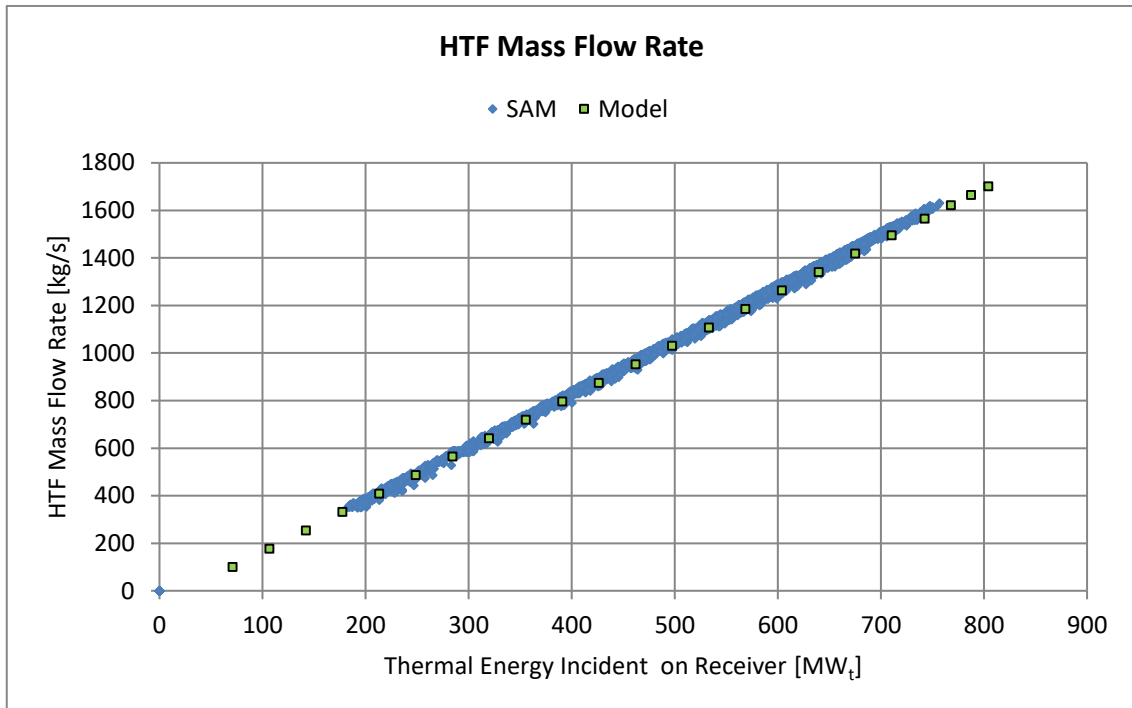


Figure 53: Results comparison in the HTF mass flow rate through the receiver

5.3. Power Block Model

The power block model has been designed according to the design parameters of the case study plant (Figure 30). The power block model has a conventional Rankine steam cycle coupled with a generator. The steam for the turbine is generated from the molten salt steam generator. This steam generator consists of a preheater, boiler, superheater and reheater. The power block is subjected to the ambient conditions as well as the thermal energy received in the steam generator. For validation of the steam generator, the results of the power block model were compared to the results from SAM and the basic design of the case study plant. For modelling the power block, SAM utilises TRNSYS as an interface. However, the case study plant was designed in Thermoflow and the corresponding heat and mass balance is presented in Table 18 along with the developed power block model's results.

Table 18: Turbine heat and mass balance correlation

Parameters	Solar-1 Basic Design		Model	
	IN	OUT	IN	OUT
HP TURBINE				
Pressure [Bar]	120	22.13	120.00	21.20
Temperature [°C]	541.7	309.7	543.36	305.39
Mass Flow [kg/s]	78.92		78.98	
IP TURBINE (1)				
Pressure [Bar]	20.33	12.67	21.20	10.66
Temperature [°C]	543.7	473.6	544.12	453.84
Mass Flow [kg/s]	72.86		74.22	
IP TURBINE (2)				
Pressure [Bar]	12.67	7	10.66	4.76
Temperature [°C]	473.6	389.6	453.84	344.23
Mass Flow [kg/s]	71.51		70.24	
LP TURBINE (1)				
Pressure [Bar]	7	2.81	4.76	1.82
Temperature [°C]	389.6	274	344.23	232.96
Mass Flow [kg/s]	67.41		66.36	
LP TURBINE (2)				
Pressure [Bar]	2.81	0.82	1.82	0.57
Temperature [°C]	274	145	232.96	118.95
Mass Flow [kg/s]	63.45		62.87	
LP TURBINE (3)				
Pressure [Bar]	0.82	0.13	0.57	0.14
Temperature [°C]	145	51.1	118.95	52.00
Mass Flow [kg/s]	59.67		59.75	
Power Block				
Gross Power [MW _e]	100.16		100.47	

The methodology followed while modelling the power block results in variance in the turbine pressures. As discussed in Section 3.6, the process for designing the power block model followed a similar approach as in Wagner (2008) by utilising fixed turbine splitter extraction phases. Exact optimisation is not required as the cycle's efficiency is weakly dependent on these pressures. The splitter stage pressures are calculated by dividing the difference in temperature between the intermediate turbine inlet temperature and low-pressure turbine outlet temperature equally. The temperatures obtained are the temperature at saturation for the splitter stage pressure.

The corresponding heat and mass balance for the condenser and low pressure-, open- and high pressure- feed water heaters are presented in Table 19. The pressure drops across the feedwater heaters are not taken into account in the power block model. The LP FWHs operate at the same pressure as the open FWH, i.e. 4.87 bar. The HP FWHs operate at the desired high pressure steam turbine inlet pressure, and boiler pressure of 120 bar.

Table 19: Condenser and feedwater heaters heat and mass balance correlation

Parameters	Basic Design		Model	
	IN	OUT	IN	OUT
Condenser				
Pressure [Bar]	0.13	0.13	0.14	
Temperature [°C]	51.10	51.10	52.00	51.90
Mass Flow [kg/s]	59.67		59.75	
LP FWH (1)				
Pressure [Bar]	10.25	9.71	4.76	
Temperature [°C]	51.66	90.62	51.97	81.76
Mass Flow [kg/s]	59.72	67.84	59.75	66.36
LP FWH (2)				
Pressure [Bar]	9.71	9.16	4.76	
Temperature [°C]	90.62	127.70	81.76	113.92
Mass Flow [kg/s]	67.84		66.36	
Open FWH				
Pressure [Bar]	9.16	9.16	4.76	
Temperature [°C]	127.70	164.50	113.92	149.91
Mass Flow [kg/s]	67.84	78.92	66.36	78.98
HP FWH (1)				
Pressure [Bar]	129.70	129.00	120.00	
Temperature [°C]	167.70	191.90	152.47	186.28
Mass Flow [kg/s]	78.92		78.98	
HP FWH (2)				
Pressure [Bar]	129.00	128.40	120.00	
Temperature [°C]	191.90	217.20	186.28	215.78
Mass Flow [kg/s]	78.92		78.98	

The heat and mass balance correlation between the basic design and the steam generating system is represented in Table 20. The pressure drop across the steam generator is not taken into consideration in the power block model. This level of detail is not required for this model. The agreement between the two steam generator systems is confirmed from these results.

A good correlation between the basic design of the case study plant and the power block model is observed at design point. The slight deviations between the numbers are as a result of the different modelling approaches used. The developed model was based on the methodology followed by Wagner (2008) in his study, whereas an advanced software package called Thermoflow was utilised for basic design.

Table 20: Steam generator heat and mass balance correlation

Parameters	Basic Design		Model	
	IN	OUT	IN	OUT
Preheater				
Pressure [Bar]	128.40	126.90	120.00	
Temperature [°C]	216.60	324.00	215.78	322.91
FW Mass Flow [kg/s]	78.92		78.98	
HTF Mass Flow [kg/s]	570.00		570.00	
HTF Temperature	339.00	287.50	338.96	287.37
Boiler				
Pressure [Bar]	126.90	126.90	120.00	
Temperature [°C]	324.00	329.00	322.91	324.68
FW Mass Flow [kg/s]	78.92		78.98	
HTF Mass Flow [kg/s]	570.00		570.00	
HTF Temperature	448.40	339.00	449.20	338.96
Superheater				
Pressure [Bar]	126.90	126.10	120.00	
Temperature [°C]	329.00	545.00	324.68	543.36
Steam Mass Flow [kg/s]	78.92		78.98	
HTF Mass Flow [kg/s]	352.40		347.41	
HTF Temperature	565.00	448.20	565.00	449.24
Reheater				
Pressure [Bar]	21.20	20.90	21.20	
Temperature [°C]	307.70	545.00	305.39	544.12
Steam Mass Flow [kg/s]	72.86		74.22	
HTF Mass Flow [kg/s]	217.70		222.59	
HTF Temperature	565.00	448.70	565.00	450.43

Thermoflow is used for detailed engineering. Various losses such as pressure drop across heat exchangers and additional thermal losses are taken into consideration. The developed model is, thus, adequate in design and the corresponding parameters are fixed and used as reference for simulation.

To validate the power block model under various operating conditions, the power block performance is measured against the simulation results from the SAM. The results from the power block model is plotted against the performance curve of the SAM simulation results, see Figure 54. The SAM results are an annual representation of the performance of the power block under various conditions. Both simulation results present the expected performance curve of the power block. Five independent graphs representing the power block model's performance under various conditions are shown in Figure 54. The aim of these graphs is to create a better understanding and to replicate the data points presented by the SAM results. The steam generator system's HTF mass flow rate was incremented under constant ambient temperatures. These three plots are similar to the performance curves used when analysing the power block at design point conditions. The bottom curve

represents the design point conditions, $T_{amb} = 32\text{ }^{\circ}\text{C}$, with an increase in heat transfer fluid mass flow rate. Therefore, the data points from SAM sharing the same performance curve characteristics represent the plant behaviour during part load operations.

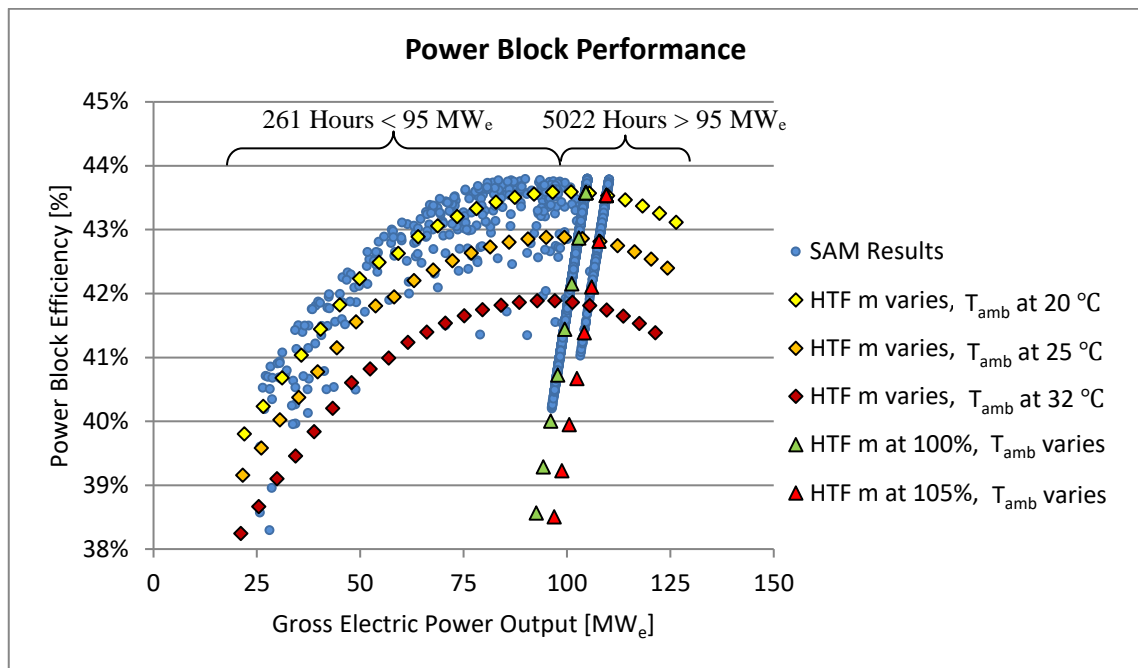


Figure 54: Power block performance validation

The second set of curves, the two seemingly obvious linear lines, are obtained by fixing the mass flow rate of the HTF to the steam generating system as specified at the design point. The second linear line is obtained by increasing the mass flow rate to 105 % of the design point parameter. From the analysis, the SAM results account for 5,022 hours with 95 % of operation time with operations above 95 MW_e. Therefore, these two lines result as the power block operates under various ambient temperatures while the HTF mass flow rate is kept constant. This phenomenon is expected to result from the SAM simulation, as the operating strategy followed in SAM is the ‘Maximise Power Generation’, thus the power block aim 100 % operation at full load.

Although, a representative correlation between the two models is obtained in a behavioural manner, the power block efficiency of the SAM model is slightly higher than the developed model’s simulation results. This can be translated to a scaling factor with the efficiency of 99 %. The modelling of the power block in both the simulation models differs as change in the thermal losses and the individual turbine efficiencies are specified independently. However, the correlation between the two models was deemed adequate and fit for purpose.

6. SIMULATION RESULTS

The optimisation of various plant operations is necessary when different operating strategies are applied. Therefore, the control logic pertaining to the plant operations has been implemented in this model. With the various systems validated in Section 5, the overall plant control and optimisation is incorporated to satisfy the research objectives.

The various operating strategies have been identified in Section 2.8 and are demonstrated through the simulation model's capabilities in this Section. The simulation results from the various operating strategies are compared to establish the key performance and financial indicators for each in the specified period. A detailed analysis on each operating strategy, its resulting parameters and simulation results are supplemented in APPENDIX C. This Section will highlight the key findings from the APPENDIX C. It is, therefore, recommended that the appendix is read first to fully understand and appreciate the simulation results discussed.

6.1. Maximise Power Generation

6.1.1. Short Term Simulation Results

The most commonly used the 'Maximise Power Generation' operating strategy imposes no system boundaries on the plant. Therefore, the plant operations are optimised to yield maximum power generation in the selected period. The 'Maximise Power Generation' and 'Maximise Plant Revenue' operating strategies coincide when the flat rate tariff structure is considered.

The following plant operations were considered for optimisation: maximise energy collection from the solar collection system; minimising energy dumping associated with a full state of charge in the hot thermal storage tank; minimising impact of plant start-ups and shut-downs; and power block efficiency associated with part load conditions. Although, the detailed analysis and user flexibility regarding this operating strategy is supplemented in the appendix, only the 'Optimised Maximum Power Generation' results are considered. This is because it truly reflects the capabilities and optimisation of the plant operations. The time period, 19th to 21st March, selected to carry out the simulation corresponds to the design point day for the plant. The design point day was the autumn equinox or the noon of 20th March. During this period, low DNI is bestowed upon the heliostat field, the ambient temperatures are fair and unwarranted cloud transients are not observed (Figure 55).

One of the objectives within the 'Maximise Power Generation' operating strategy, is to maximise energy collection from the solar collection system. Therefore, the receiver's net thermal output should be optimised. This becomes challenging especially during high DNI periods as the hot TES reach a full state of charge inducing energy dumping. Within this operating strategy minimisation of energy dumping is another optimisation objective. The receiver operations are, therefore, considered and illustrated in Figure 56.

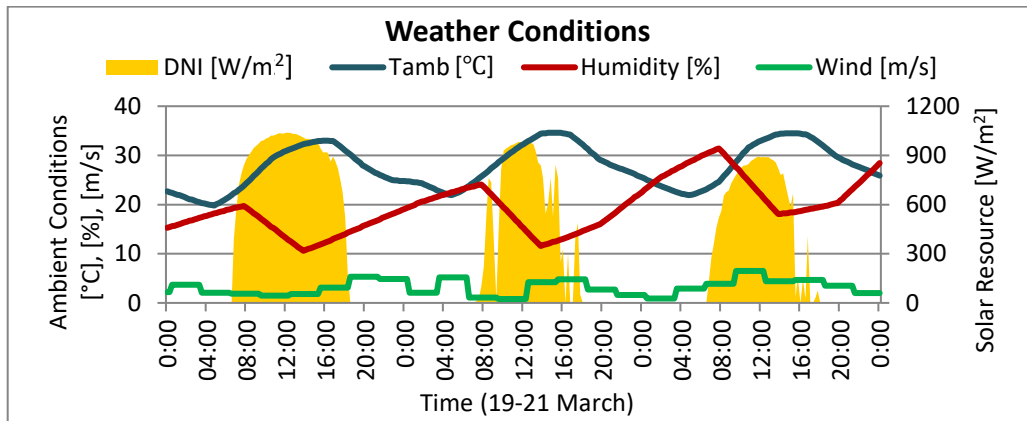


Figure 55: Weather conditions as input to simulation model

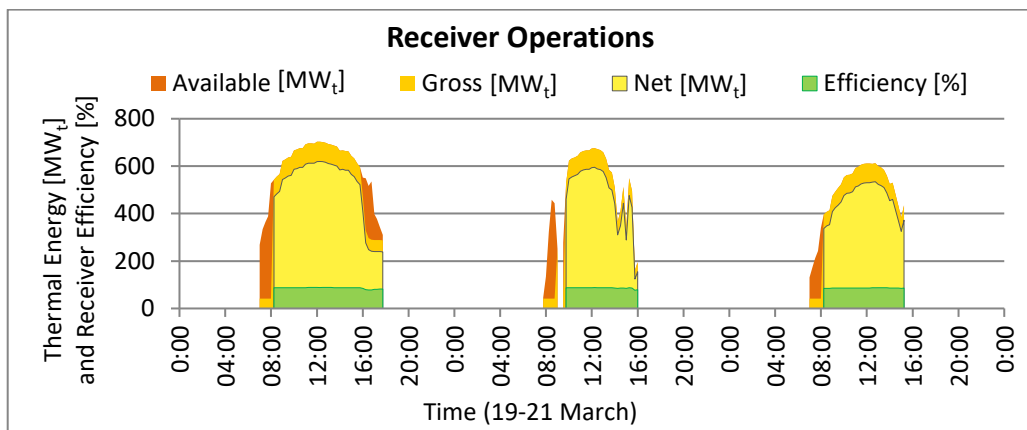


Figure 56: Graphical representation of receiver operations

From the results in Figure 56, the receiver collected all the solar energy in the last two days. However, receiver curtailment is observed during the first day. Greater amount of solar energy input was present on the first day of operation as compared to the other two days. Therefore, the TES was inadequate to accommodate all the solar energy, thus the receiver had to be curtailed. The dispatch profile and state of charge of the hot TES is shown in Figure 57.

The inference made regarding the hot TES size and receiver curtailment is confirmed when the first day is analysed (Figure 57). The model dispatched the thermal energy in the hot TES to the SGS in order to empty the hot TES before starting the receiver operations. Therefore, with the maximum turbine output observed in Figure 58 until the receiver curtailment commence, around 16h00, it is confirmed that the receiver had to curtail its operations due to the design limitations of the hot TES. By increasing the turbine output to 110 % of its nominal output, discharge from the hot TES would be greater, thus energy loss due to dumping could be recovered.

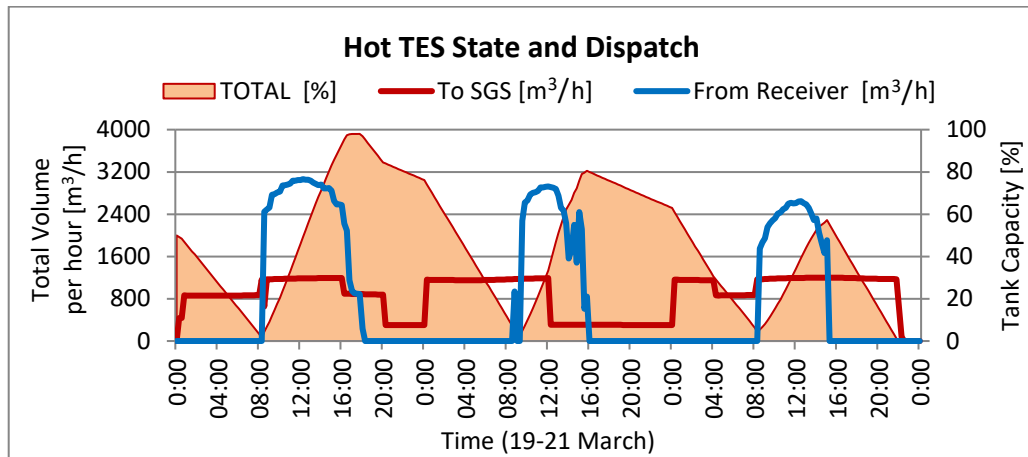


Figure 57: Hot TES dispatch profile and state of charge

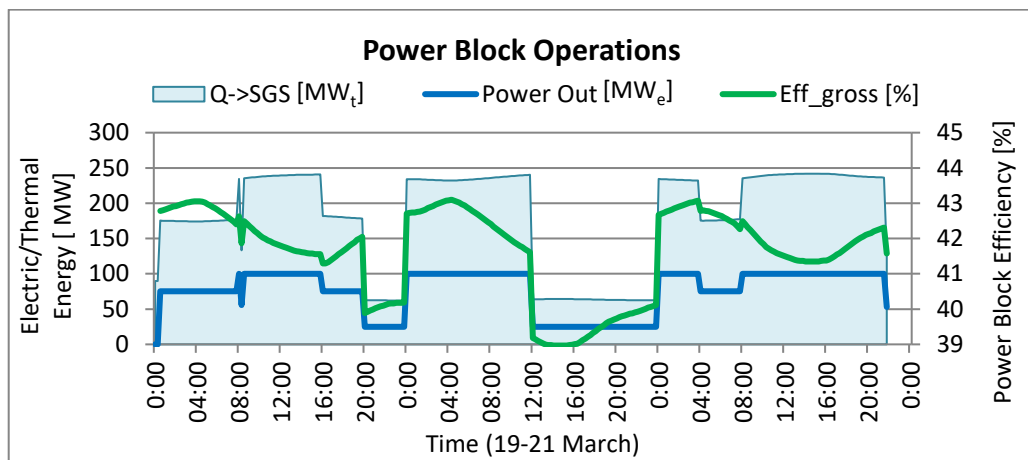


Figure 58: Power block operations under optimised maximise power generation

One of the significant findings is the use of part load operational aspect of the power block to yield maximum power generation over the selected time period. This minimises the impact of plant start-ups, shut-downs and take into consideration the efficiency of the power block associated with part load conditions. To achieve the maximum plant power generation, one suspects that the power block generates power at its full capacity for extended periods of time. By taking advantage of the high turbine efficiency, the model optimised the plant operations by reducing the turbine output to avoid turbine stops or shutdowns, shown in Figure 58. By reducing the turbine output, the energy saved from the turbine start-up increases the power block efficiency, ultimately increasing the plant efficiency. Furthermore, it is worth noting that the model calculated the thermal energy dispatched to the steam generator accurately while maintaining sufficient thermal energy in the hot TES for continuous generation of power. The thermal energy from the receiver is supplied to the hot TES just before a depletion state is reached in the hot TES (see Figure 57) at times around 08h00-09h00.

The differences in the optimised and non-optimised part load operations are illustrated in Figure 59. The results from Figure 59 visually represent the dispatch profile within the hot TES. In the optimised part load operations, the model results in a higher power block efficiency of 40.3 %, and total gross electric power of 1.53 GWh_e. Whereas, in the case of non-optimised operations, the power block efficiency of 39.5 % and total gross electric power of 1.51 GWh_e is observed. Therefore, the abovementioned hypothesis is confirmed.

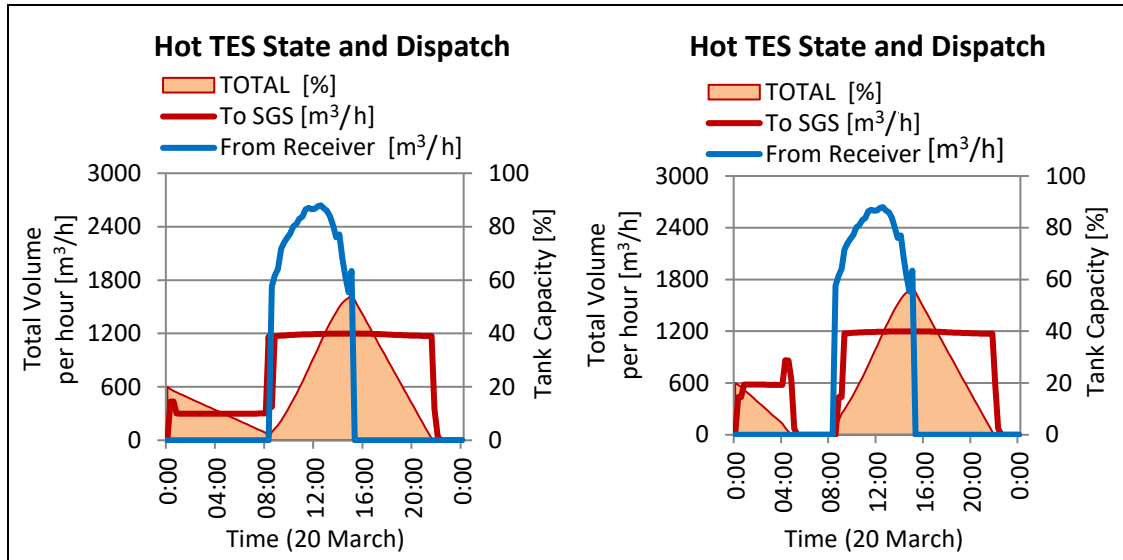


Figure 59: Power block, optimised part load (left) and non-optimised (right)

6.1.2. Annual Simulation Results

Although, the developed model is intended to simulate only for a seven day period, it is worth to analyse the annual performance of the plant operating under this operating strategy. The results would further confirm the performance of the model when compared to the simulation software package SAM. Since, SAM utilises the maximise power generation operating strategy for its plant performance, the comparison between the two models would be of great value. The simulation results, representing the annual plant performance operating under the ‘Optimised Maximise Power Generation’ operating strategy, are represented in Table 21. Comparison of these results with SAM is done. Both the models in this exercise utilised the same TMY data set as input. The plant design parameters in SAM are the same as the previously evaluated parameters in Section 5, validating the model results.

Table 21: Annual simulation results, comparative overview

Heliostat Field Annual Performance				
Parameter	MODEL	SAM	Unit	Remark
Total incident power in solar field (gross)	3880	3874	GWh _t	Total heliostat field reflecting area in relation to total annual DNI on field
Heliostat field efficiency	40.4	40.1	%	Taking into consideration energy dumping and receiver flux limitation
Receiver Annual Performance				
Parameter	MODEL	SAM	Unit	Remark
Total incident power for normal operation (gross)	1570	1552	GWh _t	Incident power onto the receiver during normal operation, energy dumping taken into consideration
Thermal power delivered by receiver (net)	1355	1354	GWh _t	Total thermal energy sent to hot TES
Receiver efficiency (net)	86.3	87.2	%	
Power block Annual Performance				
Parameter	MODEL	SAM	Unit	Remark
Total thermal energy sent to SGS	1355	1343	GWh _t	Hot TES dispatch to power block
Total electric power generated	573	544	GWh _e	Gross electric power sent to grid
Power block efficiency (gross)	42.3	40.5	%	
Plant Annual Performance				
Parameter	MODEL	SAM	Unit	Remark
Total auxiliary consumption	55	48	GWh _e	Total plant parasitics
Plant net electric power	518	496	GWh _e	Total net electric power sent to grid
Plant efficiency (gross)	14.8	14.0	%	Solar to electric energy conversion
Plant efficiency (net)	13.4	12.8	%	Solar to electric energy conversion
Plant Capacity Factor	65.5	62.1	%	Capacity Factor using total gross

The total incident power in the solar field for both models were in the order of 3,880 GWh_t. For both the models, the heliostat field reflected this solar energy onto the receiver with 40 % efficiency. The ‘total incident power for normal operation’ represents the thermal energy reflected on the receiver during the ‘normal’ operation of the receiver. Therefore, the incident power on the receiver during the receiver start-up and cloud transients operating regimes are excluded. See Section 3.5.7 for further details on the various receiver operating regimes.

The receivers of both the models delivered a net thermal energy 1,355 GWh_t. This value is coincidental as the developed model’s receiver efficiency is slightly lower than that of SAM. This can be seen in Table 21 under the entry ‘Receiver efficiency (net)’. Furthermore, in Figure 60, the receiver performance simulation results for both models are plotted with the receiver efficiency as a function of the incident power onto the receiver. The lower efficiency of the model in comparison to SAM is observed and it concurs with the earlier results shown in Figure 52.

Considering that both the models are following the maximise power generation operating strategy and have less than 1 % difference in power block efficiencies (as determined from the power block validation in Section 5.3), the total electric power generated will be similar. However, the developed model generated 3.43 % more electric power than SAM.

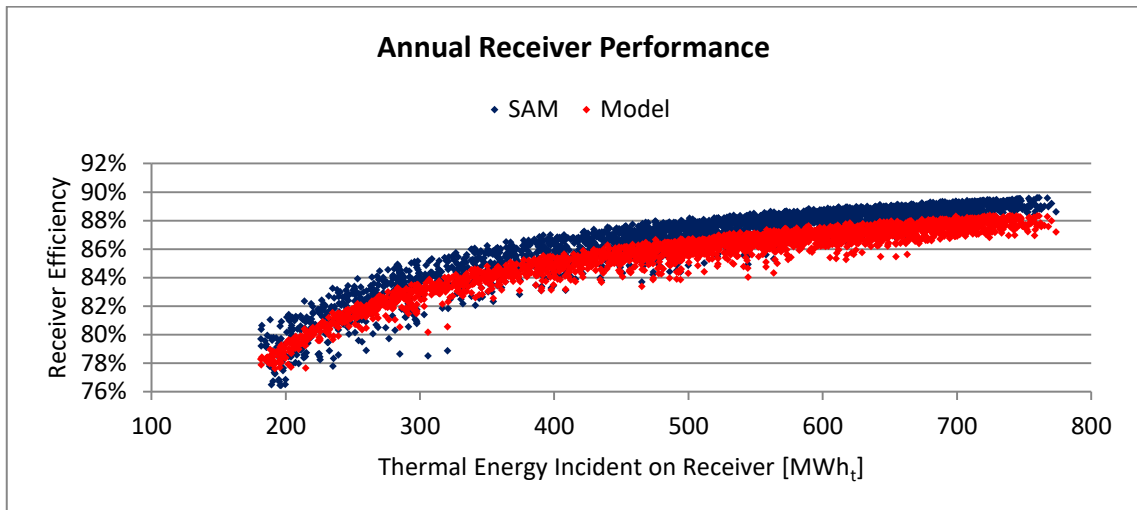


Figure 60: Annual receiver performance curve correlation between the two models

This equates to an average power block efficiency of 42.3 %, in comparison to SAM with power block efficiency of 40.5 %. It was suspected that the higher power block efficiency resulted due to part load operation of the turbine, similar to the results from Figure 59. When the annual generation breakdown report is considered (Figure 61), it is observed that the model implemented more part load operations in the power block than the SAM model. The results show that the annual generation of 57 % accounted towards 100-110 MW_e whereas no generation accounted to 35.6 %. In contrast, the developed model demonstrates part load operation ranging from 25-100 MW_e. The full load operations accounted for 48.4 % whereas part load operations accounted for 32.2 %, and no generation only 19.4 %. Therefore, by optimising the dispatch from hot TES to SGS, the effectively reduced turbine start-ups and shutdowns resulted in a higher power block efficiency.

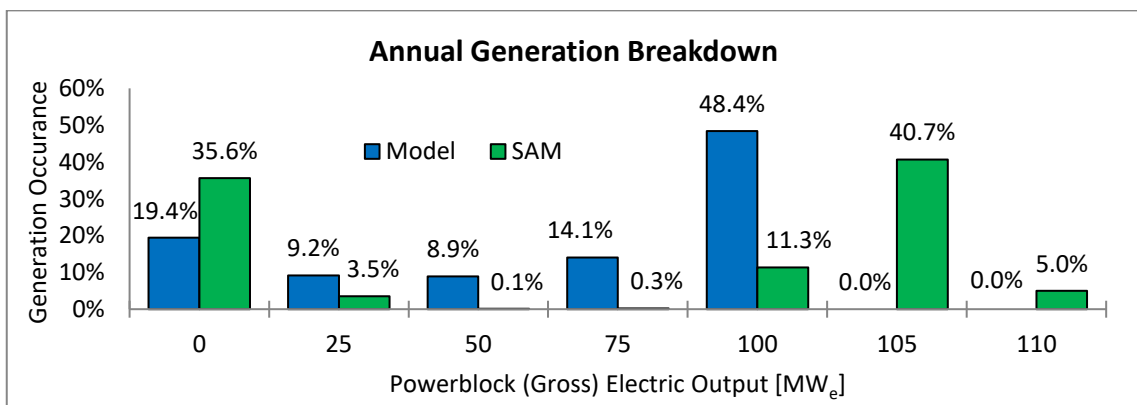


Figure 61: Annual generation breakdown comparison with generation occurrences

A higher power block efficiency is obtained in the part load operations for the following reasons. The SGS requires 179.9 MWh_t for starting up the turbine-generator from a warm start-up. The SGS requires ±64 MWh_t to generate 25 MW_e from the power block,

translating to a 39 % power block efficiency. If the plant utilises the part load operations by avoiding a power block start-up, the 179.9 MWh_t is saved which can translate to 75 MW_e additional power to be generated. Therefore, if the total thermal energy sent to SGS and the gross electric power generated by turbine is considered, the gross efficiency of the power block increased. Subsequently, less energy is required to generate more electric power. However, from the calculations the model can determine if operating at part load operations and lower turbine efficiencies could outweigh the thermal energy saved from the start-up. Thus, the model optimises the plant operations to yield the highest power block efficiency, which addresses the ‘Maximise Power Generation’ objective.

In addition, the hot TES dispatch profile from SAM is used as input for the developed model. The results from the model are compared in Table 22. The two models operating under the same hot TES dispatch profile differ only with 0.03 % between the gross power block efficiencies. Therefore, optimisation within the plant operations is confirmed in the developed model. An increase in the power block efficiency up to 1.8 % is achievable by introducing part load operations to the operating regime of the plant. An additional energy output of 29 GWh_e is added to the grid. This increases the overall plant efficiency from 12.8 % to 13.4 %. The plant capacity factor further increased from 62.1 % to 65.5 %.

Table 22: Comparison in simulation results for SAM’s hot TES dispatch profile

Parameter	SAM	Model	Unit
Total thermal energy sent to SGS ¹	1198.88	1198.88	GWh _t
Total electric power generated	510.80	511.24	GWh _e
Power block efficiency (gross)	42.61	42.64	%

Note 1: Total thermal energy sent to SGS exclude thermal energy required for start-ups

6.2. Maximise Plant Revenue

The Maximise Plant Revenue operating strategy is used to simulate the plant operations under the PPA as per Bid Window 3.5 and the model has been set up as per this strategy (Appendix C.3.4). The reference plant design did not account for these boundary conditions and therefore, the plant performance will be impacted. The reference plant design caters for a SM of 2.4 and TES size of 12 hours. During high DNI periods, the overall plant performance is severely affected due to the no payment terms in the PPA. See Appendix C.5.13, where various operating strategies were compared during periods of high DNI. Since, the hot TES was not sufficiently discharged, the receiver curtailment occurred due to high SM and state of charge in the hot TES. Therefore, lower efficiencies of the heliostat field, receiver and overall plant was recorded.

However, to illustrate the optimisation in plant operations for the ‘Maximise Plant Revenue’ operating strategy, a period of low and good DNI was selected for simulation (Figure 62). The following are the terms for the PPA Bid Window 3.5: No payments between 22h00-05h00; base tariff of R1.93/kWh for time periods, 05h00-16h30 and 21h30-22h00; and 270 % of base tariff during 16h30-21h30. The base tariff of R1.93/kWh

is the fully indexed price, the inflation was adjusted to April 2016 as presented in Section 2.1.3, Figure 3. As observed from the Figure 63, the model optimises dispatch from the hot TES to prioritise generation during the peak paying period. The distinction is clearly noted on the first two days with low DNI, when limited energy was available for power generation. However, with sufficient DNI available, maximum power generation is observed throughout the day.

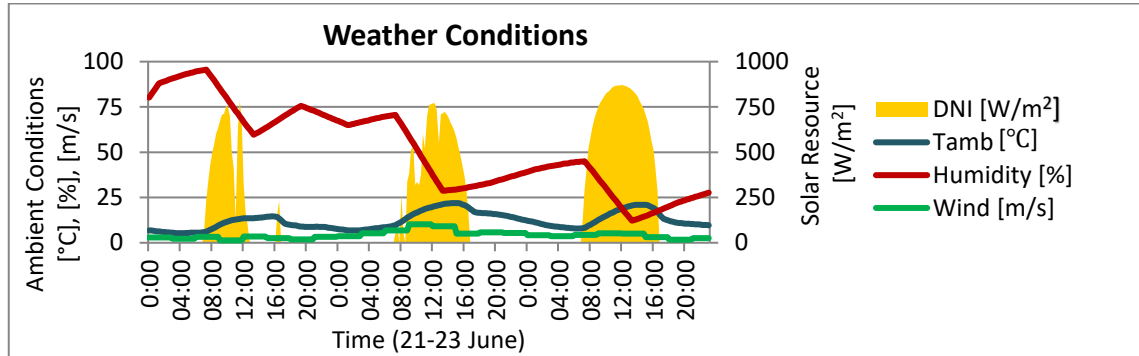


Figure 62: Weather conditions for period with limited solar resource availability

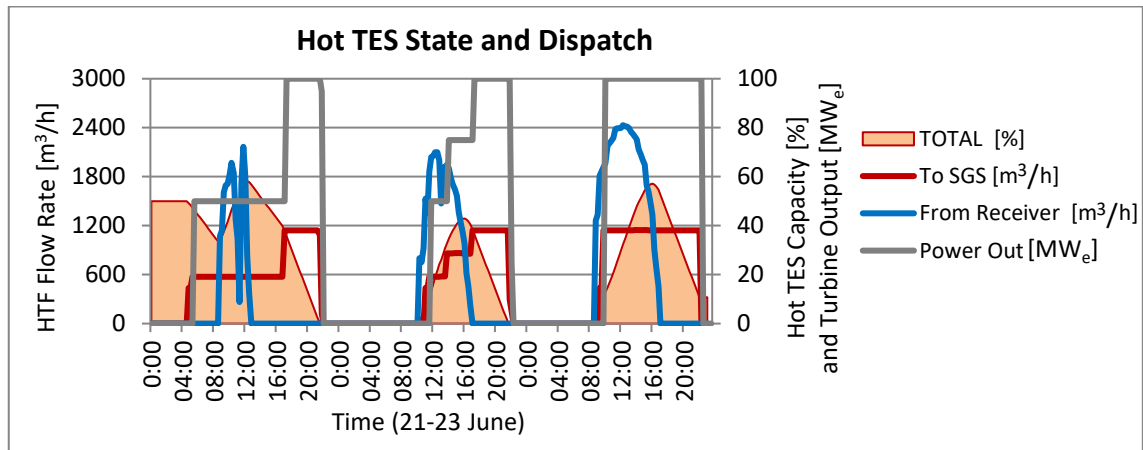


Figure 63: Hot TES dispatch profile, optimising dispatch during higher paying tier

6.3. Minimise Energy Dumping

The ‘Minimise Energy Dumping’ operating strategy is considered within almost all the operating strategies. The energy dumping refers to the act of defocusing the heliostats from the receiver, ‘dumping’ the potential energy, and affecting overall plant efficiency. Energy dumping is done due to the hot TES that is fully charged leading to shut down or curtailment of the receiver. It is also due to certain heliostats that are defocused from the receiver in order to prevent it from exceeding the maximum incident solar flux limit of the receiver material. Therefore, the energy is intentionally deflected from the receiver by heliostat field and is hence called the deflected energy. To prevent energy dumping, the plant optimises its hot TES dispatch and turbine power output to ensure that full state of charge is not reached within the hot TES. Additionally, the aiming strategy of the heliostat field can be optimised to stay within the flux limit of the receiver. In the ‘Minimise Energy

Dumping' operating strategy, all the plant operations are prioritised to ensure that no or minimal energy dumping occurs. The implementation of a weather predicting system can further enhance the optimisation capabilities regarding dispatch forecasting and peak flux limits on the receiver.

6.3.1. Short Term Simulation Results

The receiver operations of the 'Maximise Power Generation' operating strategy, as illustrated in Figure 56 is recalled and shown in Figure 64 (left). As noted, the receiver was curtailed during the first day due to the hot TES reaching a full state of charge. Furthermore, with high DNI levels present in the heliostat field, the flux limit of receiver is reached through the default heliostat field aiming strategy. Thus, the heliostats had to be deflected to reduce the thermal energy on the receiver surface, illustrated in Figure 65 (left). The implementation of the 'Minimise Energy Dumping' operating strategy and the results are presented in Figure 64 (right) and Figure 65 (right). It is clear from the results that the receiver curtailment was evaded and heliostat field aiming strategy was adjusted to prevent it from exceeding the receiver flux limitations.

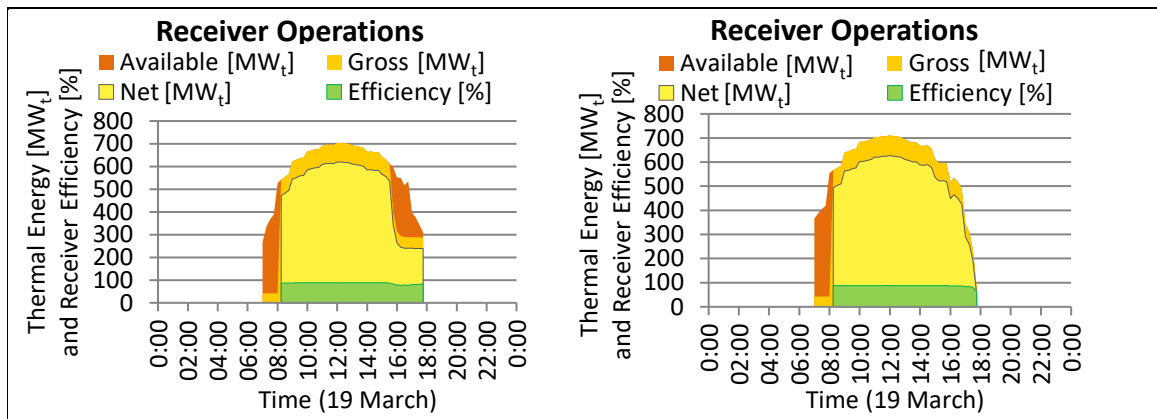


Figure 64: Maximise power generation (left), and minimise energy dumping (right)

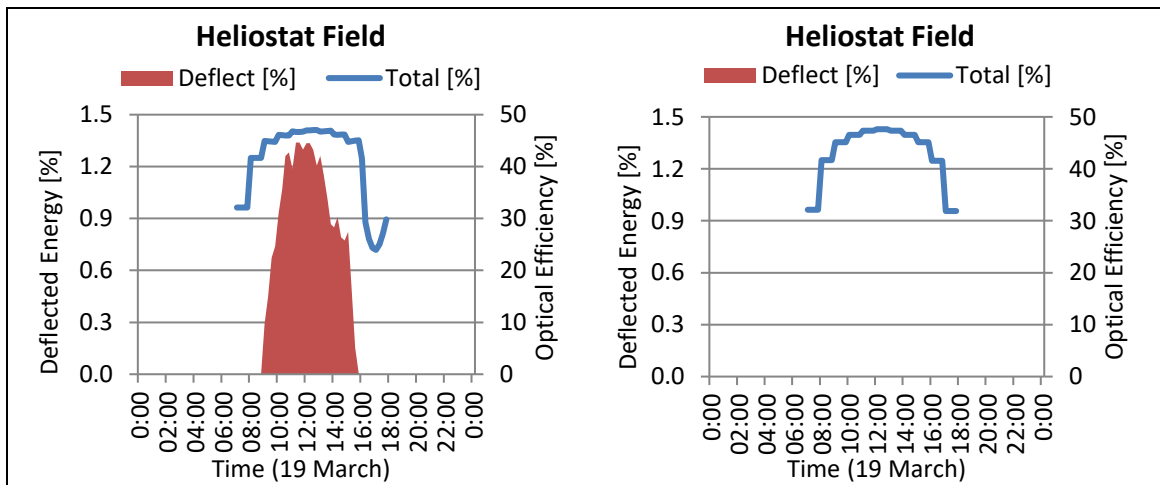


Figure 65: Maximise power generation (left), and minimise energy dumping (right)

The ‘Minimise Energy Dumping’ operating strategy utilise the dispatch potential of the hot TES to reduce the likelihood of receiver curtailment. It adapts the aiming strategy of the heliostat field to avoid exceeding the receiver flux limitations. The hot TES dispatch profile illustrated in Figure 66 clearly shows the dispatch from the hot TES to the power block to avoid reaching a full state of charge. A valuable tool for the plant operator is illustrated in Figure 67, indicating the minimum turbine output required to avoid reaching a full state of charge in the hot TES. It is also noted that the turbine output was increased to 110 % of its nominal output. It was done in order to increase the discharge rate of the hot TES. This hypothesis was put forward earlier in the ‘Maximise Power Generation’ short term results as a possible operational optimisation.

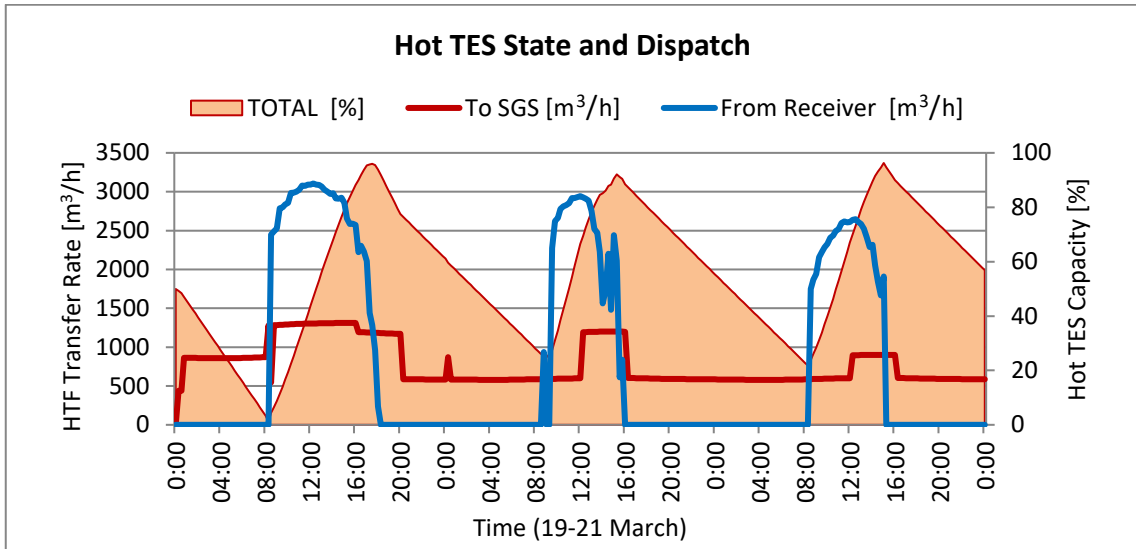


Figure 66: Hot TES dispatch profile, optimised to minimise energy dumping

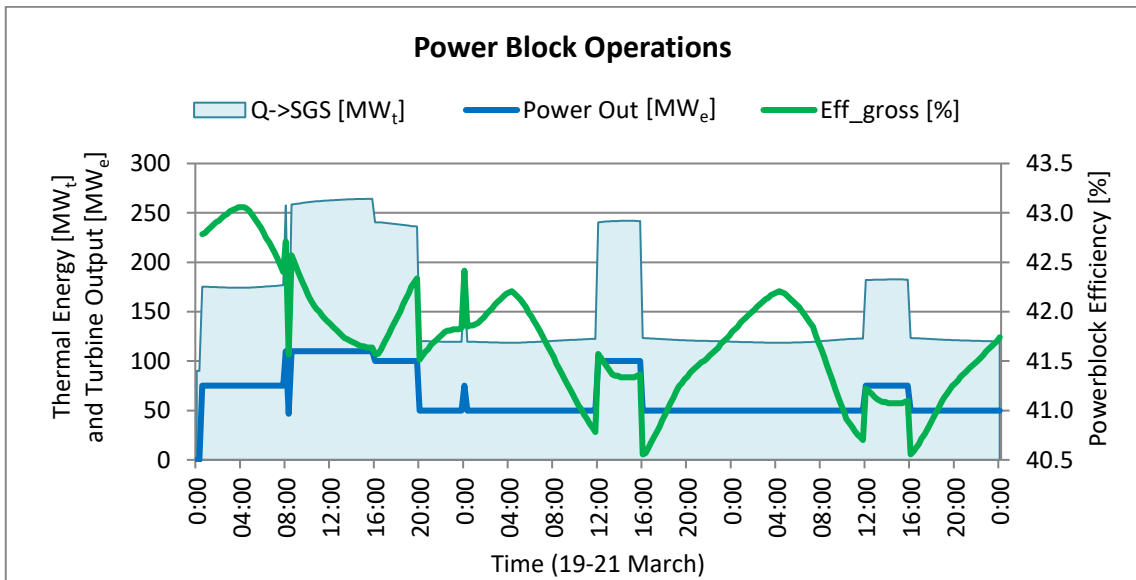


Figure 67: Minimum turbine output required to avoid energy dumping

6.3.2. Annual Simulation Results

The ‘Maximise Power Generation’ operating strategy’s annual plant performance was used to evaluate the performance of the ‘Minimise Energy Dumping’ operating strategy, represented in Table 23. The increase of 0.31 % in the parameter ‘available power for the receiver’ is due to the redistribution of flux over the receiver’s surface. This is in relation with the heliostat field aiming strategy and allowable design flux limitations of the receiver material. By optimising the hot TES dispatch to the SGS and at times increasing the turbine output to 110 MW_e, the incident power for normal operation of the receiver could be increased by 1.88 % or 29.5 GWh_t. The adapted heliostat field aiming strategy leads to the increase in the incident power to 0.31 % or 5.6 GWh_t. The ‘Maximise Power Generation’ operating strategy utilised 96.0 % of the available power during normal receiver operations whereas the ‘Minimise Energy Dumping’ utilised 97.3 %. Thus, the receiver curtailed only 2.7 % or 44.8 GWh_t of the energy instead of 4.0 %, 64.3 GWh_t. This was achievable by intermittently increasing the turbine output to 110 MW_e and effectively discharging the hot TES at faster rates. Subsequently, the receiver could charge the hot TES with more thermal energy and reduce the need for curtailment.

Table 23: Key plant performance indicators optimised, ‘Minimise Energy Dumping’

Annual Energy Yield per System	Minimise Energy Dumping	Maximise Power Generation	Units
Total incident power in solar field	3881	3881	GWh _t
Total available power for receiver	1775 (+0.31 %)	1769	GWh _t
Total incident power (normal operation)	1599 (+1.88 %)	1570	GWh _t
Net power delivered by receiver	1380 (+1.80 %)	1355	GWh _t
Total electric power generated	584 (+1.80 %)	573	GWh _e

Table 23: Key plant performance indicators optimised in ‘Minimise Energy Dumping’

Annual Efficiency per System	Minimise Energy Dumping	Maximise Power Generation	Units
Heliostat field efficiency	41.21% (+1.88 %)	40.45 %	-
Receiver efficiency	86.27% (-0.08 %)	86.34 %	-
Power block efficiency (gross)	42.31% (+0.00 %)	42.31 %	-
Plant Efficiency (gross)	15.04% (+1.80 %)	14.78 %	-
Plant Efficiency (net)	13.58% (+1.67 %)	13.35 %	-

With an increase in 1.80 % of thermal energy from the solar collecting system, the electrical energy output of the power generating system also increased by 1.80 %. Therefore, the gross plant efficiency increased by 1.80 % whereas the net plant efficiency increased by 1.67 %. The auxiliaries in the plant operation increased due to the power required for pumping as more energy was incident onto the receiver.

6.4. Optimise Electric Grid

There are three common arguments against renewables. Firstly, some stakeholders argue that renewables are not able to provide base load capabilities. Secondly, the renewables do not deliver power to the system when it is required the most. And thirdly, the renewables are unpredictable and unreliable. This Section aims to demonstrate that the developed model is capable of optimising the plant operations to provide the electric grid with these services.

Due to the inherent nature of non-dispatchable renewable energy generating technologies, these technologies can be seen by some stakeholders as unpredictable or unreliable. The argument is supported by ‘the wind is not always blowing and the sun is not always shining’. Although, wind and PV generation offer low LCOE values, a dispatchable generating technology is required to provide stability and secure supply to the electric grid. CSP with storage can provide these complimentary services to the electric grid. The model utilised the aggregated wind and PV generation profile from National Control Centre (Eskom, 2015b). It optimised the plant operations to provide a continuous generation profile, from the electric grid point of view, therefore, stabilising the grid. For illustration purposes, the plant output has been scaled to represent a ‘Solar Park’ to match the generation profile of the non-dispatchable generating technology. Further details regarding the modelling approach followed for ‘Complimentary services to wind and/or PV generation’ is supplemented in Appendix C.3.6.

6.4.1. Complimentary Services to Wind Generation

The aggregated wind generation profile for January 2015 is considered for illustration purposes (Figure 68). The CSP plant or ‘Solar Park’ aim to follow the wind generation profile to provide continuous power to the electric grid. The combined power generation from both wind and CSP is short of 1000 MWh_e. The results show that the combined generation of wind and CSP could provide the system with continuous power supply. However, the model uses the TMY data set of Upington, and on days with low DNI, the demand was not fully met. This risk can be mitigated by distributing CSP installations in various regions amongst South Africa, thus, diversifying the effects of ambient conditions on the plant operations and capabilities.

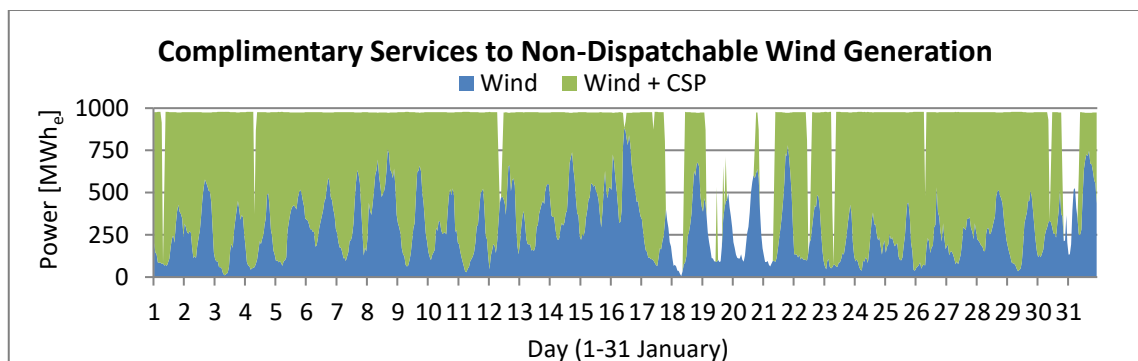


Figure 68: Generation profile, wind and CSP offering continuous output

Further analysis on the annual generation profile for the CSP plant indicates that the plant seldom had to operate at full load. The results are shown in Figure 69. This is supported by the fact that the weather is always windy in South Africa and wind farms are present in such locations. The CSP plant could not meet the demand only for 17.6 % of the year.

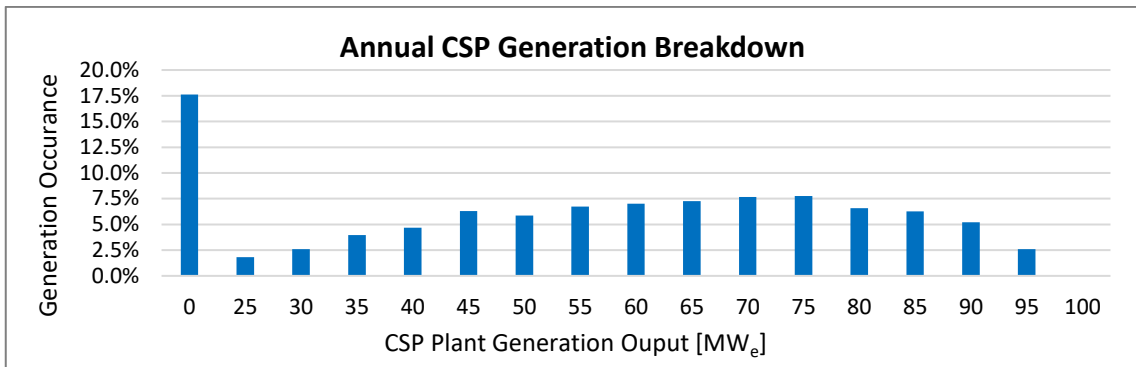


Figure 69: Annual generation profile, CSP providing complimentary service to wind

The hourly demand in South Africa plays an important role for the system operator and Eskom. It is essential to meet the power demands to avoid load-shedding, especially during peak times when the system is constrained. With the new capacity, such as Ingula, Medupi and Kusile, added to the system, an oversupply of generation is eminent with no growth in the economy. However, Figure 70 aims to illustrate the hourly annual average CSP plant generation and the combined availability of wind and CSP to contribute to the demand. The average system demand is a function of the peak demand, expressed as a percentage. The availability of wind and CSP to provide continuous power was over 93 % between 12h00-24h00. The availability peaked at 97 % between 16h00-19h00. As the hot TES is depleted throughout the night, the availability lowers as well. The lowest availability of 68 % was observed between 08h00-10h00. This concur with the hourly average generation output of the CSP plant as observed from the graph.

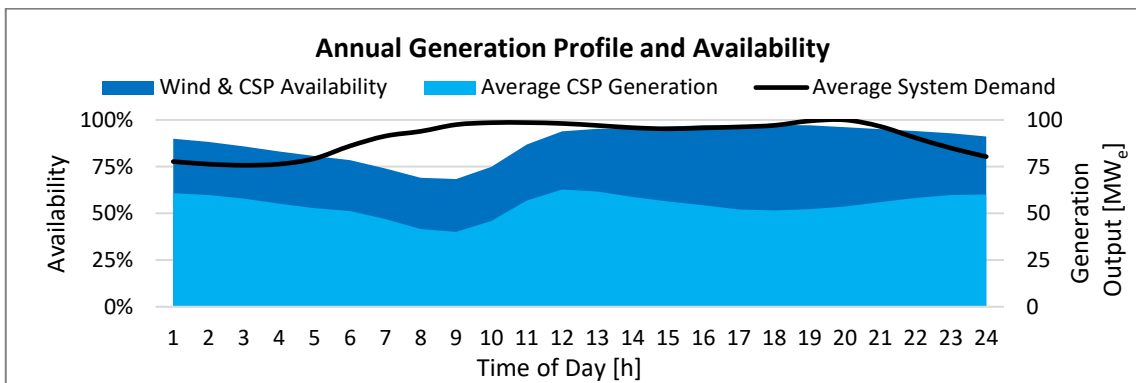


Figure 70: Annual generation profile and availability, wind and CSP generation

6.4.2. Complimentary Services to PV Generation

Predominantly part load operations were noted in the complimentary services to wind operating strategy. This, however, is not the case when PV generation is considered. As PV generation only occurs during day-time, with maximum generation in noon, the CSP plant had to provide full load when the sun sets. This operational behaviour is seen in Figure 71 and Figure 72. The plant operated at full-load 33 % of its generation time, whereas no output generation was observed at 40 %. The early morning demand with continuous full-load CSP generation could not be met as operating it at full load leads to faster depletion of the hot TES. This could be seen in Figure 73. However, PV and CSP had over 98 % availability between 11h00-18h00. Thus, CSP contribution is appreciated in the late afternoons and early evenings.

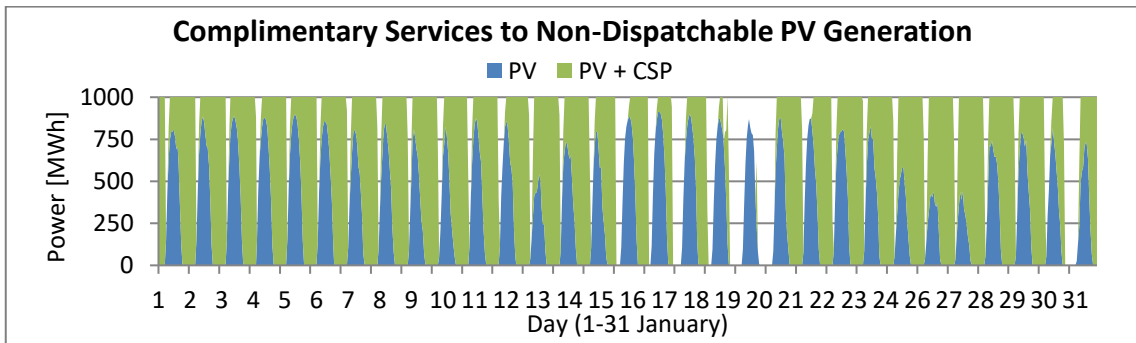


Figure 71: Generation profile, PV and CSP with continuous output

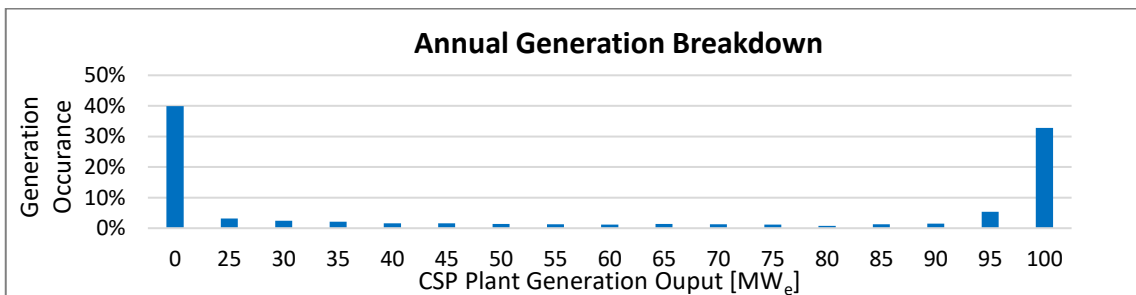


Figure 72: Annual generation profile, CSP with complimentary services to PV

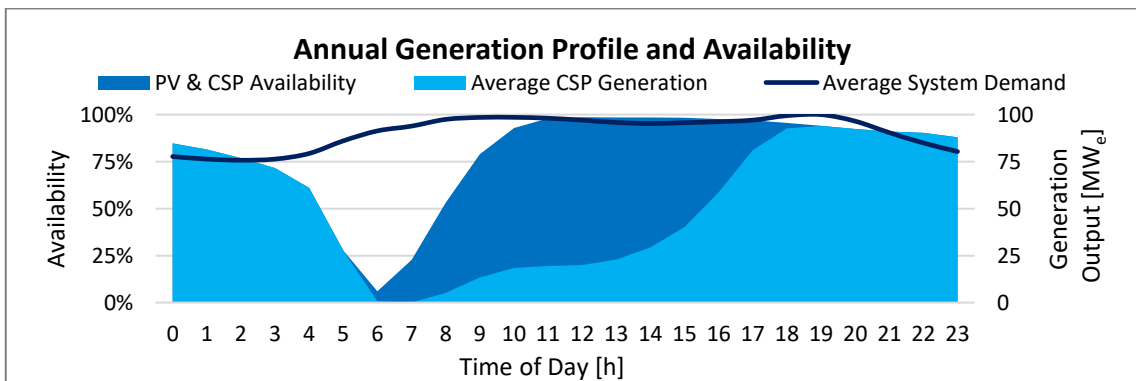


Figure 73: Annual generation profile and availability, PV and CSP generation

6.4.3. Complimentary Services to Wind and PV Generation

The effects of complimenting CSP with both wind and PV generation on the plant operations were studied. When PV contributed to the system, the CSP plant charged its hot TES. Whereas, the continuous wind generation allowed the CSP plant to operate in part load. The power delivered to the system in this case maintained a better continuity as compared to the case when only PV was used (Figure 74). The generation occurrence peaked at 80 MWe, see Figure 75, with no generation at 22 %. The contribution of wind generation assisted in part load operations for the plant, increasing the overall availability in the early morning to almost 60 %, from which about 50 % of the contribution was from CSP due to its storage, see Figure 76.

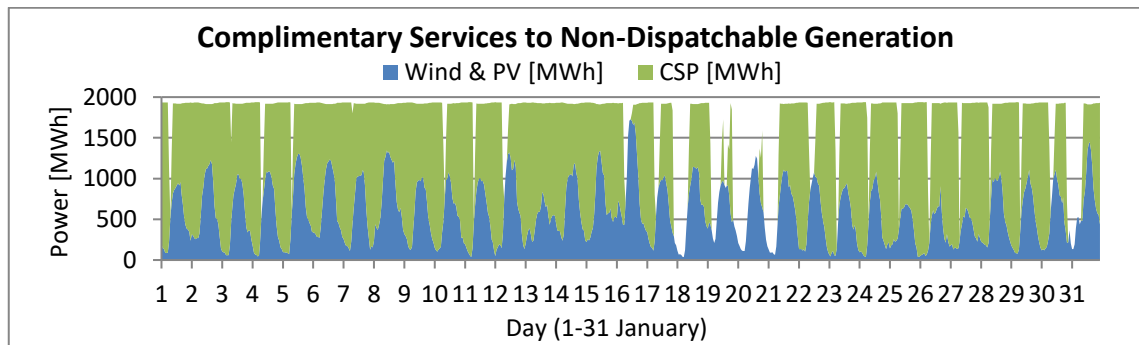


Figure 74: Generation profile, Wind-PV and CSP for continuous output

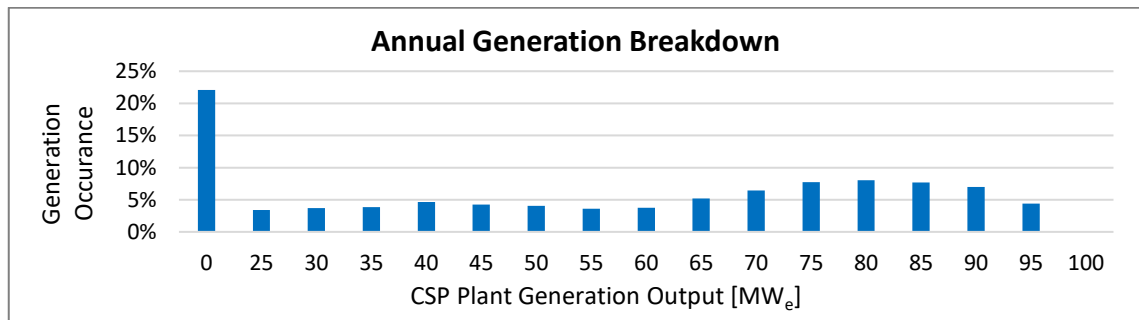


Figure 75: Annual generation profile, CSP with complimentary services to Wind-PV

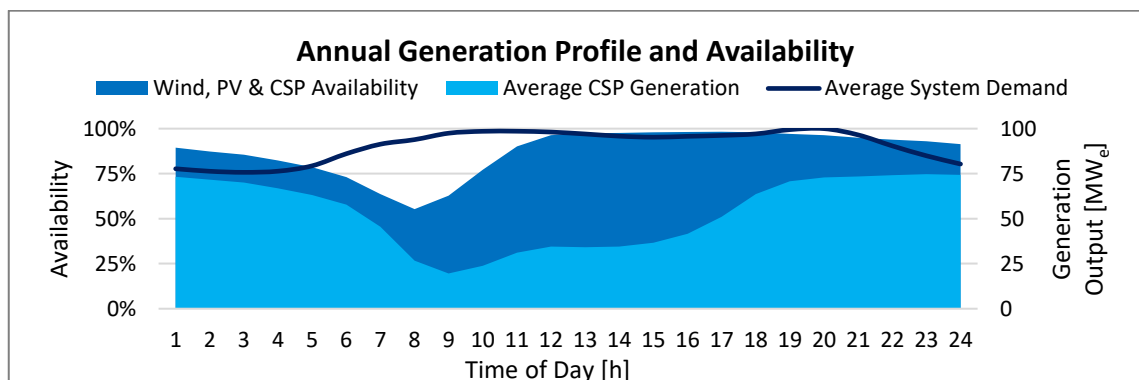


Figure 76: Annual generation profile and availability, Wind-PV and CSP generation

6.4.4. Complimentary Services Summary

The value-added contribution of CSP to the system in providing complimentary services to wind and PV generation was discussed and illustrated in the sections above. However, the plant design was intended predominately, for a maximise power generation operating strategy, to achieve a yearly plant capacity factor above 60 %. Therefore, as evident from Table 24, the plant efficiencies were greatly affected by the complimentary services of wind and PV generation that CSP offered. The three ‘complimentary services’ operating strategies are compared to the ‘maximise power generation’ operating strategy.

Table 24: Plant performance indicators, complimentary services to Wind and/or PV

Annual Energy Yield per System	Complimentary services to Wind	Complimentary services to PV	Complimentary services to Wind-PV	Maximise Power Generation
Incident power in solar field	3858 GWh _t	3858 GWh _t	3858 GWh _t	3881 GWh _t
Receiver gross thermal power	1286 GWh _t	1320 GWh _t	1317 GWh _t	1570 GWh _t
Receiver net thermal power	1137 GWh _t	1132 GWh _t	1130 GWh _t	1355 GWh _t
Total electric power generated	467 GWh _e	454 GWh _e	460 GWh _e	573 GWh _e
Annual Efficiency per System	Complimentary services to Wind	Complimentary services to PV	Complimentary services to Wind-PV	Maximise Power Generation
Heliostat field efficiency	33.3 % (-7.12 %)	34.2 % (-6.24 %)	34.1 % (-6.31 %)	40.45 %
Receiver efficiency	88.4 % (+2.10 %)	85.7 % (-0.62 %)	85.8 % (-0.58 %)	86.34 %
Power block efficiency (Gross)	41.1 % (-1.21 %)	40.1 % (-2.20 %)	40.7 % (-1.57 %)	42.31 %
Plant Efficiency (Gross)	12.1 % (-2.66 %)	11.8 % (-3.01 %)	11.9 % (-2.85 %)	14.78 %
Plant Efficiency (Net)	10.9 % (-2.48 %)	10.5 % (-2.81 %)	10.7 % (-2.66 %)	13.35 %
Plant Capacity Factor	53.36 %	51.80 %	53.36 %	65.46 %

The receiver gross thermal power for normal operation was reduced. This was due to the full state of charge in the hot TES. The plant rarely operated at full load when the receiver was in operation. The average CSP generation from each operating strategy’s annual generation profile is as in Figure 70, Figure 73 and Figure 76. Therefore, the dispatch from the hot TES was not fast enough to secure the allocation for the full potential of energy offered by the heliostat field. The heliostat field efficiency greatly reduced by 7.12 %. The power block efficiency reduced by about 1.21 - 2.20 %. The two contributing factors being the increase of power block start-ups and increase in part load operations. The complimentary services to wind generation allowed part load operations of the CSP plant. Therefore, the main contributing factor in the power block efficiency was due to reduced efficiency of part load operations. However, when PV is considered, the increase in the power block start-ups were the main contributing factor. This results in the lowest power block efficiency. Due to the increase in the part load operations the plant start-ups were decreased. This lead to the increase in the power block efficiency as the result of the combination of PV and wind generation.

Overall, the plant efficiency decreased with about 2.5 % to 2.8 %, offering complimentary services to non-dispatchable generating technologies. The dispatchability potential of CSP with TES is appreciated in this analysis. It provides continuous power and stability to the electric grid. The hourly availability on each operating strategy is

provided to better understand the contribution to the hourly demand of the system. Although, the plant design catered for the maximise power generation operating strategy, the plant design proved to be flexible in plant operations to offer these complimentary services to the system.

6.4.5. Base Load Operations

CSP with storage could further provide base load capabilities to the system. In the ‘base load’ operating strategy, the model optimised the hot TES to deliver continuous power to the system throughout the day. The results are shown in Figure 77. A sufficient amount of energy was collected from the solar collecting system to alternate the turbine output between 50 MWe to 100 MWe. The power block dispatch profile is shown in Figure 78.

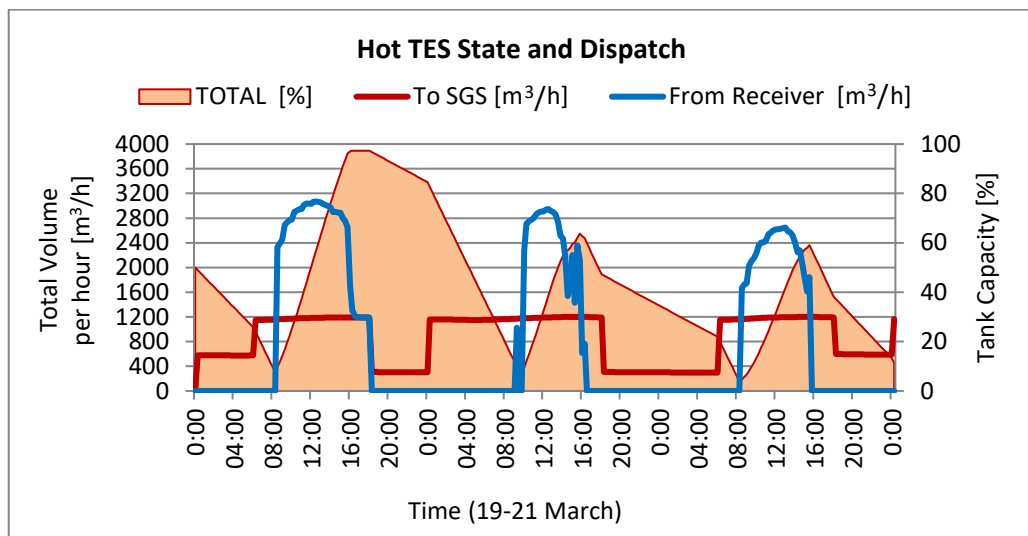


Figure 77: Hot TES dispatch control, maintaining sufficient capacity in hot TES

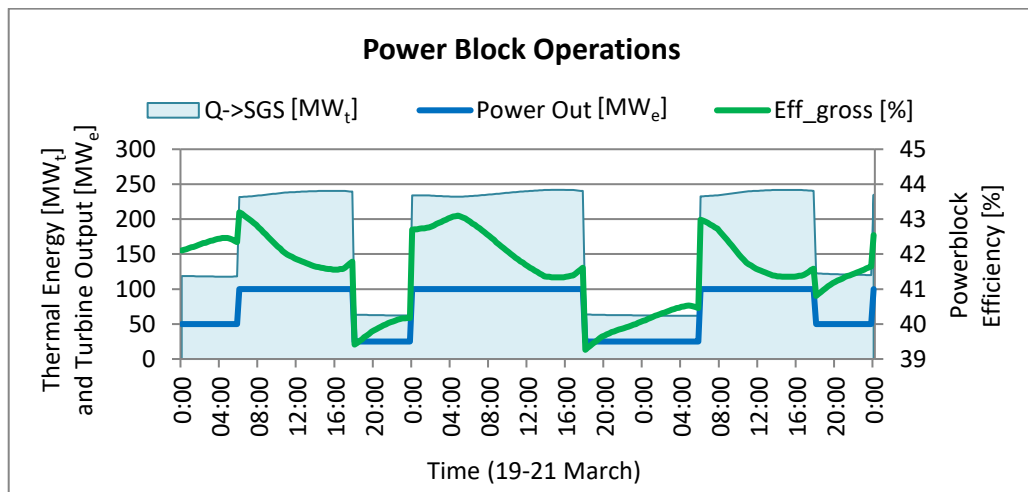


Figure 78: Power block dispatch profile to the grid, base load capability

Under high DNI conditions, excessive energy is collected from the solar collecting system, providing the hot TES with sufficient energy to maintain the base load operations. With the hot TES sufficiently charged, the power block could maintain a higher turbine output as illustrated in Figure 79.

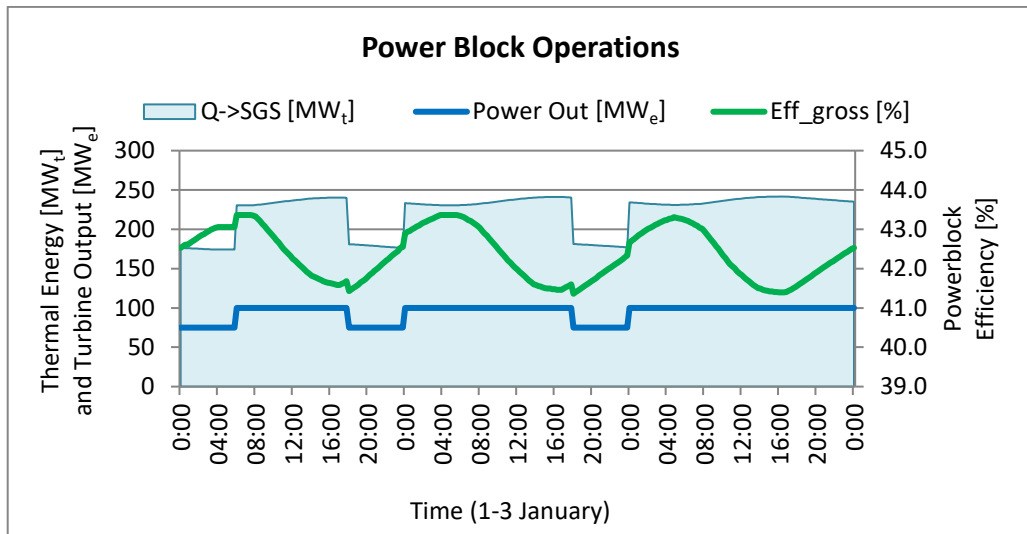


Figure 79: Base load operations while maintaining a higher turbine output

However, when low DNI periods are considered (Figure 80), the model provides continuous power by reducing the turbine output. Therefore, thermal energy attained on the first day is better utilised to provide continuous power throughout the period till the last day. The results are shown in Figure 81. The early morning turbine output was increased to make provision for the receiver's thermal output, see Figure 82.

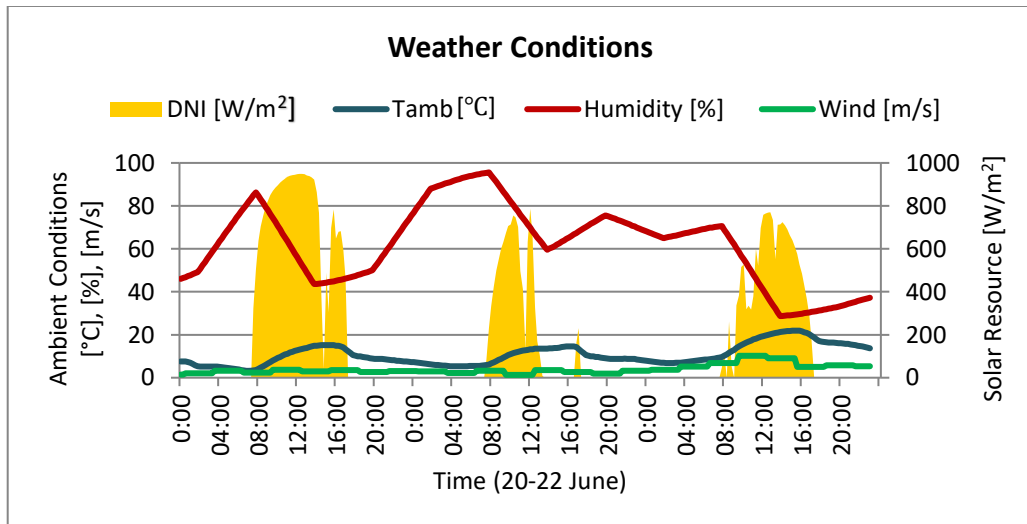


Figure 80: Weather conditions applicable for the low DNI period

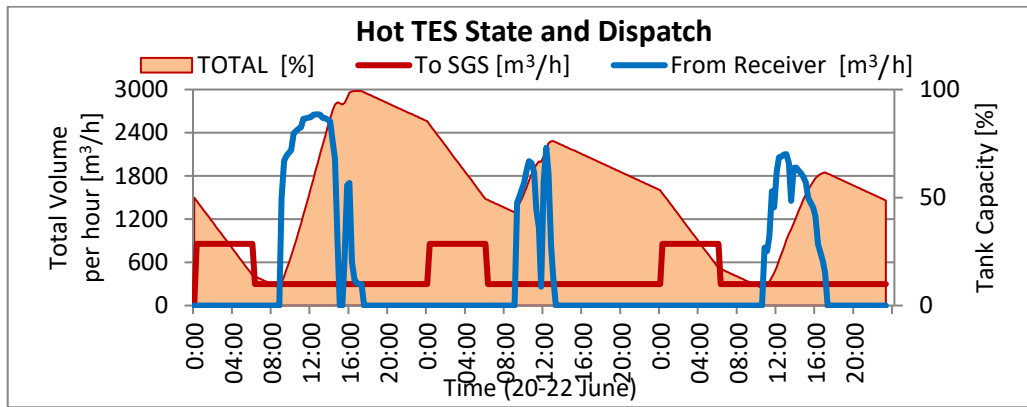


Figure 81: Hot TES dispatch during low DNI periods

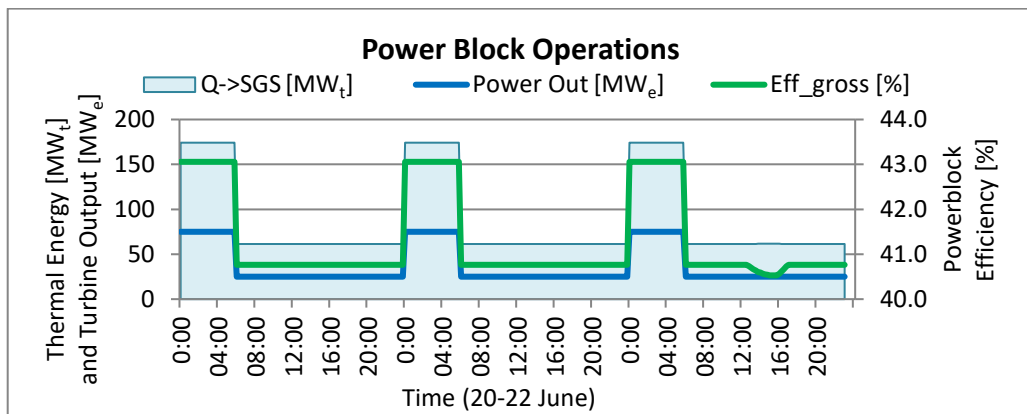


Figure 82: Lower turbine output during low DNI periods

The annual performance of the ‘Base Load’ operating strategy has been investigated and the results are shown in Figure 83. The annual results indicate higher plant availability, which was greater than 95 % from 10h00-24h00. From the annual results it was observed that on operating the plant under the base load operating strategy only 6.5 % of it accounted towards no generation output from the plant.

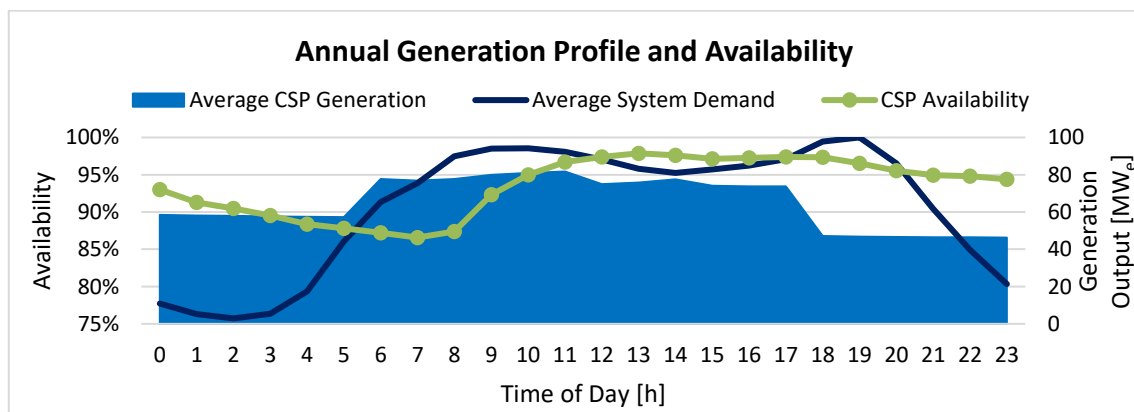


Figure 83: CSP offering base load capabilities to the system demonstrated

6.4.6. Peaking Operations

Peaking operations specify the desired turbine output at selected times. Peaking operations are less challenging as base load operations, as the receiver ideally charges the hot TES during the day. Peaking times are generally early evenings after sunset, therefore it is assumed that sufficient thermal energy would be available in the hot TES to meet these requirements. With the sufficient energy collected from the solar collecting system, the plant is able to provide electric power to the grid during the specified peak period. For illustrative purposes, 120 MW_e is required from the plant during the specified peak period of 18h00-20h00. During the 'Peaking' operating strategy, the power generation is prioritised for the specified peaking period. The model optimises the plant operation to deliver the required electric power during peak times, while maintaining a maximise power generation undertone, see Figure 84.

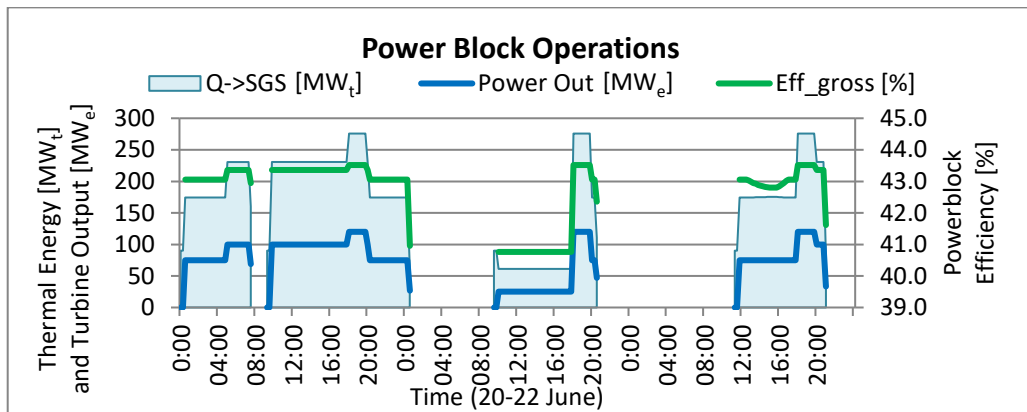


Figure 84: 'Peaking' capabilities demonstrated during low DNI period

7. CONCLUSION

7.1. Summary of Findings

The ‘Maximise Power Generation’ also known as the ‘Solar Driven’ operating strategy, is predominantly followed in the industry by CSP plant operators. Many literatures focus on optimising the plant design and operation for this operating strategy as it yields maximum electric power, high capacity factors and low LCOE values. The plant operation is simulated for this operating strategy by running the power block at full load until depletion of the hot TES (Garcia-Barberena and Erdocia, 2016, Morin, 2010 and Wagner and Wittman, 2014). This plant operation is also implemented in the SAM model used in this research, evident in the annual plant generation profile seen in Figure 61. This research found that operating the plant at selected times under part load conditions increase the gross power block efficiency (+1.8 %), plant net efficiency (+0.6 %), electric power generation (5.3 %), plant net electric power (+4.4 %) and capacity factor (3.4 %). Therefore, the common assumption made in the industry and by the literature that operating the plant at full load until depletion of the hot TES does not necessarily result in maximum power generation. Therefore, optimising plant designs under this assumption should be revisited, especially the plant with sufficient TES. Further lowering of the plant LCOE is possible through part load operational optimisation. This is achieved by lowering the operating and maintenance cost associated with cyclic stresses in the power block components that is reducing the amount of start and stops in the power block. Additionally, the increase in the generation output from the plant would reduce the LCOE by the same percentage (Wagner and Wittman, 2014).

Various literatures have investigated the optimisation of CSP plant design or operation to maximise plant revenue under various financial boundary conditions (Casella *et al.*, 2014, Petrollese *et al.*, 2017, Kost *et al.*, 2013, Dersch *et al.*, 2015, Silinga *et al.*, 2015, Dominguez *et al.*, 2012, Guedez *et al.*, 2013 and Guedez *et al.*, 2015). The focus on this operating strategy is expected as CSP plants have relatively high investment costs compared to other renewables such as wind and solar photovoltaics. Although, the thermal energy storage by the CSP plants leads to increase in the capital expenditure, it allows dispatchability of electric power to the electric grid during peak hours, when the tariffs pay the most. In a study done by Guédez *et al.*, analyses of the effect of market conditions on the profitability of a South African CSP plant were done (Guédez *et al.*, 2016). The modelling results illustrated the trade-offs between minimising investments and maximising profits under three scenarios. The scenarios were based on incentive programs and wholesale electricity prices. The optimal plant configuration for each scenario highlighted the value, in terms of profitability, for the storage offered under the time-of-day tariff structure. An economic evaluation of the plant configurations resulted in the LCOE being used as the performance indicator. Therefore, an optimal plant configuration with a selected operating strategy resulted in an accompanying LCOE. This research approach is typically applicable when the plant operator is an IPP with a PPA in place.

The plant design in this research was not optimised for a specific tariff structure. The maximise power generation and maximise plant revenue operating strategies, therefore, share the same operational objectives where a fixed price is awarded for power generation. It is for this reason that the maximise power generation optimisation also resulted in the maximum plant revenue. Although, the developed model catered for various tariff structures, it was concluded from the simulation results that the plant's heliostat field, receiver and thermal storage was overdesigned for a PPA similar to the REIPPPP Bid Window 3. A comparison between the parabolic trough and the central receiver technologies with molten salt as heat transfer fluid was conducted by Poole, 2017. This study optimised the plant design 100 MW_e, for different locations in South Africa under the flat rate and two-tier tariff structure. The outcomes of this research are of great value as the receiver and power block design parameters, as well as the performance curves are based on the simulation results of the developed model from this research. These outcomes suggest that for the flat rate tariff structure, a 100 MW_e tower plant based in Upington, 14 hours of TES and a SM of 2.9 results in the lowest LCOE. Whereas, a plant with 6 hours storage and a SM of 2.3 favour the LCOE in the two-tier tariff structure (Poole, 2017). The operating strategy for the power block followed the 'Solar Driven' operating strategy, operating the power block at full load when possible.

The 'Minimise Energy Dumping' operating strategy provides the plant operator with a forecast for the hot TES dispatch to prevent energy dumping from the solar field. The model accurately increased the turbine output to 110 % at selected times, increasing thermal energy dispatch to the power block, thus reducing energy dumping from the field. Energy dumping was reduced from 4.0 % to 2.7 %. An additional 1.8 % of electric power was generated compared to the Maximise Power Generation operating strategy, and 7.4 % greater than the results from SAM.

As South Africa progresses towards a more diverse energy mix, the system should include generation capable of starting, stopping and ramping rapidly. Therefore, serving the responsive load quickly by dispatching reserves to ensure system stability. System flexibility is the general characteristic of the ability of the aggregated set of generators to respond to the variation and uncertainty in the net load (Denholm and Hand, 2011). Highlighted by Denholm and Hand (2011), the methods of shifting demand in the system will become increasingly valuable. They found that with non-dispatchable renewable energy penetration above 50 %, electrical or thermal storage provides a critical role in integrating these technologies and reducing the curtailment of the conventional generation. These findings were supported by a recent study, that performed a case study on South Africa, highlighting the role of CSP with storage at high penetrations of wind and PV (Badeda *et al.*, 2016). The case study is a continuation of research methodology (Lunz *et al.*, 2015), determining the value of CSP in electric grids.

The role and value of thermal storage in the electric grid have been established by aforementioned references. However, the results from the 'Complimentary Services' introduced another dimension that is not considered in optimising the electric grid. The simulation results demonstrated the complimentary services to wind and/or PV generation by coupling CSP with storage. In this case, a continuous output is achieved that provides system reliability and stability. Furthermore, limitation in the grid capacity and

constraints in South Africa's transmission network is prevalent (Eskom, 2014). The transmission development plan for the period 2016-2025 set forth Eskom's infrastructure expansion programme to enable connection of future IPPs (Eskom, 2015). However, the cost, timeline and location of these upgrades may hinder connection of future generation plants in areas of good resources. Non-dispatchable generation plants such as wind and PV, do not utilise 100 % allocation on the grid. From the results shown in Table 24, complimentary services from CSP with storage could benefit the utilisation factor on these constrained areas. This opportunity greatly increases the market of CSP and emphasises the value of thermal storage. The results indicated that the plant design optimisation is required to increase the plant performance and efficiency. The optimised design configuration was investigated to provide continuous power output of 100 MW_e from a combination of CSP and PV plant by using weather data from Upington, South Africa (Pan and Dinter, 2017). Therefore, this operating strategy proved viable especially in grid constraint areas. However, plant design optimisation is required to accommodate this operating strategy.

The 'Base Load' operating strategy, also referred in literature as the 'Reduce Stops' (Garcia-Barberena and Erdocia, 2016 and Garcia-Barberena *et al.*, 2012), aims to increase the online hours of the power block and reduce the turbine start-ups required. The research conducted by Garcia-Barberena and Erdocia (2016), reduced the turbine stops by 67 % for a CSP plant with 8.5 hours of storage when operating the power block at minimum load. The turbine load increased when the hot TES reached full capacity. This approach, however, introduces the risk of energy dumping, especially for a plant with a SM greater than 2. The turbine operates further from its design point conditions, when the power block is operating on its minimum load. This reduces the power block efficiency. This is evident from the results published by them. They reported a power block gross efficiency of 34.7 % and 31.3 % for 'Solar Driven' and 'Reduce Stops', respectively. In this research, the 'Base Load' operating strategy was optimised to operate at the maximum allowable load while ensuring sufficient levels in the hot TES for continuous power generation. An increase in power generation of 3.6% was observed when it was operated at maximum allowable load. The gross efficiency of the power block was 42.2 %, compared to 42.3 % from the 'Maximise Power Generation' operating strategy. The turbine stops were reduced by 85 % to 52 stops per annum. Similarly, with the part load optimisation evident in the 'Maximise Power Generation' operating strategy, the turbine stops were reduced by 50 %. The main advantage of reducing the turbine stops is the cyclic operation stress associated with the power block components, thus reducing degradation and maintenance (Garcia-Barberena and Erdocia, 2016). Ultimately, the operation and maintenance costs are reduced, thus reducing the plant LCOE (Garcia-Barberena *et al.*, 2012).

Peaking operations are well understood in the industry and no significant findings are reported. It has been noted from literature (Garcia-Barberena and Erdocia, 2016) that an increase in turbine stops for this operating strategy is present. This is as a result of the shutdown of the power block in order to preserve sufficient energy for the peaking operations. In this research, the model has been adapted to prevent additional turbine start-ups. Thus, thermal energy for the power block start-up is conserved.

7.2. Conclusion

South Africa's progress towards a more diverse energy mix is therefore, necessary to build a better understanding of both the contribution and implications that renewable energy generating technologies have on the electric grid. IPPs and other CSP plant operators across the globe predominantly adopt the 'Maximise Power Generation' operating strategy. This research investigated the effects of an array of varying operating strategies imposed upon the plant. It is an essential exercise to determine the possible role of CSP within the South African electric grid. The three boundary conditions of weather conditions, plant status, and operating strategies, determine the operations of a CSP plant. The literature review established that no publically available model is available to optimise the plant operations under these conditions. A model was therefore developed to achieve the research objectives.

The results of the simulation demonstrated that the various operating strategies have effects on plant operations, plant performance, and finance that form the core indicators. It is concluded that when a flat rate tariff structure is applied, the 'Maximise Power Generation' and the 'Maximise Plant Revenue' operating strategies coincide. These operating strategies delivered maximum plant revenue and net power to the grid under any environmental conditions. It was often noted that the power block was curtailed to take advantage of the high turbine efficiency, which is performed to avoid turbine stops or shutdowns. By curtailing the power block, the energy saved from the turbine start-up increased the power block efficiency, ultimately increasing the plant efficiency. In 'winter' seasons where limited thermal energy was available, the power block did not curtail its output. To avoid turbine shutdown, longer periods for curtailment were required. However, energy loss due to lower turbine efficiencies outweighed the energy required for turbine start-up. Thus, the turbine shut down its operations upon depletion of the hot TES, and starts them again when it receives sufficient energy from the receiver. Therefore, as compared to the other operating strategies, the 'Maximise Power Generation' yields maximum plant revenue and efficiency under any weather conditions.

In the case of the 'Time-of-day' tariff structure, the results indicated that the reference plant used in the simulation model and the PPA tariff structure of Bid Window 3.5 did not align for either higher plant efficiencies or revenue generated. As this operating strategy was included for demonstrating the model flexibility, informative results were gathered. The importance of plant design to adhere to the PPA was highlighted. The results obtained from the moderate to high DNI periods concluded that the plant was overdesigned in terms of heliostat field size, receiver and thermal storage. The time-of-day tariff structure offered the electric grid lower purchasing costs per unit power as compared with the other operating strategies. However, in the lower DNI scenario, the system cost per unit power was higher compared to the flat rate tariff structure as the model prioritised power generation during high paying tariff periods. Although, the time-of-day tariff structure was intended for demonstrative purposes only, the results highlighted important factors to consider when drafting PPAs as well as plant designs. This model offers the ability to simulate the plant operations of a proposed plant under a given PPA. The results could further assist developers and/or policymakers to optimise the plant design or amend the PPA structure.

Further, the developed model is able to compare various operating strategies by means of a graphical representation and a data table. By analysing the overview, the user can conclude which operating strategy delivered the highest receiver efficiency, power block or plant efficiency, the highest net power output of each sub-system and highest net or gross revenue. The user can either compare the same operating strategy for various periods, pertaining to different weather conditions, or compare various operating strategies under the same weather conditions. Either way, the model would be able to determine the more preferable operating strategy given the user requirements or objectives.

The ‘Minimise Energy Dumping’ operating strategy is an additional tool at the disposal of the plant operator. It determines the minimum power block output required before energy dumping occurs. It proved to be advantageous during high DNI periods. The hot TES dispatch was optimised to limit the risk of either receiver curtailment or shutdown due to a full hot TES. Furthermore, by adapting the heliostat field aiming strategy, the deflected solar energy from the receiver due to flux limitations is regained.

Pertaining to the research objectives, the model developed is capable of demonstrating the effects that (i) weather conditions, (ii) plant status and (iii) operating strategies have on the operational capabilities of the central receiver technology. The advantages that this model offers over other similar simulation models available in literature is as follows: (i) it provides a detailed (up to seven-days) forecast of the plant operations, (ii) it implements time resolution of 15 minutes, thus, increasing the transients and results accuracy, (iii) it provides user flexibility to specify the precise boundary conditions imposed on the plant operations, and (iv) this model is capable of comparing various simulations on the basis of the key performance and financial indicators.

The research outcomes obtained and the model developed offers Eskom and the system operator with the required tools to address the specific business needs that are identified by the EPPEI program. Utilising this model, with future modifications, the system operator would be able to determine a seven-day forecast. The resulting cost of generation and performance indicators are able to assist in future PPA formulation.

There are three common arguments against renewables. First, some stakeholders argue that renewables are not able to provide base load capabilities. Second, renewables do not deliver power to the system when it is required the most. Third, and more generally, renewables are unpredictable and unreliable. This research further extended the capabilities of the model to investigate these claims. It is concluded that CSP with storage offers additional benefits and value to the electric grid. The results demonstrated that CSP is indeed capable of providing continuous power delivery to the electric grid when base load operations are considered. The value obtained utilising the dispatch capability from the plant’s storage is fully realised with the implementation of the peaking operations. The inherent dispatchability potential of CSP compliments other non-dispatchable renewable energy generation plants such as wind and PV. The value and benefit obtained from this symbiotic relationship provide the grid with continuous power, security of supply, and a reliable clean source of power generation.

7.3. Further Research Developments

The model developed during this research project was based on the Solar-1 basic design. Each subsystem of the plant is incorporated into the model to represent a central receiver CSP plant of 100 MW_e with 12 hours of storage. The results of this intended model demonstrate the plant operational optimisation in terms of weather conditions, plant status and operating strategy. With the research objectives achieved, it is envisioned that the model is extended further beyond the focus of this research project. The following areas were identified for further development.

The model in its current state represents a plant simulator. Its design is based on the design of the Solar-1 basic design. However, the successful bidder for the Solar-1 project will implement its submitted design. The bidder's submitted proposal in all likelihood will be different than the Solar-1 basic design. These changes directly affect the performance of each subsystem and consequently the developed model will no longer be applicable.

It is for this reason, the first modification to the model will allow the user to specify the heliostat field as well as receiver and power block performance curves. Furthermore, the plant auxiliary consumption curves and storage size will be user-defined. The user will also be granted with the freedom of importing the site-specific TMY data.

The software package SAM utilise the user specified system design parameters, installation and operating costs, to create results for annual plant performance predictions and cost of energy estimates. However, the methodology used to validate the model in this study can be used to extract relevant data from the SAM results to develop the performance curves required by the model. A manual accompanying the updated version will guide the user in exporting data from SAM to the model. The model will be able to form results in the form of the performance curves and relevant equations.

SAM's flexibility regarding power block optimisation lies within the user-specified dispatch profile of the power block. As this approach limits optimisation of plant operations, the developed model from this research can provide the user with a detailed plant operational report for up to seven days on any implemented operating strategy. The user can therefore be better informed regarding the proposed plant's operations and performance relating to the plant design, weather conditions and operating strategy. The advantages of the developed model highlight the plant performance and financial indicators by comparing the operating strategies in various periods. To further extend the flexibility and value of the model, the model will grant the user freedom to compare various plant designs under similar boundary conditions. This functionality further assists in plant design optimisation required due to implemented operating strategies.

With the various plant designs catered for in the updated version, the focus is shifted towards the system operator. The developed model is to be implemented at the NCC. The system operator would utilise the model as a tool to obtain a seven-day forecast for a CSP plant. In order to set up the model for the system operator, similar performance curves are to be provided by the IPP. By incorporating the weather forecast data for the site-

specific plant and the relevant PPA, the model generates the forecast, plant performance and cost of unit power for the system operator.

According to the Eskom's business requirements, additional conditions may be imposed on the operating strategies. Conditions, such as generation of dispatch order, will further determine the impact on plant operations. It is envisioned that once the system operator is engaged on this level of details, additional requirements, conditions and cost structures have to be included in the model. These requirements may include, but not limited to, pricing for complementary, regulatory and ancillary services.

The proposed future work supports Eskom's directive to further develop its competencies in CSP and enables the system operator to enhance the progression of the electric grid to cater for a diverse energy mix. The objectives related to the future work are, to establish an all-inclusive platform engaging the power industry, academia and policy makers on the detailed performance, limitations and advances CSP offers under various designs, operating strategies, PPAs and weather conditions.

Areas of Improvement:

The following areas of improvement are highlighted in the current research project:

- Receiver and turbine start-up procedures, pertaining to time and thermal energy required, i.e. cold, warm and hot start-ups as well as receiver cloud transients.
- Detailed subsystems auxiliary power consumptions, i.e. heliostat field, receiver, TES, power block, BoP, and others.
- Financial parameters of plant operations, resulting in more accurate estimates for cost of generation and revenue per unit power.
- Introduction of water usage in plant operations
- More detailed thermal losses in plant and subsystems
- Overall improvements in the Graphical User Interface of the model
- Elimination of minor programming bugs
- Optimisation of programming sequences and execution speed

REFERENCES

- Alpert, D. J. and Kolb, G. J., 1988. *Performance of the Solar One Power Plant Simulated by the SOLERGY Computer Code*. Albuquerque(NM): Sandia National Laboratories, SAND99-0321.
- Augsburger, G., 2013. *Thermo-economic optimisation of large solar tower plants*, Lausanne, Switzerland,: PhD Thesis, École Polytechnique Fédérale De Lausanne.
- Badedá, J., Stocker, P., Sauer, D. U., Mehos, M., De Meyer., O. A. J., Pitz-Paal, R., 2016. *What is the Role of CSP in the Future South African Electricity System with CO2 Emission Targets?*. https://www.researchgate.net/publication/316825652_What_is_the_Role_of_CSP_in_the_Future_South_African_Electricity_System_with_CO2_Emission_Targets [Accessed September 2016].
- Behar, O., Khellaf, A. and Mohammedi, K., 2013. A Review of Studies on Central Receiver Solar Thermal Power Plants. *Renewable and Sustainable Energy*, Issue 23, pp. 12-39.
- Bode, S. J. and Gauche, P., 2012. *Review of Optical Software for use in Concentrated Solar Power Systems*. Stellenbosch, Proceedings of SASEC 2012.
- BrightSource Energy, 2014. *Flickr*. <https://www.flickr.com/photos/brightsourceenergy> [Accessed November 2016].
- Brightsource, 2014. *BrightSourceEnergy*. http://www.brightsourceenergy.com/stuff/contentmgr/files/0/3eac1a9fed7f13fe4006aaab8c088277/attachment/ivanpah_white_paper_0414.pdf [Accessed 16 August 2014].
- Budynas, R. G. and Nisbett, J. K., 2008. *Shigley's Mechanical Engineering Design*. New York(NY): McGraw Hill, ISBN 978-007-125763-3.
- Burgaleta, J. I, Temero, A., Vindel, D., Salbidegoitia, I., and Azcarrage, G., 2012. *Gemasolar, Key Points for the Operation of the Plant*. Marrakech (Morocco), Proceedings of the 18th SolarPACES International Conference.
- Candy, D. R., 2014. *Eskom Corporate Specialist, System Operator* [Interview] (11 2014).
- Casella, F., Casati, E. and Colonna, P., 2014. *Optimal Operation of Solar Tower Plants with Thermal Storage for System Design*. Cape Town, South Africa, s.n.
- Cengel, Y. A., 2009. *Heat and Mass Transfer, A Practical Approach*. 3 ed. New York(NY): McGraw Hill.
- CMI, 2017. *CMI Groupe*. <http://www.cmigroupe.com/thermal-solar-receivers> [Accessed June 2017].
- Crane, 1986. *Flow of Fluids, Through Valves, Fittings and Pipe - Metric Edition*. London: CraneLTD.
- De Meyer, O. A. J., Dinter, F. and Govender, S., 2015. *Thermal Resistance Model For CSP Central Receivers*. Cape Town, Proceedings of the 21st SolarPACES Conference,
- De Meyer, O. A. J., Dinter, F. and Govender, S., 2014. *Research Project Proposal: Optimisation of the Solar Energy System for a 100 MW CSP Tower Plant with focus on*

the Operating Philosophy, Stellenbosch: Stellenbosch University, Mechanical & Mechatronic Engineering Department.

DEA, 2014. *South Africa's Greenhouse Gas (GHG) Mitigation Potential Analysis*, Pretoria: Department of Environmental Affairs (DEA).

Denholm, P. and Hand, M., 2011. Grid flexibility and storage required to achieve very high penetration of variable renewable electricity. *Energy Policy*, Volume 39, pp. 1817-1830.

Dersch, J., Dieckmann, S. and Hennecke, K., 2015. Annual performance calculations for CSP plants under different feed-in tariff schemes. *Energy Procedia*, Volume 69, pp. 2031-2038.

Dinter, F. and Busse, K. T. T., 2016. Overview of predictive CSP spread prospects and its opportunities. *Journal of Energy in Southern Africa*, 27(2), pp. 50-59.

Dinter, F. and Mayorga Gonzalez, D., 2013. Operability, reliability and economic benefits of CSP with thermal energy storage: first year of operation of ANDASOL 3. *Energy Procedia*, Volume 49, pp. 2472-2481..

DoE, 2011. *Electricity Regulation Act No4 of 2006. Electricity Regulations on New Generation Capacity*, SA: Department of Energy.

DoE, 2013. *Integrated Resource Plan for Electricity 2010-2030*.http://www.DOE-irp.co.za/content/IRP2010_updatea.pdf. [Accessed March 2016].

DoE, 2015. *State of Renewable Energy in South Africa*, Pretoria: Department of Energy.

DoE, 2016a. *DoE: About SA - Energy, Nuclear*. <http://www.gov.za/about-sa/energy> [Accessed 23 June 2016].

DoE, 2016b. *Independent Power Procurement Program - An Overview as at 31 March 2016*, SA: DoE.

DoE, 2017. *Department of Energy*. <http://www.energy.gov.za/IRP/irp-2016.html> [Accessed June 2017].

Dominguez, R., Baringo, L. and Conejo, A. J., 2012. Optimal offering strategy for a concentrating solar power plant. *Applied Energy*, Volume 98, pp. 316-325.

Eskom, 2012a. *Basic Design Report*. Sandton: Eskom Project Documentation: CSP, Upington Demonstration Plant. S1GM000MEM0002.

Eskom, 2012b. *Site Meteorological Data*. Sandton: Eskom Project Documentation: CSP, Upington Demonstration Plant, S1GM000MEM0008.

Eskom, 2012c. *Conventional modelling report and conventional heat balances*. Sandton: Eskom Project Documentation: CSP, Upington Demonstration Plant. S1PR000MEM0003.

Eskom, 2013. *Ancillary Services Technical Requirements for 2014/15 - 2018/19*. Sandton: Eskom, No 342-201.

Eskom, 2014. *Generation Connection Capacity Assessment of the 2016 Transmission Network (GCCA-2016)*. <http://www.eskom.co.za/Whatweredoing/GCCARepor/Documents/GCCA2016ReportREV2.pdf> [Accessed September 2017].

- Eskom, 2015a. *Integrated Report 2014/15*, SA: Eskom.
- Eskom, 2015b. *Net system demand data of South Africa*. Germiston: South Africa National Control Centre.
- Eskom, 2015. *Transmission development plan 2016-2025*. <http://www.eskom.co.za/Whatweredoing/TransmissionDevelopmentPlan/Documents/TransDevPlan2016-2025Brochure.pdf> [Accessed September 2017].
- Eskom, 2016. *Integrated Report 2015/16*, SA: Eskom.
- Falcone, P. K., 1986. *A Handbook for Solar Central Receiver Design*. Livermore(CA): Sandia National Laboratories SAND-86-8009.
- Garcia-Barberena, J. and Erdocia, I., 2016. *Simulation and comparison of different operational strategies for storage utilization in concentrated solar power plants*. s.l., AIP Conference Proceedings 1734, 070010 (2016); doi: 10.1063/1.4949157.
- Garcia-Barberena, J., Garcia, P., Sanchez, M., Blanco, M. J., and Lasheras, C., 2012. Analysis of the influence of operational strategies in plant performance using SimulCET, simulation software for parabolic trough power plants. *Solar Energy*, Vol 86, pp. 53-63.
- Garcia-Casals, X., Tellez, F. and Millian, M., 2012. *Operation Strategies, Eskom: CSP Upington Demonstration Plant, Kiwano Project, Sandton (SA): Eskom, S1GM000MEM0015 rev0*.
- Garcia, E. and Calvo, E., 2012. *One Year Operational Experience of Gemasolar Plant*. Marrakech, Proceedings of the 18th SolarPACES International Conference.
- Garcia, L., Burisch, M. and Sanchez, M., 2015. Spillage estimation in a heliostats field for solar field optimization. *Energy Procedia*, Volume 69, pp. 1269-1276.
- GeoModel, 2011. *Site Assessment of Solar Resource, Upington Solar Park*. Stellenbosch: GeoModel Solar, Ref. No. 58-01/2011 rev. 2.
- Goswami, D. Y. and Kreith, F., 2007. *Handbook of Energy Efficiency and Renewable Energy*. Boulder(CO): CRC Press, ISBN 1420003488.
- Gould, W. R., 2011. *Solar Reserve's 565 MWt Molten Salt Power Towers*. Granada, Proceedings of the 17th SolarPACES International Conference.
- Govender, S., 2013. *Thermal Sciences for Engineers*. Sandton: Crown Publications. ISBN: 978-0-922-17813-0.
- Grobler, A. and Gauche, P., 2014. *A Review of Aiming Strategies for Central Receivers*. Port Elizabeth (South Africa), Proceedings of SASEC 2014.
- Guasti, N., 2015. *Nicxco Photography*. <http://niccologuasti.com/works/abengoa-solar-power-towers/> [Accessed November 2016].
- Guedez, R., Spelling, J., Laumert, B. and Fransson, T., 2013. Optimisation of thermal energy storage integration strategies for peak power production by concentrating solar power plants. *Energy Procedia*, Issue 49, pp. 1642-1651.

- Guédez, R., Topel, M., Conde, I., and Ferragut, F., 2016. A Methodology for Determining Optimum Solar Tower Plant Configurations and Operating Strategies to Maximize Profits Based on Hourly Electricity Market Prices and Tariffs. *SME Journal of Solar Energy Engineering*, 128(2).
- Guedez, R., Topel, M., Spelling, J. and Laumert, B., 2015. Enhancing the profitability of solar tower power plants through thermoeconomic analysis based on multi-objective optimization. *Energy Procedia*, Volume 69, pp. 1277-1286.
- Ho, C. K., 2008. *Software and Codes for Analysis of Concentrated Solar Power Technologies*. Albuquerque(NM): Sandia National Laboratories, SAND08-8053.
- IRENA, 2015. *Renewable Power Generation Costs in 2014*, Bonn, Germany: International Renewable Energy Agency (IRENA).
- JG Afrika, 2017. *JG Afrika*. <http://www.jgi.co.za/projects/> [Accessed June 2017].
- Kelly, B. and Singh, M., 1995. Summary of the final design for the 10 MWe solar two central receiver project. *Solar Engineering*, Issue 1, p. 575.
- Kistler, B. L., 1986. *A User's Manual for DELSOL3: A Computer Code for Calculating the Optical Performance and Optimal System Design for Solar Thermal Central Receiver Plants*. Albuquerque(NM): Sandia National Laboratories, SAND86-8018.
- Kolb, G. J., 2011. *An Evaluation of Possible Next-Generation High-Temperature Molten-Salt Power Towers*. Albuquerque(NM): Sandia National Laboratories: SAND11-9320.
- Kost, C., Flath, C. M. and Most, D., 2013. Concentrating solar power plant investment and operation decisions under different price and support mechanisms. *Energy Policy*, Volume 61, pp. 238-248.
- Litwin, R. Z., 2002. *Receiver System: Lessons Learned from Solar Two*, Albuquerque (NM): Sandia National Laboratories, SAND2002-0084.
- Lovegrove, K. and Stein, W., 2012. *Concentrating solar power technology. Principles, developments and applications*. 21 ed. Cambridge : Woodhead Publishing Series in Energy.
- Lunz, B., Stocker, P., Pitz-Paal, R. and Sauer, D. U., 2015. *Evaluating the Value of Concentrated Solar Power in Electricity Systems with Fluctuating Energy Sources*. Cape Town, s.n.
- Morin, G., 2010. *Techno-economic design optimization of solar thermal power plants*, Braunschweig: Ph.D. thesis, Technische Universit at Braunschweig.
- Neises, T. W., Wagner, M. J. and Gray, A. K., 2014. *Structural Design Considerations for Tubular Power Tower Receivers Operating at 650'C*. Golden(CO): NREL, CP-5500-61848.
- Pacheco, J. E., 2002. *Final Test and Evaluation Results from the Solar Two Project*, Akbuquerque (NM): Sandia National Laboratories, SAND02-0120.
- Pan, C. A. and Dinter, F., 2017. Combination of PV and central receiver CSP plants for base load power generation in South Africa. *Solar Energy*, Volume 146, pp. 379-388.

- Petrollese, M., Cocco, D., Cau, G. and Cogliani, E., 2017. Comparison of three different approaches for the optimization of the CSP plant scheduling. *Solar Energy*, Volume 150, pp. 463-476.
- Poole, I. V., 2017. *Concentrating solar power in South Africa - a comparison between parabolic trough and power tower technologies with molten salt as heat transfer fluid*, Stellenbosch: MSc Thesis, Stellenbosch University.
- Radosevich, L. G., 1988. *Final Report on the Power Production Phase of the 10-MW Solar Thermal Central Receiver Pilot Plant*. Livermore(CA): Sandia National Laboratories, SAND87-8022.
- Reddy, V. S., Kaushik, S. C. and Tyagi, S. K., 2013. State-of-the-Art of Solar Thermal Power Plants - A Review. *Renewable and Sustainable Energy Reviews*, Issue 27, pp. 258-273.
- Rodriguez-Sanchez, M. R., Soria-Verdugo, A., and Almendros-Ibanez, J. A., 2014. Thermal Design Guideline of Solar Power Towers. *Applied Thermal Engineering*, Issue 63, pp. 428-438.
- SAM, 2014. *System Advisor Model V 2014.1.14. User Documentation, Power Tower Molten Salt System*, Golden, CO: NREL.
- Silinga, C., Gauche, P., Rudman, J. and Cebecauer, T., 2015. The South African REIPPP two-tier CSP tariff: Implications for a proposed hybrid CSP peaking system. *Energy Procedia*, Volume 69, pp. 1431-1440.
- Solar Reserve, 2014. *CSP-World.com*. <http://www.csp-world.com/news/20130201/00728/store-or-not-store-not-question> [Accessed 23 July 2014].
- Solar Reserve, 2016. *Solar Reserve*. <http://www.solarreserve.com/en/global-projects/csp/crescent-dunes> [Accessed November 2016].
- The Presidency, 2014. *National Development Plan 2030 - Our Future, make it work*, South Africa: National Planning Commission.
- Torresol Energy, 2010. *Torresol Energy*. <http://www.torresolenergy.com/TORRESOL/gemasolar-plant/en> [Accessed November 2016].
- Tyner, C. E., Sutherland, J. P. and Gould, W. R., 1995. Solar Two: A Molten Salt Power Tower Demonstration. *VDI Berichte*, Volume 1200, pp. 53-53.
- Wagner, M. J., 2008. *Simulation and Predictive Performance Modeling of Utility-Scale Central Receiver System Power Plants*. Madison(WI): University of Wisconsin.
- Wagner, P. H. and Wittman, M., 2014. Influence of Different Operation Strategies on Transient Solar Thermal Power Plant Simulation Models with Molten Salt as Heat Transfer Fluid. *Energy Procedia*, Volume 49, pp. 1652-1663.
- Wang, A., 2014. *Crescent Dunes Project Overview*. Santa Monica(CA): Solar Reserve.
- White, M., 2008. *Fluid Mechanics*. 6 ed. New York(NY): McGraw Hill, ISBN 978-0-07-128645-9.

Winsberg, E., 2002. *Simulated Experiments: Methodology for a Virtual World*, Tampa: Department of Philosophy, The University of South Florida.

Zavoico, A. B., 2001. *Solar Power Tower: Design Basis Document*. Albuquerque(NM): Sandia National Laboratories: SAND01-2100.

APPENDIX A: SOLAR-1 DESIGN PARAMETERS

The following design parameters were used in the development of the heliostat field, receiver and power block model.

Table A.1: Plant design parameters

	Value	Unit		Value	Unit
Heliostat Field			Power Block		
Number of Heliostats	11198	#	ACC IDT	20	°C
Heliostat Height	11.60	m	TES Capacity		
Heliostat Width	10.64	m	Hours of Storage	12	hours
Heliostat Area	123.42	m ²	TES Capacity	2877.6	MWh _t
Reflective Area Ratio	0.97		HTF Mass	24751	t
Total Mirror Area	1340638.9	m ²	HTF Volume	13611	m ³
Mirror Reflectivity	0.93		HOT Tank		
Mirror Cleanliness	0.95		Volume	14302	m ³
Heliostat Optical Efficiency	0.8835		Max Tank Height	20.0	m
Heliostat Auxiliary	0.6	MWh _e	Min Fluid Height	1.0	m
Wind stow speed	15	m/s	Tank Diameter	31.0	m
Receiver (Design)			COLD Tank		
Receiver Optical Height	208	m	Volume	12985	m ³
Receiver Height	19.24	m	Max Tank Height	20.0	m
Receiver Diameter	16.32	m	Min Fluid Height	1.0	m
Receiver Area	986.45	m ²	Tank Diameter	29.5	m
Number of Panels	16	#			
Tube Thickness	1.5	mm			
Tube Outer Diameter	50	mm			
Tube Inner Diameter	47	mm			
Interconnecting Pipe Diameter	419.10	mm			
Panel Pipe Roughness	0.005	mm			
Receiver Reflectivity	0.93				
Receiver Emissivity	0.88				
Flux Limit	1000	kW/ m ²			
Tower Riser Diameter	560.78	mm			
Tower Riser Roughness	0.15	mm			
Inlet Vessel Pressure Drop Factor	1.33				

Table A.2: Plant operational parameters

	Value	Unit		Value	Unit
Receiver (Operations)			Power Block		
Start-Up			SGS Thermal Energy Required		
Start-Up (1hour) Energy Fraction lost	0.25	hours	At Design Point (DP)	239.8	MWh _t
Total time required for Start-Up	1.25	hours	Required for start-up	0.75	%
Time required for min flow	0.5	hours	Required for stand-by	0.25	%
Fraction of Min Power for Start-Up	0.6		Start-Up time	0.5	hour
Min operating power	70	MW _t	Max. Standby time	2	hour
Min flow to receiver	168	kg/s	Min. Part Load	25	MW _e
Auxiliary used for Start-Up (No Flow)	0.461	MW _e	Max. Turbine Output	110	MW _e
Auxiliary used for Start-Up (With Flow)	1	MW _e	TES		
Piping Losses (With Flow)	0.5	MW _t	Initial volume. Hot TES	50	%
Heliostat Tracking Power (60% Required)	0.36	MW _e	Wetted Loss Coefficient	0.40	W/ m ² °C
Heat Tracing (Pipe & Equipment)	0.101	MW _e	Dry Loss Coefficient	0.25	W/ m ² °C
Light Cloud / Stand-by					
Min flow maintained to receiver	168	kg/s			
Auxiliary used for Stand-by (With Flow)	1	MW _e			
Piping Losses (With Flow)	0.5	MW _t			
Heliostat Tracking Power (60% Required)	0.36	MW _e			
Heat Tracing (Pipe & Equipment)	0.101	MW _e			
Heavy Cloud / Off					
Auxiliary used for OFF (No Flow)	0.6	MW _{h_e}			
Heat Tracing (Pipe & Equipment)	0.101	MW _{h_e}			
Normal Operation					
HTF Input Temperature from TES	289	°C			
HTF Output Temperature desired	565	°C			
Piping Losses (With Flow)	0.5	MW _t			
Heliostat Tracking Power	0.6	MW _e			

APPENDIX B: DELSOL3 FLUX MAP AND ERRORS

- SIGEL= Tracking Error in OPEN-LOOP drive systems*
SIGAZ= Foundation motion
SIGSX= Mirror waviness
SIGSY= Panel alignment error
SIGTX= Tracking Error in CLOSED-LOOP drive systems
SIGTY= Tower Sway

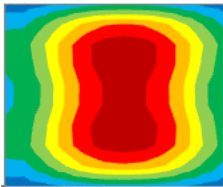
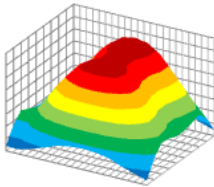
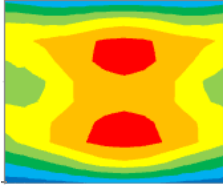
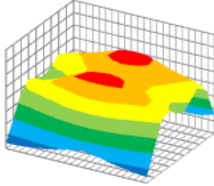
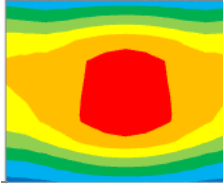
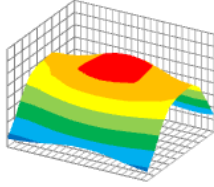
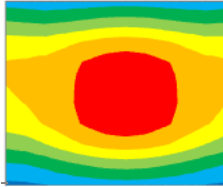
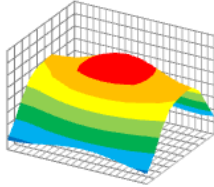
SIGEL= 0 SIGAZ= 0 SIGSX= 0 SIGSY= 0 SIGTX= 0 SIGTY= 0 #_Helio= 8965			Gross Power = 651.72 MWt (Performance) Gross Power = 660.35 MWt (Flux Map) Net Power = 87.59 Mwe				
DAY 81.00	HOUR 0.00	COSINE 0.83	SHADOW 1.00	BLOCK 0.98	AIR ATT 0.92	SPILLAGE 0.99	TOTAL 0.60
SIGEL= 0 SIGAZ= 0 SIGSX= 0.003 SIGSY= 0 SIGTX= 0 SIGTY= 0 #_Helio= 10491			Gross Power = 658.42 MWt (Performance) Gross Power = 660.75 MWt (Flux Map) Net Power = 88.54 Mwe				
DAY 81.00	HOUR 0.00	COSINE 0.80	SHADOW 1.00	BLOCK 0.98	AIR ATT 0.92	SPILLAGE 0.89	TOTAL 0.52
SIGEL= 0 SIGAZ= 0 SIGSX= 0.003 SIGSY= 0.002 SIGTX= 0 SIGTY= 0 #_Helio= 11027			Gross Power = 659.40 MWt (Performance) Gross Power = 668.62 MWt (Flux Map) Net Power = 88.68 Mwe				
DAY 81.00	HOUR 0.00	COSINE 0.79	SHADOW 1.00	BLOCK 0.98	AIR ATT 0.92	SPILLAGE 0.86	TOTAL 0.49
SIGEL= 0 SIGAZ= 0 SIGSX= 0.003 SIGSY= 0.002 SIGTX= 0 SIGTY= 0.003 #_Helio= 11252			Gross Power = 659.33 MWt (Performance) Gross Power = 670.75 MWt (Flux Map) Net Power = 88.71 Mwe				
DAY 81.00	HOUR 0.00	COSINE 0.79	SHADOW 1.00	BLOCK 0.98	AIR ATT 0.91	SPILLAGE 0.82	TOTAL 0.47

Figure B.1: Heliostat compensation for induced errors to field performance

SIGEL= Tracking Error in OPEN-LOOP drive systems
 SIGAZ= Foundation motion
 SIGSX= Mirror waviness
 SIGSY= Panel alignment error
 SIGTX= Tracking Error in CLOSED-LOOP drive systems
 SIGTY= Tower Sway

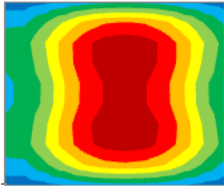
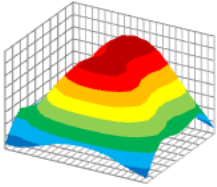
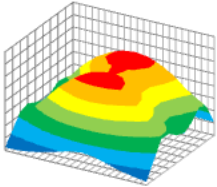
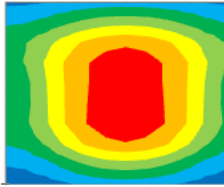
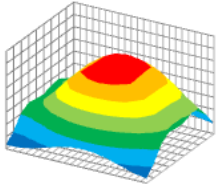
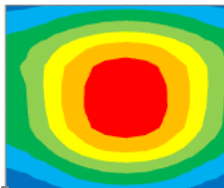
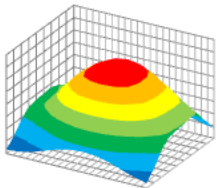
SIGEL= 0 SIGAZ= 0 SIGSX= 0 SIGSY= 0 SIGTX= 0 SIGTY= 0 #_Helio= 8965			Gross Power = 651.72 MWt (Performance) Gross Power = 660.35 MWt (Flux Map)	
DAY HOUR COSINE SHADOW BLOCK AIR ATT SPILLAGE TOTAL 81.00 0.00 0.83 1.00 0.98 0.92 0.99 0.60				
SIGEL= 0 SIGAZ= 0 SIGSX= 0.003 SIGSY= 0 SIGTX= 0 SIGTY= 0 #_Helio= 8965			Gross Power = 583.91 MWt (Performance) Gross Power = 585.50 MWt (Flux Map)	
DAY HOUR COSINE SHADOW BLOCK AIR ATT SPILLAGE TOTAL 81.00 0.00 0.83 1.00 0.98 0.92 0.89 0.54				
SIGEL= 0 SIGAZ= 0 SIGSX= 0.003 SIGSY= 0.002 SIGTX= 0 SIGTY= 0 #_Helio= 8965			Gross Power = 566.85 MWt (Performance) Gross Power = 573.39 MWt (Flux Map)	
DAY HOUR COSINE SHADOW BLOCK AIR ATT SPILLAGE TOTAL 81.00 0.00 0.83 1.00 0.98 0.92 0.86 0.52				
SIGEL= 0 SIGAZ= 0 SIGSX= 0.003 SIGSY= 0.002 SIGTX= 0 SIGTY= 0.003 #_Helio= 8965			Gross Power = 552.80 MWt (Performance) Gross Power = 562.75 MWt (Flux Map)	
DAY HOUR COSINE SHADOW BLOCK AIR ATT SPILLAGE TOTAL 81.00 0.00 0.83 1.00 0.98 0.92 0.84 0.51				

Figure B.2: Constant heliostat field, effect on performance due to induced errors

APPENDIX C: SIMULATION MODEL: STEP-BY-STEP GUIDE

C.1. INSTALLATION

C.1.1. Compatibility

The entire model is built on the Microsoft Visual Basic for Application 7.0 platform. As this research is funded by EPPEI, and Eskom utilises Microsoft Windows as its operating system across the business, compatibility with other operating systems or platforms, such as Macintosh, has not been developed. The model was tested on these platforms, which resulted in no compatibility problems. The developed model requires no installation and is accessible through the Microsoft Excel file. The user is, therefore, recommended to run the model from a Microsoft operating system, with MS Office 2010 or latest version installed.

C.1.2. Setting up the Model

C.1.2.1. Copy to a New Destination Folder

Three different models were developed accompanying this research. The main or parent folder called the ‘Simulation Models’ contains four sub-folders namely, ‘Model 1 – Receiver Thermographs and Operation’, ‘Model 2 – Power block Detailed Operation’, ‘Model 3 – Main Model’, and ‘Model Templates’. When the user wants to copy these models to a new destination, he/she should ensure that the entire parent folder ‘Simulation Models’ is copied. The ‘Model Templates’ folder contains all the templates that were used while executing the simulation. It should be noticed that an error will result if the user separates any of the models from their original structure.

C.1.2.2. Which Model to Run First

Each model developed, supplies the user with specific information relating to the plant. As per the case for Model-1, it focusses on the detailed receiver operation and rendering of the thermographs and colormaps. A ‘snapshot’ of the power block’s operation, executed in Model-2, supplies the user with the heat and mass balances of the power block under user-specified conditions. These user inputs are the ambient temperature, and the temperature and mass flow rate of the heat transfer fluid to the steam generator. Model-1 and Model-2 are supplementary models supplying the user with additional information. The objectives of this research are realised in Model-3 that focusses on optimisation of the plant operations under various boundary conditions. These boundary conditions are: weather conditions, plant status, and the operating strategy imposed on the plant. The models are able to run independently of each another. The main purpose of this guide is to familiarise the user with Model-3 and help in identifying the supplementary benefits that either/both Model-1 and Model-2 offer.

C.2. MODEL-3: OPTIMISE PLANT OPERATIONS

C.2.1. Graphical User Interface

First, the user has to open the 'MODEL 3 – Optimise Plant Operations.xlsm' which is Microsoft Excel Macro-Enabled Worksheet file. Upon opening the file, a window will appear (see Figure C.1). Two buttons will be visible for execution in the 'User' tab. During execution, the tabs at the bottom, 'Report', 'Results' and 'Compare SimResults' are populated. If the user wants to clean the workbook from the simulation results, he/she can do so by clicking the 'Clean Workbook Results' button (Please note that all information in the workbook will be deleted/cleared. The unsaved information will be lost). To start the simulation process, the user is required to click on the 'Start Simulation' button. This will open up a window from which the user can set the boundary conditions. The next section assists the user in setting up this window in order to execute the first simulation run.

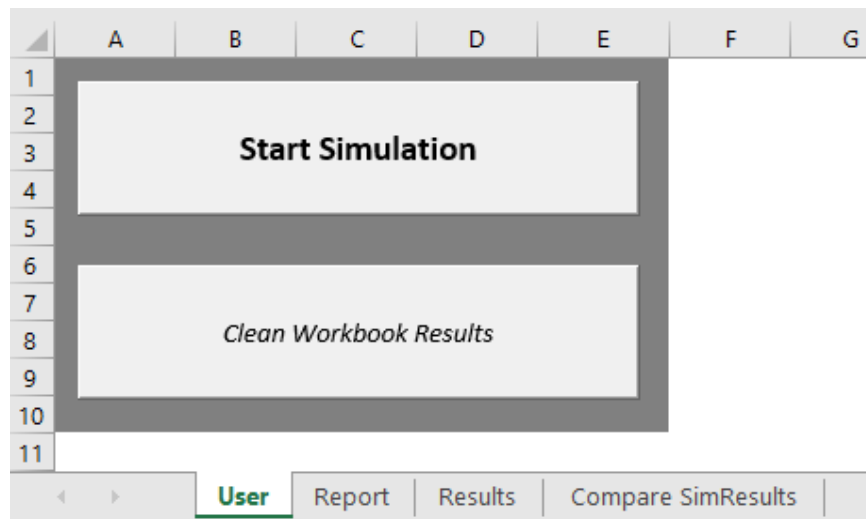


Figure C.1: Model-3 Opening window

C.2.2. Start Simulation

From the Model-3 opening window, the user can begin the simulation process by clicking on the 'Start Simulation' button. A 'Simulation Model' window will come up on the screen and it is reproduced in Figure C.2. The graphical user interface is set up in a manner to highlight the research objectives in a clear and concise manner. In Figure C.2, four main sections are noted, namely, 'Specify Simulation Time', 'Plant Status', 'Financials', and 'Operating Strategy Implemented'. These categories correspond to the research objectives, which is to optimise the plant operations based on the boundary conditions, weather conditions, plant status and operating strategy imposed on the plant. The 'Financials' category is relevant across all the operating strategies given that electrical power is sold to the grid. Therefore, it is included in the main 'Simulation Model' window.

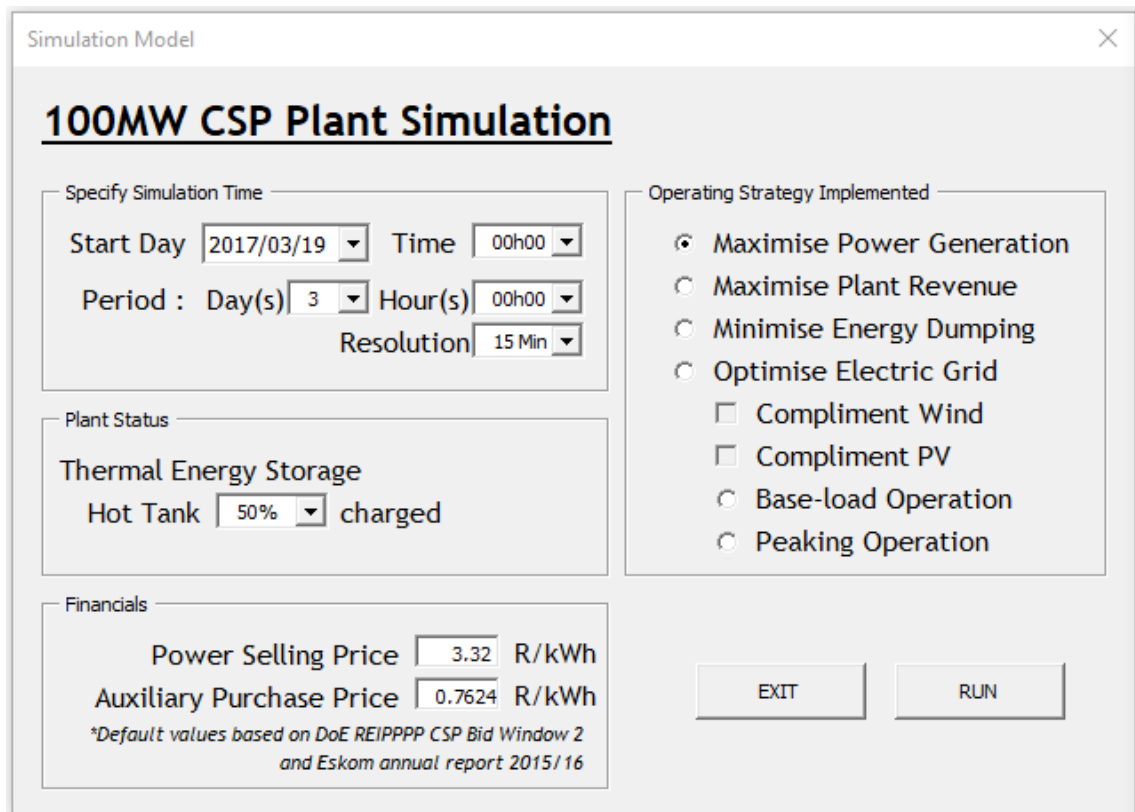


Figure C.2: 'Start Simulation' graphical user interface

C.2.2.1. Specify Simulation Time

The user has the freedom to set the start day and time of the simulation model. The period, for which the simulation model will run for, can be specified from one hour to a maximum of seven days. The upper limit of seven days is in line with the Eskom's NCC requirements requesting a plant dispatch forecast period. The time resolution of the model can be between 15 minutes to 1 hour. (Note: All the operating strategies are not able to accommodate both time resolutions. In the case of 'Maximise Plant Revenue', the operating strategy is limited to 15 minutes intervals, as the time-of-day tariffs are specified between hours. Similarly, in the 'Optimise Electric Grid – Compliment Wind and or PV' operating strategies, the model is limited to one-hour intervals, as the data obtained from National Control only publicise the hourly demand, wind contribution and PV contribution). The 'Specify Simulation Time' represents the objective to optimise the plant under various weather conditions. The specified simulation period will automatically access the weather data during this period, and this data set will be added as input to the simulation model.

C.2.2.2. Plant Status

On the basis of the plant operations, the status of the thermal energy storage fluctuates throughout the day and the year. To accommodate these fluctuations, the user can specify

the state of the hot thermal storage tank while initialising the simulation model. As soon as the model executes the first time-step, the thermal energy storage system is updated based on the plant operations. As the state of the thermal energy storage tank is updated with each time step, the objective to optimise the plant operations based on the plant status is represented under this section.

C.2.2.3. Financials

The ‘Financials’ section is applicable to all the operating strategies. The electric power generated generally sold to the grid. But sometimes, it has to be purchased from the grid for auxiliary consumption. The indicated prices should not be confused with the LCOE of the plant. The selling and purchase prices relate to a typical PPA structure where a flat rate is considered throughout the day. The default ‘Power Selling Price’ of 3.32 R/kWh is based on the DoE REIPPPP Bid Window 2 with inflation adjusted to April 2016. It is noted that future plants will come in at a lower bidding price. However, the amount 3.32 R/kWh was awarded as a flat rate tariff for the CSP plants in Bid Window 2 (Note: The user has the flexibility to introduce a time-based tariff structure under the ‘Maximise Plant Revenue’ operating strategy, more details are presented below under this operating strategy).

These financial parameters were introduced to draw a comparison between the plant revenue generated in each simulation run. The net electric power delivered to the system is by the plant leads to plant’s remuneration. The plant purchases the power from the grid when it could not generate sufficient amount of electric power to sustain its auxiliary consumption. The ‘Auxiliary Purchase Price’ of 76.24 c/kWh is the electricity revenue per kWh, including environmental levy, captured in the Eskom 2015/16 Annual Integrated Report (Eskom, 2016). The cost of electricity, excluding depreciation, for the period is 64.00 c/kWh.

C.2.2.4. Operating Strategy Implemented

The user has the flexibility to implement any of the mentioned operating strategies. Only one of the operating strategies can be executed per simulation run. As mentioned under Section C.2.2.1, certain operating strategies are limited to either a 15 minutes or 1 hour time resolutions. These time resolutions are discussed under each operating strategy in the following sections. The operating strategies may exhibit their own windows for additional information to be provided by the user before executing the simulation run.

C.3. OPERATING STRATEGIES: INPUT PARAMETERS

The user can select the operating strategy, once he/she is satisfied with specifying the simulation time, plant status and financial indicators. By elaborating on the various input parameters, this section aims to guide the user in successfully simulating each operating strategy.

C.3.1. Maximise Power Generation, 05h00 Turbine Start-Up

Once the user selects ‘Maximise Power Generation’ operating strategy, the Maximise Power Generation sub-window will appear. It is reproduced in Figure C.3. Under the heading, additional notes regarding the operating strategy will be displayed. Certain modifications in the simulation model that are applicable to this operating strategy are implementation of weather prediction system in the receiver operating regimes, imposing no system boundaries on the plant, power generation of 100% of its design capacity by the turbine, and a single turbine start/stop each day.

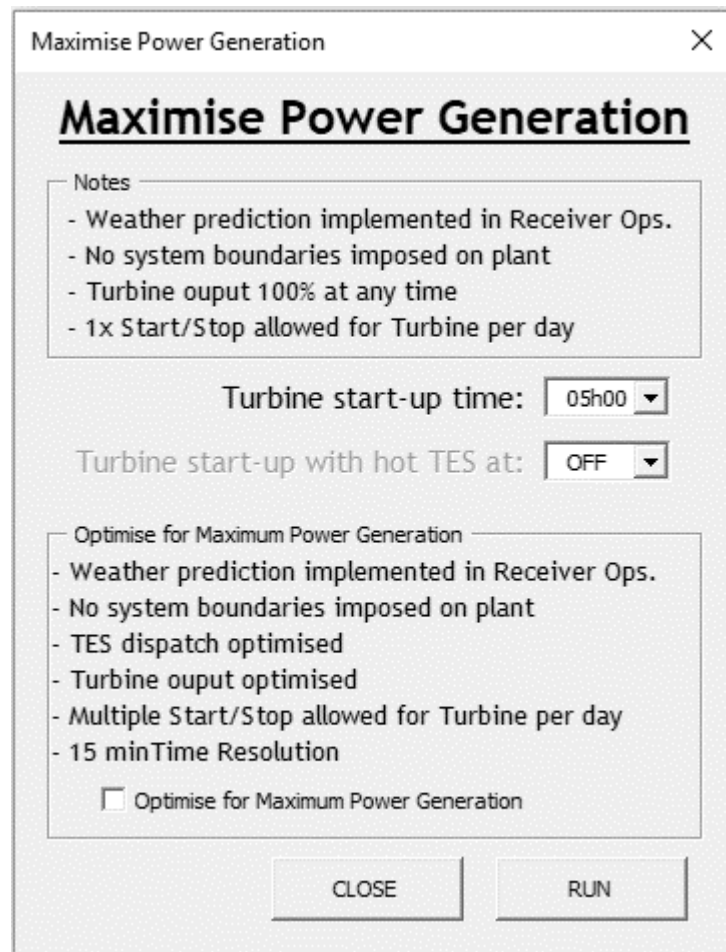


Figure C.3: Maximise Power Generation operating strategy sub-window

Although this operating strategy does not necessarily optimise the plant operations, it is a good representation of ‘how’ the plant performs when the turbine allowed for a single start/stop per day. Also, the user can specify the timings of the dispatch from the hot storage tank to the SGS. The user has two options, either he/she can specify the turbine start-up time or dispatch TES according to the user-specified capacity.

C.3.1.1. Inputs - Maximise Power Generation (User)

The first simulation run demonstrated in this guide is the ‘Maximise Power Generation’ operating strategy. The simulation model has been set up as illustrated in Figure C.4. The simulation start date is set at 19 March at 00h00. It simulates the plant operations for three days in the 15 minutes time resolution. The default values in the Maximise Power Generation sub-window are used. If the user is satisfied with the input values, he/she can continue by clicking the ‘Run’ button. The user can also close the window in case he wants to change the input values.

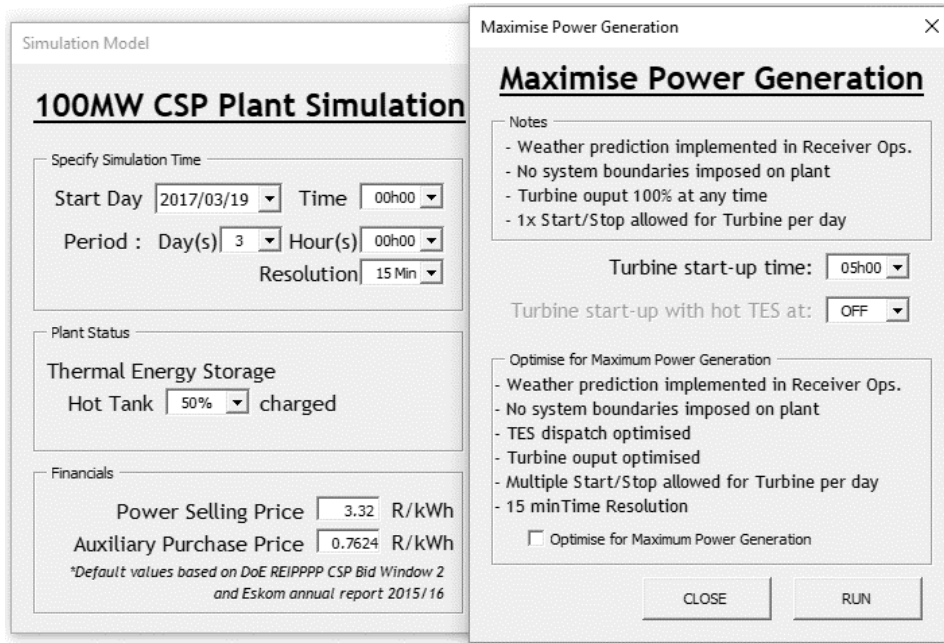


Figure C.4: Maximise Power Generation, user specified turbine start-up at 05h00

After the simulation model executes the user inputs, results are seen under three different sheets in the Excel Workbook. These are marked as ‘Report’, ‘Results’ and ‘Compare SimResults’. Under the ‘Report’ sheet, the graphical representations for the plant’s operation performance and a summary report for each system are generated and displayed. This report is accessible through the ‘Report’ tab at the bottom of the workbook. It is automatically displayed after the simulation run. For illustrative purpose, the maximise power generation operating strategy’s results are displayed in Figure C.5.

The layout of the ‘Report’ sheet is designed to provide the user with all the plant operations on a single window. The user will be able to view the details about the weather conditions, heliostat field, receiver and power block performance. The report also displays the dispatch profiles of both the cold and hot storage tanks and the plant auxiliary consumptions. For additional information, the system demand profile with wind and PV contributions are presented. For the ease of printing, the data is represented in four columns. In the following sections, the results displayed in the “Report” sheet are discussed in detail.

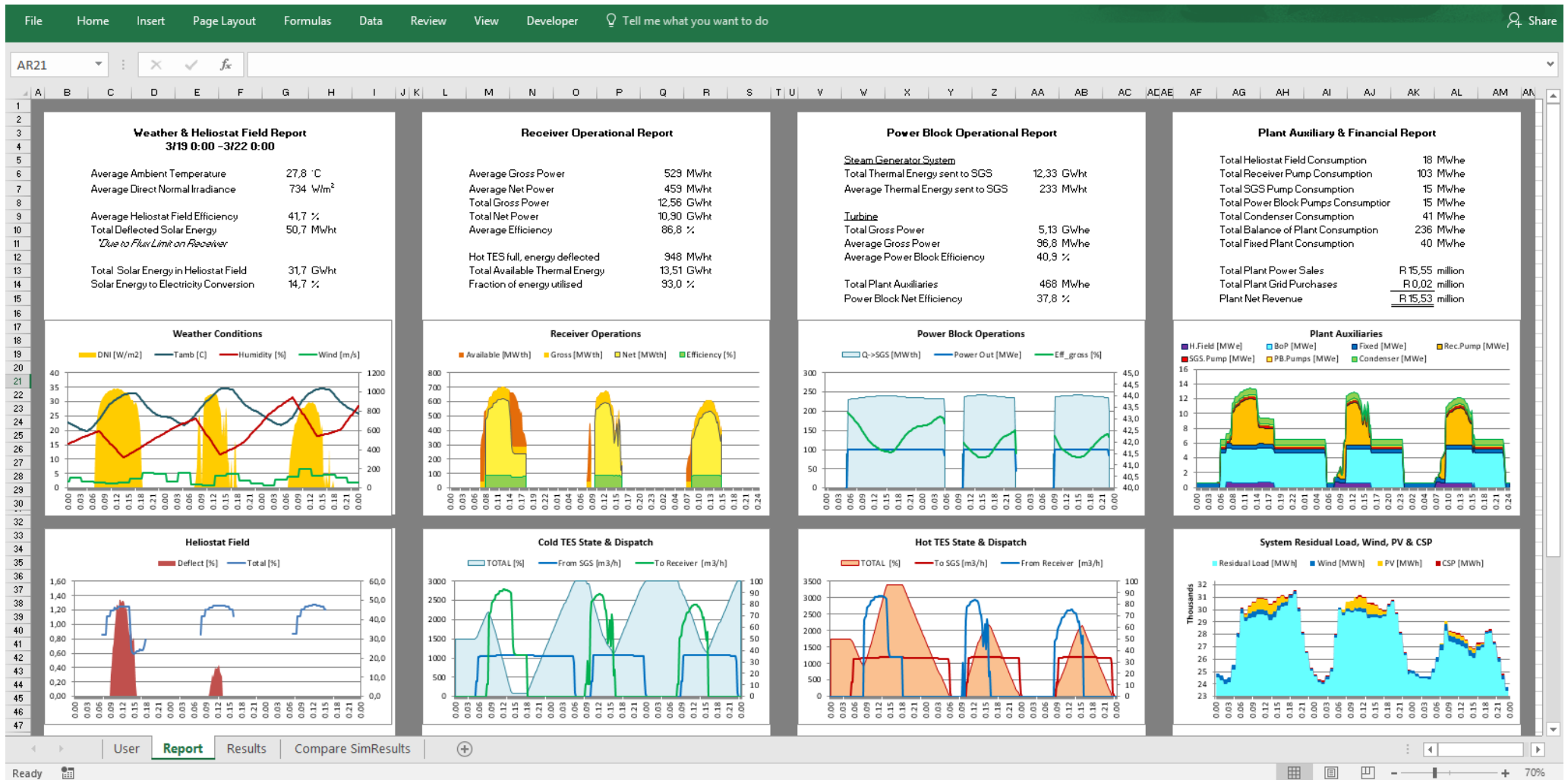


Figure C.5: Report sheet. Simulation model results with graphical representations.

C.3.1.2. Report – Weather and Heliostat Field Report

The first individual report is the ‘Weather and Heliostat Field Report’. This was reproduced from Figure C.5 and is illustrated in Figure C.6. The simulation date and time as selected by the user can be seen in the report as 19 March at 00h00. The simulation run period is for three days, that is, till 22 March 00h00.

Weather & Heliostat Field Report	
3/19 0:00 -3/22 0:00	
Average Ambient Temperature	27,8 °C
Average Direct Normal Irradiance	734 W/m ²
Average Heliostat Field Efficiency	41,7 %
Total Deflected Solar Energy	50,7 MWht
<i>*Due to Flux Limit on Receiver</i>	
Total Solar Energy in Heliostat Field	31,7 GWht
Solar Energy to Electricity Conversion	14,7 %

Figure C.6: Weather and heliostat field report - summary

Additional information on the average ambient temperature and DNI for this period are also shown in the report. A detailed report on the weather conditions for this period is represented in Figure C.7. The amount of energy received from the heliostat field is displayed in terms of average heliostat optical efficiency and total deflected solar energy values. The ‘Total Deflected Solar Energy’ value represents the amount of solar energy deflected away from the receiver when the flux limitation of the receiver material is exceeded. Thus, the excessive energy is deflected away from the receiver surface to adhere to the design limitations of the receiver material. This ‘potential energy’ loss is the result of the aiming strategy that is implemented by the heliostat field. In this instance, the aiming strategy implemented concentrated too much solar energy on a specific region on the receiver surface. Therefore, the user adjusted the aiming strategy so that the solar flux distributed evenly on the receiver’s surface and the energy lost is regained.

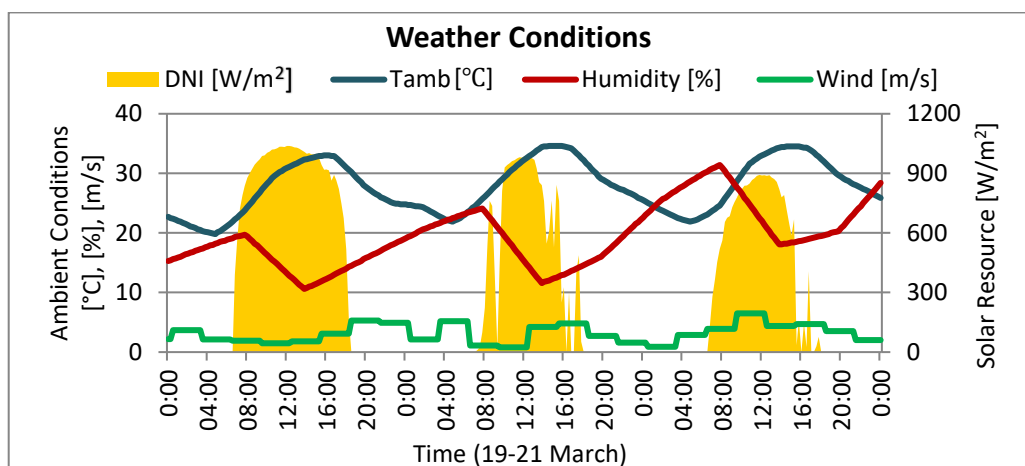


Figure C.7: Ambient conditions under which the plant operations were optimised

The results are displayed graphically in order to express the potential areas for optimisation in the plant operations and to highlight the effects of the plant operations while implementing various operating strategies for the plant. As is the case for Figure C.8, the deflected solar energy from the heliostat field highlights the requirement for optimisation in the heliostat field aiming strategy. By adjusting the aiming strategy, this potential energy could be regained. The deflected solar energy is typically observed when DNI is high.

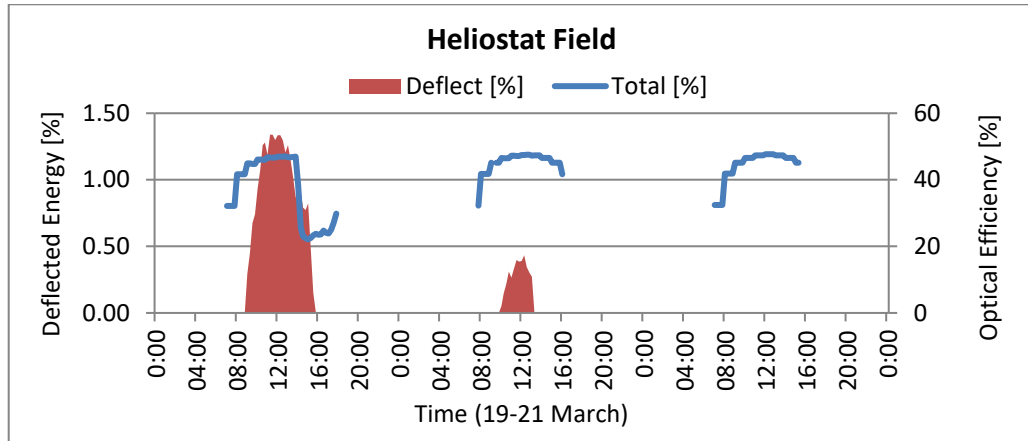


Figure C.8: Heliostat field optical efficiency and energy deflected from receiver

C.3.1.3. Report – Receiver Operational Report

The ‘Receiver Operational Report’, reproduced in Figure C.9, provides the user with important information regarding the performance of the receiver. Apart from the standard gross and net performance values, this report indicates the amount of energy that had to be deflected away from the receiver owing to the fact that the hot TES was fully charged. Additionally, the total available thermal energy and the fraction of this energy that is utilised in the receiver operation are supplied. These values allow the user to optimise the plant operations. Due to the operating strategy implemented in this case, the hot thermal storage tank was to be fully charged. This lead to defocussing the heliostats from the receiver and subsequently dumping the energy.

Receiver Operational Report	
Average Gross Power	529 MWht
Average Net Power	459 MWht
Total Gross Power	12,56 GWht
Total Net Power	10,90 GWht
Average Efficiency	86,8 %
Hot TES full, energy deflected	948 MWht
Total Available Thermal Energy	13,51 GWht
Fraction of energy utilised	93,0 %

Figure C.9: Receiver operational report – summary

Although Figure C.9 displays the necessary performance indicators, the graphical representations illustrated in Figure C.10 and Figure C.11 specifically represent the performance of the receiver and dispatch control within the cold TES. These graphical representations are a useful tool to the user to fully understand the operational aspects of the receiver. Figure C.10 shows the available power for the receiver. However, the actual amount of thermal power reflected by the heliostats onto the receiver is represented by the ‘Gross’ thermal power. During the warm up sequence, the receiver utilises a fraction of the available power. Once the receiver is fully warm, normal operation commences. During the first day, it was noticed towards the end of the afternoon that some of the solar energy was deflected or the heliostats were defocused. This led to a reduction in the receiver’s output. This phenomenon is represented in Figure C.11. When the cold TES reaches the stage of depletion, there is an insufficient amount of molten salt or the heat transfer fluid to be pumped to the receiver in order to sufficiently cool the receiver. When the volume molten salt pumped to the receiver is considered, it is observed that the output of the receiver coincides with the cold TES state. During this time, the turbine was in operation and the cold TES is charged from the SGS output. This allowed the receiver to utilise the molten salt from the SGS to be pumped to receiver, hence a reduced output is observed in the receiver. In the event when the turbine was not in operation, the receiver would shut down its operation due to insufficient capacity in the cold TES.

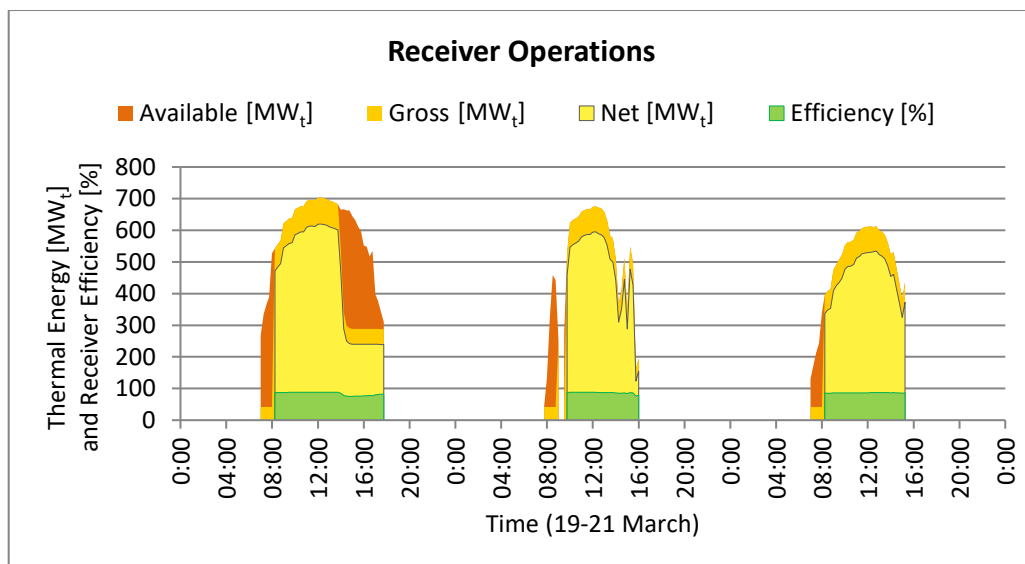


Figure C.10: Graphical representation of receiver operations

The weather prediction systems and the cloud transients that were implemented on the receiver operations are represented during the second day. In the morning, sufficient solar radiation was available to warm up the receiver. At least a fraction of this solar energy was collected before a passing cloud interrupted the receiver’s operations. The receiver operations were shut down for that period while maintaining a minimum flow through the receiver’s bypass. Although, Figure C.10 and Figure C.11 does not clearly show the required details in the graphs, the exact figures can be found in the ‘Results’ sheet at rows 128-139. These are extracted and represented below in Figure C.12.

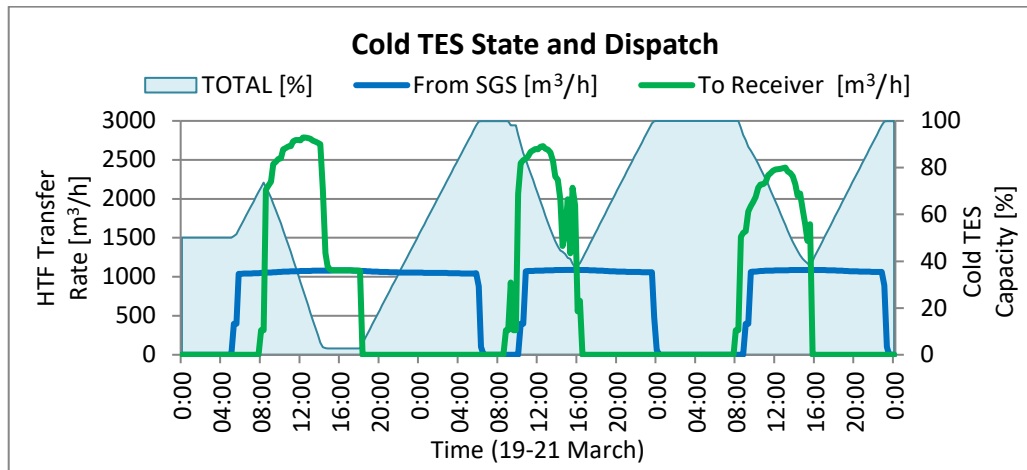


Figure C.11: Graphical representation of cold TES charge and discharge profiles

DNI [W/m ²]	Heliostat Field		Receiver Performance				Tin [C]	Tout [C]	MassFlow [kg/s]
	Total [%]	Deflect [%]	Available [MWh]	Gross [MWh]	Net [MWh]	Efficiency [%]			
11									
23									
99	32,3	0,0	46	42					
223	41,8	0,0	134	42					
536	41,8	0,0	323	42					
761	41,8	0,0	458	42			288,0	288,0	168
736	41,8	0,0	443	42			288,0	288,0	168
387	45,1	0,0	252	252	206	82,0	288,0	565,0	491
23							288,0	288,0	168
427	45,1	0,0	278	42			288,0	288,0	168
812	45,1	0,0	528	528	460	87,0	288,0	565,0	1094
929	46,6	0,1	624	624	547	87,7	288,0	565,0	1302

Figure C.12: Extraction from 'Results' sheet, rows 128-139

C.3.1.4. Report – Power Block Operational Report

The 'Power Block Operational Report' provides the most significant data to the plant and the system operator. From a plant operator's point of view, the turbine output and auxiliary consumption has a direct influence on the plant's revenue, whereas the system operator is interested in the dispatch profile of the plant. For this reason, the 'Power Block Operational Report' represents the common gross and net values of the power block, represented in Figure C.13, as well as the dispatch profile of the power block, illustrated in Figure C.14. The supplementary information regarding the thermal energy sent to the SGS and the power block efficiency are represented in Figure C.14. As in the case with the example executed, where the turbine starting time was specified as 05h00, the user input agrees with Figure C.14. However, the start-up times for the power block on these three days were 05h00, 09h30 and 08h45 respectively. Although, the specified start-up time was 05h00, the start-up was achieved on the specified time for the first day only. This was due to sufficient capacity in the hot TES. If the time specified was 16h00, the results would have been different since the hot TES would have been sufficiently charged by the energy from the solar collecting system.

Power Block Operational Report	
<u>Steam Generator System</u>	
Total Thermal Energy sent to SGS	12,33 GWht
Average Thermal Energy sent to SGS	233 MWht
<u>Turbine</u>	
Total Gross Power	5,13 GWhe
Average Gross Power	96,8 MWhe
Average Power Block Efficiency	40,9 %
Total Plant Auxiliaries	
	468 MWhe
Power Block Net Efficiency	
	37,8 %

Figure C.13: Power block operational report – summary

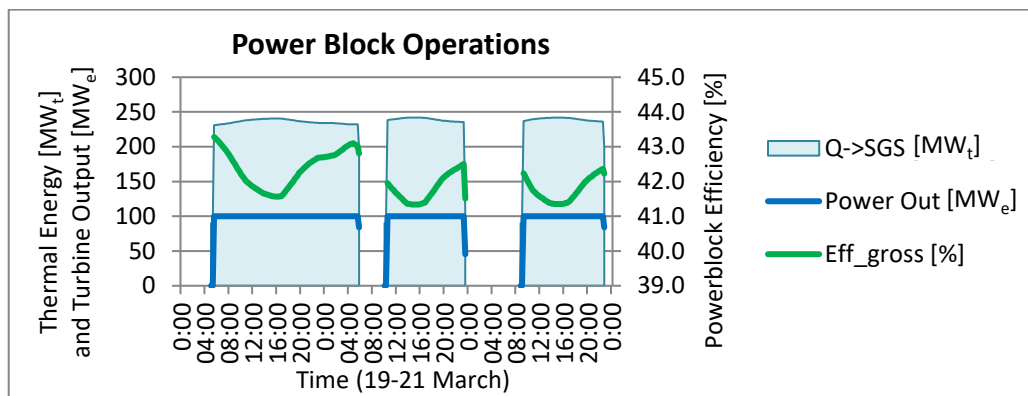


Figure C.14: Power block dispatch profile and efficiency

The power block is generally affected by the ambient temperature. This phenomenon can be noticed in the power block gross efficiency curve in Figure C.14. As the efficiency reduces, more thermal energy is required for the steam generator to generate the same electrical output from the turbine. The corresponding dispatch profile of the hot TES tank to the SGS is represented in Figure C.15. The output of the power block ceases when the hot TES depletes.

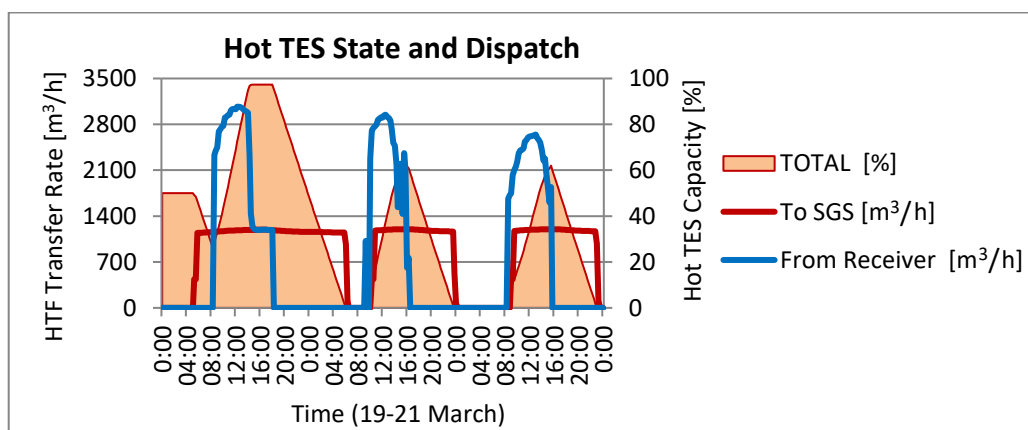


Figure C.15: Graphical representation of hot TES charge and discharge profiles

C.3.1.5. Report – Plant Auxiliary and Financial Report

The breakdown for the auxiliary consumption in a plant for a particular time period is provided by the ‘Plant Auxiliary and Financial Report’. It is as represented in the Figure C.16. The financial indicators of total power sales and grid purchases are also presented in the figure.

Plant Auxiliary & Financial Report	
Total Heliostat Field Consumption	18 MWhe
Total Receiver Pump Consumption	103 MWhe
Total SGS Pump Consumption	15 MWhe
Total Power Block Pumps Consumption	15 MWhe
Total Condenser Consumption	41 MWhe
Total Balance of Plant Consumption	236 MWhe
Total Fixed Plant Consumption	40 MWhe
Total Plant Power Sales	R 15,55 million
Total Plant Grid Purchases	R 0,02 million
Plant Net Revenue	<u>R 15,53 million</u>

Figure C.16: Plant auxiliary consumption and financial report

A graphical representation of the total plant auxiliary consumption is shown in Figure C.17. The solar collecting system operations are indicated by the heliostat field (H.Field) operation and receiver pump (Rec.Pump), whereas the power generation system is represented in the BoP, SGS pump, power block pumps and condenser operations.

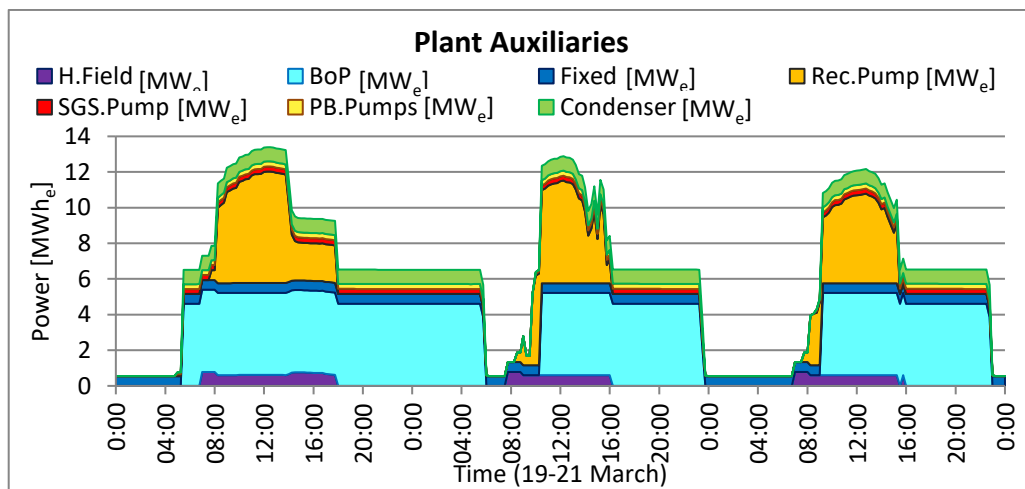


Figure C.17: Plant auxiliary consumption

For illustrative purposes, the system demand with wind, PV and CSP contributions to the grid is shown in Figure C.18. This figure is relevant to the ‘Optimise Electric Grid’ operating strategies. The peaks in the figure indicate the increased demand that a dispatchable energy generating source such as CSP with storage has to address in order to fulfil them. The data obtained from the NCC is in an hourly format, therefore, a step-wise representation is observed for selected 15 minutes time intervals.

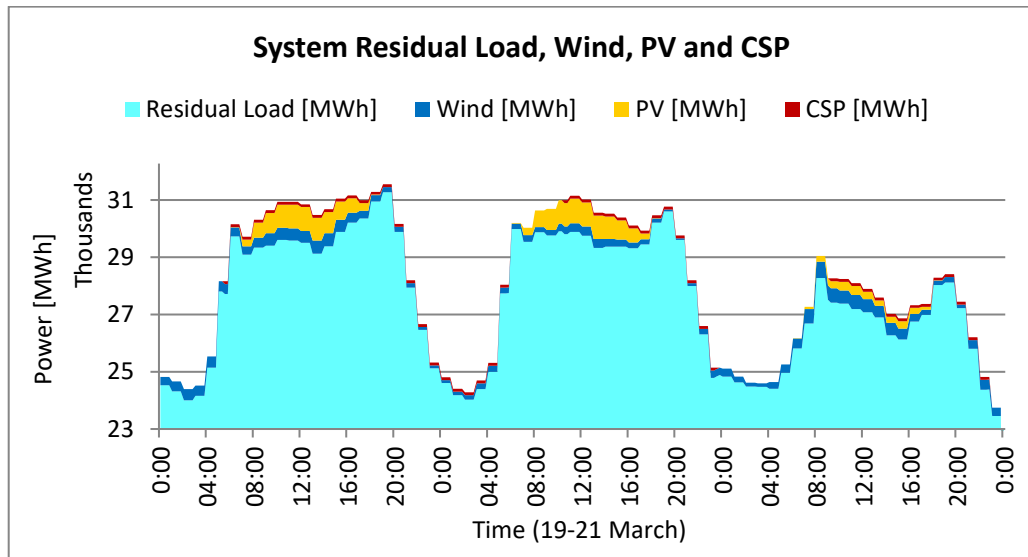


Figure C.18: System demand; represent residual load, wind, PV and CSP.

C.3.1.6.Results – Detailed Plant Performance

Figure C.19 is the graphical representation of the values that were obtained from the ‘Report’ sheet. The detailed information regarding the plant performance, weather conditions and financial indicators act as supplementary information to the results of the simulation model. At times, especially when the simulation period is set to the maximum period of seven days, the graphical representation could become encumbered with information. Although the graphs supply the user with an overview of the specific system’s performance, it is deemed useful to further extent this in the ‘Results’ sheet.

The supplementary simulation models have been provided to accompany Model 3, in case the user requires detailed information on the receiver’s performance, heliostat field aiming strategy or power block performance. For the detailed performance of the receiver, Model 1 can be accessed and the date can be specified. Under the ‘normal’ operating regime, the model gives the detailed receiver performance. The user furthermore has the option to obtain a thermographic and colormap representation of the receiver. Similarly, the heat and mass balance diagram can be obtained for the power block by accessing Model 2. The user is requested to input the ambient temperature, heat transfer fluid mass flow rate and temperature. This information can be easily obtained from the ‘Results’ sheet.

C.3.1.7. Summary

This section assisted the user to execute the first operating strategy in the simulation model. A detailed explanation of the results informed the user on how to interpret the results from the simulation mode. The following sections illustrate the execution of the other operating strategies. The noteworthy results pertaining to the selected operating strategy will be discussed in the further sections in more detail.

C.3.1.8. Compare Simulation Results

The ‘Compare SimResults’ sheet maintains a record of all the simulations and provides the user with an overview of the various systems’ performances as well as the associated financial indicators. The objective of this simulation model is to provide the user with the results for a plant for which the plant operations have been optimised. These plant operation optimisations were done considering various boundary conditions such as weather conditions, plant status and imposed operating strategy. If the initial plant status and weather conditions are kept constant, the plant performance can be compared between the different operating strategies. This functionality within the simulation program extracts the benefits and values from this model. The simulation date, time and duration have to be kept constant for drawing a comparison. When the user executed the desired operating strategies for comparison, he/she can continue by clicking on the ‘Compare Operating Strategies’ button. The ‘Compare Simulation Results’ section is revisited at the end of this Section, once the user has simulated all operating strategies in this guide.

C.3.2. Maximise Power Generation, Turbine Start-Up at Hot TES at 30 %

The second operating strategy simulated with the model is the ‘User Specified’ Maximise Power Generation operating strategy. The user is required to set up the simulation model as illustrated in Figure C.20. When the hot TES capacity is greater than 30 %, the turbine sequence will start-up. As mentioned earlier, although, the user-specified maximise power generation operating strategy does not necessarily optimise the plant operations, it is a good representation of ‘how’ the plant performs when the turbine is allowed for only one start/stop per day. It also includes an additional turbine start-up condition. The following sections briefly describe the difference between the ‘Turbine start-up time’ and ‘Turbine start-up with hot TES capacity at’.

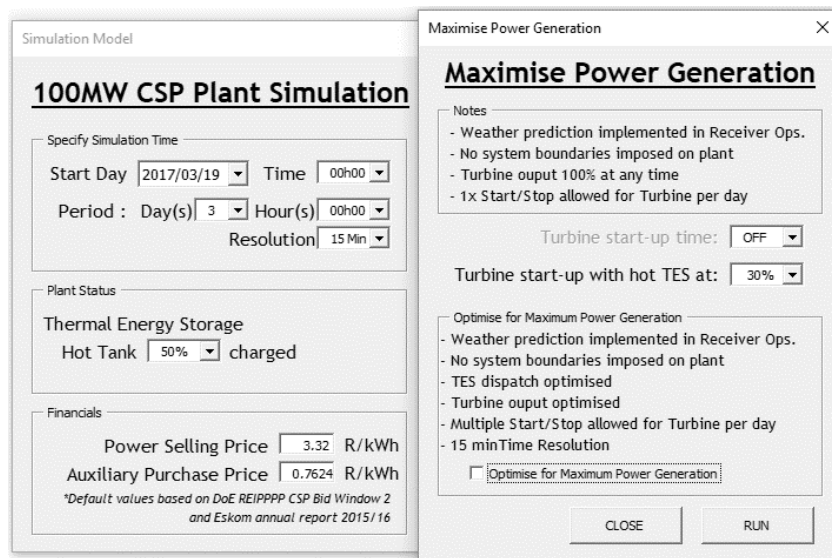


Figure C.20: Maximise Power Generation, user specified turbine start-up

Receiver Operational Report	
Average Gross Power	567 MWht
Average Net Power	493 MWht
Total Gross Power	10,77 GWht
Total Net Power	9,38 GWht
Average Efficiency	87,0 %
Hot TES full, energy deflected	40 MWht
Total Available Thermal Energy	10,81 GWht
Fraction of energy utilised	99,6 %

Figure C.21: Receiver operational report – summary

In this simulation run, the hot TES was initially 50 % charged. Therefore, the turbine start-up sequence initiated at the start of the simulation run itself. The power block, however, utilised all this energy before the receiver operated within its normal operating regime. This caused the turbine to shut down as the hot TES depleted fully. The receiver started to operate and charging the hot TES. When the hot TES was fully charged, the receiver had to shut down its operations, see Figure C.22.

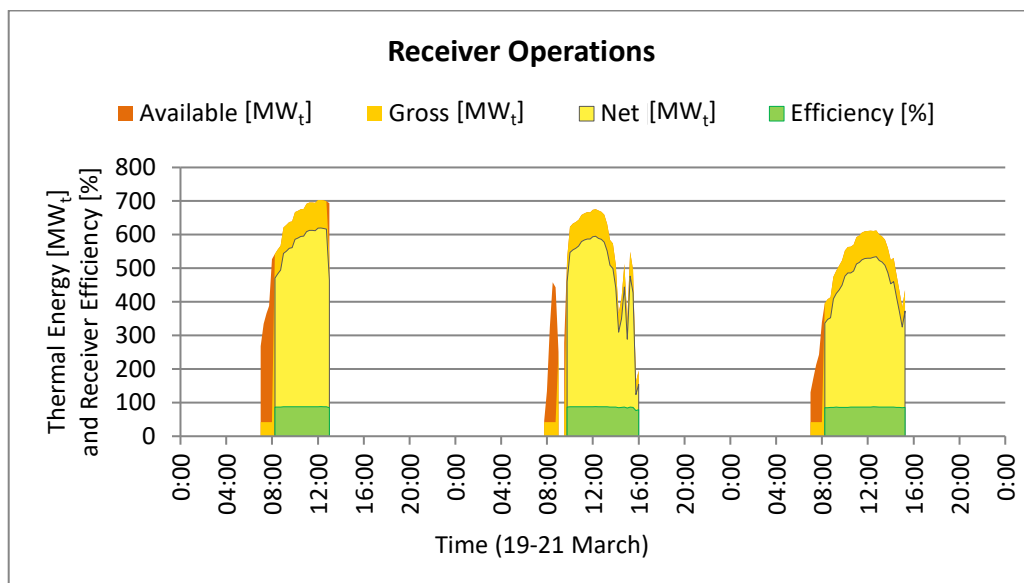


Figure C.22: Graphical representation of receiver operations

As represented in Figure C.23 and Figure C.24, the dispatch profiles for the power block and receiver operations are noticeable in the first few hours of the simulation. It is interesting to point out that if the turbine reduces its output by using less thermal energy from the hot TES tank, the turbine could have prevented its shut down. This was possible as the receiver would have supplied sufficient energy to supplement its operations. On the last day of operation, the turbine start-up initiation is observed at 11h00 when the hot TES capacity is greater than 30 % charged.

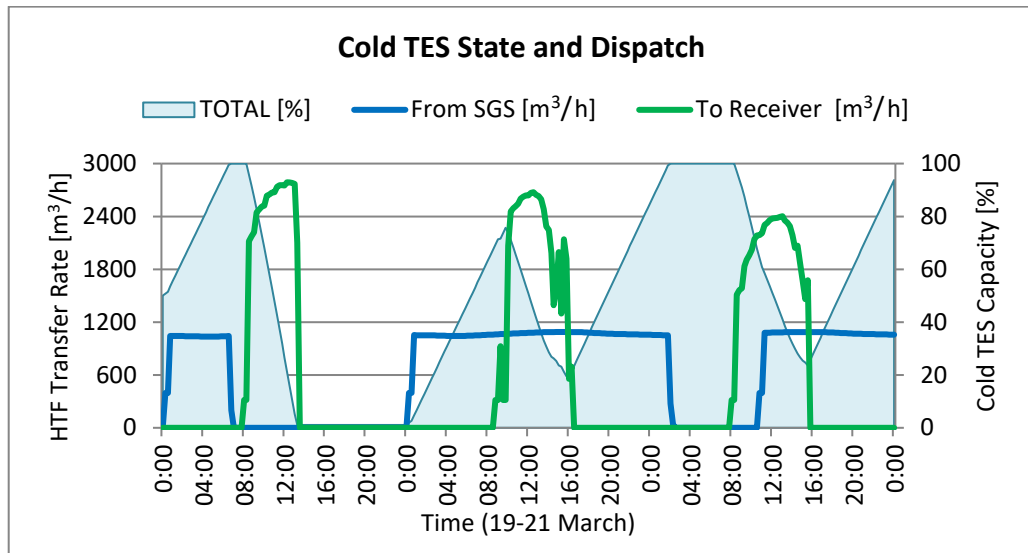


Figure C.23: Graphical representation of cold TES charge and discharge profiles

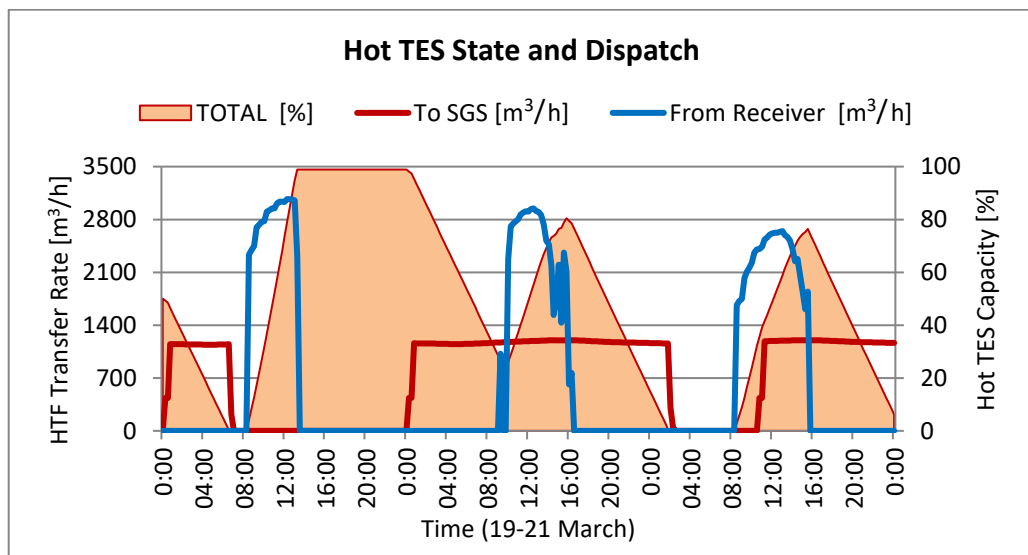


Figure C.24: Graphical representation of hot TES charge and discharge profiles

C.3.3. Optimised Maximise Power Generation

Under the user-specified turbine start up conditions, the user-specified ‘Maximise Power Generation’ operating strategies merely generated the turbines designed power of 100 MW_e. From the previous simulation results, it was clear that no optimisation in plant operations were executed. The turbine essentially kept operating until the hot TES depleted. The operation was resumed the next day when initiation of turbine start-up was done. The manner in which this operating procedure affected other systems in the plant, e.g. the receiver operations, became prominent in the graphical representations. By executing these two scenarios, the user has obtained the basic mechanisms of the CSP plant operations and the interdependency between the various systems.

With the basic understanding and appreciation of the plant operations, it is demonstrated in the following sections how to optimise the plant operations in order to maximise the plant's power generation. The user is tasked to set up the simulation input parameters as illustrated in Figure C.25. While enabling the 'Optimise for Maximum Power Generation', the user-specified turbine start-up times are disabled. This is because of the optimisation in the model's TES dispatch to the power block in order to maximise power generation. Furthermore, multiple start-ups or shutdowns in the turbine are allowed, although, this might influence the turbine operating and maintenance parameters. That is the model only focussed on the power generation. If the user is satisfied with the parameters, the 'Run' button can be clicked to start the optimisation.

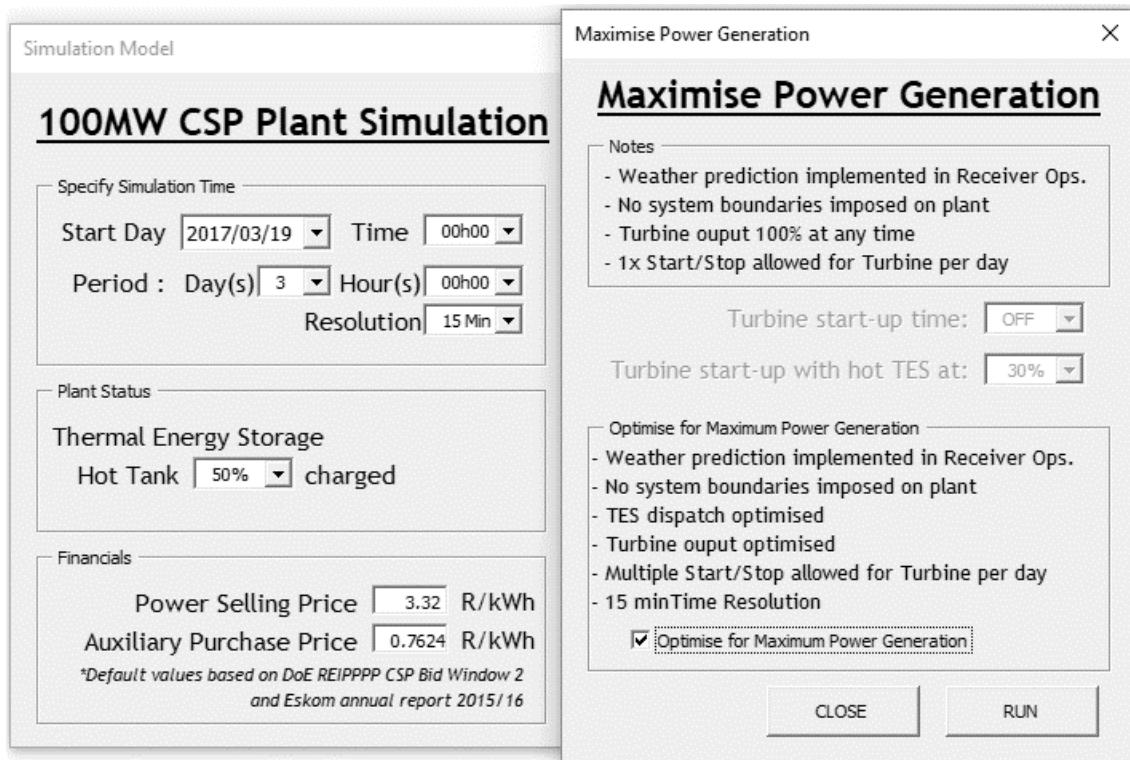


Figure C.25: Optimised Maximise Power Generation

C.3.3.1. Receiver Operational Report

The 'Maximise Power Generation' operating strategy focus on utilising most or all of the available solar energy from the heliostat field while maintaining the objective to maximise power generation from the power block. As illustrated in Figure C.26 and Figure C.27, nearly all of the available thermal energy was utilised in the receiver. Due to the fully charged state of the hot TES, 260 MWh_t of energy had to be deflected, despite the best efforts by the hot TES dispatch.

Receiver Operational Report	
Average Gross Power	558 MWht
Average Net Power	485 MWht
Total Gross Power	13,25 GWht
Total Net Power	11,53 GWht
Average Efficiency	87,0 %
Hot TES full, energy deflected	260 MWht
Total Available Thermal Energy	13,51 GWht
Fraction of energy utilised	98,1 %

Figure C.26: Receiver operational report – summary

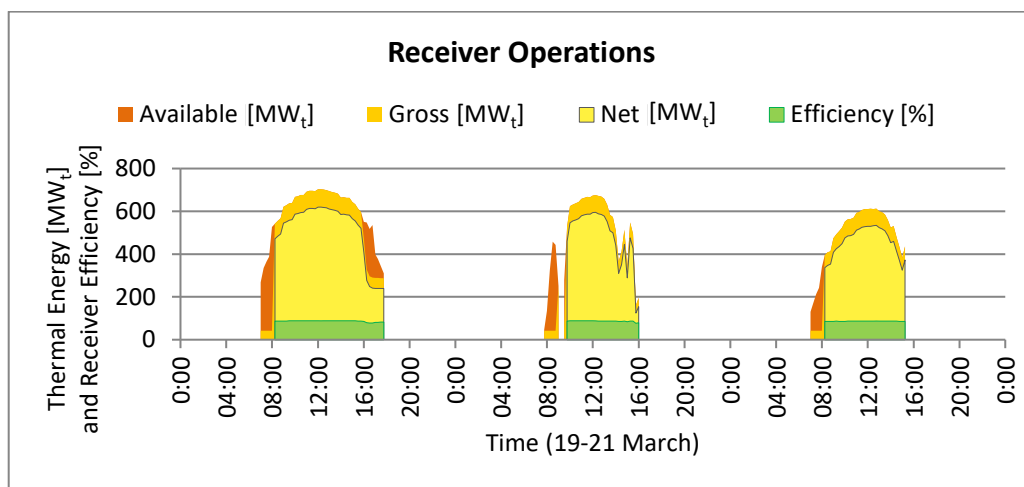


Figure C.27: Graphical representation of receiver operations

C.3.3.2. Power Block Operational Report

The ‘Power Block Operational Report’ is the most important information set demonstrating the unique optimisation capabilities of the model. The ‘Maximise Power Generation’ operating strategy maximise the gross electric power output of the power block. This is represented in Figure C.28. It will be noted that as compared to the other operating strategies for the same period, the ‘Total Gross Power’ value is higher. This indicative value is perhaps important for a plant operator when reporting on the plant’s performance. The real value drawn from these simulation results are presented in Figure C.29 and Figure C.30. These figures demonstrate, to the user or the plant operator, how to operate the plant in order to achieve the reported total gross power. When the ‘Maximise Power Generation’ operating strategy is considered initially, the operating regime that is to be considered is to operate the plant at the turbine’s designed rating. This would happen while maintaining sufficient levels in the cold TES tank for the receiver operations. When Figure C.29 is considered, the results suggest the opposite operating regime, a key piece of information resulted from this simulation model to be considered by CSP plant operators.

Power Block Operational Report	
<u>Steam Generator System</u>	
Total Thermal Energy sent to SGS	13,00 GWht
Average Thermal Energy sent to SGS	188 MWht
<u>Turbine</u>	
Total Gross Power	5,45 GWhe
Average Gross Power	79,0 MWhe
Average Power Block Efficiency	41,4 %
Total Plant Auxiliaries	502 MWhe
Power Block Net Efficiency	38,0 %

Figure C.28: Power block operational report – summary

The model optimised the plant operations in a manner that it resembles base load operations. It saves the energy required to start-up the turbine. To prevent the turbine shut down, its output fluctuates in a way to sustain sufficient capacity in the hot TES. This phenomenon is clearly represented by the hot TES dispatch profile and charged state, illustrated in Figure C.30. While taking the receiver’s thermal output in considerations, the turbine output is increased during the receiver’s operational period. This is to ensure that the hot TES does not reach a fully charged state. The simulation model maximises the gross power output of the plant by optimising the TES dispatch to the power block and receiver respectively.

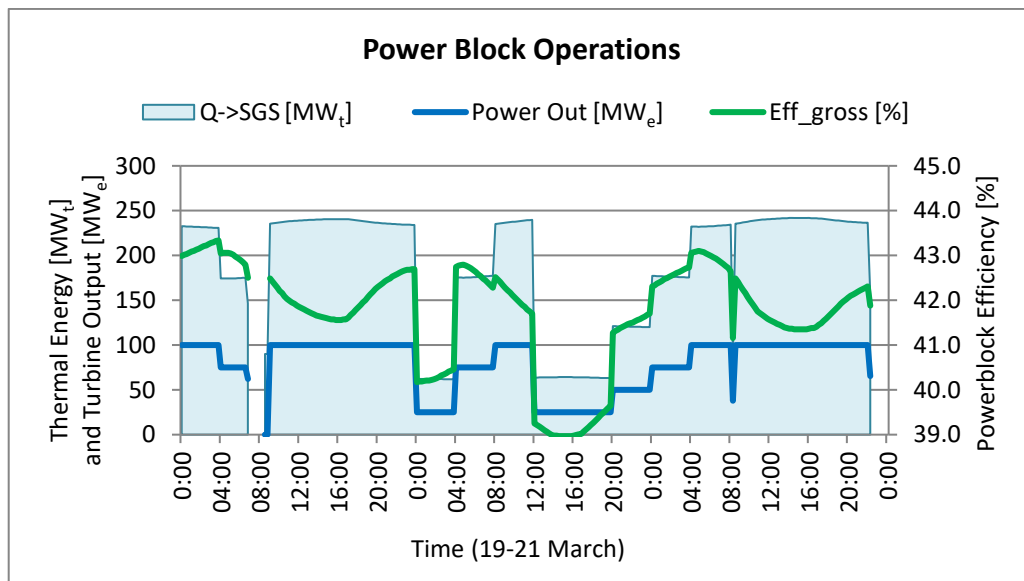


Figure C.29: Power block dispatch profile and efficiency

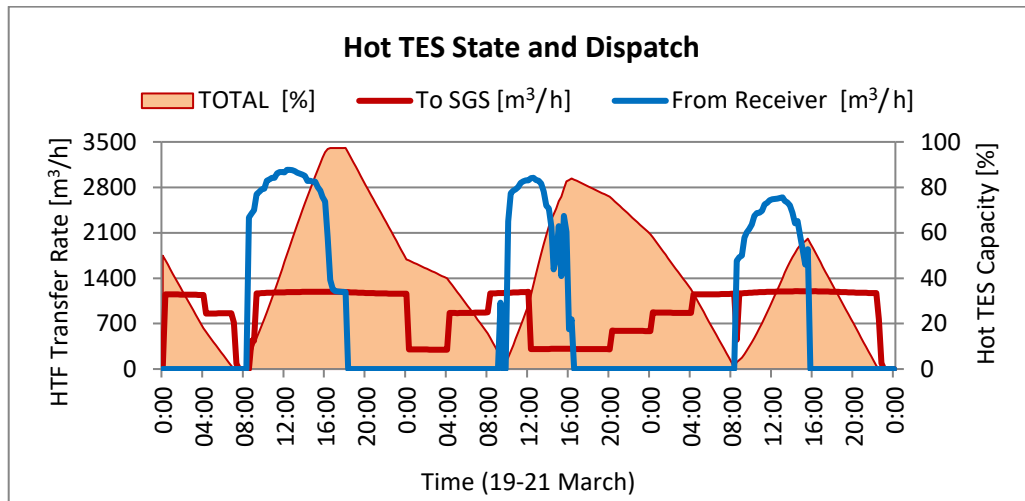


Figure C.30: Graphical representation of hot TES charge and discharge profiles

C.3.4. Maximise Plant Revenue

The ‘Maximise Plant Revenue’ strategy is of particular importance to a plant that sells the power generated to the electric grid. In South Africa, a PPA is concluded between the plant and the electric grid, i.e. IPP and Eskom. This operating strategy has been set up to reflect the current PPA time-of-day tariff structure applicable to IPP plants of Bid Window 3.5 of the REIPPPP. By the end of this section, the user will be able to fully understand and appreciate the PPA boundary conditions imposed onto the plant and its effects on the plant operations. The model has been set up to accommodate five time-of-day tariffs, as illustrated in Figure 31. This allows the user to further test the future PPA structures that are applicable to the CSP plants. There are two variations available in the optimisation process for ‘Maximise Plant Revenue’. The only difference between the ‘Plant Revenue’ and the ‘Reduced Turbine Start/Stop’ is the additional simulation time required for the latter. A quick overview is given for the first option. If the user requires further optimisation, the second option is recommended.

C.3.4.1. Maximise Plant Revenue

The case study plant on which this model is based on does not have a ‘Time-of-day Tariff’ PPA in place. However, for the demonstrative purposes of the model, this scenario is simulated. This added feature offers flexibility and additional value to the user. The user is tasked to set up the simulation model as per Figure C.31 with the ‘Plant Revenue’ option enabled. The previous simulation results demonstrated the receiver’s dependency on the charged stage of the hot and cold TES. Thus, the simulation results for this operating strategy do not focus on the receiver’s operations but rather on power block operations. The optimisation for maximising the plant revenue is directly influenced by the PPA structure. It subsequently optimises the dispatch of the hot TES to the power block. No thermal energy is dispatched to the power block in times where no payment for generated power is awarded; this is clearly illustrated in Figure C.32 by the non-generation correlating to the ‘Time-of-day Tariff’ structure.

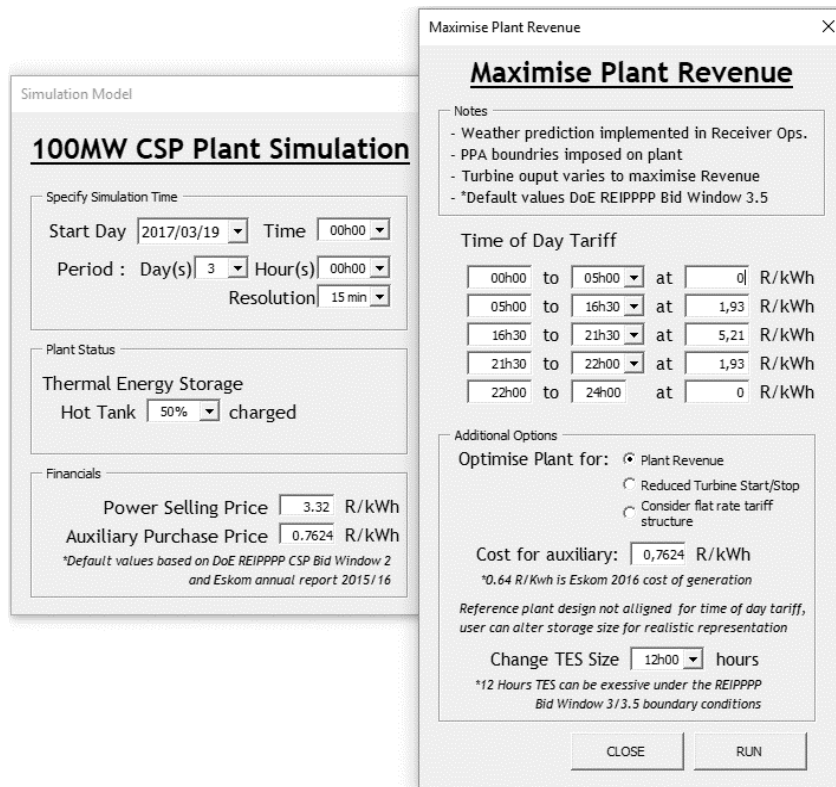


Figure C.31: Maximise Plant Revenue, Time-of-day Tariff – Optimise Net Power

To generate power at full load from the power block, the hot TES tank was sufficiently charged by the receiver for a selected time period. However, a turbine start/stop sequence can be present at times when the hot TES is depleted before the receiver could supplement the offset used by the power block. As this model could be utilised as a tool to the CSP plant operator, the operator would rather delay the turbine start-up or reduce the turbine output to compensate for this anomaly. The simulation model considers this situation and the user has the flexibility to further optimise the power block output by selecting the ‘Reduced Turbine Start/Stop’ option.

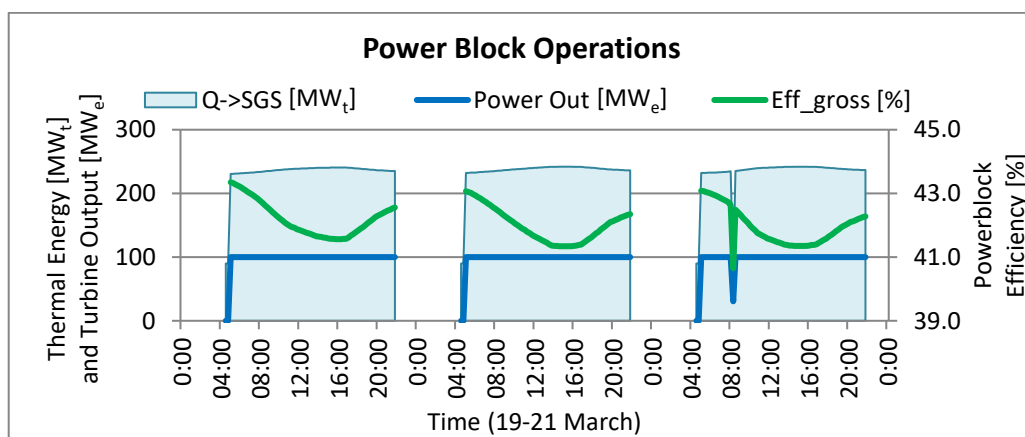


Figure C.32: Power block dispatch profile and efficiency

C.3.4.2.Reduced Turbine Start/Stops

The ‘Reduced Turbine Start/Stop’ optimisation is accessible under the ‘Maximise Plant Revenue’ menu, as seen in Figure C.31. Once executed for the same period and under the same boundary conditions, the optimised simulation results will be obtained. Figure C.33 presents these optimised simulation results. As observed, the turbine start-up is delayed which prevents the turbine to stop and restart later on.

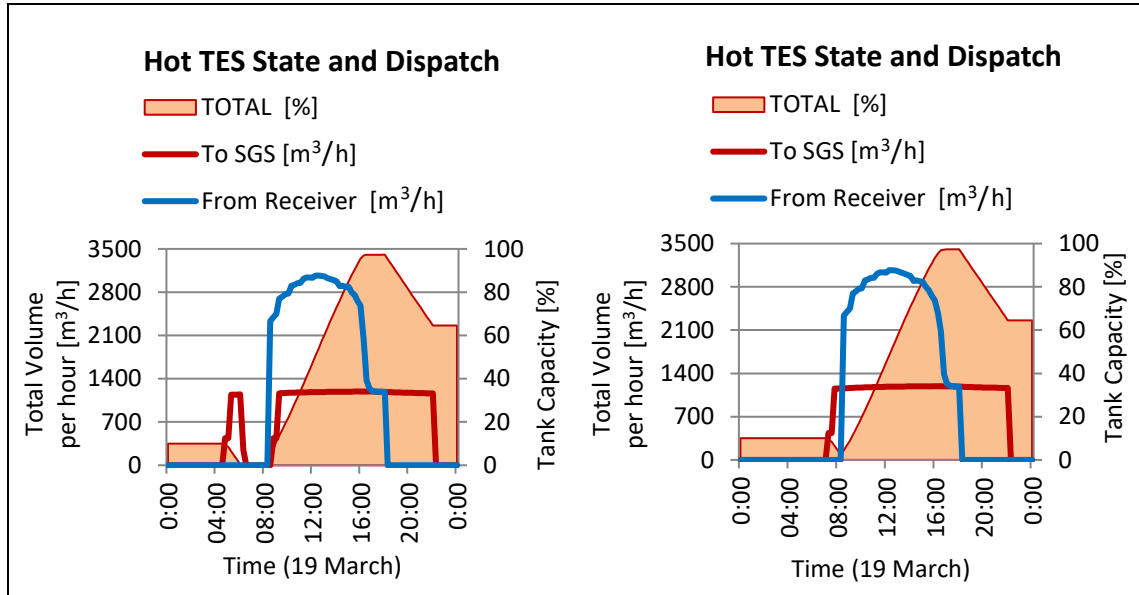


Figure C.33: Hot TES dispatch profile

C.3.4.3.Additional User Functionality

The ‘Maximise Plant Revenue’ operating strategy offers the user the flexibility to implement various PPAs for the plant. By specifying a time-of-day tariff and setting the different period to suit the user’s need, this simulation model strives to cover the current South African conditions regarding the REIPPPP. It is, therefore, important to test and analyse the impact of various PPA structures on the plant operations and plant design. One of the design limitations that is noticed in the discussed PPA example is the oversized TES.

The present simulation model is based on the referenced power plant that did not bring in to consideration what impact the illustrated PPA will have when it is implemented. This plant, however, belongs to the same entity as the electric grid. It is for this reason the TES of the plant is optimised to offer a wider dispatchability potential to the grid, aiming to achieve a capacity factor of 60 %. Nevertheless, the user is provided with an option to alter the plant’s TES size. This is as illustrated in Figure C.34. It is only available for the ‘Maximise Plant Revenue’ operating strategy to simulate the dispatch from the TES under various implemented time-of-day tariffs. It should, however, be noted that the receiver in this case will be oversized for smaller TES sizes. The SM at design point is 2.4. Thus, the energy might be deflected due to the fully charged state of the hot TES.

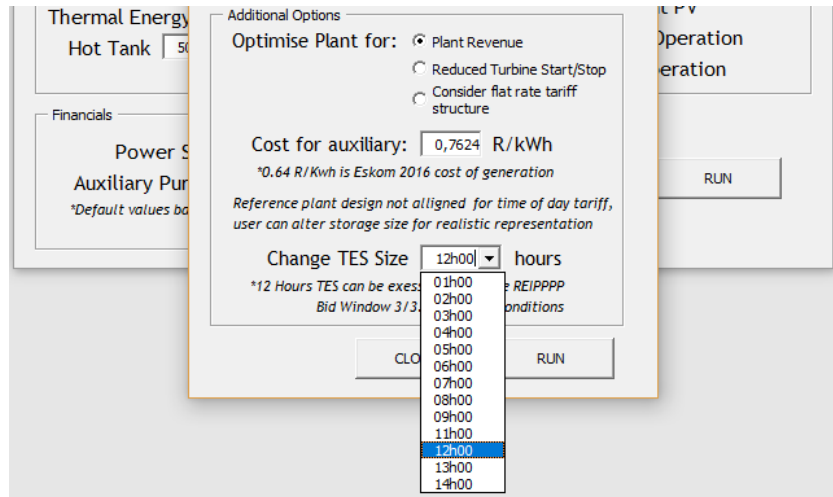


Figure C.34: Change TES size, adapted from Figure C.31

C.3.4.4. Change TES Size for Maximise Plant Revenue

The user is tasked to repeat the simulation run of the ‘Maximise Plant Revenue’ the TES size of ‘8 hours’. From the simulation results, it is clear that the receiver is overdesigned for this scenario, as the output of the receiver was curtailed to accommodate the TES size. This resulted in an increase in the deflected energy, as seen in Figure C.35.

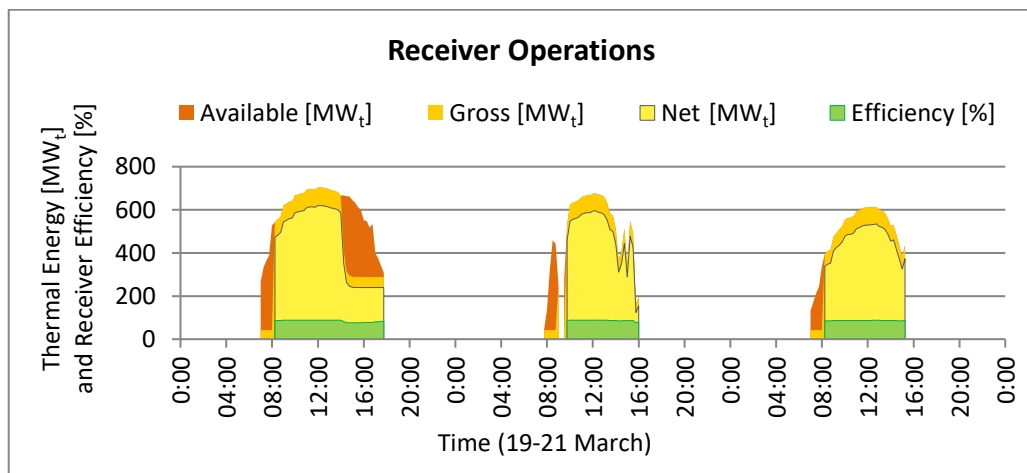


Figure C.35: Receiver curtailment due to TES size reduction

Furthermore, an increase in the turbine starts and stops are observed when the output of the power block is considered. The turbine output is fixed for the specific period, i.e. 05h00-16h30. If the hot TES is charged sufficiently for the power block to start up, the start-up sequence will initiate depleting the hot TES before the receiver could supplement the offset. The user is, therefore, tasked to optimise the turbine start/stops. These results are illustrated in Figure C.36.

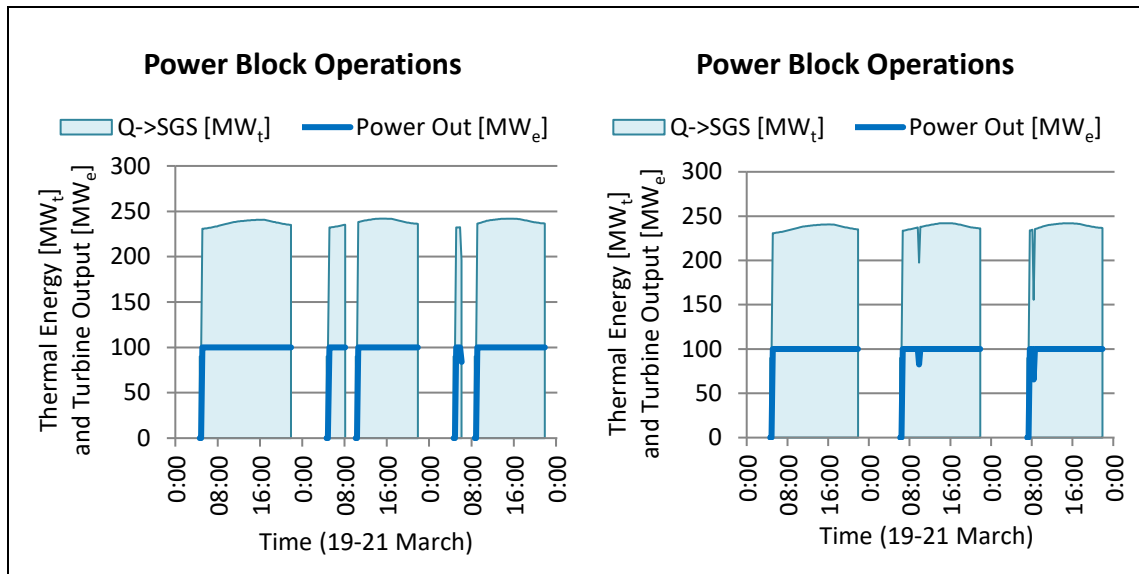


Figure C.36: Increase in turbine start/stops due to reduction in TES (left), Reduce turbine start/stops by delaying turbine start-up (right)

C.3.4.5. Maximise Plant Revenue with Flat Rate Tariff

The ‘Maximise Power Generation’ and ‘Maximise Plant Revenue’ operating strategies coincide when the flat rate tariff structure is in place. Therefore, the execution of simulation run by the user for the ‘Optimised Power Generation’ operating strategy leads to execution of the ‘Maximise Plant Revenue’ with a flat rate tariff.

C.3.5. Minimise Energy Dumping

The phenomenon of ‘Energy Dumping’ was observed during the first simulation results of Section C.3.1.2. The following figures, Figure C.8 and Figure C.10, are reconsidered for the ‘Minimise Energy Dumping’ operating strategy.

The ‘Deflected Solar Energy’ presented in Figure C.8 accounts for the amount of solar energy deflected away from the receiver due to the exceeding flux limitations of the receiver material. This ‘potential energy’ loss resulted due to the implemented aiming strategy of the heliostat field. As previously discussed, the aiming strategy implemented for the heliostat field concentrated too much of the solar energy onto a specific region on the receiver’s surface. The user will accordingly be able regain this lost energy. The lost energy can be regained by adjusting the solar flux to attain uniform flux distribution over the surface of the receiver. The receiver control system implements this safety precaution through the heliostat field aiming strategy. By adjusting the aiming strategy, this potential energy could be regained.

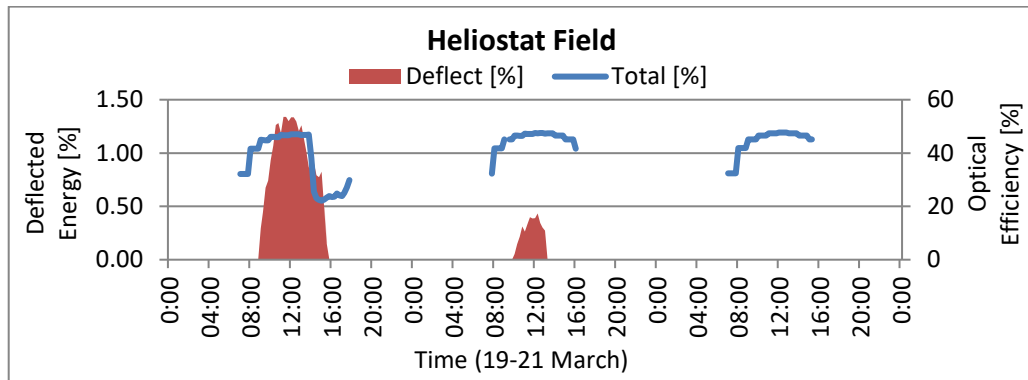


Figure C.8: Heliostat field optical efficiency and energy deflected from receiver

The second phenomenon to be considered in the ‘Minimise Energy Dumping’ operating strategy is the energy loss due to the status of the hot TES. When the hot TES is fully charged and the power block is not operational, the receiver is shut down. The receiver output can also be curtailed to supplement the discharge used by the power block. In Figure C.10, the notable energy dump on the first day of the simulation results was due to the operating strategy implemented. The strategy involved turbine start-up at 05h00 resulting in a full state of charge for the TES during receiver operation.

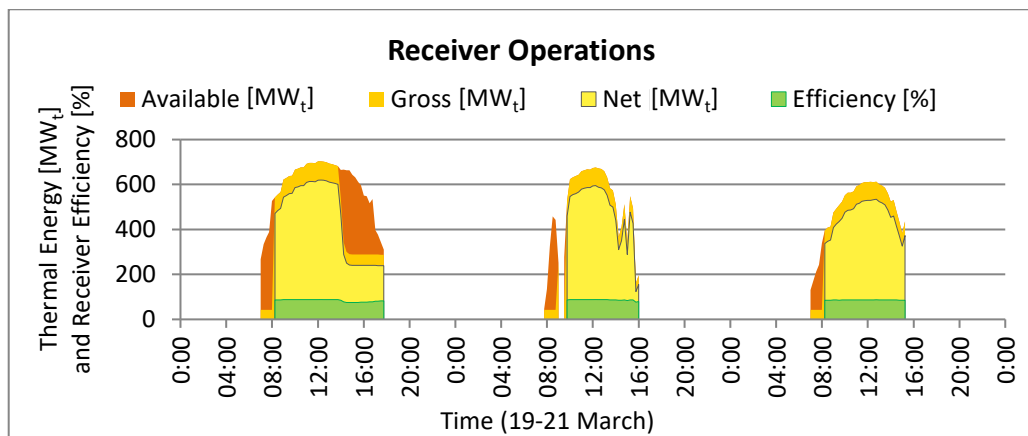


Figure C.10: Graphical representation of receiver operations

It is evident from these two scenarios that the heliostat field and receiver operations can be optimised to reduce the deflected and/or dumped energy and the energy dumping can be minimised. The user is tasked to enable the ‘Minimise Energy Dumping’ operating strategy as illustrated in Figure C.37. The simulation results, illustrated in Figure C.38 and Figure C.39, show that there is no deflected energy resulting from the heliostat field or the receiver operations. To incorporate the deflected solar energy, the heliostat field aiming strategy was adjusted and this was achieved by shifting the excess flux found in high concentrations to the regions with lower flux concentrations on the receiver. This phenomenon resulted in a higher gross power to the receiver. The dispatch control of the hot TES allowed for a 100 % receiver energy utilisation.

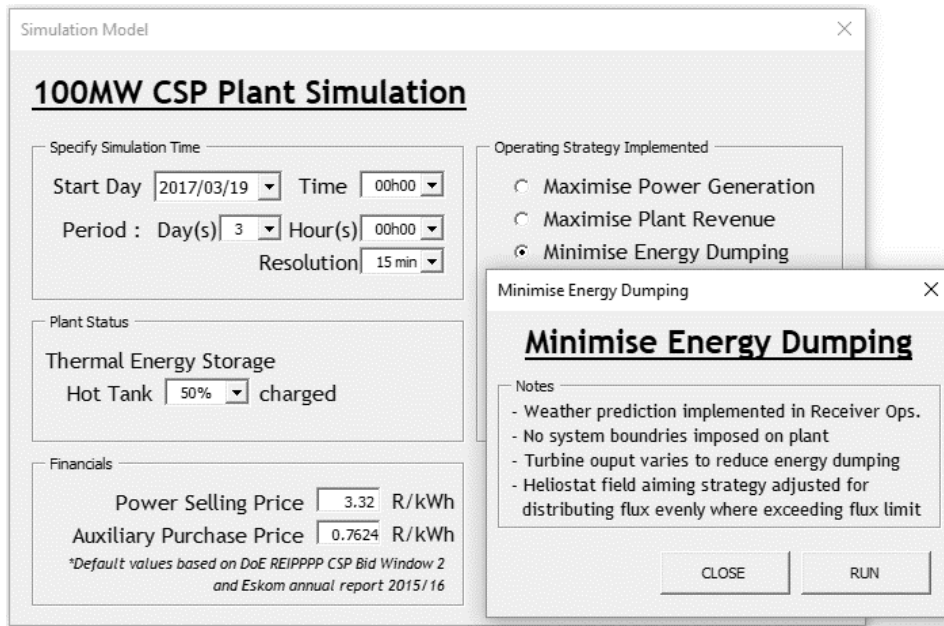


Figure C.37: Minimise energy dumping operating strategy

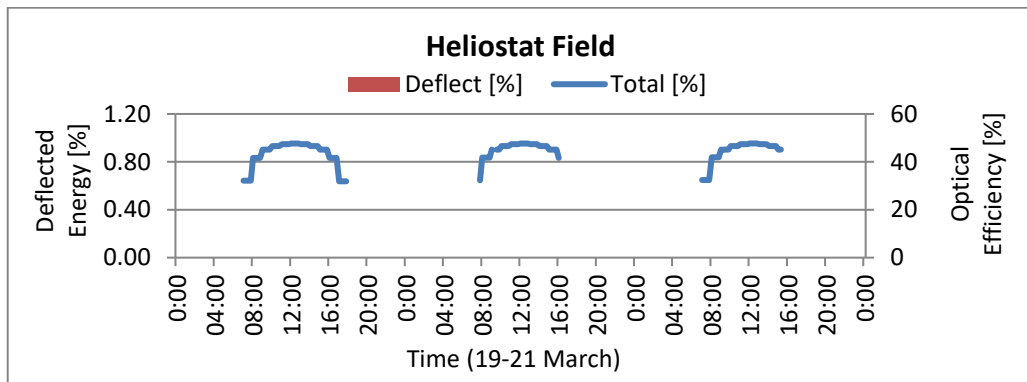


Figure C.38: Heliostat field optical efficiency, no solar energy deflected

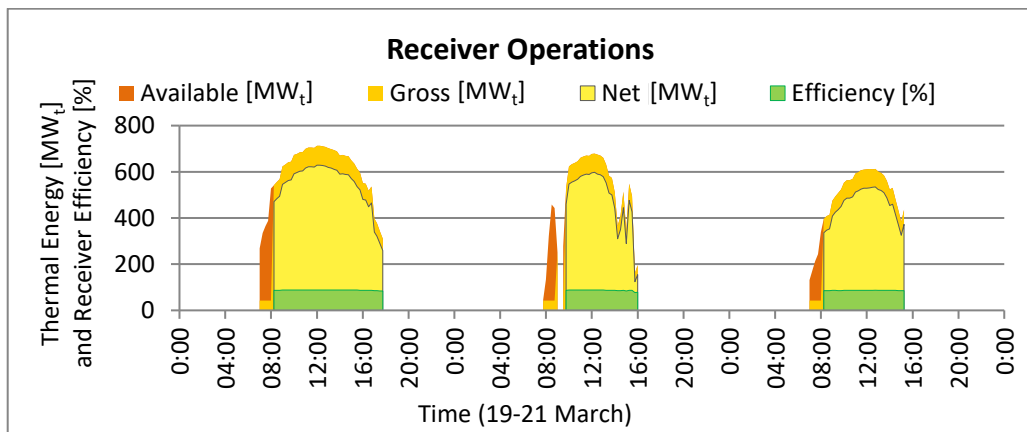


Figure C.39: Receiver operations, no solar energy deflected

For this particular operating strategy, the simulation results illustrate the power block operations in a manner to inform the user or plant operator about the possible TES constraints. The model implemented a lower boundary condition for the power block and step up the turbine output to highlight the minimum required turbine output, given the state of charge of the TES. The TES constraints are illustrated in Figure C.40 and Figure C.41. In this operating strategy, the receiver operations were prioritised for maximum thermal output.

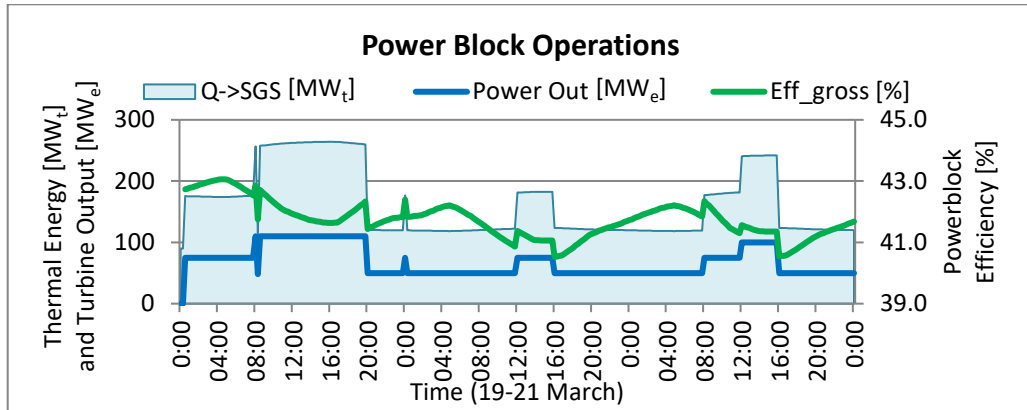


Figure C.40: Reduce turbine start/stops by delaying turbine start-up

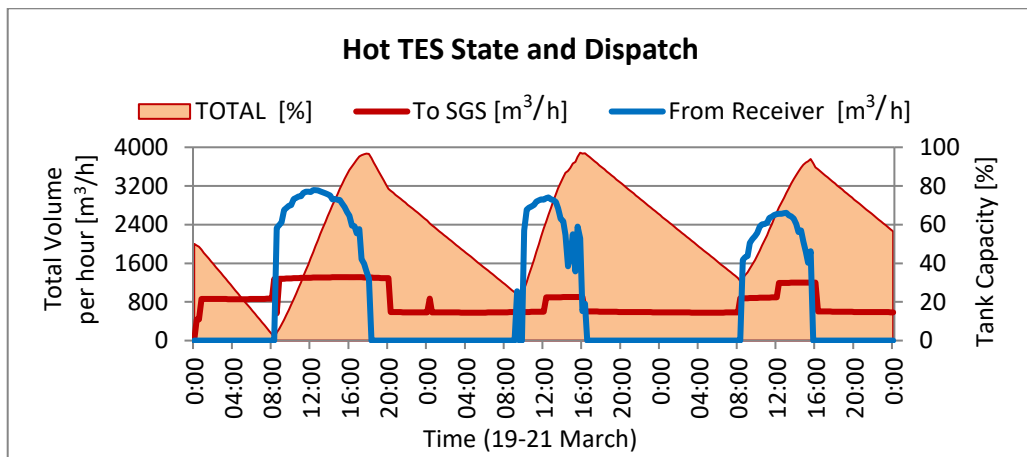


Figure C.41: Hot TES dispatch control highlighting areas of constraint

It is interesting to note from Figure C.40 the dispatch control to the power block to avoid the hot TES reaching a full state of charge. During each day within the simulation, it is noticeable that the dispatch volume to the power block increases. For comparison, results from the heliostat field and receiver performances of three relevant operating strategies are shown in Table C.1. The first simulation used is the user operating strategy set out in Section C.3.1 and no optimisation was implemented. The second operating strategy used was ‘Maximise Power Generation’ simulation whose results are considered as executed in Section C.3.3. The ‘Maximise Power Generation’ operating strategy strives to utilise as much of the solar energy from the heliostat field as possible. The higher receiver output causes the hot TES state to be charged with more thermal energy. This subsequently leads

to delivery of higher output from the power block. This can be clearly observed in the ‘Available Energy Utilised’ entry in Table C.1. The main differences between the ‘Minimise Energy Dumping’ and ‘Maximise Power Generation’ operating strategies are the heliostat field aiming strategy implemented for each. The ‘Maximise Power Generation’ operating strategy utilise the aiming strategy developed for the model, whereas the ‘Minimise Energy Dumping’ operating strategy adjust the total gross power onto the receiver by considering the deflected energy. Furthermore, the receiver output is optimised in the ‘Minimise Energy Dumping’ whereas the power block output is optimised within the ‘Maximise power Generation’.

Table C.1: Plant revenue comparison between two variances in simulation model

	Minimise Energy Dumping	User Specified Operations Section 3.1	Maximise Power Generation	Units
Heliostat Field				
Deflected Solar Energy (flux limitations)	0	50.7	50.4	MWh _t
Receiver:				
Total Gross Power	13.56	12.56	13.25	GWh _t
Total Net Power	11.81	10.90	11.53	GWh _t
Energy deflected	0	948	260	MWh _t
Available Energy utilised	100	93.0	98.1	%

C.3.6. Optimise Electric Grid

The ‘Optimise Electric Grid’ operating strategy demonstrates the value of CSP with storage capabilities within the electric grid. Often the argument is made by the electric grid stakeholders that the renewables do not offer base load capabilities or security of supply. These statements are discredited by the operating strategies that are discussed in this section. They demonstrate the value and offerings of CSP in the electric grid. The five operating strategies discussed in this section include Compliment Wind, Compliment PV, Compliment Wind and PV, Base load Operation, and Peaking Operation. The operating strategies complimenting wind and PV generation demonstrate the dispatch potential of CSP storage when non-dispatchable renewable generating technologies are considered.

C.3.6.1. Optimise Electric Grid - Compliment Wind

The user is tasked to set up the simulation model for ‘Complimentary Services to Wind Generation’ as illustrated in Figure C.42. Due to the installed capacity of a 100 MW_e CSP plant, the contribution from one CSP plant on the electric grid is insignificant when the total system installed has the capacity for 9,697 MW_e wind and 9,650 MW_e PV. For this reason, the output of the plant is scaled up to the level of a ‘Solar Park’ to better illustrate the contribution that CSP makes on the system by matching the equivalent maximum wind and/or PV supply. During the complimentary services, the operations of the CSP plant is optimised to provide stability to the electric grid.

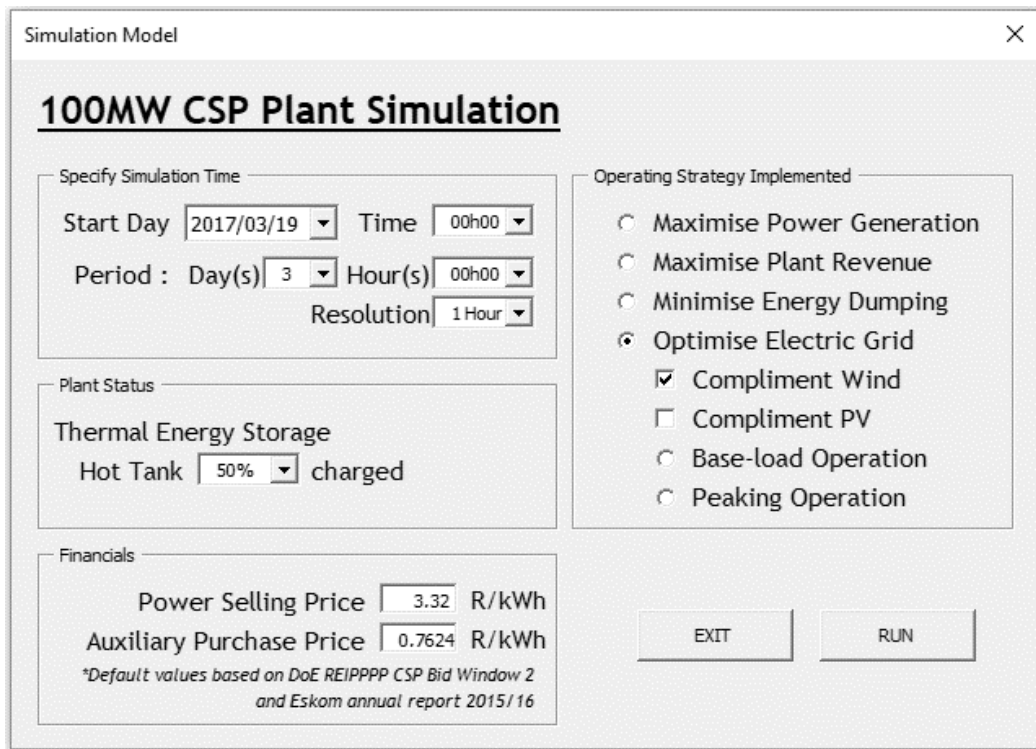


Figure C.42: Complimentary services to Wind generation

When the complementary services to wind or PV generation are simulated, a new graph is produced in the 'Report' sheet. This graph illustrates the relationship between the generating technologies. The graph (Figure C.43) clearly shows that a 'Solar Park' of 625 MW_e is able to compliment the wind generation profile. Sometimes the Solar Park gives no output due to hot TES depletion. The system's security of supply can be achieved by combination of these two technologies and a gas-turbine plant. In fact, the combination of these two technologies may even resemble base load capabilities. This graph essentially encapsulates the value offering of CSP plants with storage capabilities.

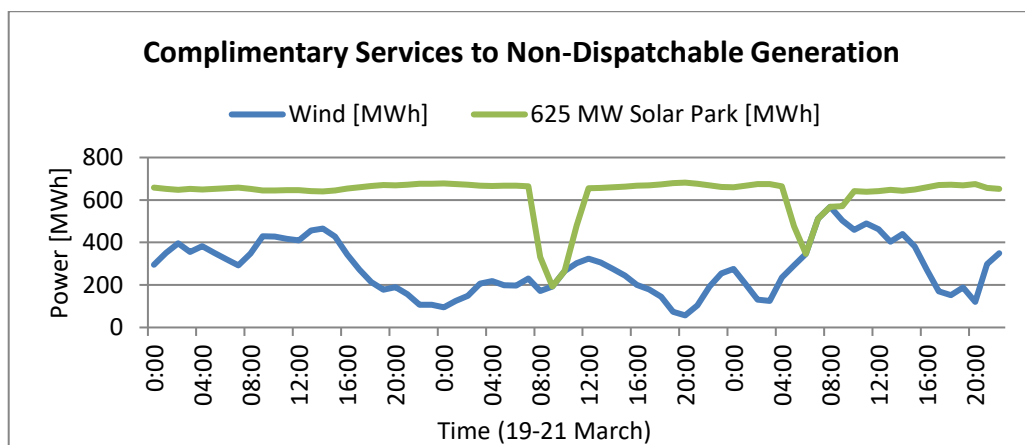


Figure C.43: CSP complimentary services to wind generation, stacked line

However, a significant disadvantage is experienced when the plant is operated to compliment the generation of another generating technology. Hence, there is a sacrifice to the efficiency of the CSP power plant. An increase in the deflected solar energy from the receiver totalling 2,500 MWh, and a lower power block efficiency at 36.2 % is observed. The resulting effects are presented in Figure C.44 and Figure C.45. Although, the overall efficiency of the plant is compromised, the benefits of complimenting wind generation are still achieved. The wind generation provides continuous power to the electric grid. If the plant is compensated financially for these services that it provides to the electric grid, this operating strategy may promote value-added services to the electric grid.

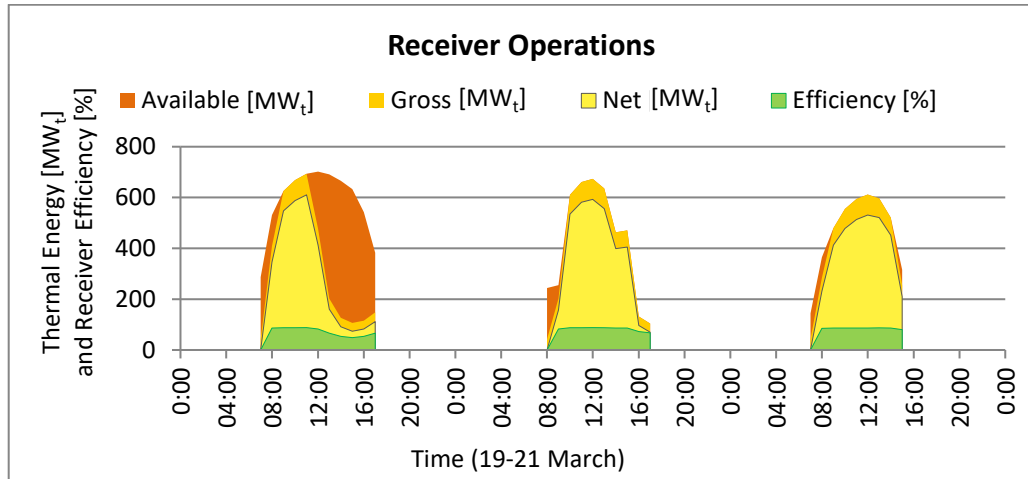


Figure C.44: Increase in deflected solar energy for complimenting wind generation

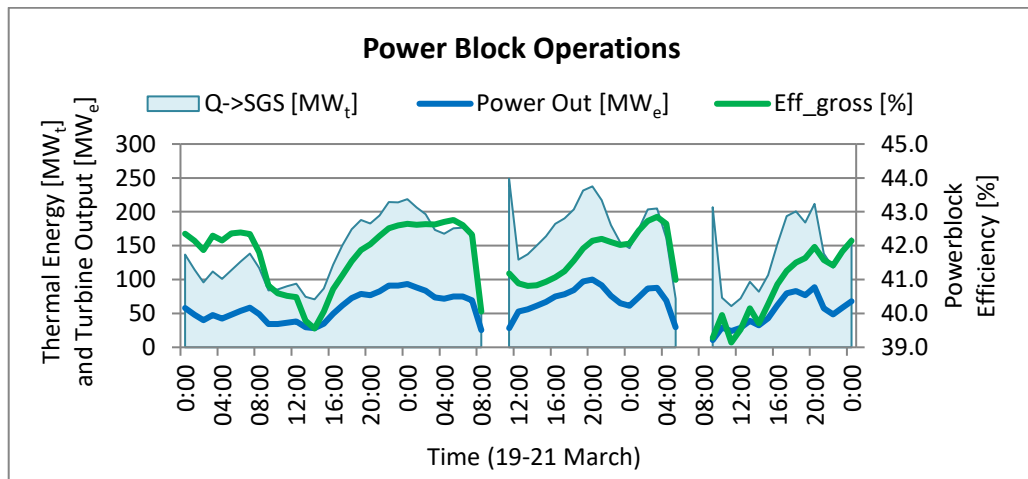


Figure C.45: Power block dispatch profile, complimenting wind generation

As a point of interest, the sharp ‘spikes’ observed in the power block operations, as illustrated in Figure C.45, are due to the power block start-up sequence. The thermal energy required for the start-up and for power generation results in a higher thermal energy sent to the SGS.

C.3.6.2. Optimise Electric Grid - Compliment PV

The user is tasked to set up the model as for the ‘Compliment Wind’ scenario, and to select the ‘Compliment PV’ option. Similarly, the ‘Complimentary Services to Non-Dispatchable Generation’ graph is produced and is as illustrated in Figure C.46. The CSP plant dispatch power to the grid when the PV contribution to the system drops below 95 % of the projected maximum generated power for the selected period. This operating strategy is of particular interest as continued generation of power into evening peaks is served by offering CSP as a complimentary service to PV generation.

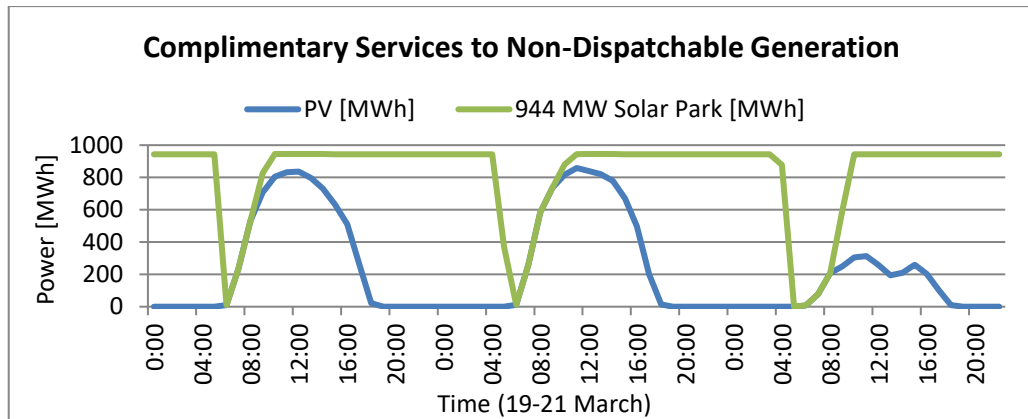


Figure C.46: CSP complimentary services to wind generation, stacked line

In the case of ‘Complimentary Services to Wind’, the CSP plant efficiency is affected. When the PV plants experience high amounts of solar irradiance, very little or no complimentary services are required from the CSP plants. When this happens, the hot TES is charged from the receiver, and it may reach its full capacity. This results in dumping of excessive energy. In this scenario, the TES storage system of the CSP plant acts essentially as a ‘battery’ for PV generation. It is represented by Figure C.47. The CSP plant obtains its energy from the TES, when the sun sets, and PV generation is reduced.

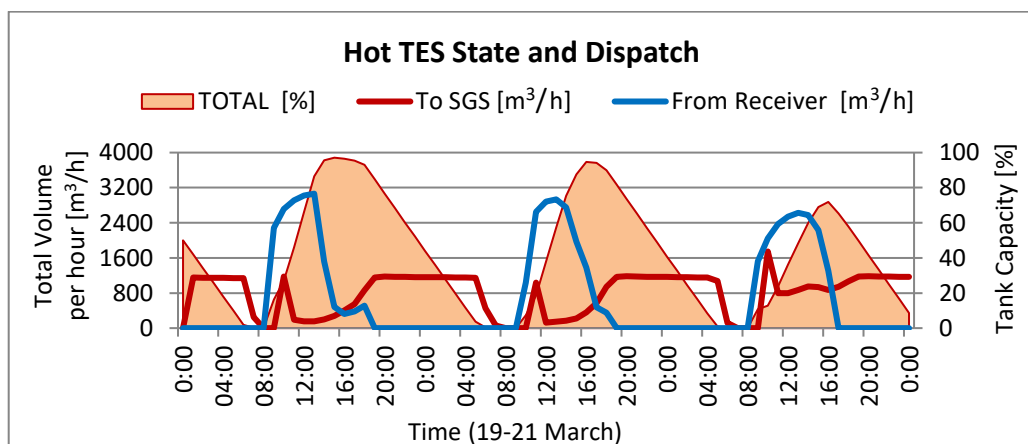


Figure C.47: CSP storage acting as a ‘battery’ for PV generation

Furthermore, the simulation model is capable of demonstrating the complimentary services to PV during cloud transients. From Figure C.46, it could be seen that on Day 3 during the cloud transients, the CSP plant utilises the stored power to provide continuous supply to the electric grid. This type of operation is more favourable on the receiver operations as the hot TES system is utilised. This reduces the probability of energy dumping.

C.3.6.3. Optimise Electric Grid - Compliment Wind and PV

The symbiotic relationship between the three generating technologies that is wind, PV and a solar park with an installed capacity of a 1380 MW_e, in providing a continuous supply to the electric grid is illustrated in Figure C.48.

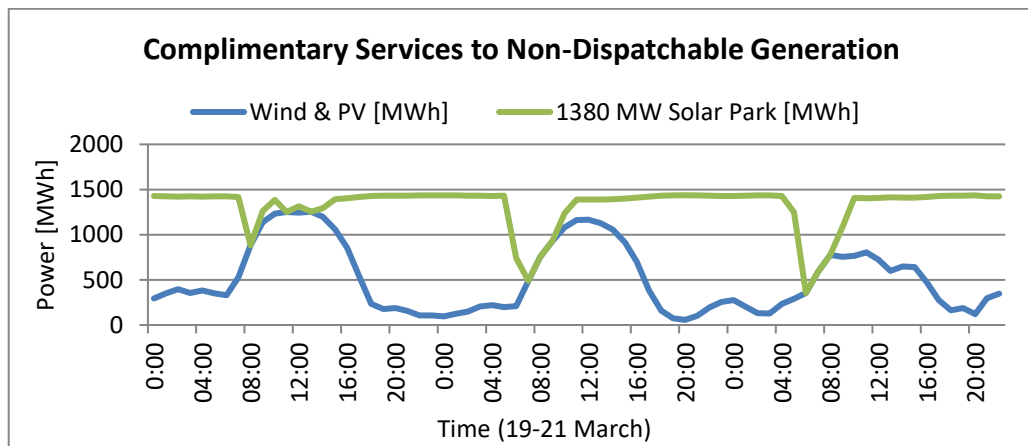


Figure C.48: CSP complimentary services, wind/PV generation, stacked line

C.3.7. Demonstrating CSP Base Load Capabilities

Under the ‘Base load operation’ operating strategy, the model optimises the plant operations to demonstrate its capability for base load operations. The maximum power output from the plant while maintaining base load operations is illustrated in Figure C.49. The corresponding dispatch profile and state of charge of the TES is seen in Figure C.50.

C.3.8. Demonstrating CSP Peaking Capabilities

Under the ‘Peaking Operations’ menu, the user is given freedom to specify the peaking operations’ time and time for delivering power from the power block. This is illustrated in Figure C.51. Furthermore, the power block output can be increased to 110 % in order to reduce energy dumping due to a hot TES state of charge. The results for peaking operation delivering 120 MW_e during period 18h00-20h00 is shown in Figure C.52. The plant operations are optimised to prioritise the peaking period while maintaining a maximise power generation operating strategy.

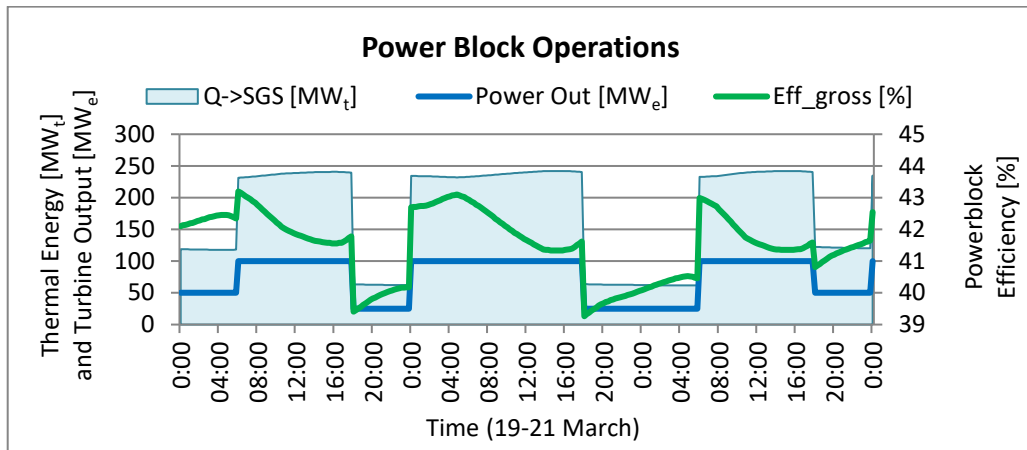


Figure C.49: Power block dispatch profile to the grid, base load capability

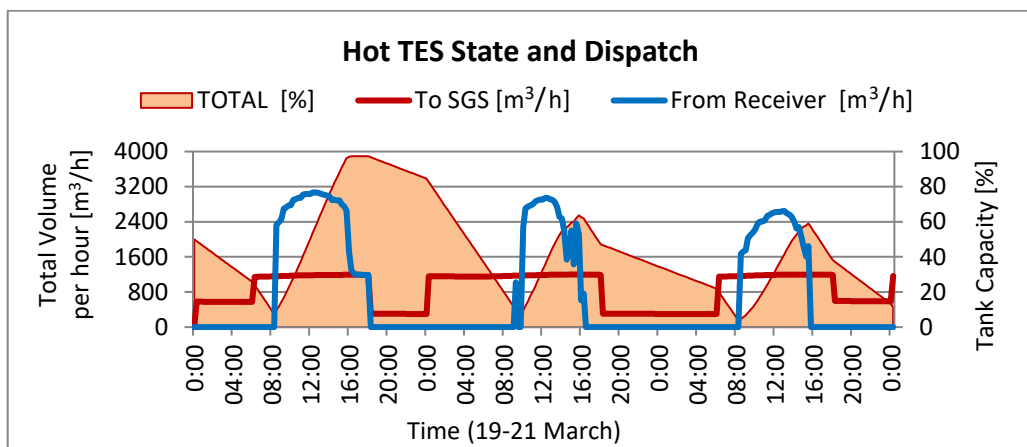


Figure C.50: Hot TES dispatch control, maintaining sufficient capacity in hot TES

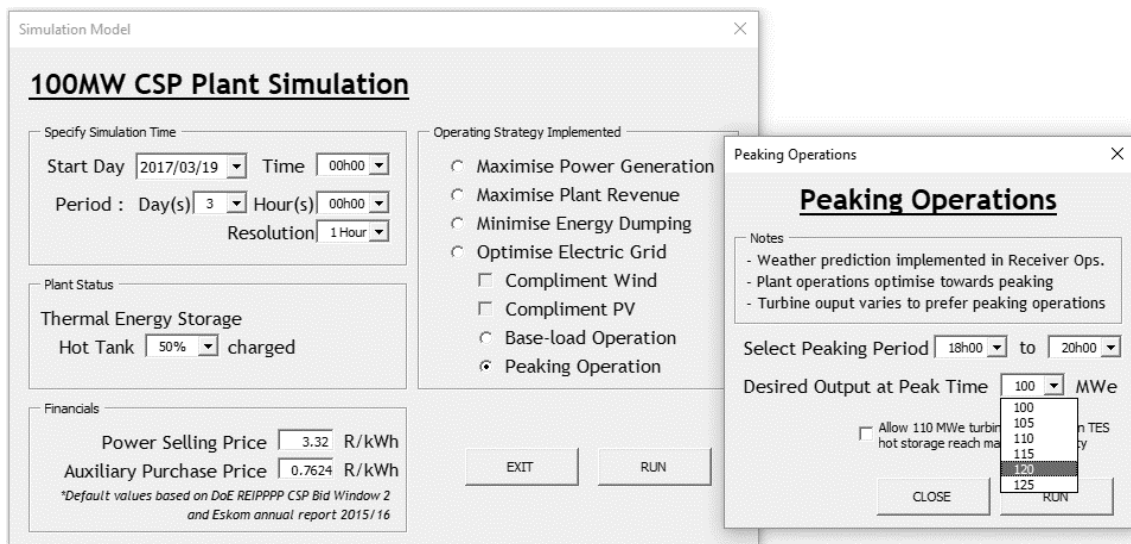


Figure C.51: Peaking operations simulation set up

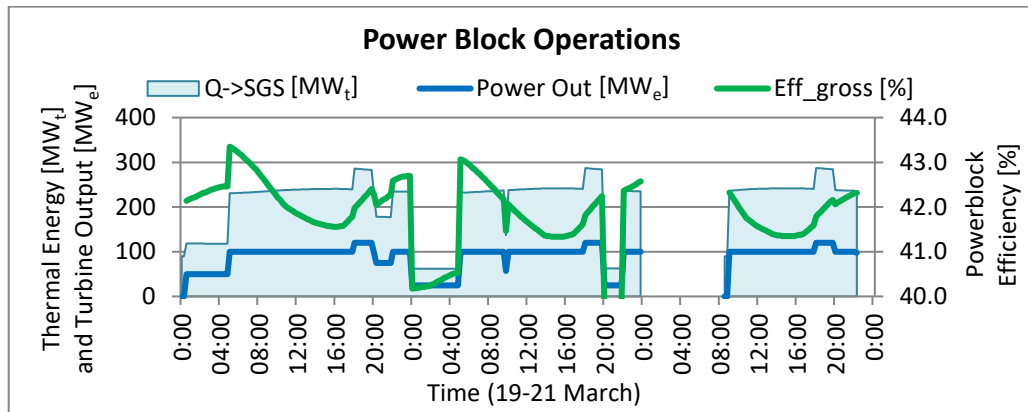


Figure C.52: Power block dispatch profile to the grid, peaking capability

C.4. COMPARE OPERATING STRATEGIES RESULTS

The above Section C.3 illustrated the ability of the simulation model to successfully simulate the plant operations under various operating strategies and specified user inputs. Therefore, in this section the user is provided with a holistic overview of the simulation results. By the end of this section, the user will be in a position to make informed conclusions on the plant’s performance for the selected time period. A comparative overview is created in the Excel workbook under the ‘Compare SimResults’ sheet. This sheet maintains a record of all the simulation results. It also provides insights into the specificities of the heliostat field, receiver, power block and the performance of the plant. The 13 simulation results for the selected period, 19th to 21st March, are provided below in a tabulated form. The applicable section and additional user inputs specified for each operating strategy is noted, see Table C.2.

Table C.2: List of operating strategies with specified user inputs in Section 3

No	Operating Strategy	Section	User Inputs
1	Max. Power Generation (User)	Section C.3.1	Power block start time at 05h00
2	Max. Power Generation (User)	Section C.3.2	Power block start at hot TES 30 % charged
3	Max. Power Generation (Optimised)	Section C.3.3	Optimised Power Generation selected
4	Max. Plant Revenue, Time-of-day tariff	Section C.3.4.1	TES size 12 hours
5	Max. Plant Revenue, Time-of-day tariff	Section C.3.4.6	TES size 8 hours
6	Reduce Turbine Start/Stop	Section C.3.4.6	TES size 8 hours
7	Max. Plant Revenue, Flat rate tariff	Section C.3.4.7	Flat rate tariff selected
8	Min. Energy Dumping	Section C.3.5	No additional inputs required
9	Complimentary services to Wind	Section C.3.6.1	No additional inputs required
10	Complimentary services to PV	Section C.3.6.2	No additional inputs required
11	Complimentary services to Wind/PV	Section C.3.6.3	No additional inputs required
12	Demonstrate Base Load Capabilities	Section C.3.7	No additional inputs required
13	Demonstrate Peaking Capabilities	Section C.3.8	Peak Time 18h00-20h00 with Turbine Output set at 120 MW _e

C.4.1. Compare SimResults Sheet

The simulation model automatically populates the ‘Compare SimResults’ sheet in order to maintain a record of various simulations. Furthermore, the user is presented with the functionality to graphically compare different operating strategies based on the receiver, power block and plant performances. Additional financial indicators are also calculated and presented under this sheet. An overview of the ‘Compare SimResults’ sheet is illustrated in Figure C.53. The user is tasked to select the ‘Compare Operating Strategies’ button for the simulation model to graphically represent these comparisons.

The additional information regarding the simulation is stored at the end of each entry, under the column ‘Notes’. This information aids the user to distinguish between various operating strategies based on the user-specified inputs. For example, the user is able to compare the plant performance and financial indicators based on specific ‘Time-of-day’ tariff structures. The user does not have to memorise all the combinations that he/she specified for each simulation. This model conveniently captures these user-specified inputs under the column ‘Notes’.

The following sections elaborate on the method used to compare the various operating strategies. It is important for the user or the plant operator to identify the best operating strategy to implement on the plant. Based on the user’s (the plant operator or the system operator) objectives, the comparative results would inform which plant operations are to be followed. Although, these results stem from only single time period, that is 19th to 21st March, a definitive conclusion should incorporate the period in question. Thus, results obtained from this period should not be used across board. The period being analysed is influenced by the ambient conditions, which ultimately affects the plant operations and performance. For this reason, similar method has been applied to two other periods for additional variability and information. These results further address the research objective that involves optimisation of the plant operations based on the weather conditions. The two additional periods represent the periods with high and low DNI. These results are captured in Section C.5 and Section C.6 of this manual.

C.4.2. Compare Receiver Performance

The two key performance indicators that are considered while comparing the receiver’s performance for the various operating strategies are the total net power delivered by the receiver and the average efficiency during the selected period. The receiver’s performance for 13 simulations as per Table C.2 is plotted and represented in Figure C.54. The horizontal axis in Figure C.54 represent the operating strategy followed from Table C.2.

Considering the ‘Total Net Power’ output of the receiver, it is assumed that the ‘Minimise Energy Dumping’ would result in the highest power output. The lowest net power for the receiver would be associated with occurrences during the hot TES fully charged state. Analysing the comparative results from Figure C.54, the operating strategies 3, 7-8 and 12-13 were amongst the best performers in terms of receiver net power output.

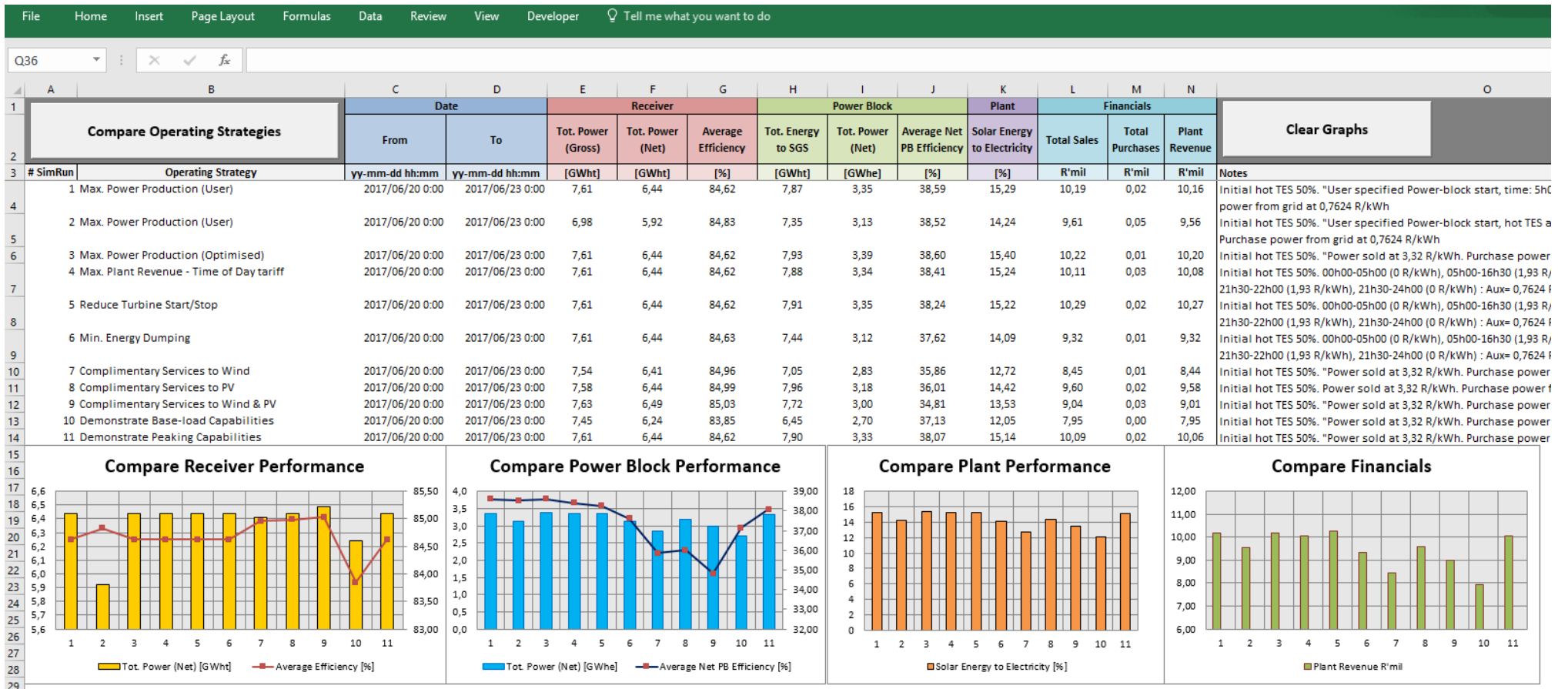


Figure C.53: Comparison of simulation results executed in Section 3 presented in the 'Compare SimResults' sheet

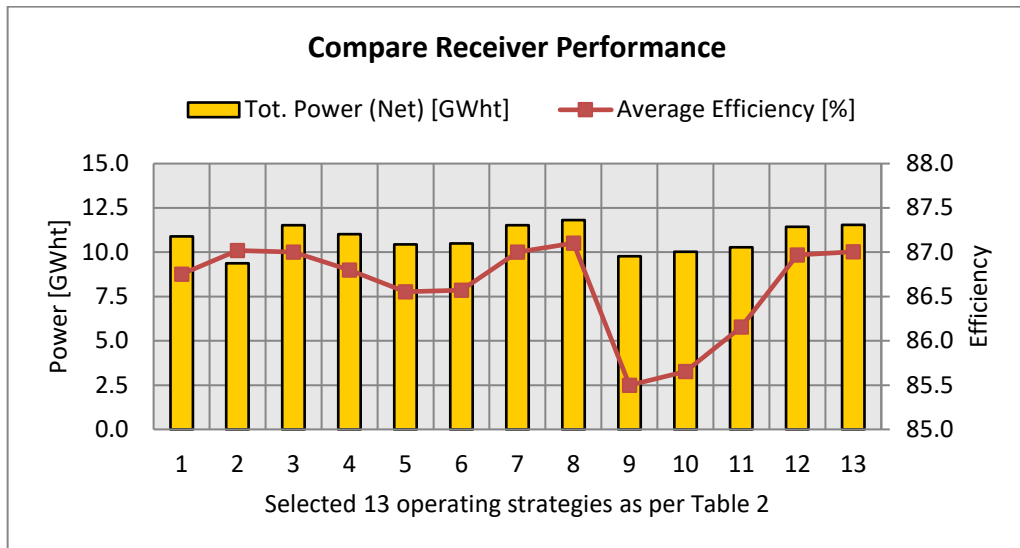


Figure C.54: Comparison of the simulation results for the receiver performance

The high performing operating strategies include ‘Maximise Power Generation’, ‘Maximise Plant Revenue with Flat Rate tariff structure’, ‘Minimise Energy Dumping’, ‘Base load Operations’ and ‘Peaking Operations’. The values tabulated in the ‘Compare SimResults’ sheet show that the ‘Minimise Energy Dumping’ operating strategy performed the best with a total of 11.81 GW_{ht} net power delivered. The ‘Maximise Power Generation and Revenue’ and ‘Peaking’ operating strategies generated power of the order of 11.54 GW_{ht}. The higher output presented in the ‘Minimise Energy Dumping’ operating strategy is due to the adjusted heliostat field aiming strategy and optimised dispatch of hot TES.

The operating strategies 2 and 9-11, from Figure C.54, delivered the least net thermal power. These operating strategies include the ‘User Specified Maximise Power Generation’ and the ‘Complimentary services to Wind, PV and Wind-PV generation’. The hot TES reaches its fully charged capacity in the scenarios when the plant was not performing well. Consequently, the receiver operations had to be reduced or they had to be completely shut down. The low performing operating strategies relevant to the receiver’s performance in this case, indicate that the dispatch from the hot TES was not optimised sufficiently for the receiver operations and thermal output. A difference of only 1.5 % was observed between the lowest and highest average receiver efficiencies and it can be observed in Figure C.54. However, the relative difference in these values correlates to the operations of the plant. The higher average receiver efficiencies were observed for the operating strategies 2-3, 7-8 and 12-13. These operating strategies did not excessively curtail the receiver’s operations. Therefore, operating at higher thermal flux or higher gross thermal power and resulting in higher efficiencies.

The average receiver efficiencies were the lowest for operating strategies 5-6 and 9-11. The operating strategies 5-6 reduced the TES size to 8 hours. This resulted in the hot TES reaching fully charged state at a much faster rate. This subsequently curtails the receiver’s output. This phenomenon can be observed in the receiver operations graphs reproduced in Figure C.55. The operating strategies curtailing the receiver’s output resulted in lower

receiver performance. This may be due to the receiver operating at lower thermal flux or gross thermal power. Similar is the case for the operating strategies 9-11 that are ‘Complimentary Services to Wind and PV generation’. The relatively higher receiver performances indicated by operating strategy 2 is due to the shutting down of the receiver’s operations instead of curtailing them (see Figure C.56). Although, the ‘Net Power’ recorded was less, the average receiver performance is higher.

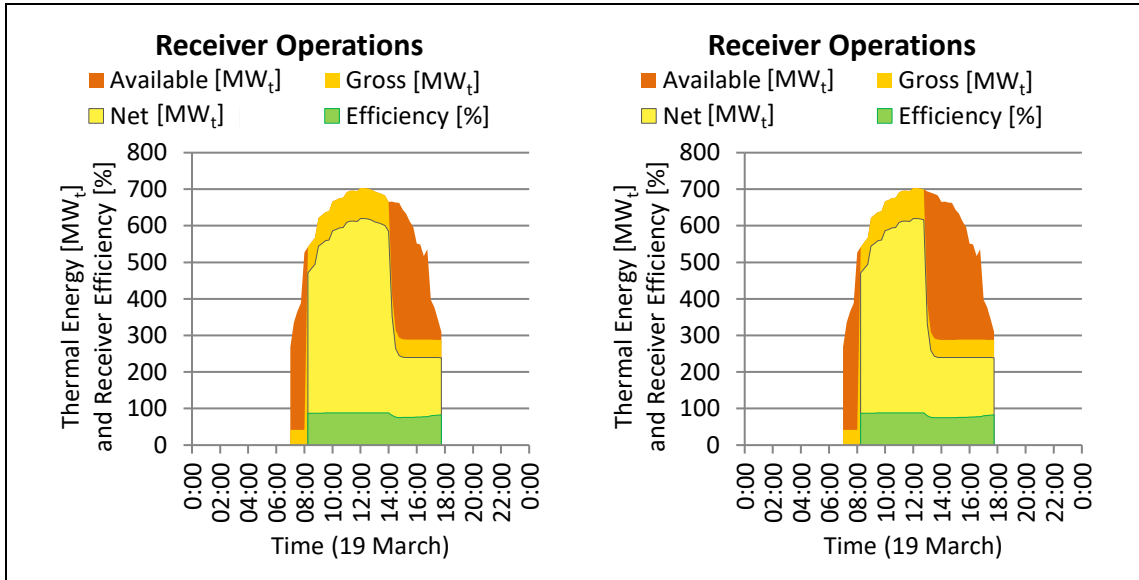


Figure C.55: TES size reduction (left) 12 hours (right) 8 hours

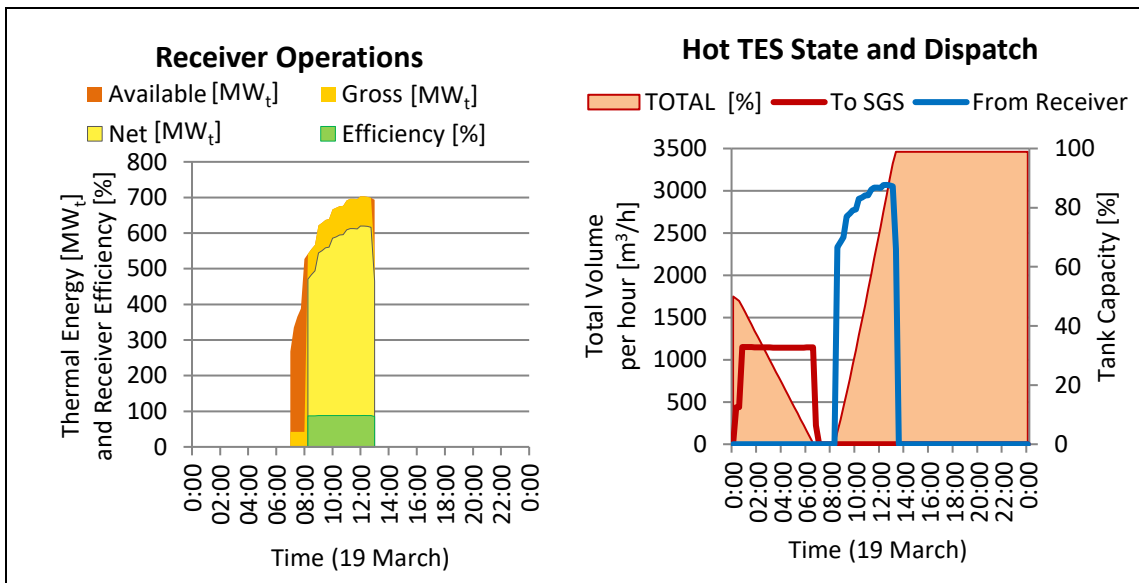


Figure C.56: Receiver shutting down due to TES state of charge

C.4.3. Compare Power Block Performance

In the ‘Compare Power Block Performance’ graph, illustrated in Figure C.57 with Table C.2 as reference, the total net power delivered to the electric grid and the average net power block efficiency is presented for comparison. In this case, the operating strategies that focus on maximising the power output of the plant are assumed to be amongst the best performers. Analysing the total net power output of the power block, the operating strategies 3, 7 and 12-13 deliver the highest amount of power to the grid. These operating strategies are namely ‘Optimised Maximum Power Generation’, ‘Maximise Plant Revenue with Flat Rate tariff structure’, ‘Base load operations’ and ‘Peaking operations’. The results obtained are in concurrence to the objectives of these operating strategies. The objectives are to maximise or optimise the electric power generated by the plant. The ‘Peaking’ operating strategy coincide with the turbine output of 120 MW_e during the specified peak period, while maintaining a maximise power generation undertone. The ‘base load operations’ operating strategy is aimed to provide continuous power while maintaining the maximise power generation undertone.

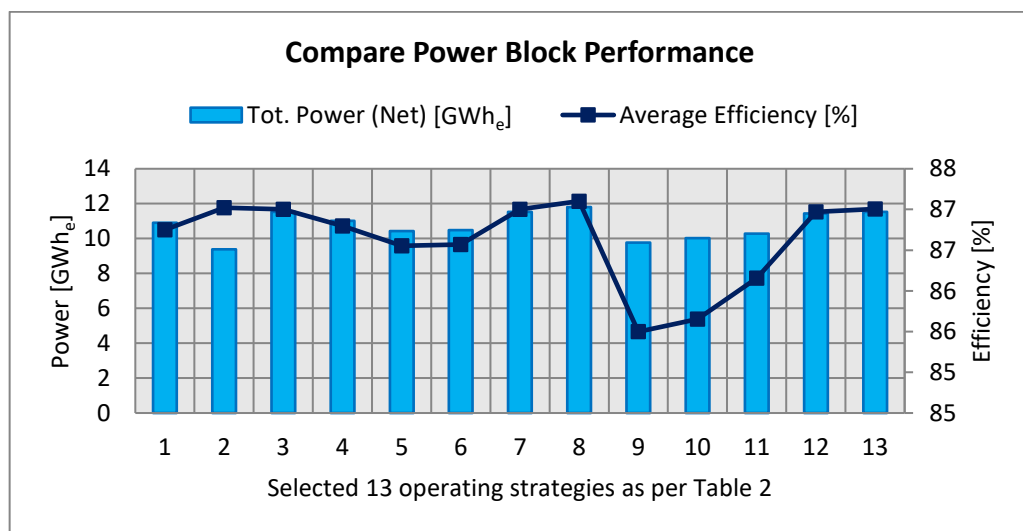


Figure C.57: Comparison of the simulation results, power block performance

The ‘Complimentary services to Wind and/or PV generation’ had poor performance, in terms of the average net efficiency for the power block. The optimisation strategy was not implemented for the power block as the plant or ‘Solar Park’ complimented the load profile of the corresponding generating technology that is the wind and/or PV for continuous power supply to the grid. Furthermore, the efficiency of the power block was most affected when its output fluctuated to sustain security of supply. This phenomenon is expected as the plant is not operating within its design point or nominal conditions, where the optimum efficiency for the power block is realised.

C.4.4. Compare Plant Performance

The plant performance best describes how well the plant converted the ‘solar energy’ bestowed onto the heliostat field into the ‘net electric power’ generated. This is represented in Figure C.58. The overall plant performance takes into account all aspects of the plant’s operations, although, the plant may have performed well in one of the sub-systems: the receiver or the power block. This is particularly the case for operating strategy 2 where the higher average receiver and power block net efficiencies were recorded.

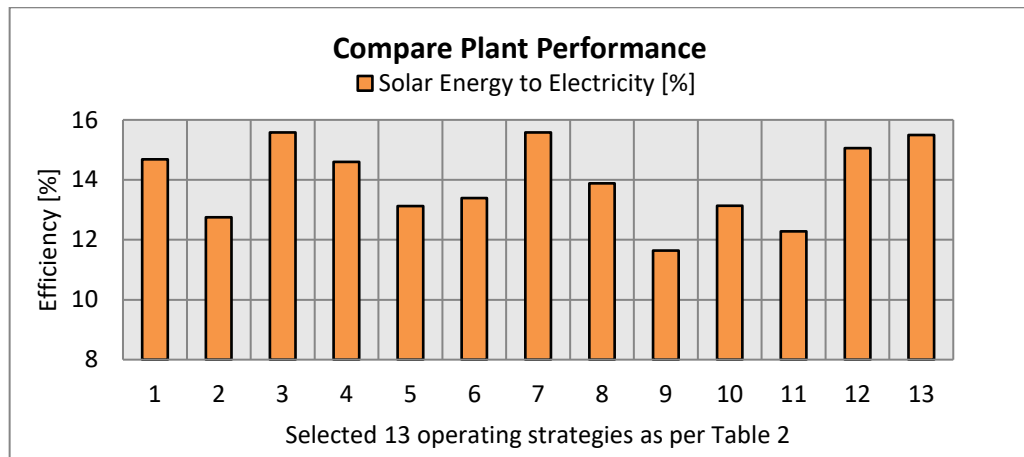


Figure C.58: Comparison of the simulation results, overall plant performance

It is anticipated that the ‘Maximise Power Generation’ operating strategy would result in the highest plant efficiency. Figure C.58 confirmed this assumption by analysing the comparative results of operating strategies 3 and 7. The ‘Base load’ and ‘Peaking’ operating strategies also performed well in this regard. Both these operating strategies prioritise the turbine output to meet the objectives of the operating strategy while maintaining a maximise power generation undertone. The ‘Peaking’ operating strategy increased the turbine output to 120 % during the specified peak period, therefore, utilising the TES effectively. The plant efficiency was reduced when the operating strategies lead to curtailment of the receiver’s output as a result of the state of charge of hot TES. The efficiency of the plant is directly affected by energy dumping. This was noticed for operating strategies 5 and 6, where the TES size was reduced to 8 hours. Similarly, complimenting wind and PV generation leads to lower plant efficiency as the plant operates to accommodate the shortcomings of these generating technologies, i.e. on demand dispatchability potential. If the operating strategy 8 (‘Minimise Energy Dumping’) coincides with the ‘Maximise Power Generation’ operating strategy, the plant would result in the highest plant efficiency. Subsequently, all the available solar energy is utilised to maximise the electric power generated from the plant.

C.4.5. Compare Financial Indicators

The last comparative overview for the various simulations is the financial indicators of the performing plant. It is important to note that various operating strategies showcase different objectives for the plant and system operators. In the case of an IPP with a time-of-day tariff

PPA in place, the plant operator would operate the plant to maximise the revenue during these times. As for the other operating strategies like the complimentary services to the grid, the system operator obtains value from the plant's contribution to the grid. Throughout the simulations, the auxiliary purchase price of 0.7624 R/kWh and the flat rate tariff for selling power to the grid at 3.32 R/kWh were kept constant. Although, the time-of-day tariff structure was simulated with PPA's tariffs from Bid Window 3.5, this PPA was not intended for the reference plant. These simulations provided the user with the plant's information regarding its performance, revenue and operations under these boundary conditions.

Nonetheless, the 'Maximise Plant Revenue' operating strategy should yield the highest plant revenue. The plant revenue for all the operating strategies are shown in Figure C.59, where operating strategies 3, 7 and 12-13 yielded the highest plant revenues. 'Maximise Power Generation', 'Maximise Plant Revenue with flat rate tariff structure', 'Base load', and 'Peaking' operating strategies were considered. The 'Maximise Plant Revenue' operating strategy has been discussed in earlier sections when it coincided with the flat rate tariff structure. The 'Time-of-day tariff' operating strategy did not perform well in terms of revenue generated for the plant. Although, the plant generated power at full load while paying tiers. This is mainly because of the large TES size that other operating strategies utilised more effectively, generating more power.

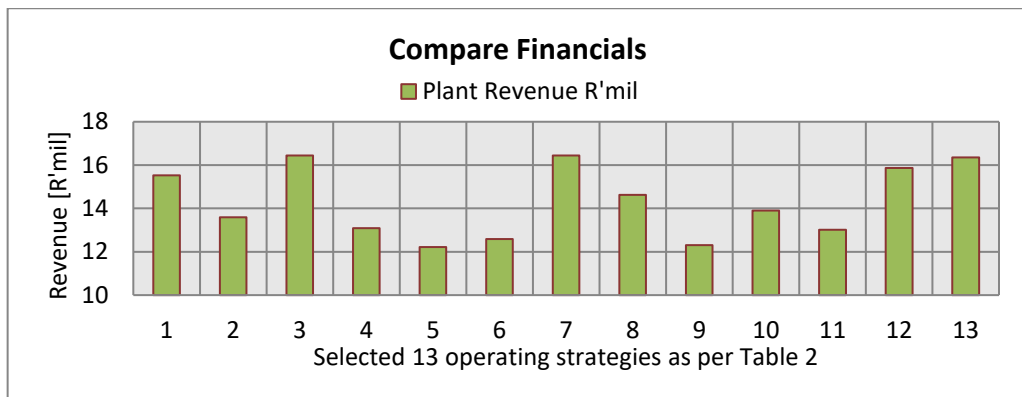


Figure C.59: Comparison of the simulation results, plant revenue generated

C.4.6. Conclusion

This Section evaluated the simulation model results in a holistic manner in order to inform the user about various plant performances and financial indicators. Here, the indicators were directly affected by the operating strategy imposed on the plant. It was observed that the 'Maximise Power Generation' operating strategy performed the best across all the platforms. Comparatively, the 'Complimentary services to wind and PV generation' strategy did not perform well. This does not indicate that the latter operating strategy should be completely discarded. On the contrary, further investigation is required to determine the precise values that the system operator obtains from these operating strategies. Scientifically, the results shown in this section are tangible and are related to quantitative measures. The discussion regarding the value of particular operating strategies is determined by the subjective view of the relevant stakeholder.

C.5. OPERATING STRATEGIES DURING A HIGH DNI PERIOD

C.5.1. Introduction

The aim of this section is to illustrate the performance of various operating strategies during a period with high DNI bestowed upon the heliostat field. The simulation period, which commences on 1st January and continues for three consecutive days, inputs data of high DNI and relatively high ambient temperatures into the model (see Figure C.60 and Figure C.61). The total solar energy recorded on the heliostat field for this period was 50.9 GWh_t. The high DNI onto the heliostat field is the reason for higher deflected energy from the receiver. This is due to the interception of a higher flux density on the receiver's surface. An increase in receiver's curtailment is expected due to the higher thermal output from the receiver to the hot TES. This results in faster charging of the TES to attain a fully charged state.

Weather & Heliostat Field Report	
1/1 0:00 -1/4 0:00	
Average Ambient Temperature	26,6 °C
Average Direct Normal Irradiance	921 W/m ²
Total Solar Energy in Heliostat Field	50,9 GWh _t

Figure C.60: Ambient conditions and heliostat performance for high DNI period

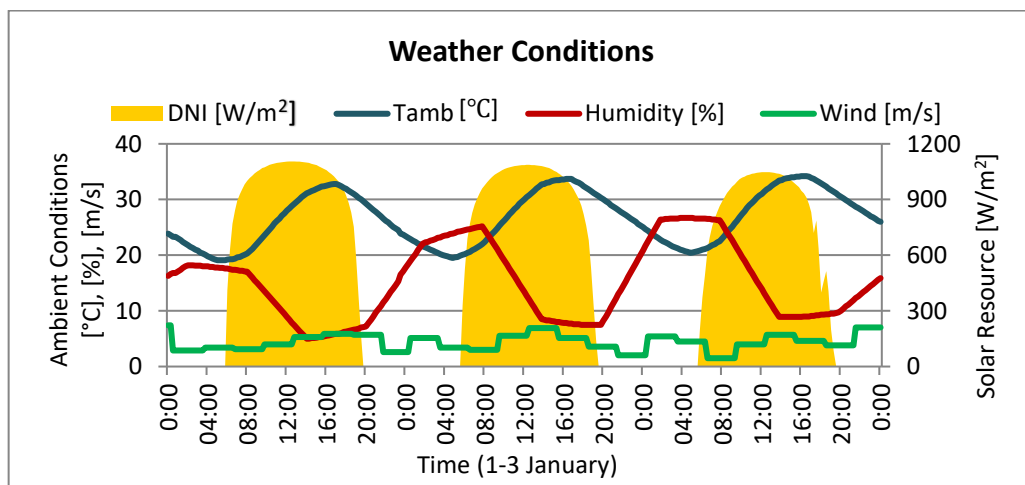


Figure C.61: Weather conditions applicable for the high DNI period

The input to various operating strategies simulated for this period is similar to Section 3. However, not all of the operating strategies and combinations of user inputs have been demonstrated in this section. The operating strategies demonstrating the plant operations optimisation under different ambient conditions, particularly high DNI, are worth mentioning. The list of operating strategies mentioned in the Table C.3 are simulated. A brief overview for each operating strategy is discussed in the following sections.

Table C.3: List of operating strategies simulated with specified user inputs

No	Operating Strategy	Section	User Inputs
1	Max. Power Generation (User)	Section C.3.1	Power block start time at 05h00
2	Max. Power Generation (User)	Section C.3.2	Power block start at hot TES 30 % charged
3	Max. Power Generation (Optimised)	Section C.3.3	Optimised Power Generation selected
4	Max. Plant Revenue, Time-of-day tariff	Section C.3.4.1	TES size 12 hours
5	Reduce Turbine Start/Stop	Section C.3.4.6	TES size 12 hours
8	Min. Energy Dumping	Section C.3.4.6	No additional inputs required
9	Complimentary services to Wind	Section C.3.4.7	No additional inputs required
10	Complimentary services to PV	Section C.3.5	No additional inputs required
11	Complimentary services to Wind/PV	Section C.3.6.1	No additional inputs required
12	Demonstrate Base Load Capabilities	Section C.3.6.2	No additional inputs required
13	Demonstrate Peaking Capabilities	Section C.3.6.3	Peak Time 18h00-20h00 with Turbine Output set at 120 MW _e

C.5.2. Maximise Power Generation, Turbine Start-Up at 05h00

The results from this operating strategy highlight the effects of the hot TES reaching a full state of charge during the receiver's operation. This is illustrated in Figure C.62. The receiver's output is curtailed when the power block and the receiver are in operation at the same time. In this case, the user specified turbine start-up time was at 05h00. Subsequently, the receiver efficiency is affected due to operating conditions in a lower gross power region.

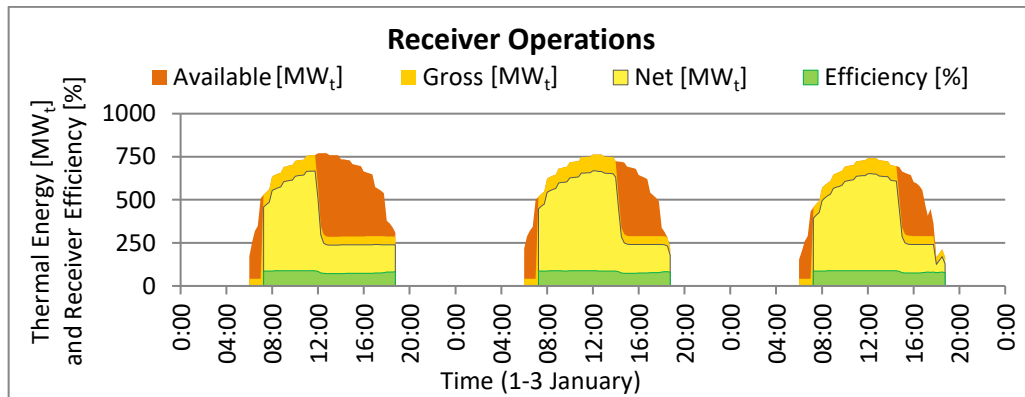


Figure C.62: Receiver output curtailed due to hot TES state of charge

C.5.3. Maximise Power Generation, Turbine Start-Up at Hot TES at 30 %

Similar results to a turbine start-up time of 05h00 are obtained in the receiver operations. However, with the user specified turbine start-up for the hot TES at 30 % charged, the hot TES depleted before the receiver could commence its normal operations. This resulted in turbine shutdown and subsequent receiver's shutdown when the hot TES reached full state of charge. The results shown in Figure C.63 corresponds to the first day of operation.

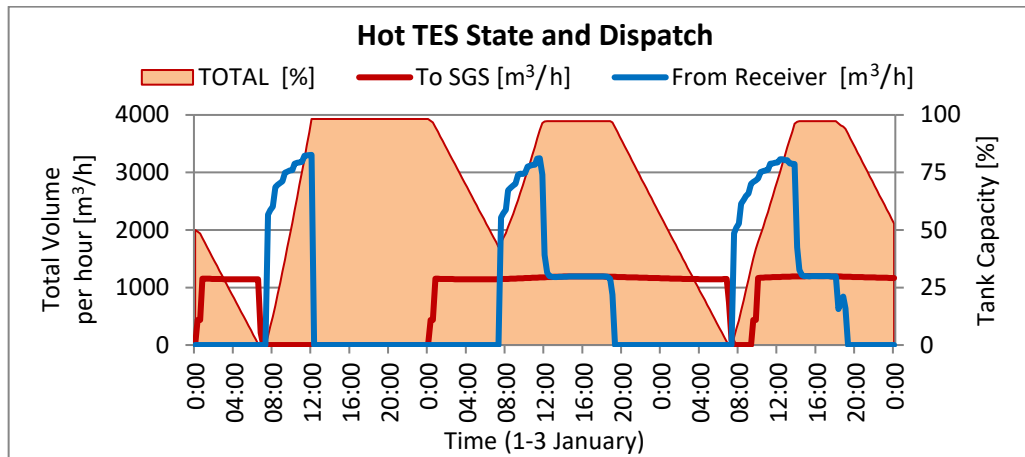


Figure C.63: Receiver operation shut down due to full hot TES

C.5.4. Optimised Maximise Power Generation

The ‘Maximise Power Generation’ operating strategy primarily optimises the power block operations. One of the significant contributions from this operating strategy is that the energy lost during the power block’s start up is minimised. The turbine output is reduced to ensure that sufficient capacity in the hot TES is available until the receiver commences its normal operations. This is illustrated in Figure C.64.

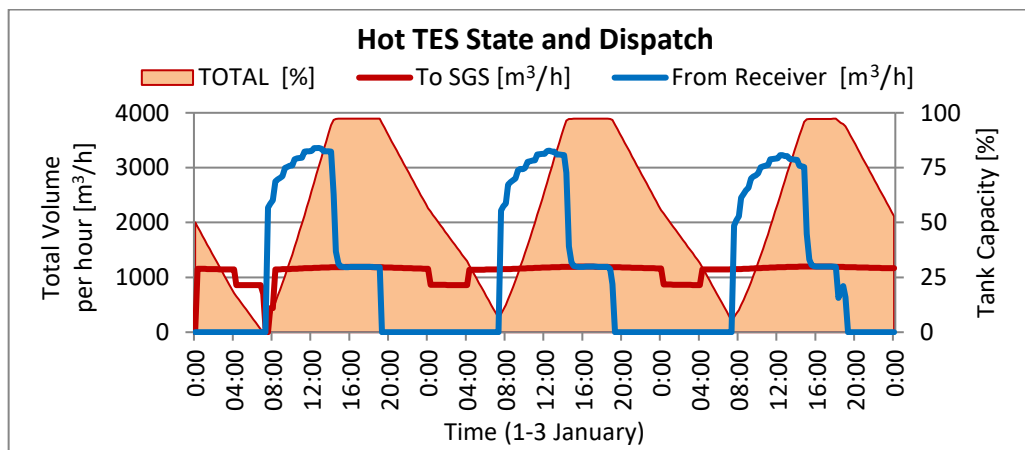


Figure C.64: Hot TES dispatch, reducing turbine start/stop for energy conservation

Although, the hot TES dispatch was optimised and the receiver’s normal operations effectively started with the available capacity of the hot TES, the receiver’s output was curtailed towards the end of the day (see Figure C.65). This potential energy loss due to the plant’s design limitations can be avoided by increasing the turbine output during receiver operations or by increasing the TES size. Essentially discharging the hot TES at faster rates, ensures that more TES capacity is available for the receiver to charge. This is a potential operational optimisation strategy that needs to be considered. This further make the ‘Maximise Power Generation’ operating strategy’s objectives stronger.

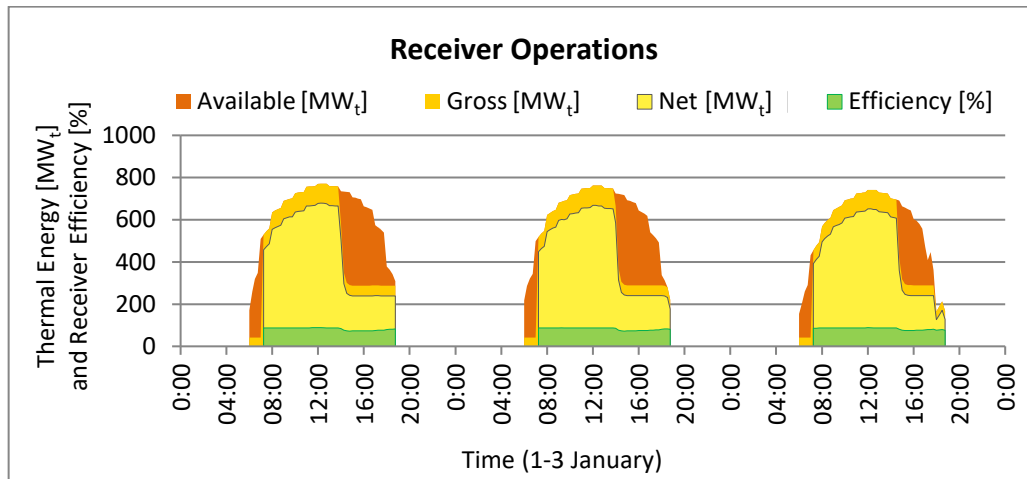


Figure C.65: Receiver output curtailed due to hot TES state of charge

C.5.5. Maximise Plant Revenue

The plant maximises its revenue for the specified period under the PPA boundary conditions, see Figure C.66. However, as the capacity within the hot TES remained primarily above 50 % charged, an increase in energy dumping is observed at the receiver. The plant efficiency is directly affected by the increase in energy dumping, or receiver’s curtailment.

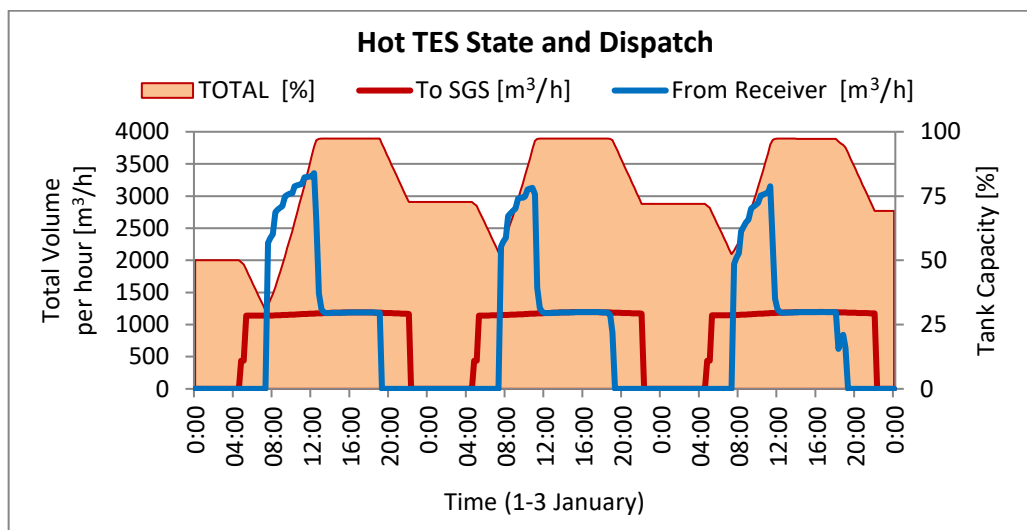


Figure C.66: Time-of-day tariff boundary conditions on turbine output

C.5.6. Maximise Plant Revenue with Reduced Turbine Start/Stop

Since, no start or stops in the turbine operations were present, the ‘Maximise Plant Revenue with reduced Turbine Start/Stop’ did not have any effect on the plant operations.

C.5.7. Minimise Energy Dumping

When the primary aim of an operating strategy is energy conservation, the ‘Minimise Energy Dumping’ operating strategy is considered to be one of the most important ones. Particularly for high DNI periods, the plant may encounter design limitations during operations. These design limitations include maximum allowable flux on the receiver’s surface or the size of TES. This section discusses two examples, namely, the receiver’s design and turbine rated power. In both the cases, the size of the TES plays an important role in their capabilities. Due to the flux limitations for the receiver’s material, an increase in the deflected solar energy is observed when high DNI is bestowed upon the heliostat field (see Figure C.67). This occurrence resulted due to the implemented heliostat field aiming strategy yielding higher concentrations of solar energy on the receiver’s surface. Subsequently, the receiver thermal output is increased owing to the fact that the receiver operates under higher gross power conditions. Therefore, the hot TES full state of charge is reached faster.

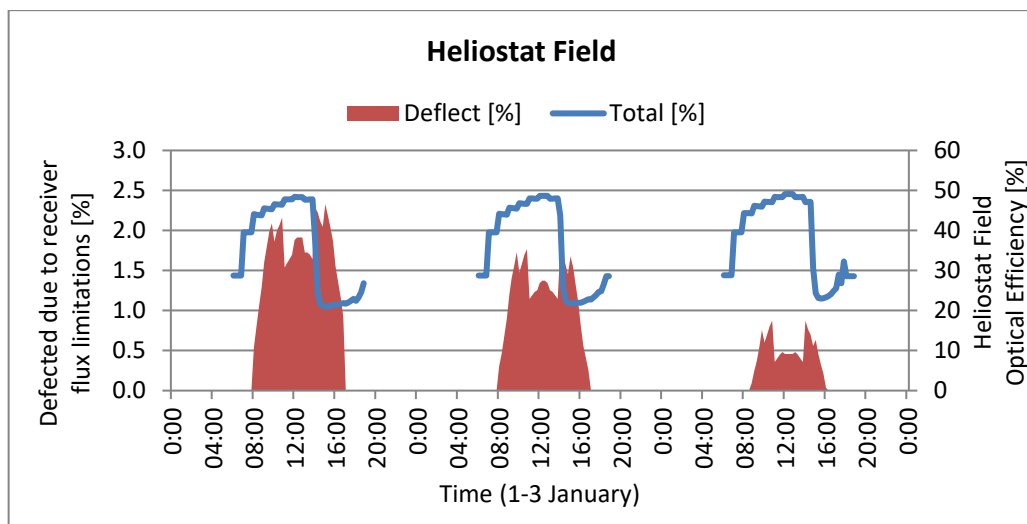


Figure C.67: Field operations before optimised in Minimise Energy Dumping

The power block utilises the energy from the hot TES to ensure that sufficient TES capacity is available for the receiver operations. As illustrated from the results presented in Figure C.68, the receiver started its normal operations with a fully depleted hot TES. However, the power block continued operating with the full load utilising the energy from the hot TES. Although, the turbine operated at its rated power and at 110 % nominal output, the receiver charge to the hot TES was greater than the discharge to the power block. At the end of the day, the receiver had to curtail its operations.

The power block operations are considered in Figure C.69 where at times, the turbine output increased to 110 % of its nominal output. It is thus concluded that the energy lost due to deflecting heliostats, are not attainable through optimising the plant operations, i.e. optimising the power block operations.

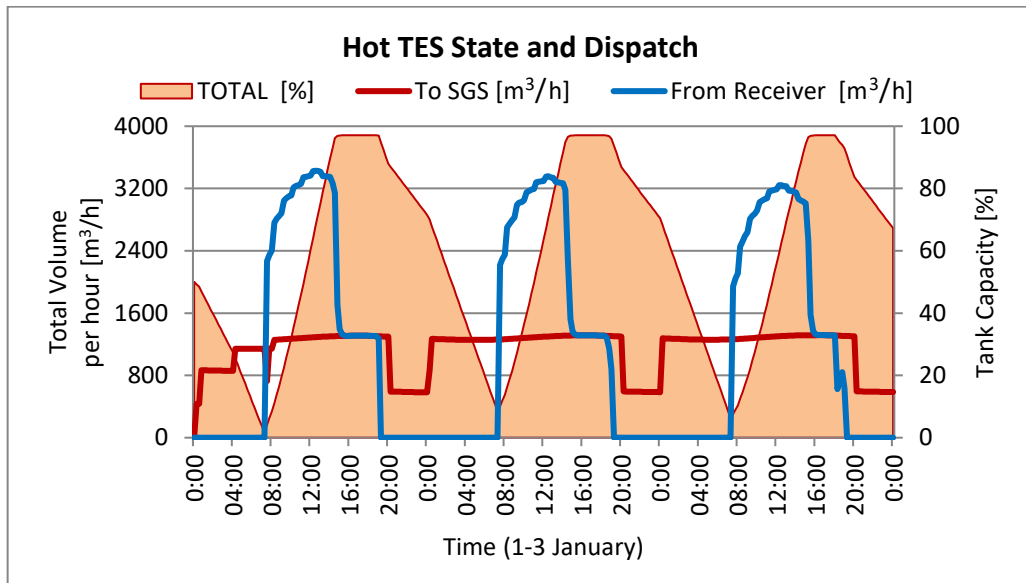


Figure C.68: Hot TES discharge and charge profile

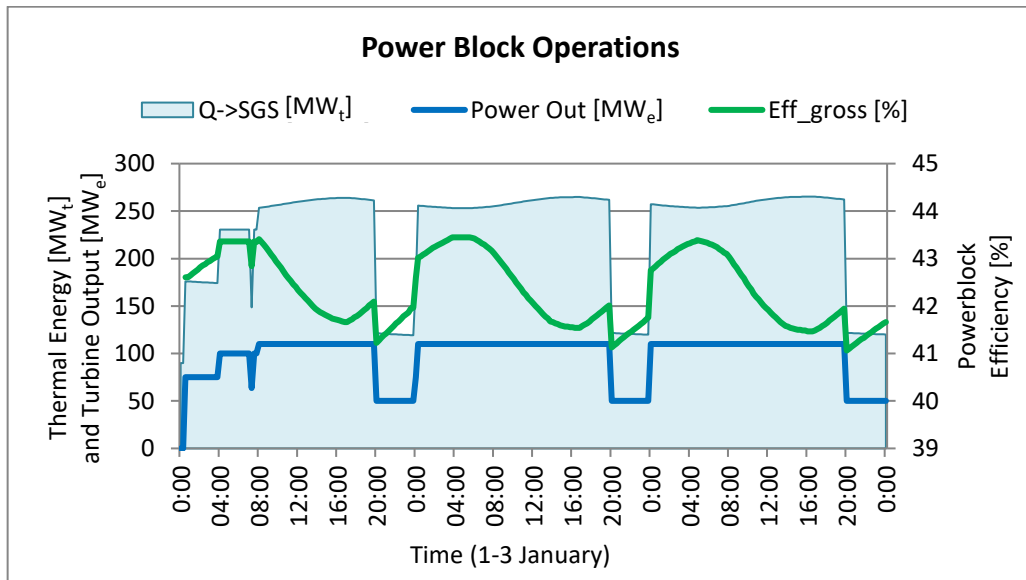


Figure C.69: Turbine output increased to 110 % nominal output

C.5.8. Optimise Electric Grid - Compliment Wind

Due to the high DNI bestowed upon the heliostat field during this period, the TES was generally in a fully charged state. Less thermal energy was required during the part load operations of the power block, therefore the receiver to lower its charge rate of the hot TES. This is clearly visible in the charge and discharge profile of the hot TES shown in Figure C.70. The accompanying receiver curtailment is noted in Figure C.71. The high DNI period favoured the complimentary services to wind generation as the relatively full hot TES could provide continuous power output to the system, as seen in Figure C.72.

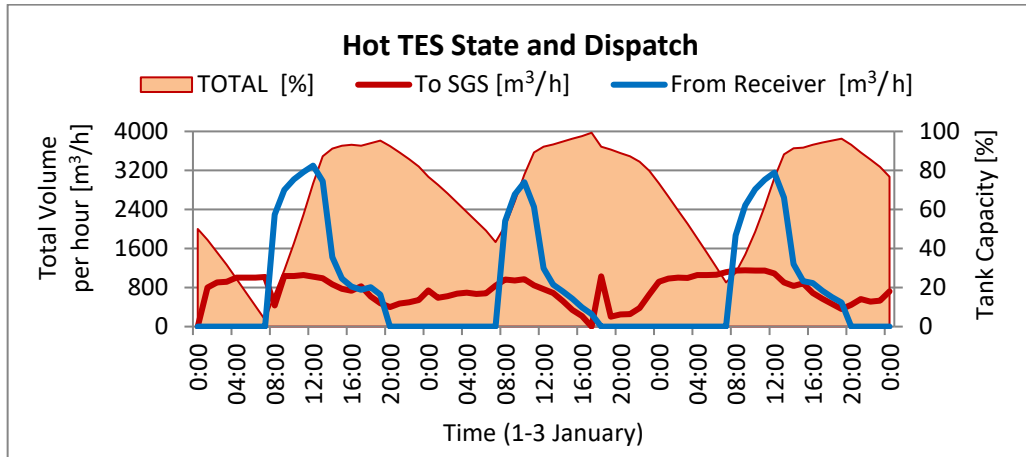


Figure C.70: Hot TES discharge and charge profile

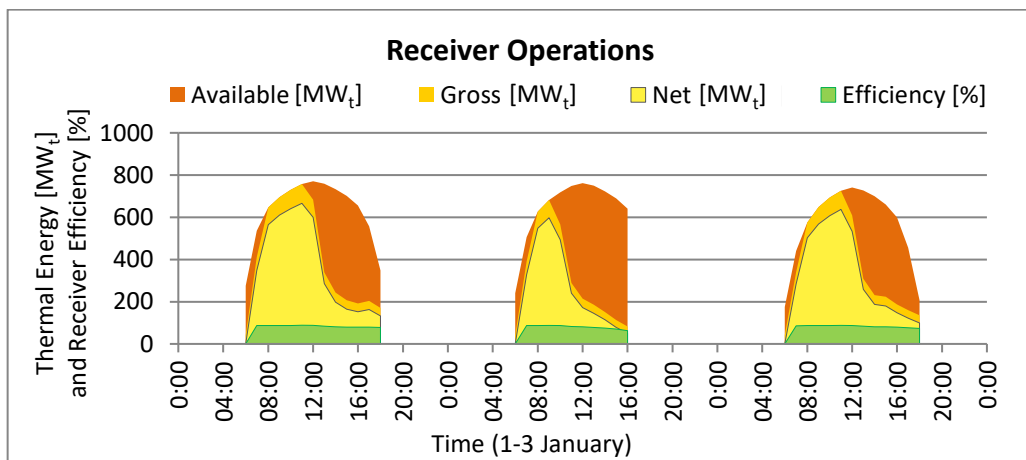


Figure C.71: Receiver output curtailed due to hot TES state of charge

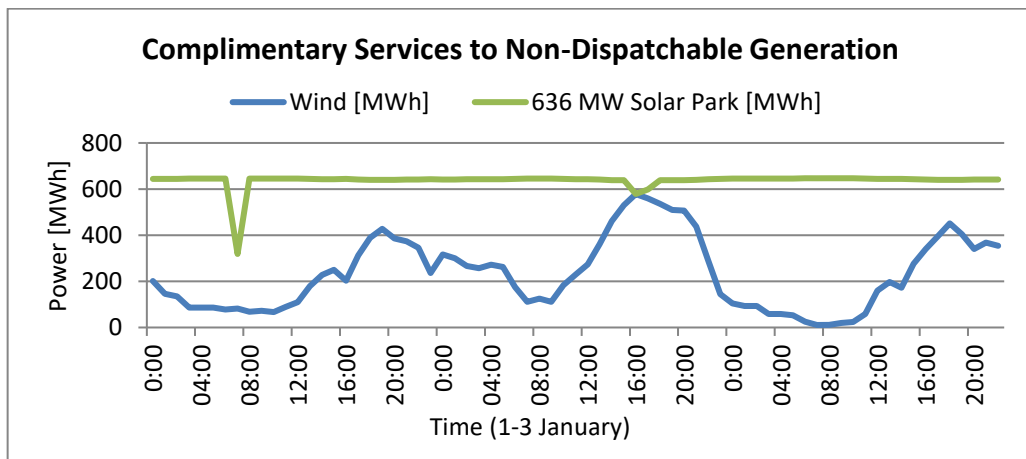


Figure C.72: CSP complimentary services to wind generation, stacked line

C.5.9. Optimise Electric Grid - Compliment PV

During the high DNI periods, the complimentary services to PV generation are accomplished. But for wind generation, the receiver is curtailed due to the part load operations of the power block (see Figure C.73). During the day, the system was supported by the PV plants. They relied lesser on the CSP plants. However, in the evenings when no contribution was made from the PV plants, power was provided from the CSP plant's TES operating at full load, see Figure C.74.

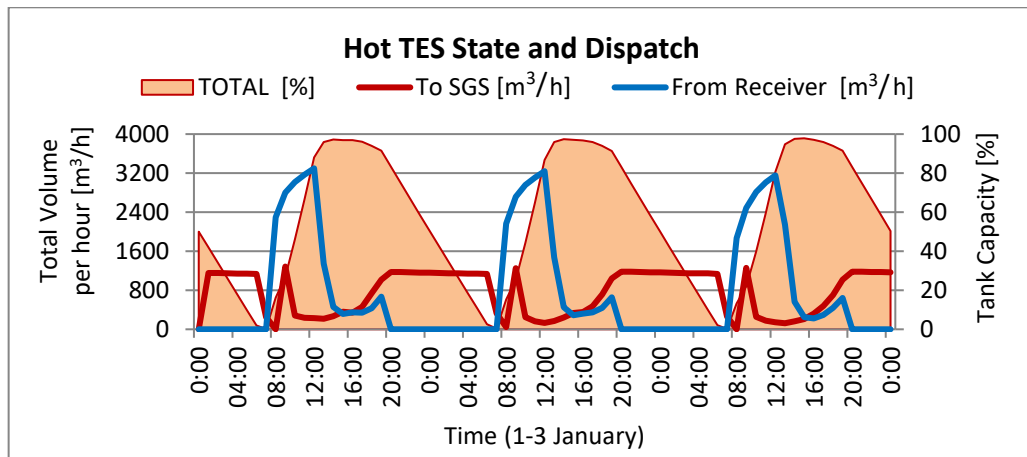


Figure C.73: Hot TES discharge and charge profile

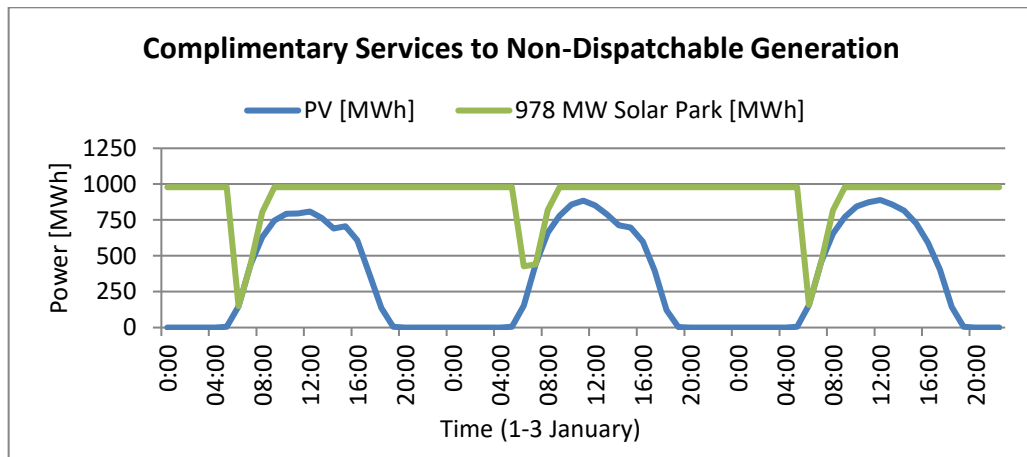


Figure C.74: CSP complimentary services to PV generation, stacked line

C.5.10. Optimise Electric Grid - Compliment Wind and PV

The CSP complimentary services of PV and wind generation provided a continuous output from the power block. The contribution of wind generation on this operating strategy lowers the demand on the CSP plant, thus it operates under part load conditions. As the load on the CSP plant is reduced, continuous power is delivered to the electric grid. This is illustrated in Figure C.75.

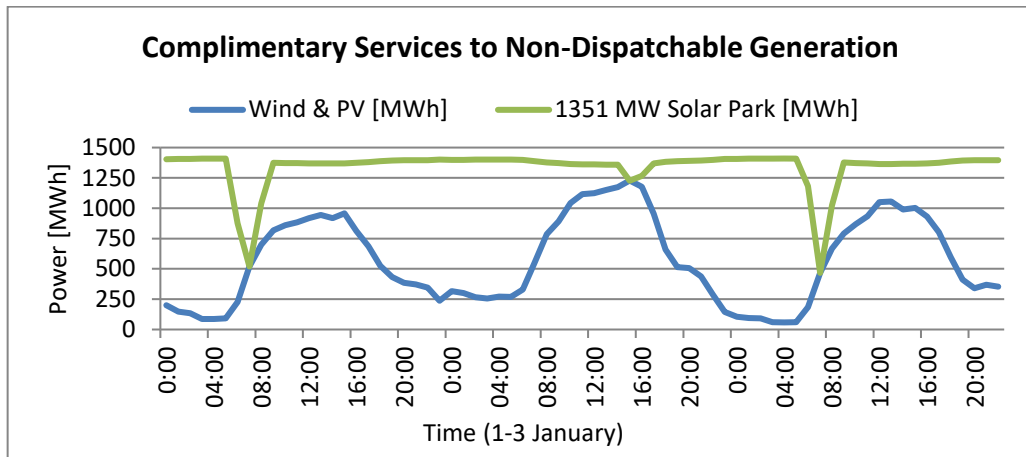


Figure C.75: CSP complimentary services to wind and PV generation, stacked line

C.5.11. Demonstrating CSP Base Load Capabilities

The base load capabilities for the plant have been demonstrated in Section C.5.4 and Section C.5.7. The excessive energy is collected from the solar collecting system when the DNI is high. This energy is used by the hot TES to maintain the base load operations. With the hot TES sufficiently charged, the power block could maintain a higher turbine output. This is illustrated in Figure C.76.

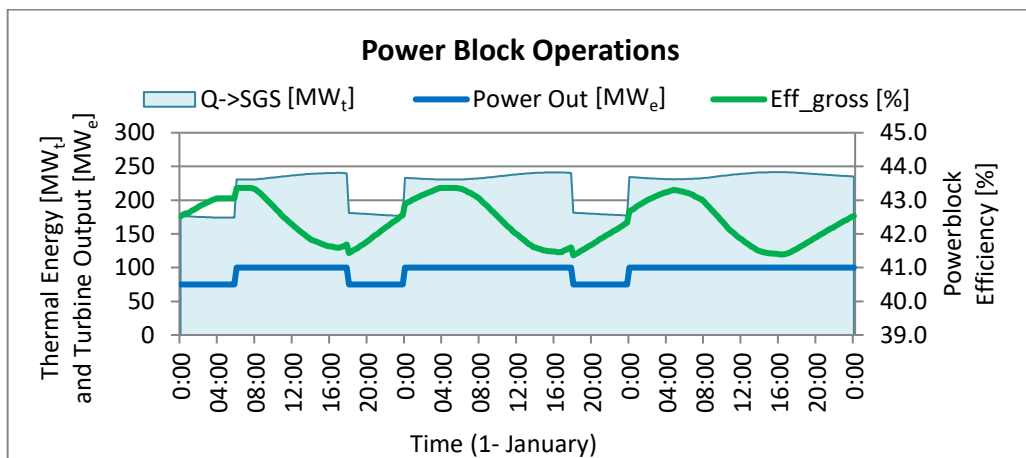


Figure C.76: Base load operations while maintaining a higher turbine output

C.5.12. Demonstrating CSP Peaking Capabilities

With sufficient energy collected from the solar collecting system, the plant is able to provide electric power to the grid during the specified peaking period. Therefore, 120 MW_e is delivered during the specified peaking period of 18h00-20h00.

C.5.13. Compare Operating Strategies for High DNI period

The 11 operating strategies, denoted in Table C.3 and recalled below, were compared based on their system performance and financial indicators. The graphs represented in this section was produced with the functionality in the ‘Compare SimResults’ sheet.

Table C.3: List of operating strategies simulated with specified user inputs

No	Operating Strategy	Section	User Inputs
1	Max. Power Generation (User)	Section C.3.1	Power block start time at 05h00
2	Max. Power Generation (User)	Section C.3.2	Power block start at hot TES 30 % charged
3	Max. Power Generation (Optimised)	Section C.3.3	Optimised Power Generation selected
4	Max. Plant Revenue, Time-of-day tariff	Section C.3.4.1	TES size 12 hours
5	Reduce Turbine Start/Stop	Section C.3.4.6	TES size 12 hours
8	Min. Energy Dumping	Section C.3.4.6	No additional inputs required
9	Complimentary services to Wind	Section C.3.4.7	No additional inputs required
10	Complimentary services to PV	Section C.3.5	No additional inputs required
11	Complimentary services to Wind/PV	Section C.3.6.1	No additional inputs required
12	Demonstrate Base Load Capabilities	Section C.3.6.2	No additional inputs required
13	Demonstrate Peaking Capabilities	Section C.3.6.3	Peak Time 18h00-20h00 with Turbine Output set at 120 MW _e

C.5.13.1. Compare Receiver Performance

The receiver’s performance is illustrated in Figure C.77. In this case, the operating strategy 6 the ‘Minimise Energy Dumping’, delivered the maximum amount of thermal power to the hot TES. The operating strategies 3, 10-11 namely the ‘Maximise Power Generation’, ‘Base Load’ and ‘Peaking’ operating strategies, also delivered high thermal outputs by the receiver. The reason stems primarily from these operating strategies following the ‘Maximise Power Generation’ undertone with optimisation realised in the power block pertaining to each operating strategy. Minimum power was delivered by the operating strategies 4 and 7-9, when the receiver was shut down or curtailed due to the hot TES state of charge.

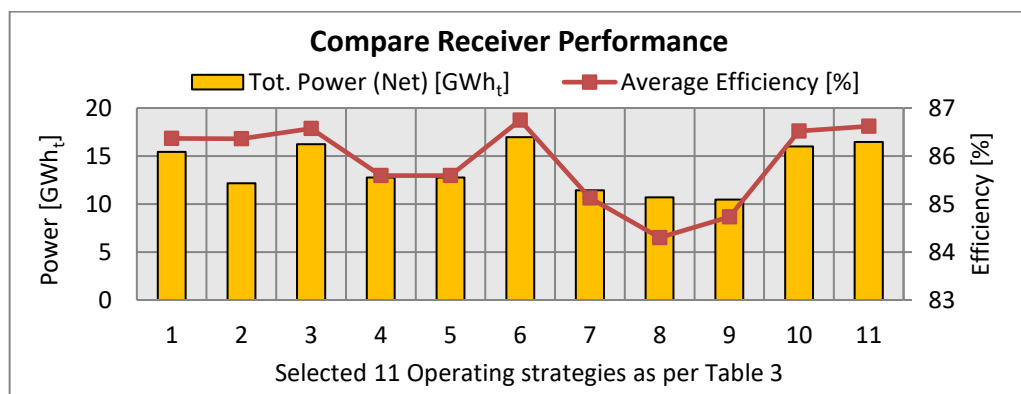


Figure C.77: Comparison of the simulation results, receiver performance

While considering the receiver’s efficiency, the best performance was shown by the operating strategies where the receiver was curtailed for the least amount of times. This is the case for operating strategies 3, 6 and 10-11. These outcomes are expected due to the optimisation in dispatch of the hot TES to the power block.

C.5.13.2. Compare Power Block Performance

The excessive energy, which is bestowed onto the heliostat field during high DNI periods, is collected by the solar collecting systems. This ensures that there is always sufficient energy in the hot TES for the power block. When Figure C.78 is considered, it assumed that under these conditions, all the operating strategies should have high total net power outputs. This is indeed the case for the operating strategies 1-3, 6 and 10-11. Since the operating strategies 4-5 relates to the time-of-day tariff structure, no power was generated during non-payment periods. When operating strategies 7-9 are considered, ‘Complimentary services to wind and PV generation’ a combination of receiver curtailment and part load operating conditions imposed on the power block results in low values for the total net power out from the power block.

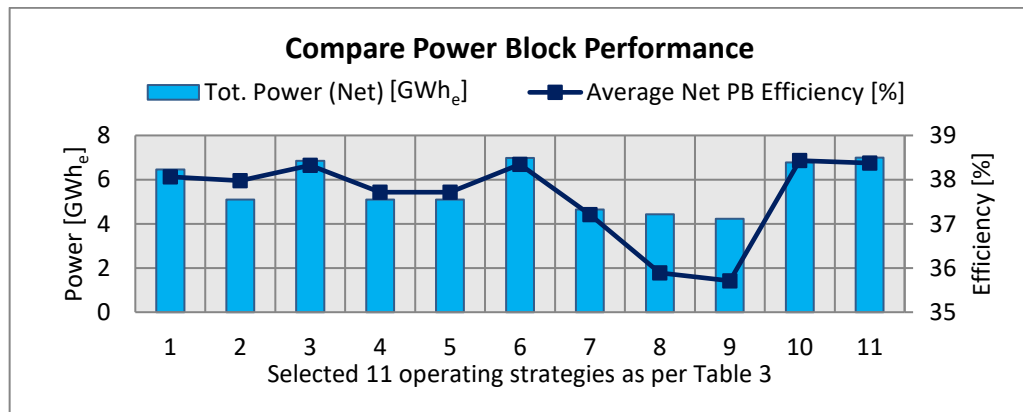


Figure C.78: Comparison of the simulation results, power block performance

The power block efficiency is consistent for all the operating strategies, except the ‘Complimentary services to wind and PV generation’ strategy. Lower power block efficiencies are recorded as the power block is operated under part load operating conditions to supplement these generating technologies. The frequency of the turbine start-ups further decreases the efficiency of the power block due to the energy required during the turbine start-ups.

C.5.13.3. Compare Plant Performance

The plant performance graph gives a good indication about the efficiency of the plant operations to convert the available solar energy to the electric power. Since the period selected had high DNI conditions along with the operating strategies applied to optimise the receiver’s thermal outputs, while maintaining maximum power generation from the power block, should result in high plant efficiencies. The operating strategy 6 ‘Minimise Energy

Dumping’, resulted in the highest plant efficiency followed by operating strategies 3 and 11, as seen from Figure C.79. The ‘Minimise Energy Dumping’ operating strategy had a slightly higher efficiency due to the heliostat field’s redistribution of thermal flux on the receiver to attain deflected solar energy. Operating strategies optimising and maximising power generation fared well whereas ‘Complimentary services to wind and PV generation’ were among the lowest.

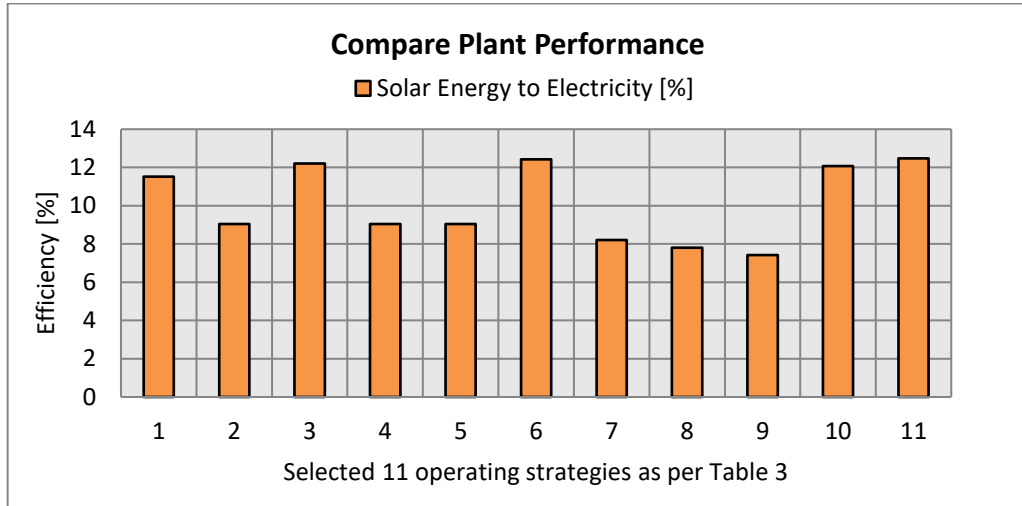


Figure C.79: Comparison of the simulation results, plant performance

C.5.13.4. Compare Financial Indicators

The financial indicators presented in the Figure C.80 indicate that operating strategies delivering high plant revenue coincide with the operating strategies delivering the highest net power to the system. These results are in accordance with the Figure C.77, where the operating strategies 3, 6 and 10-11 generated the highest income for the plant. The ‘Complimentary services to wind and PV generation’ is expected to be the least preferred operating strategies for generating plant revenue. Furthermore, the time-of-day tariff structure did not fare well due to the non-payment period in the PPA.

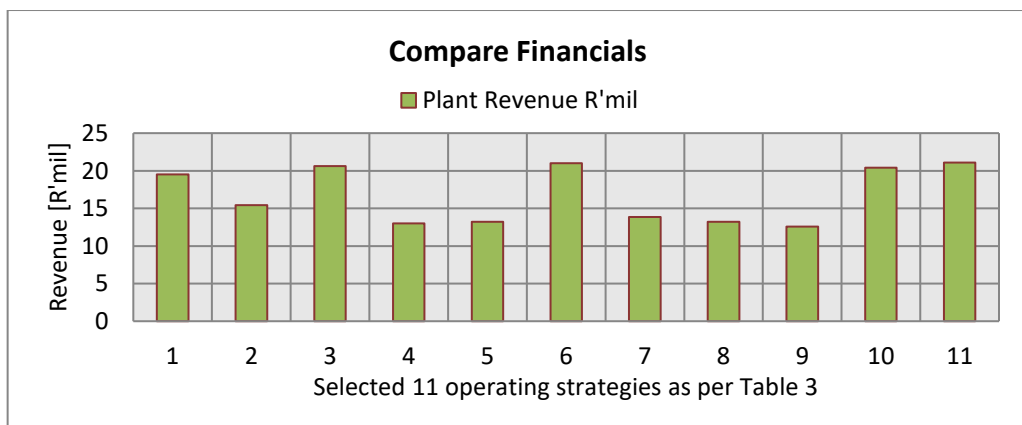


Figure C.80: Comparison of the simulation results, plant revenue generated

C.6. OPERATING STRATEGIES DURING A LOW DNI PERIOD

C.6.1. Introduction

The aim of this section is to illustrate the performance of various operating strategies during a period with low DNI conditions. The simulation period, which commences on 20th June and runs for three consecutive days, inputs data for low DNI and relatively low ambient temperatures into the model, see Figure C.60 and Figure C.61. The total solar energy on the heliostat field for this period was recorded to be 19.9 GWh. Since the thermal energy in the hot TES is insufficient, a large number of turbine starts/stops are expected.

Weather & Heliostat Field Report 6/20 0:00 - 6/23 0:00	
Average Ambient Temperature	10,7 °C
Average Direct Normal Irradiance	587 W/m ²
Total Solar Energy in Heliostat Field	19,9 GWh

Figure C.81: Ambient conditions and heliostat performance for low DNI period

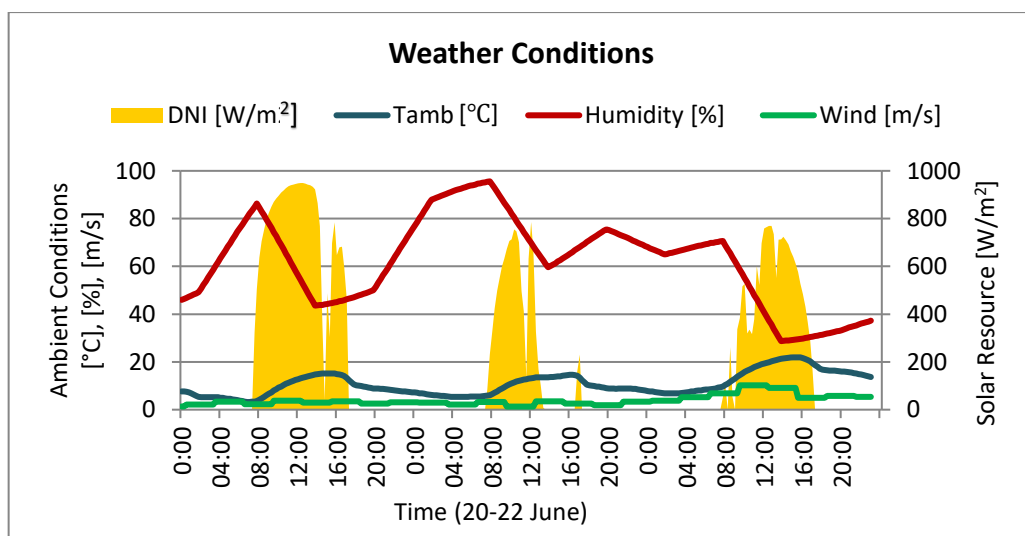


Figure C.82: Weather conditions applicable for the low DNI period

The input to various operating strategies simulated for this period is similar to Section C.3. However, not all of the operating strategies and combinations of user inputs have been demonstrated in this section. The operating strategies, that showed plant operations optimisation under different ambient conditions, particularly low DNI, are worth mentioning. The list of the simulated operating strategies is presented in Table C.3. A brief overview for each operating strategy is discussed in the following sections.

Table C.3: List of operating strategies simulated with specified user inputs

No	Operating Strategy	Section	User Inputs
1	Max. Power Generation (User)	Section C.3.1	Power block start time at 05h00
2	Max. Power Generation (User)	Section C.3.2	Power block start at hot TES 30 % charged
3	Max. Power Generation (Optimised)	Section C.3.3	Optimised Power Generation selected
4	Max. Plant Revenue, Time-of-day tariff	Section C.3.4.1	TES size 12 hours
5	Reduce Turbine Start/Stop	Section C.3.4.6	TES size 12 hours
8	Min. Energy Dumping	Section C.3.4.6	No additional inputs required
9	Complimentary services to Wind	Section C.3.4.7	No additional inputs required
10	Complimentary services to PV	Section C.3.5	No additional inputs required
11	Complimentary services to Wind/PV	Section C.3.6.1	No additional inputs required
12	Demonstrate Base Load Capabilities	Section C.3.6.2	No additional inputs required
13	Demonstrate Peaking Capabilities	Section C.3.6.3	Peak Time 18h00-20h00 with Turbine Output set at 120 MW _e

C.6.2. Maximise Power Generation, 05h00 Turbine Start-Up

The results from this operating strategy illustrates that during the low DNI periods when the turbine start-up is commenced at 05h00, operating at full load, the hot TES has sufficient capacity for normal receiver operations. The receiver output was not curtailed during this period as illustrated in Figure C.83. As the hot TES depleted each day, the turbine start-up is initiated when thermal energy is supplied to the hot TES by the receiver. This is observed in Figure C.84. Although, the turbine start-up was later, the receiver output was not curtailed for the period.

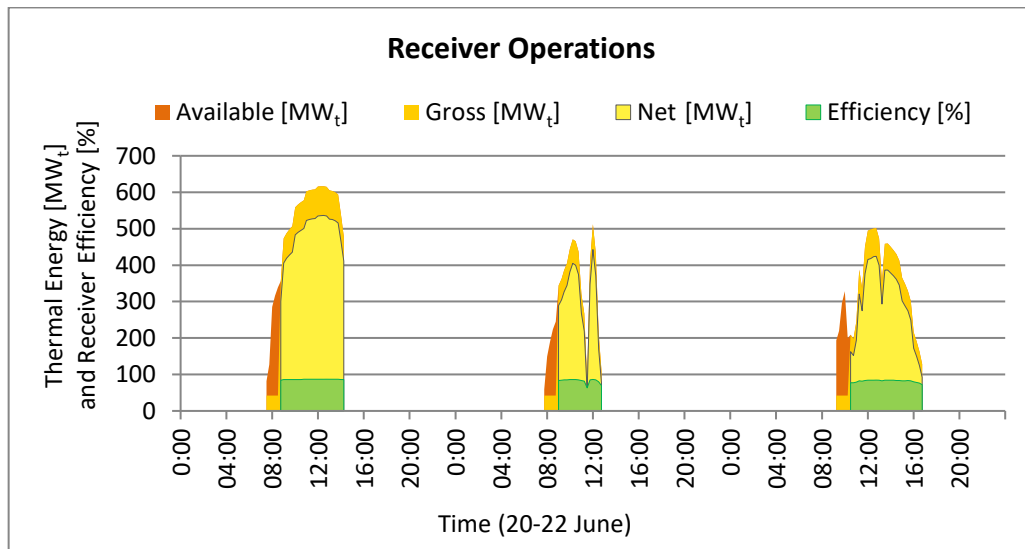


Figure C.83: Receiver output not curtailed in low DNI period

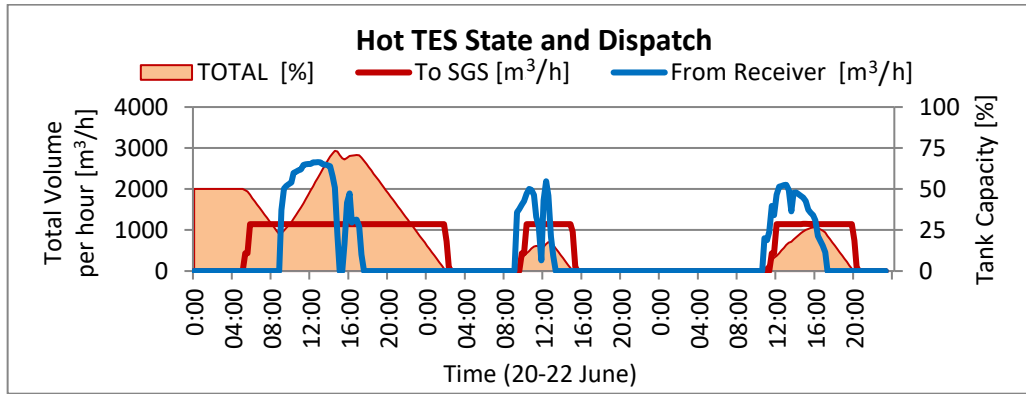


Figure C.84: Receiver output not curtailed, sufficient capacity in hot TES

C.6.3. Maximise Power Generation, Turbine Start-Up at Hot TES at 30 %

Unlike the case for a turbine start-up at 05h00, the hot TES is fully depleted before the receiver normal operations could commence. On comparing Figure C.85 to the graph obtained in Section C.5.3, Figure C.63, it is observed that the receiver start-up commenced later. This phenomenon is due to the late sun rise times during winter. Nonetheless, the receiver is shut down due to a full state of charge in the hot TES as illustrated in Figure C.86.

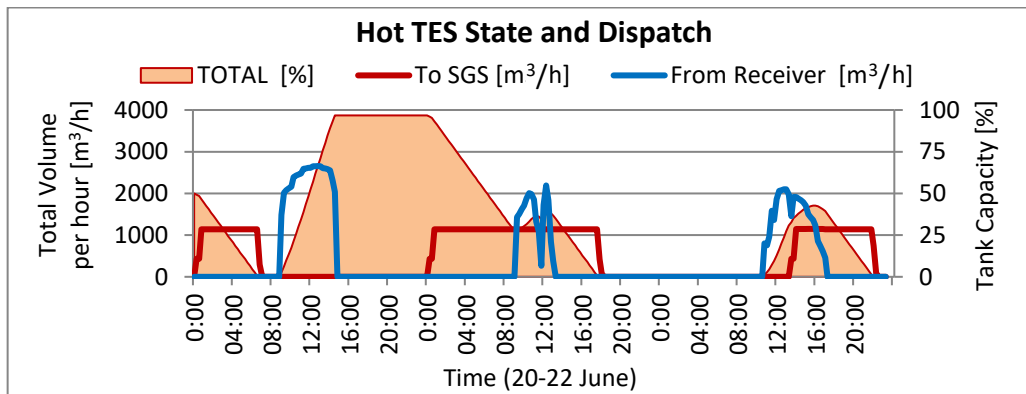


Figure C.85: Receiver operation shut down due to full hot TES

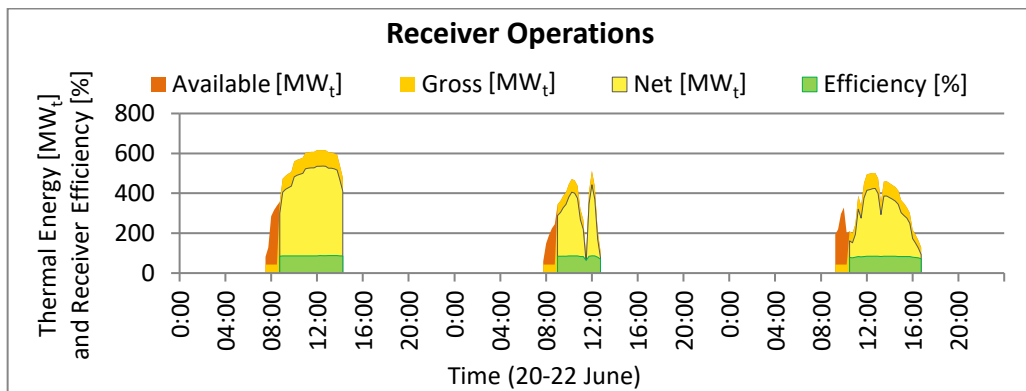


Figure C.86: Receiver operation shut down due to full hot TES

C.6.4. Optimised Maximise Power Generation

The ‘Maximise Power Generation’ operating strategy primarily optimises the power block operations. One of the significant contributions of this operating strategy is that it minimised the energy loss due to power block start-ups. However, in this scenario the power block did not curtail its power output for the third day, see Figure C.87. This operating strategy is preferred because higher thermal energy is lost while operating the turbine at part load conditions for long durations as compared to the energy loss on stopping the turbine and starting it up again. Thus, the thermal energy loss due to part load operations exceeds the thermal energy requirements for starting up the turbine.

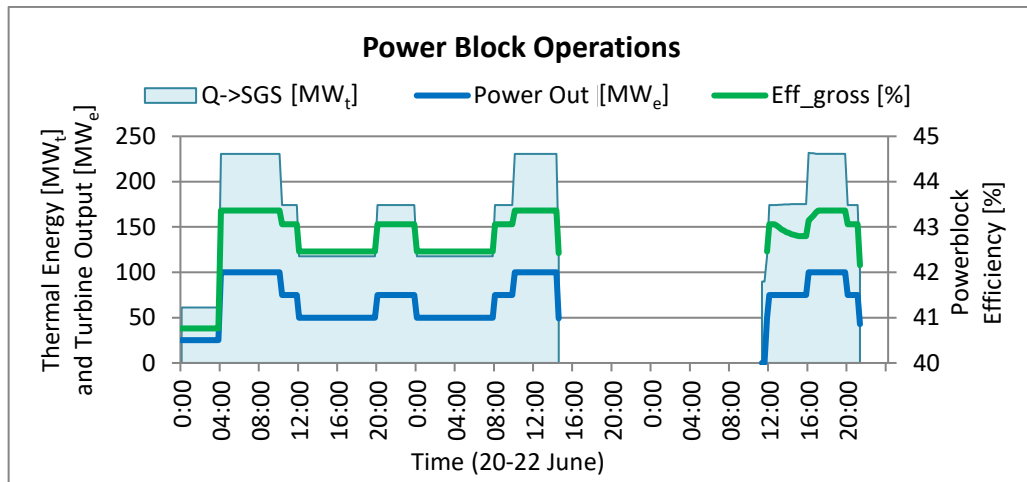


Figure C.87: ‘Maximise Power Generation’, low DNI and ambient temperatures

C.6.5. Maximise Plant Revenue

In this simulation, the plant operations were optimised to generate power during the high paying tariff periods as illustrated in Figure C.88.

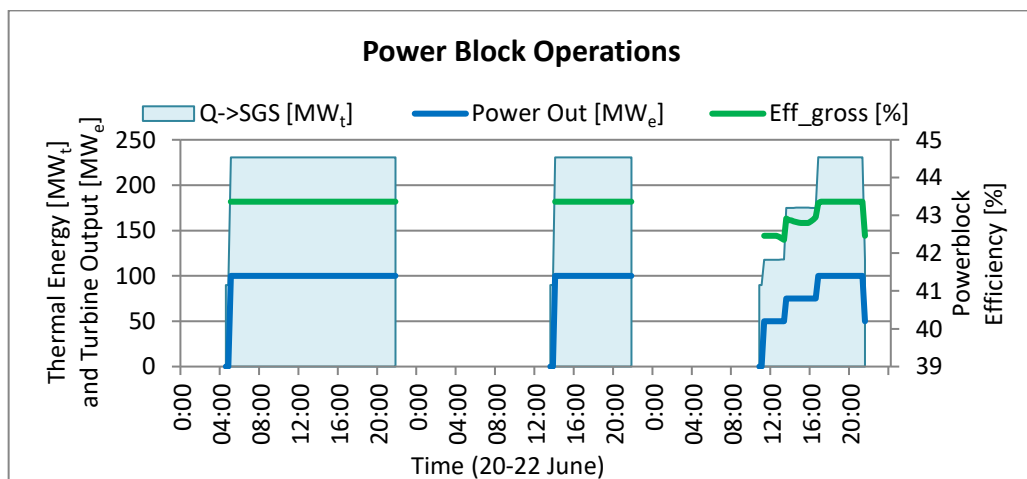


Figure C.88: Power block operations for ‘Maximise Plant Revenue’

C.6.6. Maximise Plant Revenue with Reduced Turbine Start/Stop

Optimisation done to lower the turbine starts/stops had no effect on the plant operations.

C.6.7. Minimise Energy Dumping

The ‘Minimise Energy Dumping’ operating strategy is mainly applied in conditions when high DNI is available to the heliostat field. The likelihood of energy dumping increases due to excessive flux concentrations on the receiver or a full state of charge from the hot TES. However, the excessive flux concentrations on the receiver’s surface had to be deflected by some of the heliostats, see Figure C.89. By implementing the ‘Minimise Energy Dump’ operating strategy, the heliostat field aiming strategy is adjusted and energy is attained.

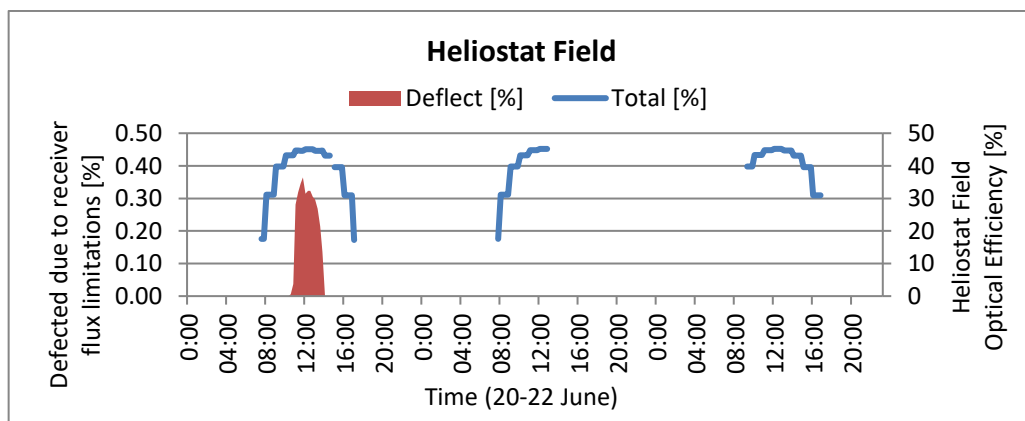


Figure C.89: Heliostat field optical efficiency and deflected solar energy

C.6.8. Optimise Electric Grid - Compliment Wind

The ‘Complimentary services to Wind and/or PV generation’ operating strategies aim to provide continuous output to the electric grid from the combined power generating technologies. In case of the wind generation, the CSP plant had to operate in part load conditions for majority of the time as there are continuous fluctuations in the wind energy throughout the day. Therefore, the hot TES was sufficiently charged with lower thermal output from the receiver during this low DNI period. However, during the second day, limited thermal energy attained from the solar collecting system failed the power block to provide complimentary services to wind throughout the third day, see Figure C.91.

C.6.9. Optimise Electric Grid - Compliment PV

Considering ‘Complimentary services to PV generation’, the plant provided the system with continuous power as long as sufficient thermal energy was available in the hot TES, see Figure C.92. During the day time when the PV contribution to the system was high, the hot TES charged. However, on other times when PV goes off-line the TES gets discharged to generate power. The dependency on the hot TES is clearly noted on the second day when exceptionally low DNI was present.

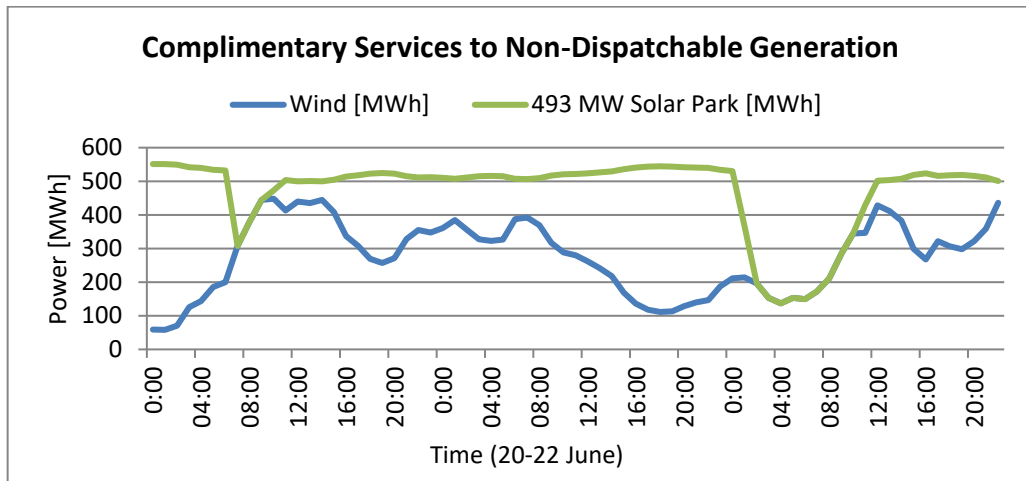


Figure C.90: CSP complimentary services to wind generation, stacked line

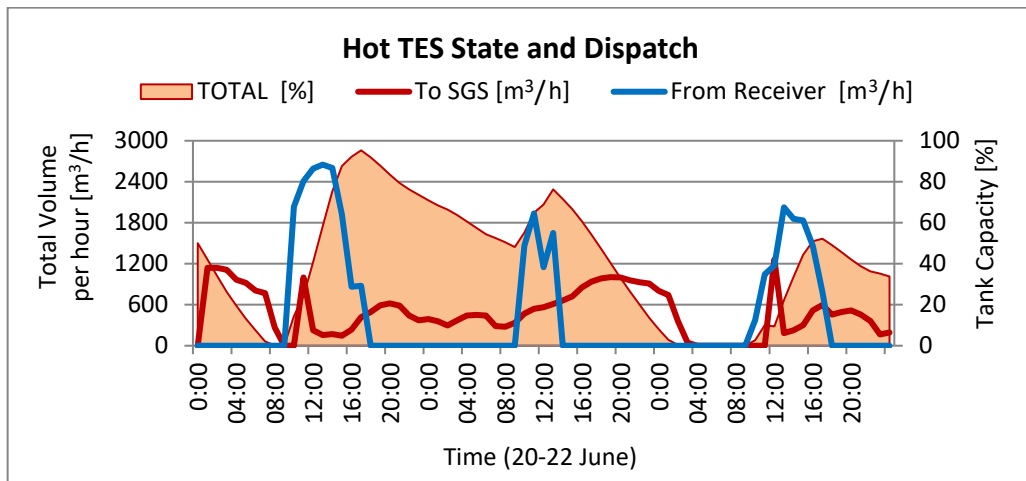


Figure C.91: Hot TES dispatch profile to provide complimentary services to wind

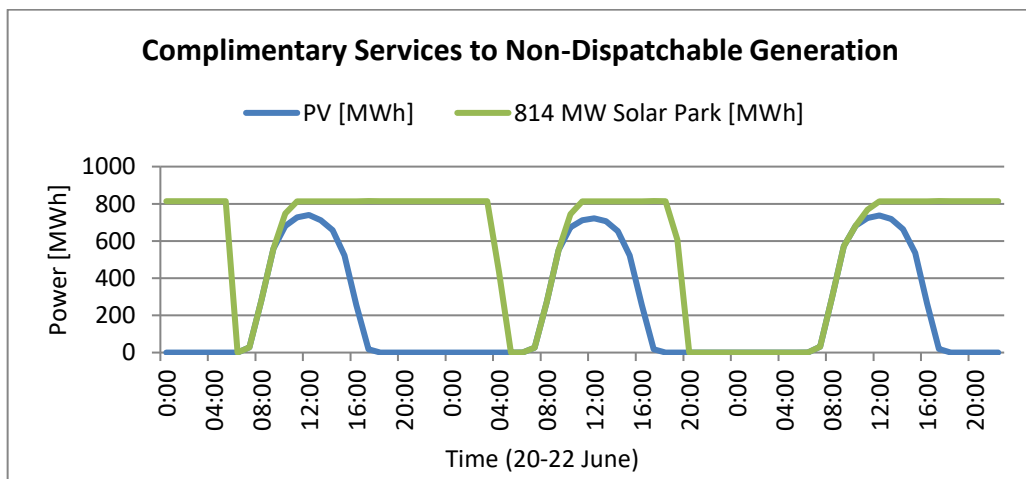


Figure C.92: CSP complimentary services to PV generation, stacked line

C.6.10. Optimise Electric Grid - Compliment Wind and PV

The ‘Complimentary services to PV generation’ alone did not perform well during low DNI periods, while combining it with wind generation offers greater results. Due to the contribution of wind to the PV generation profile, the CSP plant is able to charge its hot TES during the day, when the output is not required owing to PV contribution. In the evening, when PV generation declines, CSP supplement the power grid at a reduced turbine output due to the wind generation, see Figure C.93. Thus, continuous power for a longer period was provided.

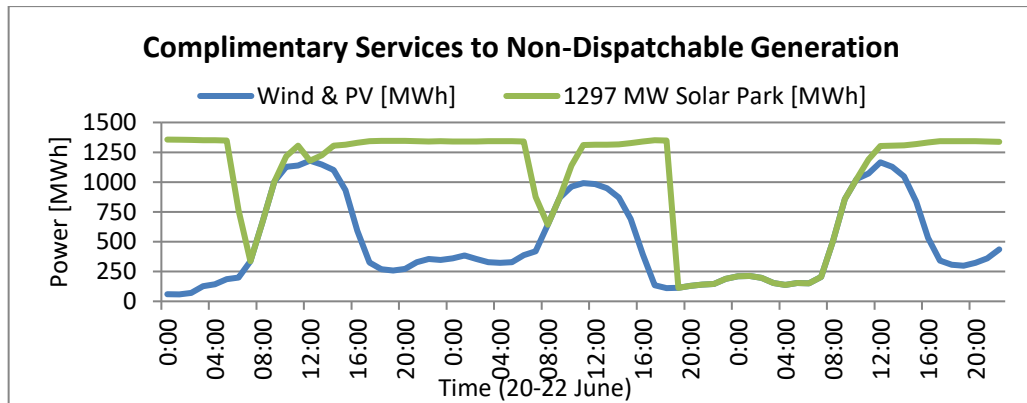


Figure C.93: CSP complimentary services to wind and PV generation, stacked line

C.6.11. Demonstrating CSP Base Load Capabilities

The most challenging to operate is the ‘Demonstrate CSP Base Load Capabilities’ operating strategy during low DNI periods. In this case, sufficient energy in the hot TES is required to sustain the energy requirements of the power block. As periods with low DNI offer low thermal energy from the receiver, this operating regime is challenged. As observed in Figure C.82, very low DNI conditions are observed on the second day.

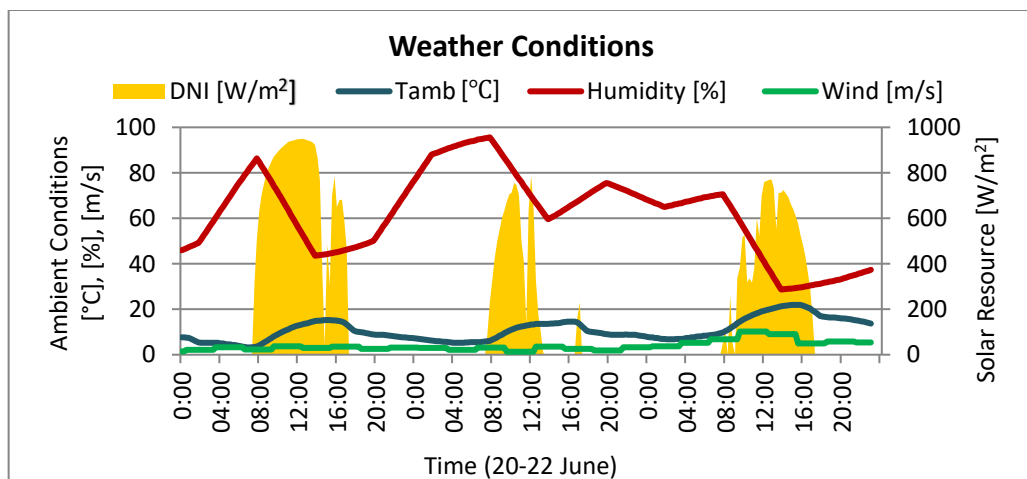


Figure C.82: Weather conditions applicable for the low DNI period

Simulating the ‘Base load Capabilities’, the model optimises the output of the turbine to provide continuous power for each day while maintaining the maximise power generation operating strategy undertone. This optimisation is represented in Figure C.94 and Figure C.95, working well in periods where the hot TES can be charged sufficiently. However, for low DNI periods, no energy generation is observed towards the end of the second day. This is because the thermal energy was utilised during the first day in order to maximise the power generation. Therefore, optimisation of the hot TES dispatch is required for the entire period of operation.

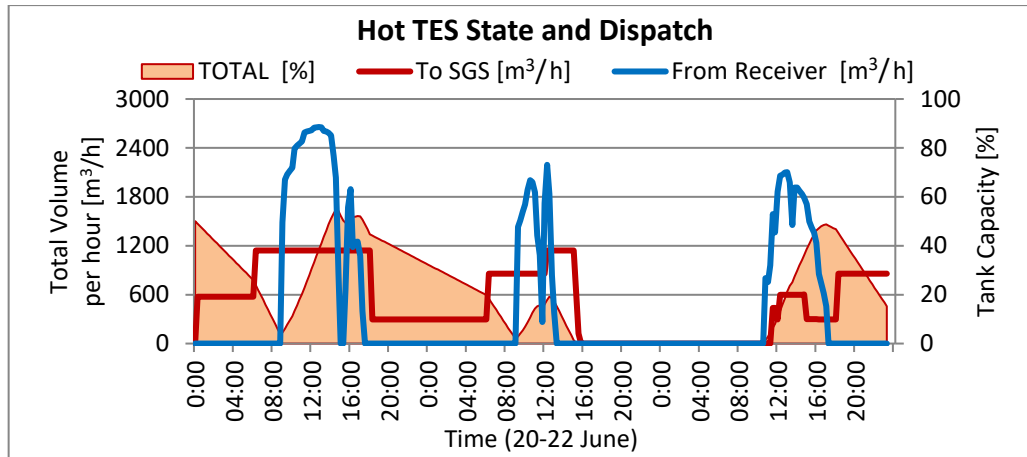


Figure C.94: Hot TES dispatch during low DNI periods

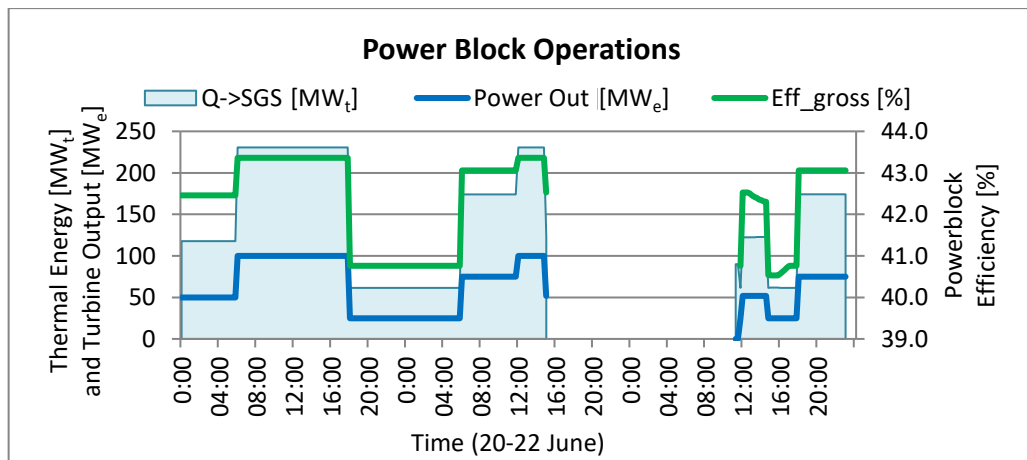


Figure C.95: Turbine output during low DNI periods

Continuous power is provided by the model by reducing the turbine output. Thus, it utilised the thermal energy produced on the first day of operation till the last day. This optimisation can be selected in the sub-menu when the ‘Base Load Operation’ operating strategy is chosen, see Figure C.96. The results are shown in Figure C.97 and Figure C.98. The hot TES was able to provide continuous power with a lower turbine output throughout the day, acting as a base load operating plant throughout the time. The turbine output was increased in early morning times to make provision for the receiver thermal output.

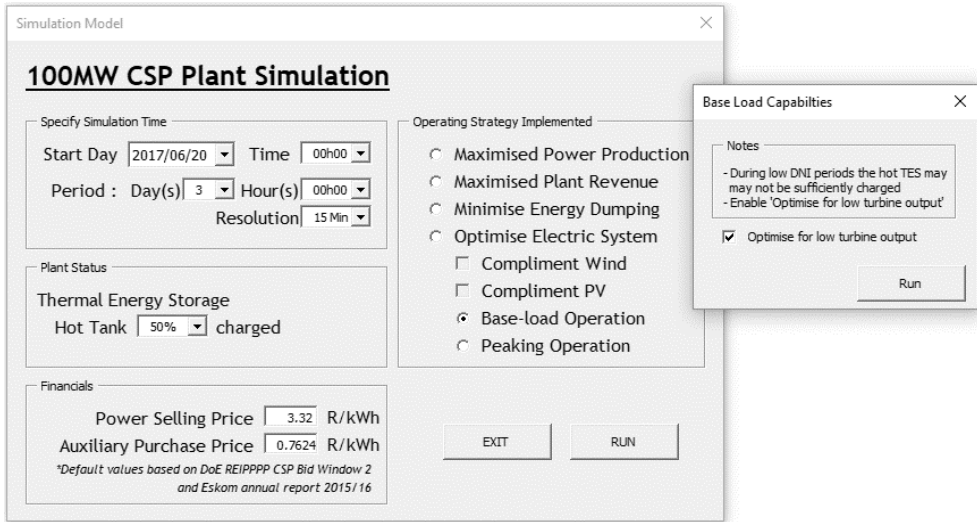


Figure C.96: Optimise for low turbine output

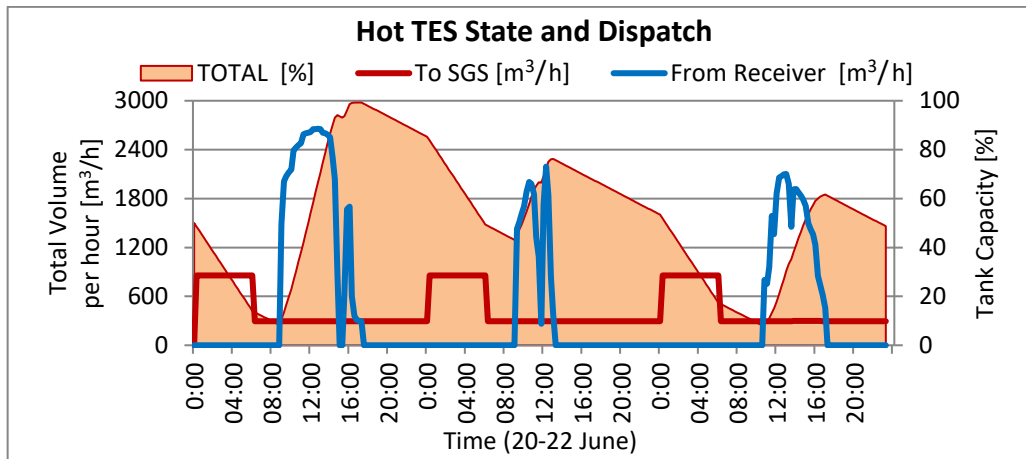


Figure C.97: Re-optimised hot TES dispatch during low DNI periods

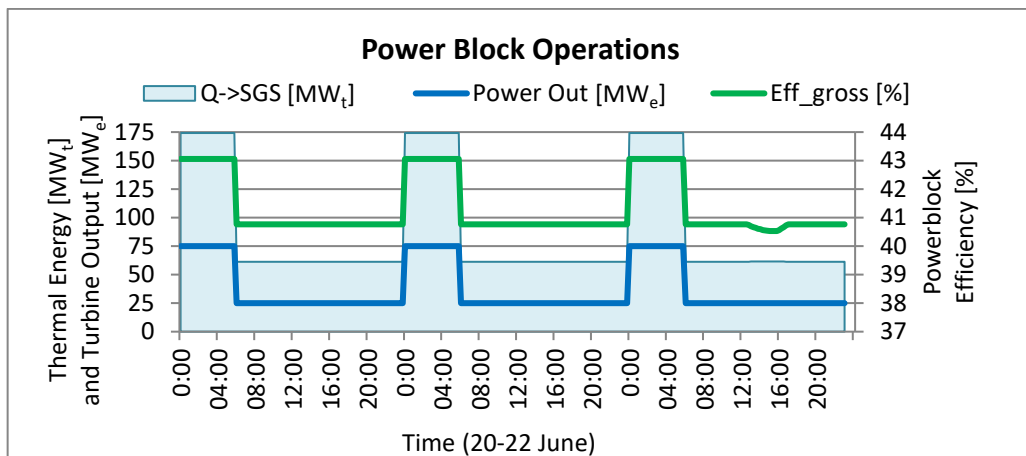


Figure C.98: Re-optimised lower turbine output during low DNI periods

C.6.12. Demonstrating CSP Peaking Capabilities

In the ‘Peaking’ operating strategy, power generation is prioritised for the specified peaking period. The model optimises the plant operation to deliver the required electric power during the peak times, while maintaining a maximise power generation undertone. Although, the low DNI period provided a limited amount of thermal energy from the receiver, the plant was able to satisfy the ‘Peaking’ operating strategy, see Figure C.99.

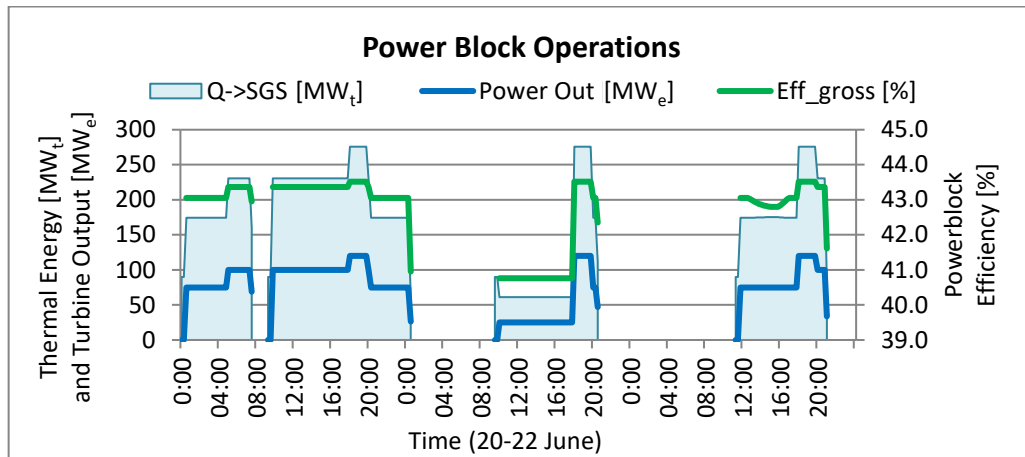


Figure C.99: ‘Peaking’ capabilities demonstrated during low DNI period

C.6.13. Compare Operating Strategies

The 11 operating strategies, denoted in Table C.3, were compared based on their system performance and financial indicators. The graphs represented in this section were produced with the functionality in the ‘Compare SimResults’ sheet.

Table C.3: List of operating strategies simulated with specified user inputs

No	Operating Strategy	Section	User Inputs
1	Max. Power Generation (User)	Section C.3.1	Power block start time at 05h00
2	Max. Power Generation (User)	Section C.3.2	Power block start at hot TES 30 % charged
3	Max. Power Generation (Optimised)	Section C.3.3	Optimised Power Generation selected
4	Max. Plant Revenue, Time-of-day tariff	Section C.3.4.1	TES size 12 hours
5	Reduce Turbine Start/Stop	Section C.3.4.6	TES size 12 hours
8	Min. Energy Dumping	Section C.3.4.6	No additional inputs required
9	Complimentary services to Wind	Section C.3.4.7	No additional inputs required
10	Complimentary services to PV	Section C.3.5	No additional inputs required
11	Complimentary services to Wind/PV	Section C.3.6.1	No additional inputs required
12	Demonstrate Base Load Capabilities	Section C.3.6.2	No additional inputs required
13	Demonstrate Peaking Capabilities	Section C.3.6.3	Peak Time 18h00-20h00 with Turbine Output set at 120 MW _e

C.6.13.1. Compare Receiver Performance

The receiver's performance, in terms of total power output and efficiency, for the various operating strategies was good. When Figure C.100 is considered, all the operating strategies were able to attain the full power output of the receiver except operating strategies 2 and 10. The reduced thermal output from these simulations is due to the curtailment and/or shutting down of the receiver operations. The receiver was shut down, when higher receiver efficiencies are observed with a relatively low thermal output. This is exhibited in operating strategy 2.

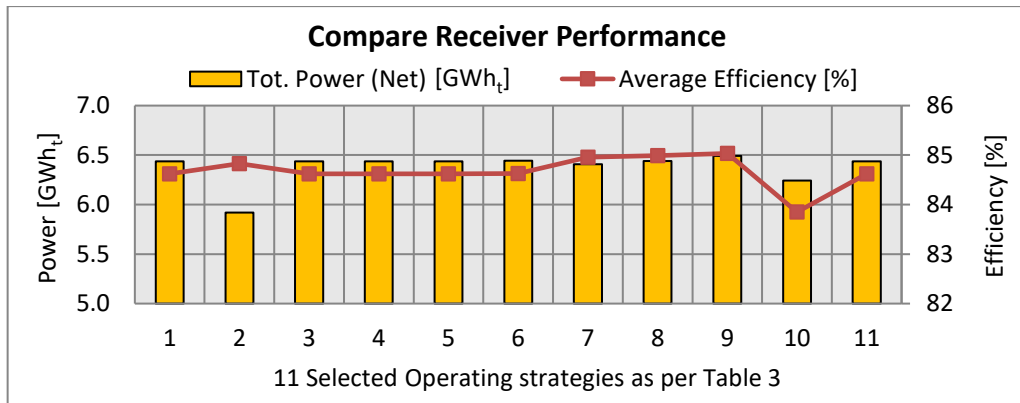


Figure C.100: Comparison of the simulation results, receiver performance

C.6.13.2. Compare Power Block Performance

Overall, the operating strategies implemented relatively performed well in terms of total net power delivered and their efficiencies, see Figure C.101. However, the 'Complimentary services to wind and/or PV generation' did not perform as well as other operating strategies. The PV delivered higher power block efficiencies compared to the wind generation, and the reason for this is the part load operations during complimentary services during wind generation. Furthermore, the auxiliary consumption in ratio to the gross power delivered to the system was higher for these complimentary services.

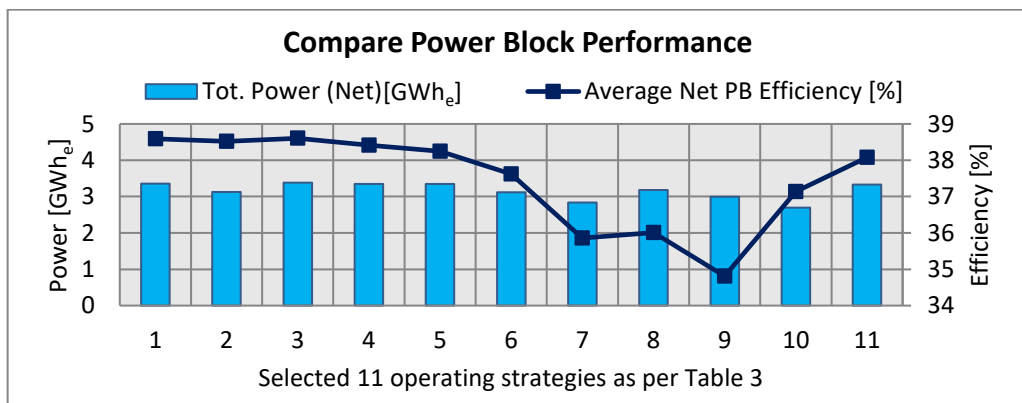


Figure C.101: Comparison of the simulation results, power block performance

C.6.13.3. Compare Plant Performance

The overall plant performance is illustrated in Figure C.102. Higher plant efficiencies are attained by operating under strategies that aim to maximise power generation and revenue. The operating strategies offering complimentary services to wind and/or PV generation resulted in lower margins. This was mainly due to the combined effect of a poor receiver and power block efficiencies.

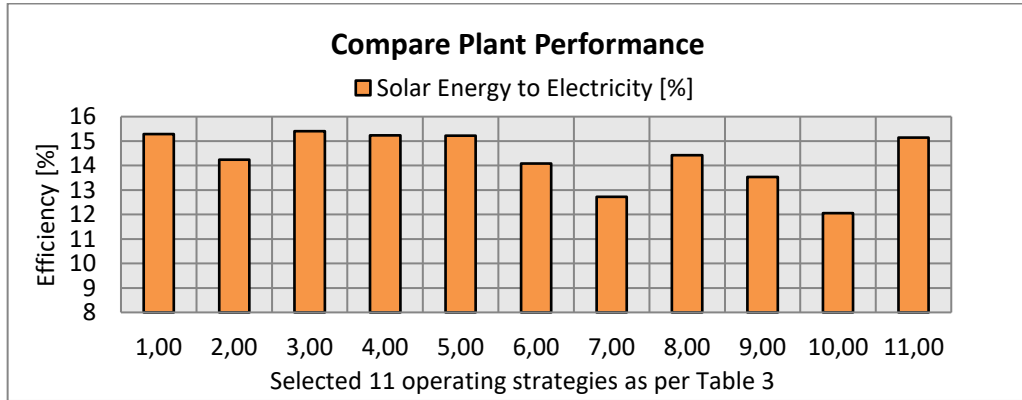


Figure C.102: Comparison of the simulation results, plant performance

C.6.13.4. Compare Financial Indicators

The plant revenue during the low DNI period is expected to be lower as compared to the results obtained during a high DNI period. With the limited thermal energy available to the power block, the plant operations were optimised to deliver the highest possible revenue. When Figure C.103 is considered, attention is drawn to operating strategies 3-5 that represents the 'Maximise power generation with flat-rate tariff structure' and 'Time-of-day tariff structure' strategies. In the previous simulation results, the 'Time-of-day tariff structure' operating strategies resulted in the lowest plant revenue. Considering that these operating strategies are on par with the other operating strategies, the time-of-day tariff structure worked in favour of the plant operations.

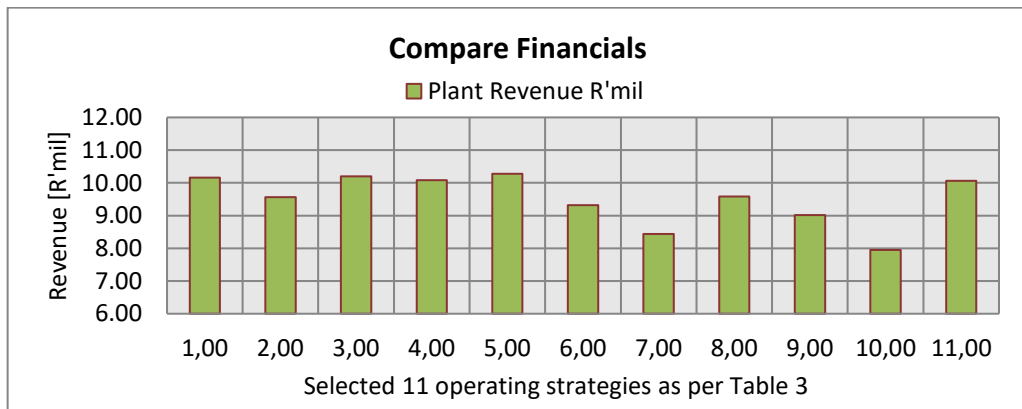


Figure C.103: Comparison of the simulation results, plant revenue generated